Assessment of Uncertainties affecting Dosimetric Calculations for the Intake of Radon and NORM

Zur Erlangung des akademischen Grades eines

DOKTORS DER INGENIEURWISSENSCHAFTEN (Dr.-Ing.)

von der KIT-Fakultät für Elektrotechnik und Informationstechnik des Karlsruher Instituts für Technologie (KIT)

angenommene

DISSERTATION

von

M.Sc., Makumbi, Thomas

geboren in: Kampala, Uganda

Tag der mündlichen Prüfung: 13.11.2025

Hauptreferent: Dr.rer. nat. Bastian Breustedt

Korreferent: Prof. Dr.-Ing. Maria Francesca Spadea

DECLARATION

I Thomas Makumbi declare to the best of my knowledge that this work has been done by myself and it reflects the work I have been able to do during the last 48 months of my doctoral study in Electrical Engineering at the Institute of Thermal Energy Technology and Safety (ITES) of the Karlsruhe Institute of Technology (KIT) Campus North.

Candidate

Thomas Makumbi

Date: 14.04.2026

ABSTRACT

This study evaluates uncertainties in dosimetric calculations for radon and naturally occurring radioactive material (NORM) intakes in underground mines. We developed INTDOSKIT, an R-based tool implementing the International Commission on Radiological Protection (ICRP) methodology for internal dose assessment, validated against ICRP data and extended with Monte Carlo simulations to assess uncertainties in dose coefficients. Probability distributions for model parameters were established through an extensive literature review, with Monte Carlo iterations optimized using the central limit theorem. A parameter uncertainty analysis was performed for radon progeny and uranium ore dust inhalation, focusing on two exposure scenarios: Job 1 (wet drilling with good ventilation) and Job 4 (dry drilling with poor ventilation).

The results show that Job 4 results in higher committed equivalent lung dose coefficients than Job 1, with geometric means (GM) of 61.87 mSv/ (mJh/m³) and 47.05 mSv/ (mJh/m³), respectively, and geometric standard deviations (GSD) of about 1.6. The 95% confidence intervals (CI) ranged from 18.59 to 104.74 mSv/ (mJh/m³) for Job 1 and from 24.83 to 133.09 mSv/ (mJh/m³) for Job 4. In both scenarios, the alveolar-interstitial region of the lung had the greatest uncertainty, with uncertainty factors (UFs) of 3.32 for Job 1 and 3.13 for Job 4. Bronchial secretory cells received the highest doses. Among the systemic organs, the kidneys received the highest doses and had the largest uncertainties.

Sensitivity analysis identified particle deposition parameters, in particular tidal volume, as key contributors to dose uncertainty. Reducing uncertainties in lung dose estimates requires more accurate measurements of activity parameters, including respiratory rate, nasal fraction, tidal volume and time spent in each activity. These factors need to be carefully considered to refine lung dose estimates for radon progeny inhalation in underground mines.

For uranium ore dust inhalation, Job 4 also resulted in higher doses than Job 1, with GMs of 0.0435 mSv/ (kBqh/m³) and 0.0308 mSv/ (kBqh/m³), respectively, and GSDs of about 2.3. The 95% CIs ranged from 0.00653 to 0.145 mSv/ (kBqh/m³) for Job 1 and from 0.00850 to 0.208 mSv/ (kBqh/m³) for Job 4. The alveolar-interstitial region again showed the greatest uncertainty, with UFs of 6.11 for Job 1 and 6.12 for Job 4. Bronchiolar secretory cells received the highest doses. Among the systemic organs, the bone received the highest doses, while the greatest uncertainties were observed in the stomach (UF = 5.48) for Job 1 and in the heart (UF = 5.67) for Job 4.

These results underline the need to refine biokinetic models to improve the accuracy of dose predictions and highlight the importance of tailored protection measures such as improved ventilation, stricter air quality standards and advanced personal protective equipment. By effectively managing the risks of radon exposure, mining regulators and industry leaders can better protect miners from the long-term health effects associated with the inhalation of radon progeny as well as long lived radionuclides in uranium ore dust and ensure safer and healthier working conditions in underground mines.

KURZFASSUNG

Diese Studie untersucht Unsicherheiten bei dosimetrischen Berechnungen für die Aufnahme von Radon und natürlich vorkommendem radioaktivem Material (NORM) in Untertagebergwerken. Wir entwickelten INTDOSKIT, ein R-basiertes Tool, das die Methodik der Internationalen Strahlenschutzkommission (ICRP) zur internen Dosisbewertung implementiert, anhand von ICRP-Daten validiert und mit Monte-Carlo-Simulationen erweitert wurde, um Unsicherheiten bei Dosiskoeffizienten zu bewerten. Wahrscheinlichkeitsverteilungen für Modellparameter wurden durch eine umfassende Literaturrecherche ermittelt, wobei Monte-Carlo-Iterationen mithilfe des zentralen Grenzwertsatzes optimiert wurden. Es wurde eine Parameterunsicherheitsanalyse für die Inhalation von Radonfolgeprodukten und Uranerzstaub durchgeführt, wobei der Schwerpunkt auf zwei Expositionsszenarien lag: Job 1 (Nassbohren mit guter Belüftung) und Job 4 (Trockenbohren mit schlechter Belüftung).

Die Ergebnisse zeigen, dass Job 4 zu höheren Lungenäquivalentdosiskoeffizienten führt als Job 1, mit geometrischen Mittelwerten (GM) von 61,87 mSv/(mJh/m³) bzw. 47,05 mSv/(mJh/m³) und geometrischen Standardabweichungen (GSD) von etwa 1,6. Die 95%-Vertrauensintervalle (CI) lagen zwischen 18,59 und 104,74 mSv/(mJh/m³) für Job 1 und zwischen 24,83 und 133,09 mSv/(mJh/m³) für Job 4. In beiden Szenarien war der alveolar-interstitielle Bereich der Lunge mit Unsicherheitsfaktoren (UFs) von 3,32 für Job 1 und 3,13 für Job 4 am unsichersten. Die höchsten Dosen erhielten die bronchialen sekretorischen Zellen. Unter den systemischen Organen erhielten die Nieren die höchsten Dosen und wiesen die größten Unsicherheiten auf.

Sensitivitätsanalysen identifizierten Partikelablagerungsparameter, insbesondere das Atemzugvolumen, als Hauptfaktoren für die Dosisunsicherheit. Um die Unsicherheiten bei der Abschätzung der Lungendosis zu verringern, sind genauere Messungen von Aktivitätsparametern wie Atemfrequenz, Nasenfraktion, Atemzugvolumen und der Verweildauer bei jeder Aktivität erforderlich. Diese Faktoren müssen sorgfältig berücksichtigt werden, um die Abschätzung der Lungendosis bei Inhalation von Radonfolgeprodukten in Untertagebergwerken zu verfeinern.

Beim Einatmen von Uranerzstaub führte Job 4 ebenfalls zu höheren Dosen als Job 1, mit GMs von 0,0435 mSv/(kBqh/m³) bzw. 0,0308 mSv/(kBqh/m³) und GSDs von etwa 2,3. Die 95%-KIs lagen zwischen 0,00653 und 0,145 mSv/(kBqh/m³) für Job 1 und zwischen 0,00850 und 0,208 mSv/(kBqh/m³) für Job 4. Der alveolar-interstitielle Bereich wies erneut die größte Unsicherheit auf, mit UFs von 6,11 für Job 1 und 6,12 für Job 4. Die bronchiolären sekretorischen Zellen erhielten die höchsten Dosen. Unter den systemischen Organen erhielt der Knochen die höchsten Dosen, während die größten Unsicherheiten im Magen (UF = 5,48) für Job 1 und im Herzen (UF = 5,67) für Job 4 beobachtet wurden.

Diese Ergebnisse unterstreichen die Notwendigkeit, biokinetische Modelle zu verfeinern, um die Genauigkeit von Dosisvorhersagen zu verbessern. Sie unterstreichen die Bedeutung maßgeschneiderter Schutzmaßnahmen wie verbesserter Belüftung, strengerer Luftqualitätsstandards und moderner persönlicher Schutzausrüstung. Durch ein effektives Management der Radonrisiken können Bergbauaufsichtsbehörden und Branchenführer Bergleute besser vor den langfristigen gesundheitlichen Folgen schützen, die mit der Inhalation von Radonfolgeprodukten sowie langlebigen Radionukliden im Uranerzstaub verbunden sind, und sicherere und gesündere Arbeitsbedingungen in Untertagebergwerken gewährleisten.

ACKNOWLEDGEMENT

I would like to thank my academic mentors Dr. rer. nat. Bastian Breustedt and Dr.rer. nat. Christian Staudt for the help and support throughout this journey. Thank you for all the knowledge and useful advice as well as the insightful discussion aimed at ensuring that I succeeded in my PhD task. I would also like to extend my sincere gratitude to my professional mentors Wolfgang Raskob, Dr.rer.nat. Sadeeb Simon Ottenburger and Dr.rer.nat. Angelika Bohnstedt for the facilitation and guidance and for offering me the opportunity to undertake my studies at the ITES-RESIS research group of KIT campus north. Special thanks go to all members of ITES-RESIS for welcoming me to the group and ensuring that I had a comfortable stay during my studies.

Special thanks also go out to my countrymen Mr and Mrs. Ssemujju who supported me physically and emotionally throughout my time of the PhD studies in Karlsruhe, Dr. Michael Kyesswa of the Institute of Applied Informatics (IAI) of KIT for his technical assistance with running my simulations.

I would also like to extend my gratitude to the RadoNorm project for funding my research and for the facilitation. Special thanks go to all the WP3 members for the encouragement, academic and emotional support. I look forward to our fruitful cooperation even after the PhD.

DEDICATION

This report is dedicated to my late guardian Mrs. Ruth Mugenyi. Thanks for the love and support throughout my academic career. The report is also dedicated to my spouse and my children Joshua Williams Mayengo and Vanessa Nicole Nansubuga for the patience, understanding and encouragement and for bearing with me for the period I was away from you while pursuing the PhD. You demonstrated a highly level of understanding, maturity and resilience. I am forever grateful and indebted to you.

Preface

The PhD candidate confirms that the work presented in this thesis contains significant scientific contributions by himself. This thesis reuses material from the following publications:

Makumbi, T., Breustedt, B., & Raskob, W. (2024a). Parameter uncertainty analysis of the equivalent lung dose coefficient for the intake of radon in mines: A review. Journal of Environmental Radioactivity, 276(1-4):107446. https://doi.org/10.1016/j.jenvrad.2024.107446

Makumbi, T., Breustedt, B., Raskob, W., & Ottenburger, S.S. (2024b). Application of INTDOSKIT tool for assessment of uncertainties on dose coefficients for ingestion of uranium by workers. Radiation Physics and Chemistry. 226(1): 112247. https://doi.org/10.1016/j.radphyschem.2024.112247

Makumbi, T. & Spielmann, V. (2024c). Assessment of uncertainties affecting dosimetric calculations for the intake of radon and thoron progeny in underground mines. https://www.radonorm.eu/wp-content/uploads/file_exchange/D3.4_Report-on-the-uncertainties-affecting-dosimetric-calculations.pdf

Breustedt, B., Chavan, N., & Makumbi, T. (2025). An R Code for calculation of dose coefficients and studying their uncertainties. Health Physics. 129(2):50-60. http://dx.doi.org/10.1097/HP.0000000000001833

Makumbi, T., Breustedt, B., Raskob, W., & Ottenburger, S.S. (2025). Parameter uncertainty analysis of the committed equivalent dose coefficients from inhalation of radon progeny in underground uranium mines. Journal of Environmental Radioactivity. 289: 107751. https://doi.org/10.1016/j.jenvrad.2025.107751

The research leading to these results has been accomplished with the financial support of the Euratom research and training program 2019-2020 under grant agreement No 900009 (RadoNorm). The analyses and results interpretation in Breustedt et al. (2025) were performed by Bastian Breustedt who also wrote the manuscript with support from the candidate and Niranjan Chavan. While the analyses and results from Makumbi et al. (2024a), Makumbi et al. (2024b) and Makumbi et al. (2025), were solely performed by the candidate who also wrote the manuscript with advice from Bastian Breustedt, Wolfgang Raskob and Sadeeb Simon Ottenburger and comments from all co-authors.

The candidate confirms that appropriate credit has been given within the thesis where reference has been made to the publications of others.

Table of Contents

List of Figures

List of Tables

1. INTRODUCTION

1.1 Research motivation

Radiation protection is a field concerned with the protection of humans from the harmful effects of ionizing radiation. For radionuclides incorporated in the body, internal dosimetry is used to assess the dose to body organs and tissues at risk (Li, 2018). Intakes of radionuclides may occur during routine operations in a range of industrial, medical, educational and research facilities. They may also occur after an incident involving the release of radioactive substances followed by inhalation of particles or ingestion of contaminated foods (Paquet et al., 2016).

An adequate assessment of internal dose resulting from intakes of radionuclides is essential for the optimization of radiological protection of workers, for the assessment of the health consequences of releases of radioactive materials to the environment for members of the public and for retrospective demonstration of compliance with regulatory requirements. The International Commission on Radiological Protection (ICRP) has defined the quantities equivalent and effective dose and developed and formalized the methodology for internal dose assessment. ICRP has also published reference biokinetic and dosimetric models to be used in internal dose assessment (ICRP, 1991, 2007; Harrison and Day, 2008).

However, it should be noted that during internal dose assessment, the parameters used in physics, human anatomy and physiology as well as computational techniques are subject to large uncertainties (Puncher and Harrison, 2012). Moreover, the biokinetic models provided by ICRP are reference models whose parameters are representative of a reference person. By definition, these model parameter values are fixed numbers with no uncertainties (Paquet et al., 2016). Therefore, sensitivity analysis and the estimation of associated parameter uncertainties in biokinetic models need to be performed to give a better understanding of the models and to estimate the influence of single parameters on the model predictions and hence dose coefficients (Breustedt et al., 2017, 2018). However, since most of the software used for internal dose assessment is commercial and designed to strictly follow the ICRP methodology for internal dose assessment, it cannot be used to perform studies on uncertainty analysis which was the main purpose of this work.

For this work, which is a part of the RadoNorm project (https://www.radonorm.eu), studies on uncertainty and sensitivity of the dose calculation following intakes of radon and other naturally occurring radionuclides (NORM) have been undertaken. For performing such studies, a dedicated software tool needed to be developed.

Therefore, the aim of this work was first to develop a software tool implementing ICRP's methodology for calculation of doses after incorporation of radionuclides into the body and secondly to extend the tool to perform uncertainty and sensitivity analysis on the calculated doses for selected exposure scenarios for intake of radon and other naturally occurring radioactive material (NORM) in underground uranium mines. The results of this work will provide information about the reliability of assessed doses and indications to selective sensitive parameters for a better fit of the models to monitoring data.

1.2 Exposure scenarios of humans to naturally occurring radioactive material

The use of NORM can expose humans and wildlife to ionizing radiation. These exposures typically follow a source-pathway-receptor model. In the context of NORM, two primary sources have been identified: direct release of radionuclides into the environment and presence of radionuclides in Technologically Enhanced Naturally Occurring Radioactive Materials (TENORM). Figure 1 depicts the distinct transmission routes of each source to receptors.

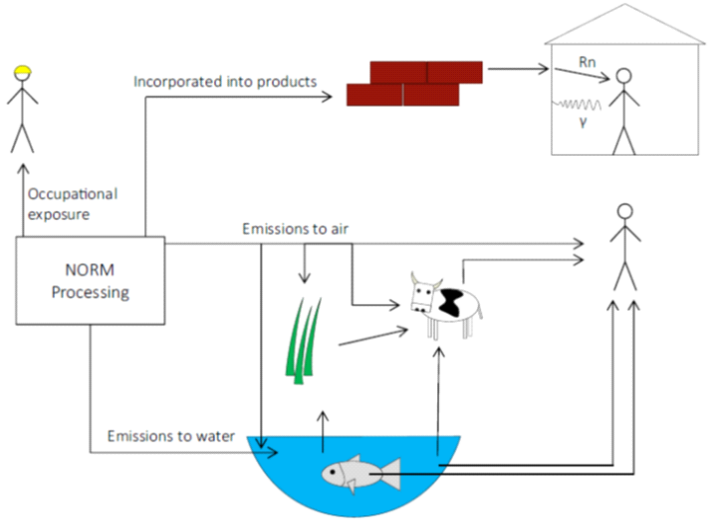

Figure 1: Human exposure pathways to ionizing radiation (Source: Joyce et al., 2017)

The mining sector is one of the main contributors to human exposure to NORM and radon. Mining operations generate significant volumes of tailings that may contain high levels of radioactivity. This issue is not limited to uranium and thorium mines, but also affects other types of mines, including those for copper and gold. Radionuclides can leach from these tailings and potentially contaminate groundwater, thereby exposing nearby populations. For instance, high levels of Ra-226 in produced water from coal mining can lead to environmental contamination, particularly when stored in open ponds. Similarly, the phosphate fertilizer industry produces large quantities of phosphogypsum, a by-product containing elevated levels of Ra-226 that is stored in extensive landfills.

Radionuclides emitted from NORM sources disperse through the environment and can reach human and non-human receptors via deposition, ingestion, inhalation, and bioaccumulation mechanisms (IAEA, 2011). For example, radionuclides emitted through stacks can be inhaled directly or deposited on plants and forage, entering the food chain in the process. These contaminants can also settle in bodies of water, affecting aquatic life and potentially being consumed by humans. Similar pathways apply to the direct discharge of radionuclides into water during NORM processing activities.

Elements such as uranium, thorium, and radium are naturally present in the Earth's crust and can act as continuous sources of radon gas. Radon can escape from soil and rock formations through diffusion or convection, resulting in its presence in both indoor and outdoor air (Makumbi et al., 2024a). Accumulation of radon and its short-lived decay products in enclosed environments, such as underground mines or water treatment facilities, increases radiation exposure risks (ICRP, 2017). Radon can migrate over a meter through soil, so the ground beneath buildings significantly contributes to indoor radon levels (Brudecki et al., 2014; Mirsch et al., 2020). In contrast, thoron (Rn-220) has a much shorter half-life of 56 seconds and travels shorter distances. It is primarily released from building materials, especially those that incorporate NORM-enriched waste. Prolonged occupancy in such environments can lead to exposure. Due to its 4-second half-life, actinon (Rn-219) contributes minimally to exposure.

Consequently, radon isotopes Rn-222 and Rn-220, along with their progeny, are considered the primary sources of indoor radiation exposure (Mirsch et al., 2020; Wang et al., 2021). Decay products from the U-238 and Th-232 series contribute less significantly to indoor inhalation exposure (UNSCEAR, 2008).

Human exposure to NORM can occur during the processing and disposal of materials. There are occupational exposure risks at sites where raw ores, residues, and final TENORM products are handled or stored, including TENORM waste landfills. The extent of exposure from environmental discharges during processing varies depending on the material type and processing technique. Although the concentrations of radionuclides in raw materials may be low, the large-scale processing seen in industries such as phosphate, steel, and oil and gas can lead to significant radioactive enrichment. Examples include Ra-226 in phosphogypsum from phosphate production, Po-210 in steel production residues, and oil and gas sludge containing Ra-226, Pb-210, and Po-210.

The International Commission on Radiological Protection (ICRP) categorizes ionizing radiation exposure into three main groups to address various exposure scenarios: occupational, public, and medical exposure. In occupational settings, inhalation is the predominant exposure route, though ingestion and dermal absorption (especially through cuts or wounds) are also possible. For the general public, ingestion through food and water is the primary exposure route, with inhalation playing a secondary role unless a nuclear accident occurs. In that case, inhalation can become the dominant exposure route. In medical contexts, radionuclides are primarily introduced into the body via intravenous injection, though oral intake occurs to a lesser extent.

Once inside the body, these substances can accumulate in organs such as the lungs or gastrointestinal tract. They can also enter the bloodstream, migrate to various tissues, and be excreted through urine and faeces. These internal processes are modelled through biokinetic frameworks.

1.3 Research Objectives

Uncertainty and sensitivity studies for selected scenarios with intakes of radon and NORM were performed to support epidemiological studies on the biological effects of naturally occurring radionuclides. This PhD project was embedded in work package 3 “Dosimetry” of the European Commission (EC) funded RadoNorm project. The main objective of the study was providing

reasonable uncertainties of the doses used in the cohort studies. To achieve this objective, it was sub-divided into five specific subtasks;

1. *Literature review and definition of scenarios.*

Here the relevant literature was reviewed and the scenarios, to be studied defined. The latter was done in collaboration with the partners of RadoNorm.

2. *Development of a software tool for internal dose assessment.*

A dedicated software tool (INTDOSKIT) was developed to calculate dose coefficients using ICRP biokinetic and dosimetry models. The tool was validated using ICRP reference data.

3. *Dose calculation for selected scenarios.*

Dose coefficients for the selected scenarios were calculated with INTDOSKIT tool using reference values for the model parameters.

4. *Extension of the software to perform uncertainty and sensitivity analysis for selected scenarios.*

INTDOSKIT was extended to allow sampling of the model parameters from a statistical distribution. A Monte Carlo approach was implemented to derive a posterior distribution of the doses from a series of repetitions. Methods to characterize the dose distributions by statistical quantities were also implemented in the tool.

5. *Uncertainty and sensitivity analysis on calculated doses for selected scenarios.*

The studies on uncertainty and sensitivity of the dose coefficients calculated in subtask 3 were performed in this subtask and dose distributions obtained.

1.4 Thesis overview

This thesis presents an assessment of the uncertainties on calculated doses for the intake of radon and uranium ore dust in underground mines. A brief overview of the core chapters in the thesis is presented as follows;

Chapter 2: Development of software for internal dose calculations

In this chapter, the biokinetic and dosimetric models used in internal dose calculations for the intake of radon and uranium ore dust by underground miners are presented. The chapter also presents the ICRP methodology for internal dose assessment. Furthermore, a brief description of the software tool INTDOSKIT used for internal dose calculations as well as its application for internal dose calculations is presented. Lastly, the validation of the software tool using ICRP data for radon and NORM material is presented and discussed.

Chapter 3: Dose calculations for selected scenarios in underground mines

This chapter presents and discusses the selected scenarios for inhalation of radon and thoron progeny in underground mines. This chapter further presents the application of INTDOSKIT tool to calculate radiation doses after intake of radon and thoron progeny as well as uranium ore dust for selected scenarios in underground mines.

Chapter 4: Extension of the software to perform uncertainty and sensitivity analysis

This chapter presents the methodologies for uncertainty and sensitivity analysis in internal dosimetry. It further discusses the modification of INTDOSKIT to perform a Monte Carlo simulation. Lastly, probability distributions for the biokinetic model parameters used in the selected scenarios for radon and thoron progeny inhalation are presented.

Chapter 5: Uncertainty and sensitivity analysis for selected scenarios

Selected results for the uncertainty and sensitivity analysis for the selected scenarios for radon and thoron progeny as well as inhalation of uranium ore dust in underground mines are presented in this chapter.

Chapter 6: Conclusions and Recommendations

This chapter presents the conclusions and recommendations for future study drawn from the findings of this study.

2. INTERNAL DOSE ASSESSMENT

This chapter describes the ICRP models used in radiation protection. It also describes the ICRP methodology for internal dose assessment, the application of the ICRP methodology for internal dose assessment to develop a software tool (INTDOSKIT) that was used in this work for internal dose assessment and to perform uncertainty studies. It further describes the operation of INTDOSKIT tool for internal dose assessment and concludes with the validation of INTDOSKIT against ICRP data.

2.1 Biokinetic and Dosimetric Models of ICRP

Radionuclides can enter the human body accidentally or deliberately through various routes, including inhalation, ingestion, injection, skin absorption, entry through wounds, instillation, and entry through body orifices. These pathways are particularly relevant in nuclear medicine, where radioactive substances are intentionally administered for diagnostic or therapeutic purposes (Li, 2018).

Once inside the body, radionuclides undergo a series of physiological processes collectively referred to as biokinetics. These processes include intake, absorption, distribution, retention, translocation to different organs, elimination, and eventual excretion. These processes determine the internal movement and fate of radionuclides, as illustrated in Figure 2.

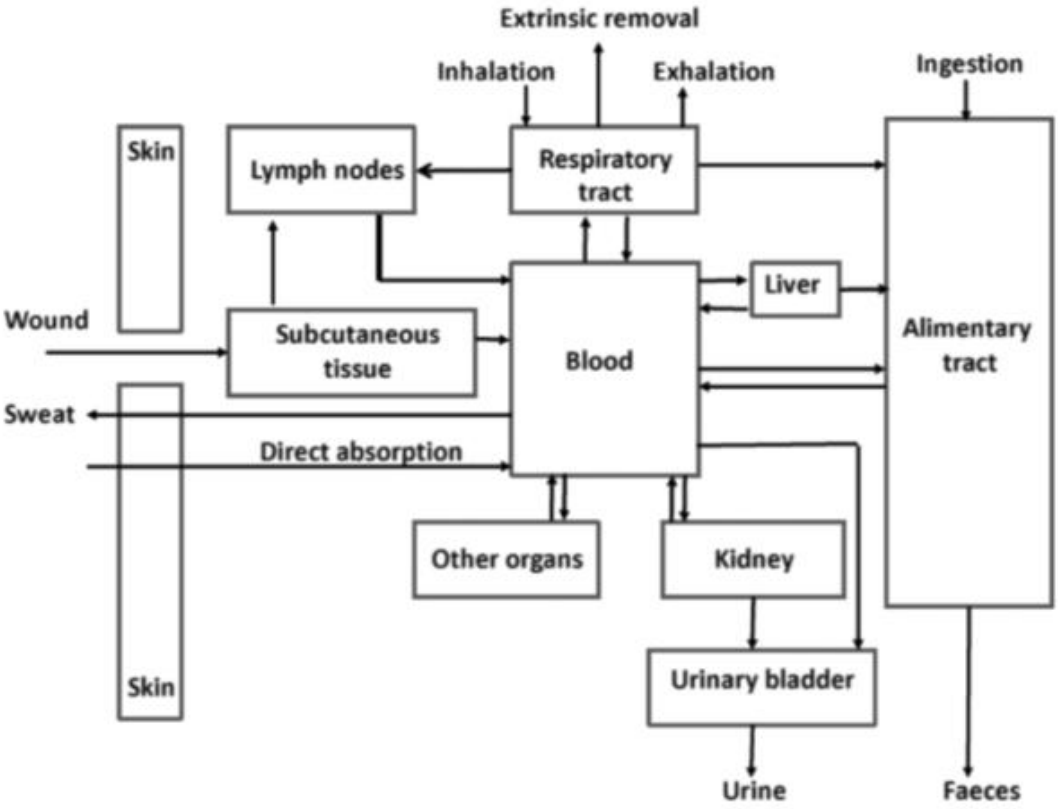

Figure 2: Main routes of intake, transfer and excretion of radionuclides in the body (Source: ICRP, 2015)

Biokinetic models are essential tools for describing the distribution of radionuclides within the human body over time and for assessing internal radiation doses. The International Commission on Radiological Protection (ICRP) has developed reference models that simulate the behaviour

of radionuclides in a standardized "reference person." These models are element-specific and estimate the total number of radioactive decays, or nuclear transformations, within specific tissues, organs, or anatomical regions, referred to as source regions, over a set time frame. Typically, this is 50 years for adults and up to 70 years for children (Paquet et al., 2016; Breustedt et al., 2018). This is achieved by calculating the time-integrated activity within each source region.

The ICRP's approach to biokinetic modelling is compartmental. This means that the body is divided into distinct compartments, or "pools of activity," where radionuclides are exchanged. Each compartment exhibits uniform kinetic behaviour and may represent individual organs, tissues, or organ systems, all of which are aligned with anatomical structures. The movement of radionuclides between these compartments is mathematically described using a system of first-order differential equations derived from a mass balance. Solving these equations enables the prediction of radionuclide behaviour over time in terms of retention and excretion functions.

Retention functions describe how long the radionuclide remains in a given compartment, while excretion functions describe how the radionuclide is eliminated through urine or faeces. Integrating retention functions over time estimates the total number of decays after intake, which serves as a proxy for determining the original level of internal contamination. However, these models must consider various influencing factors, such as the radionuclide’s chemical form, isotopic identity, route of intake, and, for inhalation, particle size. Each of these factors can significantly affect how radionuclides behave within the body (Breustedt et al., 2018).

The ICRP models include inhalation and ingestion pathways for adults and children. Generic models of the alimentary and respiratory tracts describe how radionuclides move through the body after ingestion or inhalation. Ultimately, this leads to their absorption into the bloodstream or elimination from the body. These intake-specific models can be applied to all radionuclides if the correct parameters are selected. Once absorbed, element-specific models describe the behaviour of radionuclides in the systemic circulation by tracking distribution, retention, and excretion. To simulate an intake scenario, the various models are connected through physiological transfer routes. For example, this could be the transfer of a radionuclide from the small intestine to the blood.

Accurate internal dose assessments require determining the biokinetic profile of the radionuclide in question. According to Li (2018), this information is primarily obtained from animal studies and clinical data from individuals who are severely ill, have been accidentally exposed, or are healthy volunteers. The ICRP biokinetic models and the parameters and data sources on which they are based are discussed further in the following sections.

2.1.1 The Human Respiratory Tract Model (HRTM)

The HRTM, developed by ICRP, describes the deposition, clearance, and dosimetry of inhaled radioactive materials in the lungs. The HRTM is essential for calculating dose coefficients resulting from occupational and public exposures through inhalation (ICRP, 1994; Puncher et al., 2008). The HRTM strikes a balance between physiological accuracy and practical usability. It has proven valuable in radiation protection and epidemiological research, particularly in assessing lung doses in nuclear workers exposed to radionuclides such as plutonium and other actinides (Bailey and Puncher, 2007).

The subsequent availability of new experimental findings and critical evaluation of existing datasets led to a revision of the HRTM. The updates refined the representation of particle transport within the bronchial (BB), bronchiolar (BB), and alveolar-interstitial (AI) regions and improved the modelling of deposition and clearance from the extrathoracic (ET) airways (Puncher et al., 2013). The HRTM has three main components: a deposition model that determines where inhaled particles settle, a clearance model that tracks how particles are removed from the respiratory system, and a dissolution/absorption model that describes the solubilization and uptake of particles into the body.

To gain a more comprehensive understanding of the HRTM's structure and function, readers are encouraged to consult ICRP Publications 66 (ICRP, 1994) and 130 (ICRP, 2015), which thoroughly detail the model.

2.1.1.1 Morphometry

The HRTM is divided into two main parts, as shown in Figure 3. The first component represents the ET region, comprising the anterior (ET_1) and posterior (ET_2) nasal passages, as well as anatomical structures such as the larynx, pharynx, and mouth. The second component corresponds to the thoracic (TH) region, which includes the BB, covering airway generations 0 to 8; the bb, covering airway generations 9 to 15; and the AI region, spanning from the first respiratory bronchioles to the alveolar sacs, including the associated interstitial connective tissues starting from generation 16 (ICRP, 2015).

The ET and TH regions are both linked to their respective lymph nodes. The ET region is linked to extrathoracic lymph nodes (LN_{ET}), and the TH region is linked to thoracic lymph nodes (LN_{TH}). Within each respiratory region, target cells are identified. These are the cells most sensitive to radiation and most relevant for dosimetry. For instance, basal cells of the epithelium are target cells in both the ET regions, whereas basal and secretory cells are target cells in the BB epithelium, and secretory cells are target cells in the bb region. Reference tissue dimensions are established to facilitate accurate dose calculations and define the mass of tissue containing these target cells. These reference values are standardized and considered independent of age and sex, ensuring broad applicability in radiation protection modelling (ICRP, 1994, 2015; Bailey and Puncher, 2007).

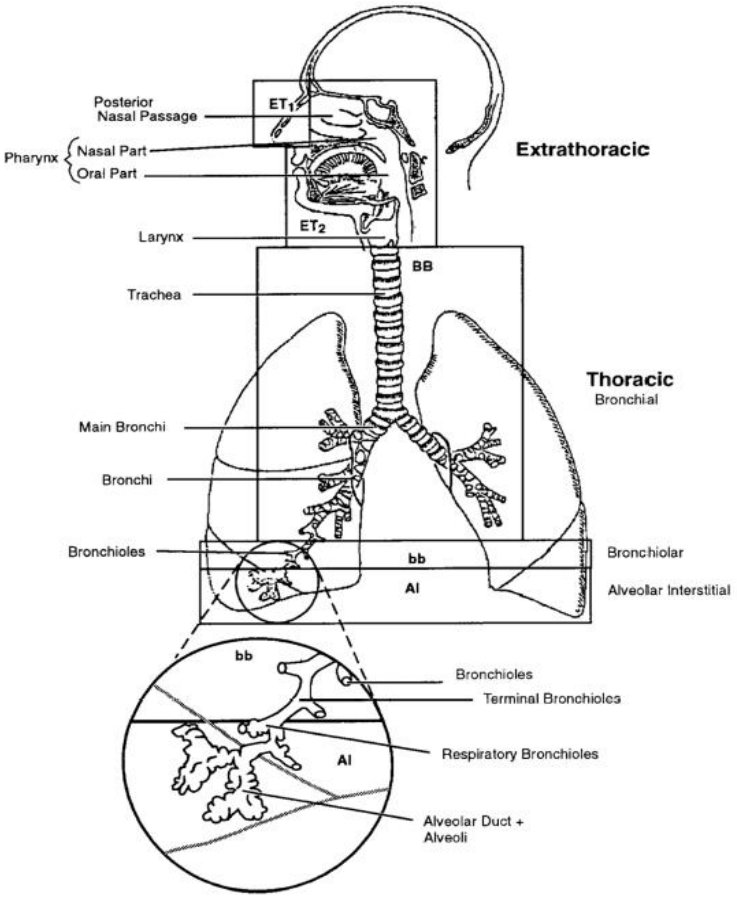

Figure 3: Respiratory tract regions defined in the HRTM (Source: ICRP, 2015)

2.1.1.2 Physiology

The key respiratory parameters considered in the HRTM are the ventilation rate (V_E), measured in cubic meters per hour (m^3/h); the respiratory frequency (f_R), expressed in breaths per minute (min^{-1}); and the tidal volume (V_T), the volume of air inhaled or exhaled per breath, measured in liters. These parameters vary according to an individual's age and level of physical activity (ICRP, 1994; Bailey and Puncher, 2007; Puncher et al., 2008). Additional physiological factors that influence respiratory dynamics include the distribution of inhaled air between the nose and mouth (F_n) and breathing mode (i.e., nasal or oral).

The ICRP (1994), provides reference values for these parameters across four standard levels of physical activity typically encountered in occupational settings: sleeping, sitting, light work, and heavy work. Combining these parameters with data from habit surveys allows for the estimation of reference inhalation quantities per work shift or per day for a given individual. Furthermore, in the context of radon progeny dosimetry, these respiratory parameters are crucial for determining intake per unit exposure, necessary for internal dose assessments (Marsh et al., 2012).

2.1.1.3 Particle Deposition

The deposition of particles in the respiratory tract depends on the physical properties of the aerosols, such as mean size, size distribution, density, and shape factor, as well as subject parameters, such as breathing mode, ventilation rate, and age. Deposition is particularly influenced by particle size. Large particles are represented by their activity median aerodynamic

diameter (AMAD), and smaller particles are represented by their activity median thermodynamic diameter (AMTD). AMAD characterizes aerosols whose deposition is dominated by sedimentation and inertial impaction mechanisms. Fifty percent of the activity is characterized by an equivalent aerodynamic diameter (d_{ae}) greater than the AMAD. d_{ae} is defined as the diameter of a sphere of unit density that has the same settling velocity in air as the particle of interest (Bolch et al., 2001). These aerodynamic effects are important for particle sizes above 0.1 µm and increase with size (ICRP, 1994; Bailey and Puncher, 2007).

When diffusion (Brownian motion) dominates particle deposition, the aerosol is characterized by an AMTD, meaning 50% of the activity is associated with particles larger than the AMTD. The thermodynamic equivalent diameter (d_{th}) describes particle behaviour and is defined as the diameter of a spherical particle with the same diffusion coefficient in air as the particle of interest (Bolch et al., 2001). Diffusion is an important thermodynamic effect for particle sizes below 0.1 µm and increases with decreasing size (ICRP, 1994; Bailey and Puncher, 2007).

The HRTM deposition model evaluates the fraction of activity in the inhaled air that is deposited in each airway region. These regions are treated as successive filters during inhalation and exhalation. The efficiency of each filter is determined by considering competing aerodynamic and thermodynamic processes. This is illustrated in Figure 4 (ICRP, 1994). Values of fractional deposition in each region of the respiratory tract of the reference worker are given in Table 1 for aerosols with an AMAD of 5 µm.

Table 1: Regional deposition of inhaled aerosols with AMAD of 5 µm for a reference worker (Source: ICRP, 2015).

Region	**Deposition (%)**
ET_1	47.94
ET_2	25.82
BB	1.78
Bb	1.10
AI	5.32
Total	81.96

ET_1, anterior nasal passage; ET_2, posterior nasal passage, pharynx and larynx; BB, bronchial; bb, bronchiolar; AI, alveolar-interstitial. The reference worker is assigned parameter values of a healthy, non-smoking, normal breathing adult male at light work. Light work is defined on the following basis i.e., 2.5h sitting with amount inhaled being 0.54 m^3/h and 5.5h light exercise during which the amount inhaled is 1.5 m^3/h. For both levels of activity, all the air inhaled enters through the nose.

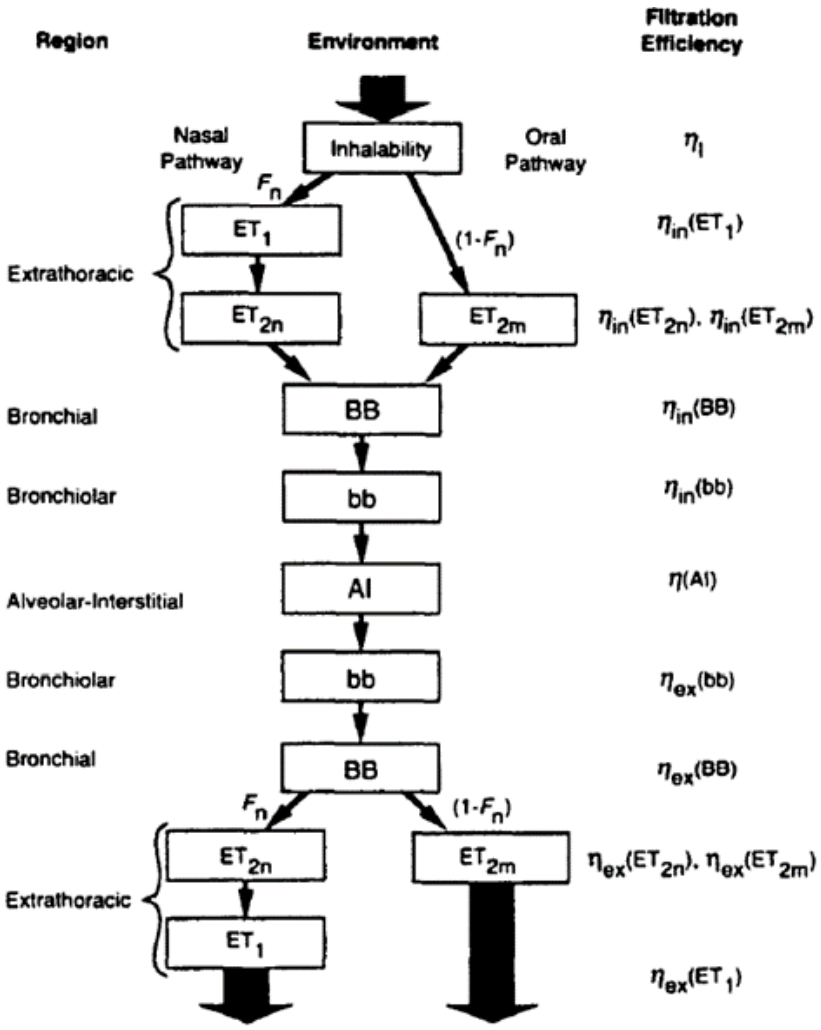

Figure 4: Empirical determination of particle inhalability and deposition in HRTM (Source: ICRP, 1994).

The deposition of inhaled gases depends on their chemical properties rather than their physical properties (ICRP, 2015). However, this is not the case for noble gases, such as radon, where no deposition occurs. When radon gas is inhaled, its activity concentration in the inhaled air is assumed to be in equilibrium with that in the ambient air (ICRP, 2017). Leggett et al. (2013) demonstrated that inhaled radon gas is partially absorbed into the arterial blood, transported to other parts of the body, and then transported back to the respiratory tract via venous blood. There, it is partially exhaled and partially reabsorbed into the arterial blood. This cycle continues until the body burden is depleted through the exchange of pulmonary blood and respiratory air, as well as loss of radon gas in exhaled air.

2.1.1.4 Particle transport

The model structure and the values of the parameters that represent or describe physiological processes are usually assumed to be the same for all elements, even though the latter are expected to vary among individuals within a population. According to the ICRP (2015), mechanical processes remove deposited material from ET_1, which has an eight-hour biological half-life. Approximately two-thirds of the material is transferred to ET_2; the remaining fraction is released into the environment through extrinsic means, such as sneezing and nasal wiping (ICRP, 2015; Hu et al., 2020).

Mucociliary clearance transports the deposited material from all regions of the airways to ET_2. From there, it is transported to the digestive tract, which has a biological half-time of 10 minutes. However, mucociliary clearance is slower in the lower lung region than in the upper lung region. The biological half-times are 230 days from AI to BB, 3.5 days from bb to BB, and 1.7 hours from BB to ET_2. Mechanical transport to the regional lymph nodes occurs from all regions except ET_1. With the exception of the AI region, 0.2% of deposited material is assumed to be transported to lymph nodes, which has a biological half-life of 1.9 years. Within the AI region, the model assumes that one-third of the deposited material is transported to the lymph nodes, with a biological half-life greater than 600 years (ICRP, 2015). Figure 5 shows the HRTM particle transport model.

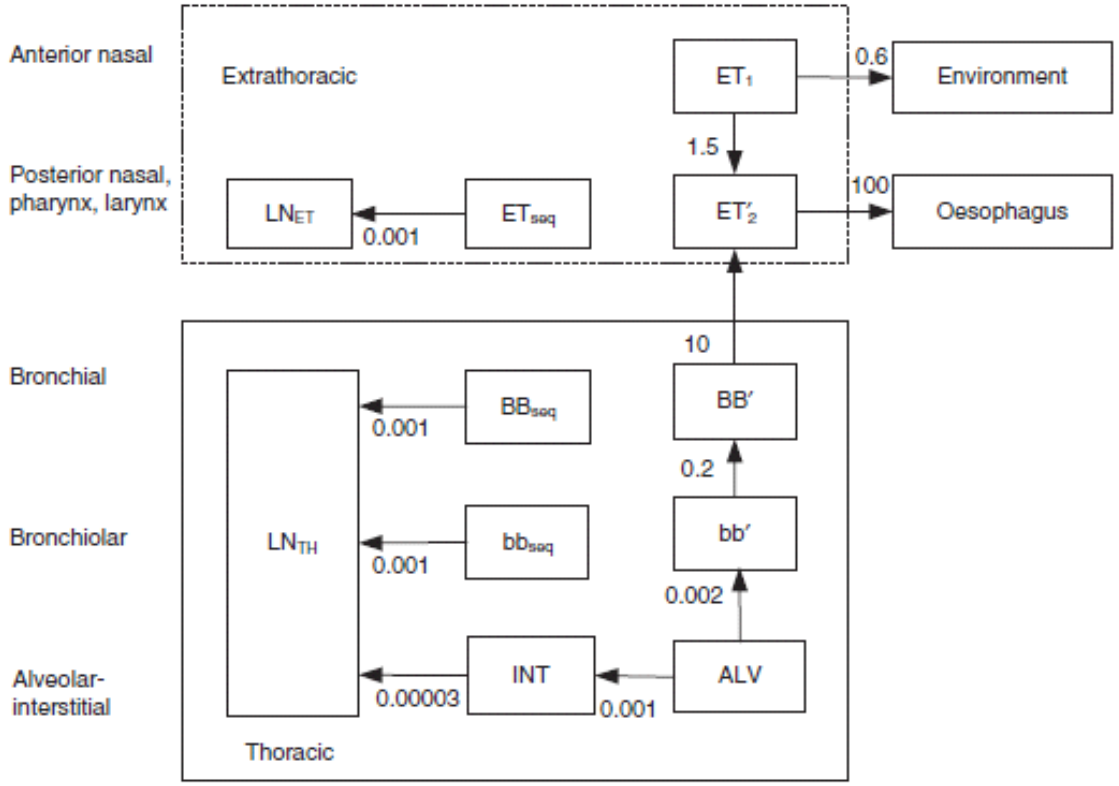

Figure 5: Compartmental model representing HRTM particle transport (Source: ICRP, 2015).

2.1.1.5 Dissolution and absorption

Figure 6 shows the HRTM dissolution/absorption model. The HRTM uses a simple compartmental model to represent time-dependent dissolution. In this model, the absorption of material deposited in ET_2 and the thoracic airways into the blood occurs in two steps. First, the inhaled material dissolves. This process is described by three parameters i.e., the fraction of material that dissolves rapidly (f_r), the dissolution rate of the rapid fraction (s_r), and the dissolution rate of the remaining fraction ($1-f_r$) (s_s). However, note that any time-dependent dissolution behaviour represented by the model in Figure 6a can also be represented by the model in Figure 6b with suitable parameter choices. Therefore, if the dissolution rate decreases over time, as is often the case, either system can be used to produce similar results with equations (2.1–2.3), although the reverse is not true.

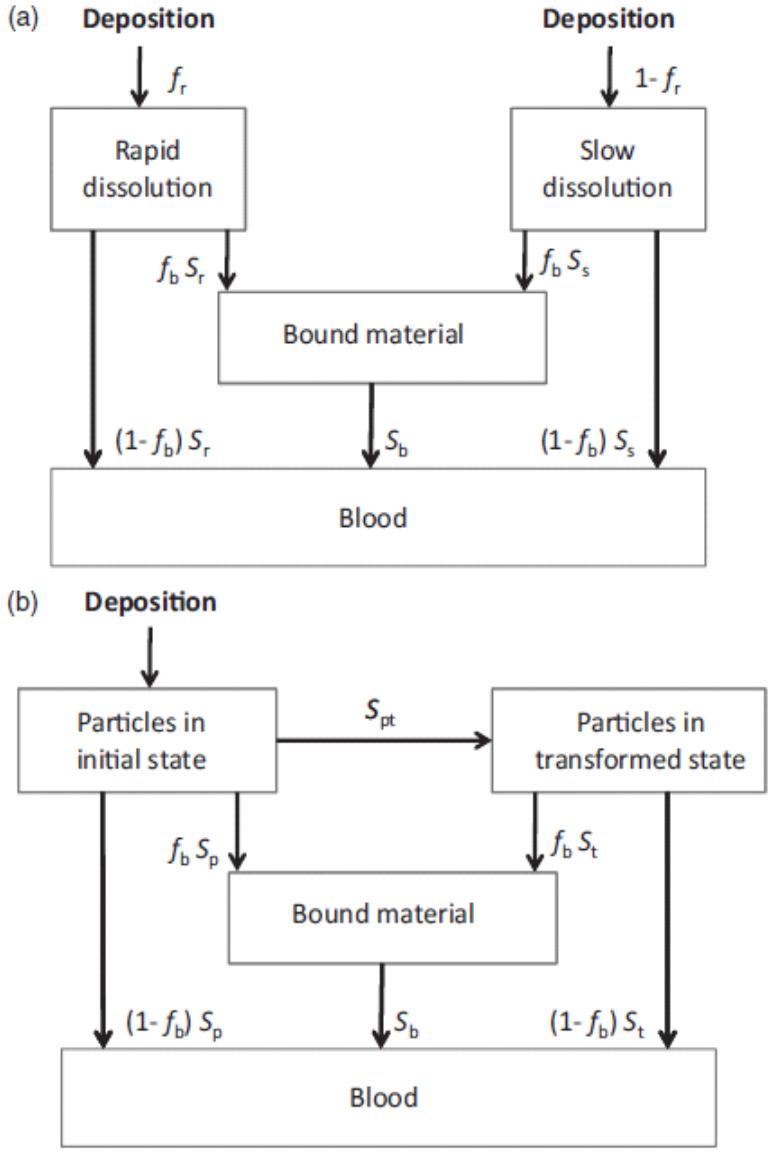

Figure 6: Alternative models representing time-dependent absorption into blood (Source: ICRP, 2015).

The dissolution parameters are assumed to be determined by the physicochemical properties and chemical form of the inhaled material (Hu et al., 2020). Dissolution is then followed by the instantaneous uptake of the dissolved material into the blood unless the dissolved ions of the radionuclide bind to the airway walls. The fraction of material that becomes bound after dissolution is represented by the bound fraction, f_b. Since the ionic form of the radionuclide determines the extent of the bound state, this is assumed to be independent of the chemical form of the inhaled radionuclide. Uptake of material into the blood from the bound state occurs at a rate s_b (Puncher and Burt, 2013; Puncher, 2014a, 2014b).

Absorption into the blood from each region (compartment) of the respiratory tract, except for ET_1 where no absorption is assumed, occurs at the same transfer rate, generally with fast and slow components. Since absorption rates depend on solubility, the ICRP has defined default

rates F, M, and S for fast, moderate, and slow absorption, respectively. The ICRP also provides compound-specific parameters where relevant data are available (ICRP, 2015). Table 2 shows the dissolution/absorption parameters for radon progeny.

Table 2: HRTM dissolution/absorption parameters for radon progeny (Source: ICRP, 2017).

Radon progeny	**Dissolution parameter values**			**Uptake parameter values**		**Absorption from the alimentary tract, f_A**
	f_r	**$s_r(d^{-1})$**	**$s_s(d^{-1})$**	**f_b**	**$s_b(d^{-1})$**	
Polonium	1.00	3.00	0.00	0.00	0.00	0.10
Lead	0.10	100	1.70	0.50	1.70	0.20
Bismuth	1.00	1.00	0.00	0.00	0.00	0.05

2.1.1.6 Dosimetry

For dosimetric purposes, the thoracic airways are divided into three regions: BB, bb, and AI. Lymphatic nodes are also associated with the thoracic airways. However, the dose to the lymphatic nodes can be ignored for radon progeny because almost all progeny decay before reaching the lymphatic nodes (Marsh et al., 2008). Radiosensitive target cells identified in the thoracic region include basal and secretory cells in the BB epithelium, Clara cells (a type of secretory cell) in the bb epithelium, and endothelial cells, such as those in capillary walls, as well as type II epithelial cells in the AI region (ICRP, 1994).

The definition of radiosensitive cells and their depth within tissue is key to understanding the dose received from alpha radiation. According to the ICRP (2015), these cells are distributed throughout the airway (AI) region and regional lymph nodes. In other areas, they are assumed to be within a tissue layer at a certain depth in the airways. In the ET region, the cell layers are assumed to be basal cells at a depth of 40–50 µm. In the BB region, the cell layers are assumed to be secretory cells (10–40 µm) and basal cells (35–50 µm). In the bb region, the cell layers are assumed to be secretory cells (4–12 µm). The dose to the BB region is calculated as the arithmetic mean of the dose values for secretory and basal cells. The dose to the ET region is calculated as the weighted average of the dose values for the nasal passage (ET_1: 0.001) and the oral cavity/larynx (ET_2: 0.999).

The lung dose is calculated as the sum of the dose values for the BB, bb, and AI regions. The doses to the LN_{TH} and LN_{ET} are included in the lymphatic tissue dose calculation (0.08 each). To account for differences in tissue sensitivity, the equivalent dose to each region (H_i) is multiplied by an apportionment factor (A_i), which represents the region's estimated sensitivity relative to the whole organ. The recommended values of A_i are given in Table 3.

Table 3: Target regions of the HRTM (Source: ICRP, 2017)

Tissue	Region	Target cells	Depth of target cell* (µm)	Mass of target region* (kg)		Assigned fraction A_i of *
				Male	Female	
ET	ET_1	Basal	40-50	2.000E-05	1.729E-05	0.001
	ET_2	Basal	40-50	4.500E-04	3.890E-04	0.999
TH	BB	Secretory (BB_{sec})	10-40	8.648E-04	7.771E-04	0.333#
		Basal (BB_{bas})	35-50	4.324E-04	3.885E-04	
	bb	Secretory	4-12	1.949E-03	1.874E-03	0.333
	AI			1.100	0.904	0.333

*Reference values are given with sufficient precision for calculation purposes which may be greater than would be chosen to reflect the certainty with which the average value of each parameter is known. For the BB, bb and AI regions, each value of AI is exactly one-third.

#The dose to BB (H_{BB}) is calculated as the arithmetic mean of the doses to BB_{sec} and BB_{bas}.

The effective dose from inhaling radon is determined primarily by the lung dose received from alpha radiation. This means that radiation and tissue weighting factors are applied directly. A tissue weighting factor of 0.12 is used for the lungs, and a radiation weighting factor of 20 is applied for alpha radiation (Hu et al., 2020). The weighted sum of the equivalent dose, H_i, to each region is the equivalent dose to the ET or TH airways, respectively, as shown in equations 2.4 and 2.5.

$$H_{ET} = H_{ET_1}A_{ET_1} + H_{ET_2}A_{ET_2} \dots\dots\dots\dots\dots (2.4)$$

$$H_{TH} = H_{BB}A_{BB} + H_{bb}A_{bb} + H_{AI}A_{AI} \dots\dots\dots\dots\dots (2.5)$$

Where H_{ET} is the committed equivalent dose coefficient to the ET region (mSv/ (mJh/m^3)),

H_{ET1} is the committed equivalent lung dose coefficient to the ET_1 region (mSv/ (mJh/m^3)), H_{ET2} is the committed equivalent lung dose coefficient to the ET_2 region (mSv/ (mJh/m^3)) and A_{ET1} and A_{ET2} are the apportionment weighting factors for ET_1 and ET_2 respectively.

H_{TH} is the committed equivalent lung dose coefficient for the TH region (mSv/ (mJh/m^3)), H_{BB} is the committed equivalent dose coefficient to BB (mSv/ (mJh/m^3)), H_{bb} is the committed equivalent dose coefficient to bb region (mSv/ (mJh/m^3)), H_{AI} is the committed equivalent dose coefficient to the AI region (mSv/ (mJh/m^3)). A_{BB}, A_{bb} and A_{AI} are the apportionment weighting factors for the BB, bb and AI regions.

2.1.2 The Human Alimentary Tract Model (HATM)

The HATM, presented in ICRP Publication 100 (ICRP, 2006), depicts the entry of a radionuclide into the oral cavity through ingestion or into the oesophagus via particle transport from the respiratory tract. The HATM illustrates the sequential transfer of radionuclides through all regions of the alimentary tract, including the oral cavity, oesophagus, stomach, small intestine, and colon, followed by excretion in faeces (ICRP, 2015).

2.1.2.1 Morphology

As shown in Figure 7, the alimentary tract consists of compartments, including the oral cavity, teeth, oral mucosa, and oesophagus, which is subdivided into two compartments before material is transferred to the stomach, which is also split into two compartments, i.e., contents and wall. The upper and lower large intestines extend to the right and left, as well as to the rectosigmoid part, each with contents and wall compartments. Radionuclides may enter the alimentary canal directly through ingestion or indirectly through inhalation and mucociliary transport of particles from the respiratory tract to the oropharynx and oesophagus. They may also enter through secretions, such as saliva, bile, or gastric juice. Alternatively, radionuclides can be produced in the alimentary canal through the decay of a parent radionuclide (ICRP, 2015).

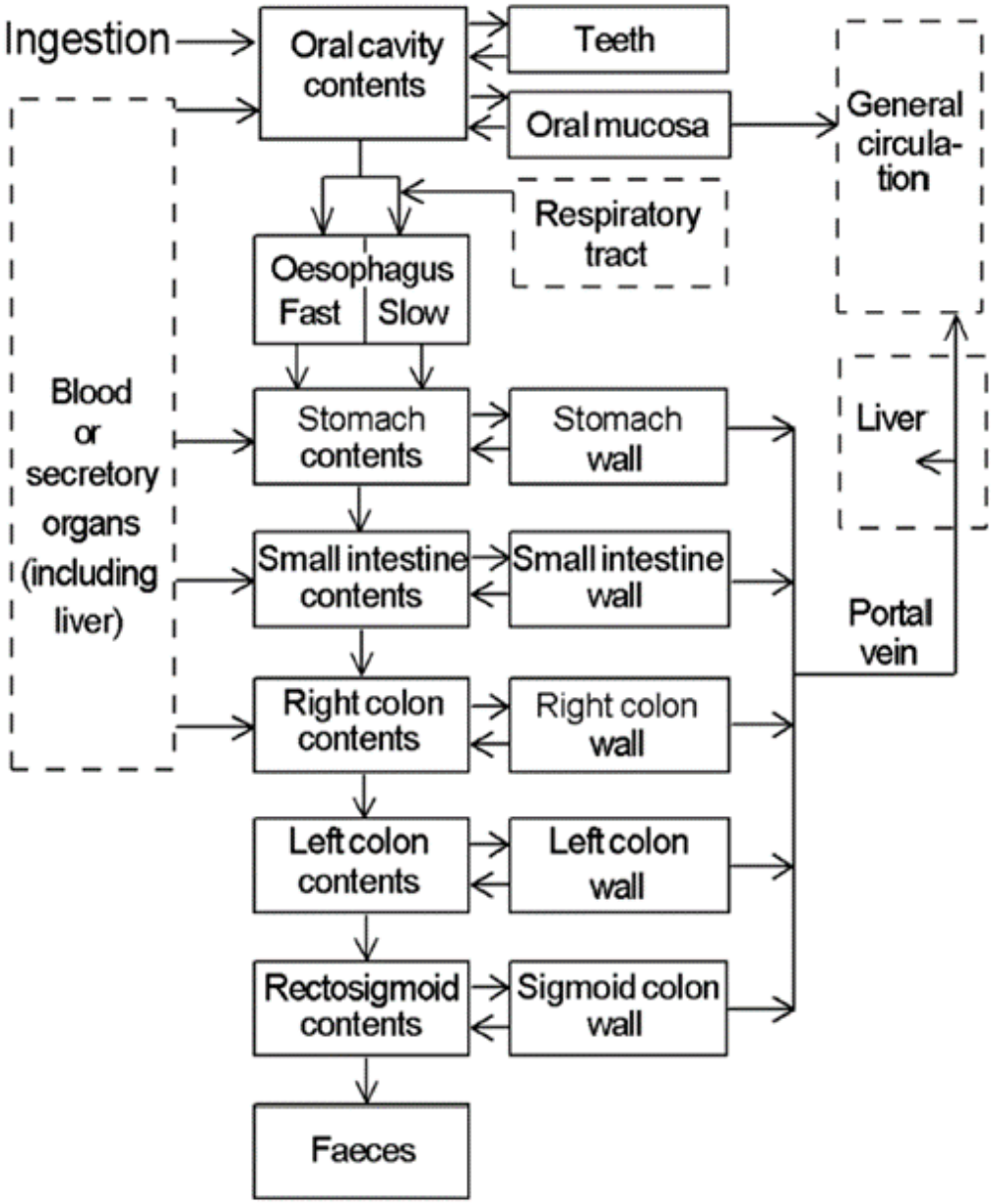

Figure 7: Structure of the HATM (Source: ICRP, 2006).

The dashed boxes are included to show connections between HATM and the HRTM and systemic biokinetic models.

2.1.2.2 Particle transport

Table 4 summarizes the transfer coefficients (per day) for the movement of alimentary tract contents between compartments for a reference worker.

Table 4: Default HATM transfer coefficients for total diet for the reference worker (Source: ICRP, 2015).

From	To	Transfer coefficient (d^{-1})
Oral cavity contents	Oesophagus (fast)	6480
Oral cavity contents	Oesophagus (slow)	720
Oesophagus (fast)	Stomach contents	12343
Oesophagus (slow)	Stomach contents	2160
Stomach contents	Small intestine contents	20.57
Small intestine contents	Right colon contents	6
Right colon contents	Left colon contents	2
Left colon contents	Rectosigmoid contents	2
Rectosigmoid contents	Faeces	2

Source: ICRP, 2015

2.1.2.3 Particle absorption

The HATM specifies the absorption of radionuclides into the blood as a fraction of the amount that enters the alimentary tract. Total absorption is denoted as f_A. The model structure allows the use of absorption data from any region for which data is available, and the default assumption is that all absorption occurs in the small intestine ($f_A = f_{SI}$). The fraction of material absorbed from the HATM into the bloodstream is the most important HATM parameter and is calculated using equation 2.6. The extent to which radionuclides are absorbed depends on the element and its chemical form (ICRP, 2006). Changes in chemical form are likely to occur during digestion, beginning in the mouth and primarily occurring in the stomach and small intestine. These changes determine the radionuclide's availability for absorption and, consequently, the extent of its uptake through the intestinal epithelium into the bloodstream. However, if transfer data from the alimentary tract regions is available, it should be used in biokinetic modelling.

$$\lambda_{SI,Blood} = \frac{f_A . \lambda_{SI,RC}}{1 - f_A} \dots\dots\dots (2.6)$$

Where $\lambda_{SI,Blood}$ is the transfer rate from small intestine contents to blood (d^{-1}) and $\lambda_{SI,RC}$ is the transfer rate from small intestine to the right colon contents (d^{-1}).

2.1.2.4 Dosimetry

The HATM enables the explicit calculation of the dose to target regions for cancer induction within each region of the alimentary tract, taking into account the doses from radionuclides in the region's contents and the mucosal retention of radionuclides, when appropriate.

The oesophagus and oral cavity receive very low doses from ingested radionuclides due to their short transit times in these regions (ICRP, 2006). However, they are included because a specific tissue weighting factor is assigned to the oesophagus, and retention in the mouth and on teeth, for example, can result in a significant increase in dose to the oral mucosa (ICRP, 2007). The regions of the alimentary tract that are generally more important in dose assessment and cancer risk are the stomach and colon (ICRP, 2006). Although the small intestine may receive higher doses than the stomach, it is not sensitive to radiation-induced cancer. Therefore, it is not

assigned a specific tissue weighting factor and is considered part of the organs and tissues that constitute the remainder (ICRP, 2007).

The location of sensitive cells in the different regions of the tract is modelled explicitly in the HATM (ICRP, 2006; Leggett et al., 2007). The targets for all effects are the epithelial stem cells, which are located some distance from the tract's lumen. The assigned depths of target cells in adult males are given in Table 5.

Table 5: Target cell depths and masses for each target region of the HATM for adult males (Source: Leggett et al., 2007).

Region	Target cell depth (µm)	Target cell mass (g)
Oral cavity	190-200	0.23
Oesophagus	190-200	0.091
Stomach	60-100	0.62
Small intestine	130-150	3.6
Right colon	280-300	1.3
Left colon	280-300	1.2
Rectosigmoid colon	280-300	0.73

Source: Leggett et al., 2007

2.1.3 Systemic models

Systemic biokinetic models describe the transfer and retention of radionuclides through the blood to internal organs and tissues. A systemic biokinetic model is developed for each element based on available human data from environmental, accidental, or medical exposure, as well as animal experiments. These models range in complexity from those that assume entire-body distribution, as in the case of hydrogen and caesium, to multi-compartment recycling models that consider movement within and between organs and tissues, as in the case of plutonium, lead, uranium, and strontium (ICRP, 1989; Harrison and Day, 2008).

The most complex models are those developed for bone-seeking alkaline earth and actinide elements, such as strontium, plutonium, radium, and thorium. These models represent the behaviour of these elements within bone by considering initial deposition on bone surfaces, exchange with or burial within bone material, and movement to bone marrow (Harrison and Day, 2008). Figures 8 and 9 show the model structures for actinides and bone-seeking alkaline earth elements, respectively. According to the ICRP (2015), the main difference between these two model structures is that the compartments representing bone marrow and gonads are omitted from the model structure for bone volume seekers since these elements do not accumulate in high concentrations in these sites.

The principle of building a systemic biokinetic model is to create a compartment that represents an organ or tissue region. Sometimes, several compartments are used for one organ or tissue region if the activity of the subregion is available. The connection of the organ or tissue to the blood is based on human physiology. A compartment called "soft tissues" or "other" represents activity not distributed to a specific organ or tissue. This compartment comprises all organs not explicitly included in the biokinetic model (Li, 2018). A central compartment representing blood/plasma is often included in the systemic biokinetic model. Depending on the nuclide, this compartment may include a sub-compartment representing red blood cells or a sub-compartment representing the process by which the nuclide bound to a protein in the blood (Li, 2018).

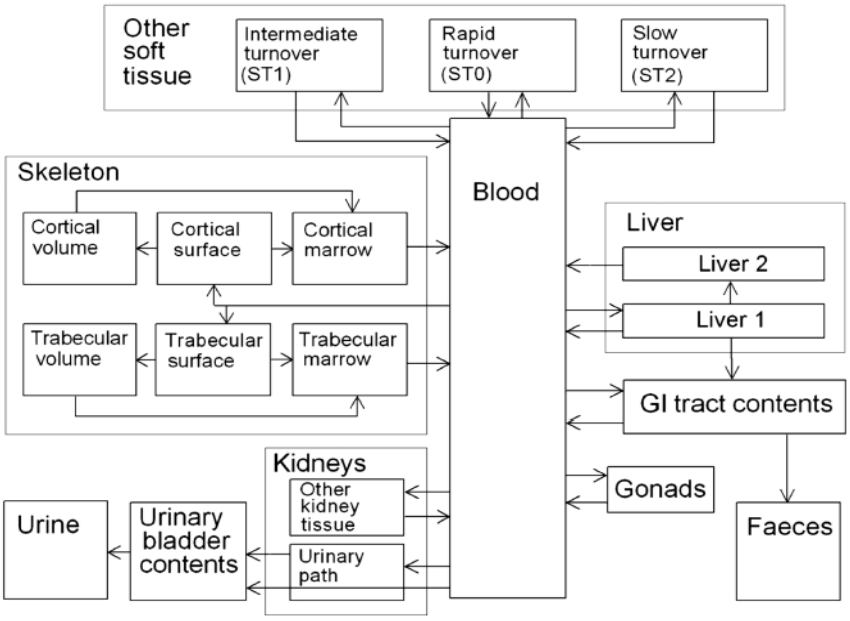

Figure 8: Biokinetic model structure for actinide elements (Source: ICRP, 2015).

The soft tissues merge into one compartment, or sometimes three sub-compartments: rapid turnover (ST0), intermediate turnover (ST1), and slow turnover (ST2). These are connected to the blood compartment. For many nuclides, certain organs are explicitly represented in a systemic model, e.g., the brain, heart, pancreas, spleen, and lungs. Organs or tissues not explicitly represented in the model are assumed to be part of the soft tissue compartment (ST0, ST1, and ST2). For bone-seeking nuclides, a skeleton compartment is usually connected to the blood. In the skeleton compartment, six sub compartments are typically assumed: cortical and trabecular surface, cortical and trabecular deep, and cortical and trabecular shallow (Li, 2018).

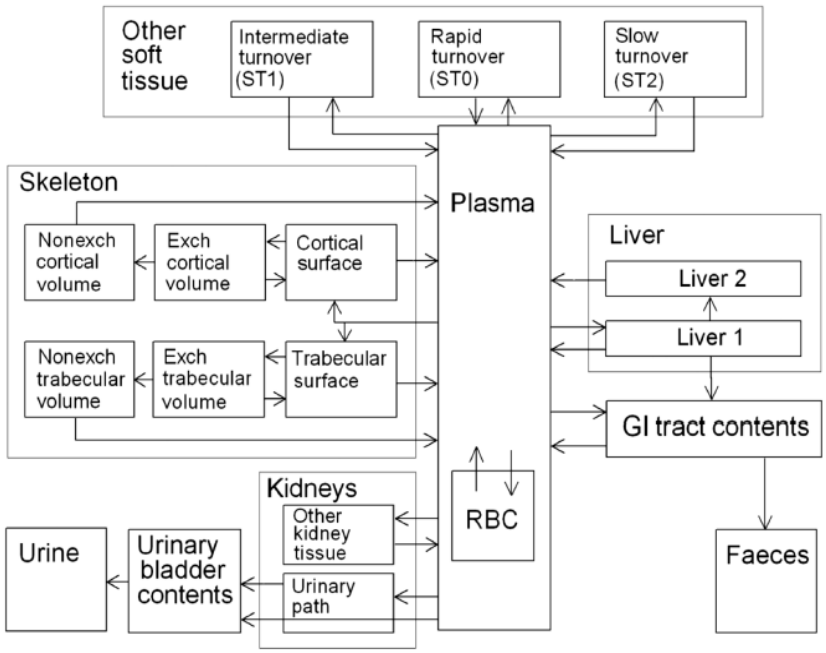

Figure 9: Biokinetic model structure for alkaline earth elements (Source: ICRP, 2015).

For most nuclides, compartments 1 and 2 of the liver are used to model materials transferred through the liver to the alimentary tract (biliary pathway), which are then excreted from the

body through faeces. Through this excretory pathway, radionuclides can be transferred directly from the blood to the intestinal wall and excreted in faeces. The mechanism of urine formation and excretion, as well as its compartmental model, is generally part of the systemic biokinetic model. The urinary excretion model includes a compartment of kidney tissue for nuclide exchange with the blood and a urinary pathway that serves as a nuclide pathway to the urinary bladder.

2.2 ICRP methodology for internal dose assessment

The term "internal dosimetry" is often used for incorporated radionuclides. It refers to the scientific methodology of measuring, calculating, estimating, assaying, predicting, and quantifying the radiation energy absorbed by the ionization and excitation of atoms in human tissues due to the emission of energetic radiation by internally deposited radionuclides (Li, 2018). Internal dosimetry mainly covers workplace exposure control, medical intervention, and compliance with existing standards and regulations.

To assess dose, biokinetic models are first used to model the distribution of accumulated radioactivity in different organs and tissues. The retention of radionuclides in organs is driven by physiological processes and depends on the element and its chemical form (ICRP, 2009; 2017). The main assumption is that ICRP models use a compartmental approach, dividing the body into several activity pools (compartments) that exchange activity. These pools can represent organs, tissues, or groups of organs linked to anatomical structures (Breustedt et al., 2018). The ICRP also assumes that material entering a given pool is immediately available for transport to another pool. To implement the system, a set of first-order ordinary differential equations (ODEs) describing the activity content in the compartments can be derived by performing a mass balance on each compartment. Equation (2.7) describes the general form of the rate of change of activity of a radionuclide in a compartment.

$$\frac{dA_i(t)}{dt} = \sum_r k_{ri}A_r(t) - \sum_j k_{ij}A_i(t) - \lambda A_i(t) + b_i(t) \dots\dots\dots\dots (2.7)$$

Where A_i is the retention in compartment i, k_{ij} is the transfer coefficient of material from compartment i to compartment j (the first term represents the input to the compartment i from the rest of compartments and the second term represents the output from the compartment i to other compartments). λ is the physical decay constant and $b_i(t)$ is the input from outside the system.

Breustedt et al. (2025) describe this compartmental system as a network of interconnected pools, and the system of differential equations representing the mass balances of all the pools constitutes the mathematical model. To facilitate the modelling process, ICRP (2015) recommends a linear, first-order kinetics approach. This approach allows the kinetics of transfer between pools/compartments to be described using a reference rate, known as a transfer coefficient. The transfer between pools is set to be directly proportional to the amount of material in the pool. This approach provides the opportunity to describe a biokinetic model as a matrix of transfer coefficients and a vector of compartment contents. Compartments connected by a flow of material are assigned positive values in the matrix element [from, to],

while the other elements are assigned zero. The compartment vector provides the contents of the compartments at a given time, t.

The compartments in the model can be interpreted as different states of the nuclide in the body. These states can be a pool in part of an organ, the whole organ, or distributed over multiple organs (soft tissues). For dose calculations, each compartment of the biokinetic model must be associated with the corresponding dosimetric source region to allocate decays to anatomical regions in the body. Radioactive decay can be added as an additional loss to the environment for single radionuclides or to a compartment of the biokinetic model for corresponding progeny during the implementation of decay chains. This is given a transfer rate (d^{-1}), which is calculated from the radioactive half-life of the radionuclide.

This set of differential equations can be solved using an ODE solver and numerical techniques. For a unit intake of activity, the initial conditions for inhalation are determined from ICRP (2015) (see Table 1). For ingestion and injection, the entire input can be introduced to the oral cavity and blood, respectively. Solving the biokinetic model yields bioassay functions (i.e., retention and excretion functions), and the integral of these functions over time gives the number of decays in the source regions. The number of decays that occur in the source regions (r_s) during the commitment period (18,250 days for adults) can be calculated using equation 2.8.

$$\acute{A}(r_s) = \sum_i \int_0^{18250} A_i(t)dt \ldots\ldots\ldots\ldots\ldots (2.8)$$

Where 18250 days represents the commitment period for an adult. The summation in equation (2.8) above is over the association of compartments i forming source region r_s. The number of decays per activity intake in the source region r_s is also given by equation (2.9).

$$\acute{a}(r_s) = \frac{\acute{A}(r_s)}{\sum_i A_i(0)} \ldots\ldots\ldots\ldots\ldots\ldots\ldots\ldots\ldots (2.9)$$

Where A_i (0) represents the initial deposition fraction for each compartment.

To model the decay chains of NORM, each compartment is linked through the decay chain of the parent nuclide to the corresponding compartment of the next progeny. Since the biokinetics of the progeny are independent of the parent nuclide's biokinetics, the model structures and transfer coefficients of the progeny are not necessarily identical to those of the parent. The approach used in ICRP Publication 71 (ICRP, 1995) is employed, whereby biokinetic parameters are assigned to source regions in the chain that are not included in the member's biokinetic behaviour. Unidentified source regions in the member's biokinetic data are assigned the biokinetics of "other" with transfer rates into compartments based on a mass fraction of the transfer rate from blood to corresponding "other" compartments. The transfer rates from blood to the "other" compartments can be reduced to maintain the system's total mass balance. The removal rates of the "other" compartments are assigned to the corresponding source region compartments. Then, the number of decays is computed.

To calculate the dose coefficients, multiply the number of decays in the source regions, calculated using the biokinetic model, by the corresponding S-Coefficient. An S-coefficient

represents the dose in the target tissue per decay in the source region. These values must be calculated for each combination of source region and target tissue using the radiation type and yield from the radionuclide's decay data (e.g., ICRP, 2008) and the specific absorbed fractions (e.g., ICRP, 2016). The general form of the S-coefficient is given by equation (2.10).

$$S_w(r_T \leftarrow r_s) = \sum_R w_R \sum_i E_{R,i} Y_{R,i} \Phi(r_T \leftarrow r_s, E_{R,i}) \dots\dots\dots\dots\dots\dots (2.10)$$

Where w_R is the radiation weighting factor for radiation type R (ICRP, 2007). E_{Ri}, is the energy of the i^{th} radiation of type R emitted in the nuclear transformations of the radionuclide (J); Y_{Ri}, is the yield of the i^{th} radiation of type R per nuclear transformation (/Bqs) (ICRP, 2008); $\emptyset(r_T \leftarrow r_s, E_{R,i})$ is the specific absorbed fraction denoted as SAF (kg^{-1}) (ICRP, 2016). For the compartment other tissues in the biokinetic models, the SAF is calculated using equation (2.11).

$$\Phi(r_T \leftarrow Other) = \frac{1}{M_{other}} \sum_{rs} M_{rs} \Phi(r_T \leftarrow r_s) \dots\dots\dots\dots\dots\dots\dots\dots (2.11)$$

The methods and SAF described in ICRP Publication 133 (ICRP, 2016) can be used to calculate S-coefficients. The contribution of a source region to the dose of a target tissue is calculated by multiplying the number of decays by the corresponding S-coefficient. The dose to the target tissue is then calculated as the sum of the contributions from all source regions. The committed equivalent doses in the target region for reference adult males and females are calculated using equations 2.12 and 2.13, respectively (ICRP, 2015, 2016).

$$h^M(r_T) = \sum_{rs} \acute{a}(r_s) S_w^M(r_T \leftarrow r_s) \dots\dots\dots\dots\dots\dots (2.12)$$

$$h^F(r_T) = \sum_{rs} a(r_s) S_W^F(r_T \leftarrow r_s) \dots\dots\dots\dots\dots\dots\dots (2.13)$$

Where $S_w^M(r_T \leftarrow r_s)$ and $S_w^F(r_T \leftarrow r_s)$ are the S-Coefficients for adult male and adult female respectively. For target tissues that are comprised of several target regions, there is an associated fractional weighting factor given by ICRP. The committed equivalent dose for those regions is calculated following recommendations from ICRP Publications 130 (ICRP, 2015) and 133 (ICRP, 2016). The committed equivalent dose for those regions is calculated using equation (2.14) and equation (2.15) for adult male and adult female respectively.

$$h_T^M = \sum_{rT} f(r_T.T) h^M(r_T) \dots\dots\dots\dots\dots\dots\dots\dots (2.14)$$

$$h_T^F = \sum_{rT} f(r_T.T) h^F(r_T) \dots\dots\dots\dots\dots\dots\dots\dots (2.15)$$

Where $f(r_T.T)$ is the regional fractional weight. These values are taken from ICRP (2016). The committed effective dose coefficient can be calculated as a product of the summation of tissue

weighting factors and the average of the adult male and female committed equivalent dose coefficients, see equation (2.16). Figure 10, (taken from Li, 2018), gives a summary of the ICRP methodology used in internal dose assessment for the different intake modes of radionuclides into the human body.

$$e(50) = \sum_{T} w_T \left(\frac{h_T^M + h_T^F}{2} \right) \ldots\ldots\ldots\ldots\ldots\ldots (2.16)$$

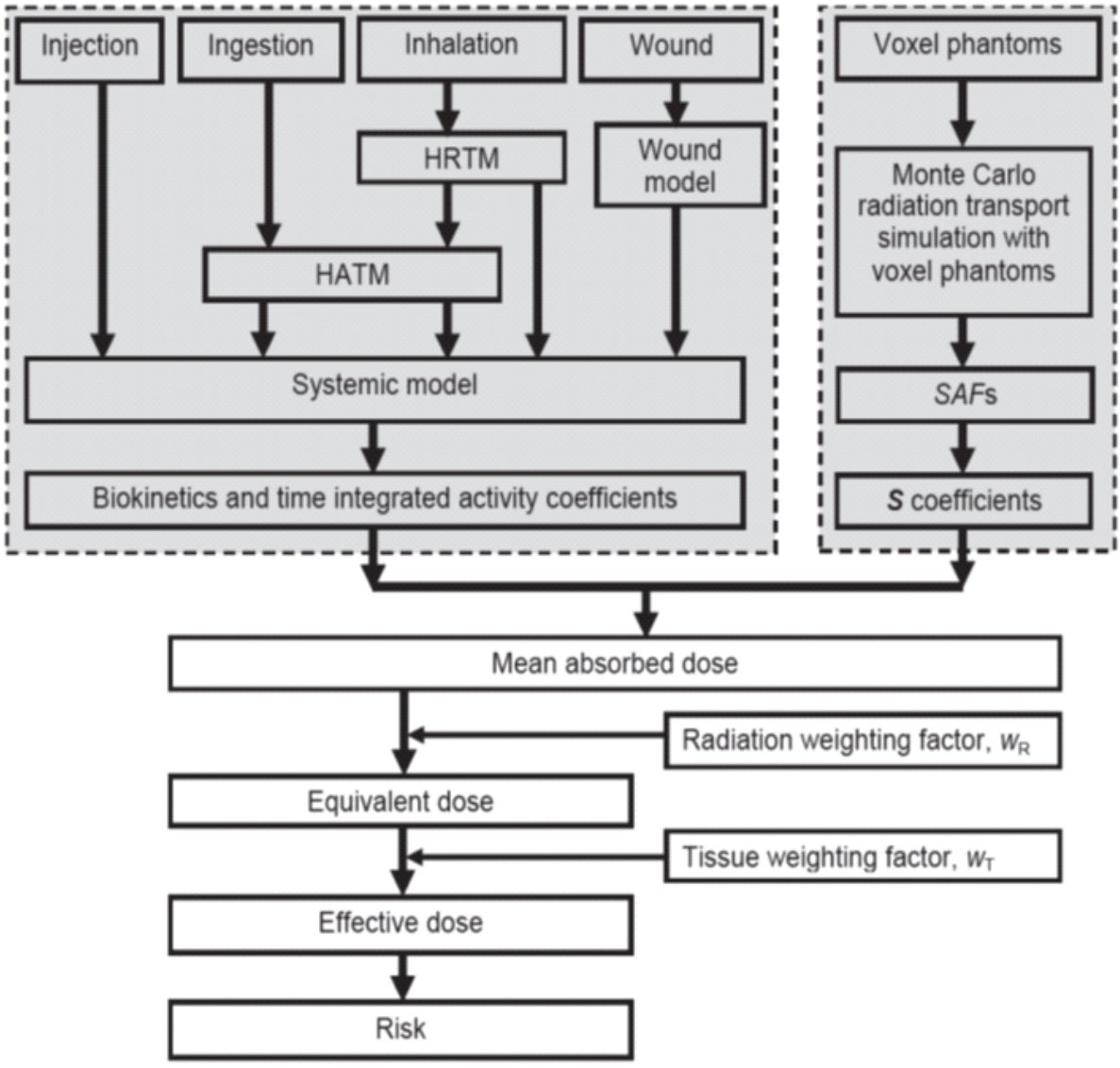

Figure 10: ICRP methodology for internal dose assessment (Source: Li, 2018).

2.2.1 Development of software for internal dose assessment (INTDOSKIT)

The software used for this study, INTDOSKIT, was developed with the R programming language and R Studio as the integrated development environment (Posit, 2023). R was chosen for this study because of its excellent performance in statistical computations. Second, R is open source with a vast number of packages for various computational tasks. Additionally, R is highly compatible with many other popular programming languages, such as C, C++, Java, Python, and FORTRAN, and can be used to produce efficient code. Furthermore, R allows for

the use of compartment names instead of indices to access individual elements of arrays and matrices, enhancing its human readability and avoiding mistakes resulting from the use of incorrect indices. Lastly, R is a proven, reliable language that has already been used in dosimetry applications (Lamart, 2007; Hernández, 2023).

The main idea behind INTDOSKIT is that it is designed to import all biokinetics and dosimetry information from plain text input files. This makes it possible to handle any radionuclide without modifying the source code, in addition to minimizing the size of the source program. It should be noted that INTDOSKIT consists of four major libraries: 1) the deposition model functions library, which is an R-file that calculates deposition fractions in different respiratory tract regions of the HRTM after inhaling radioactive aerosols; 2) the biokinetic functions library, which is an R-file containing functions that read and solve a biokinetic model to determine retention and excretion of activity in compartments over time, as well as calculate the number of decays in ICRP source regions; 3) the dosimetric functions library which is an R-file containing functions for calculating S-coefficients, effective dose, and doses to ICRP target and radiosensitive tissues. The fourth library contains useful constants, such as radiation and tissue weighting factors, unit conversion factors, a list of source and target organs, and recommended time steps for calculating retention and excretion curves. These libraries are sourced at the beginning of dose calculations, so the required functions can be called during program execution instead of being hard coded in the main program.

Templates of R scripts for common tasks were developed, and the INTDOSKIT documentation (Breustedt et al., 2025) provides guidance on their use. All code files are extensively commented to help users understand and modify the functions according to their needs. Plain text files in a defined format are used to describe models and to import and export data (e.g., SAF values for calculating S-coefficients). Functions for reading these files and exporting calculation results are also provided. The latter allows to produce comma-separated values (.csv) files that can be imported into spreadsheet applications, such as Microsoft Excel, for further processing. Interested readers can find more information about INTDOSKIT in Breustedt et al. (2025). Figure 11 provides an overview of the ICRP methodology steps for calculating dose coefficients as implemented in INTDOSKIT.

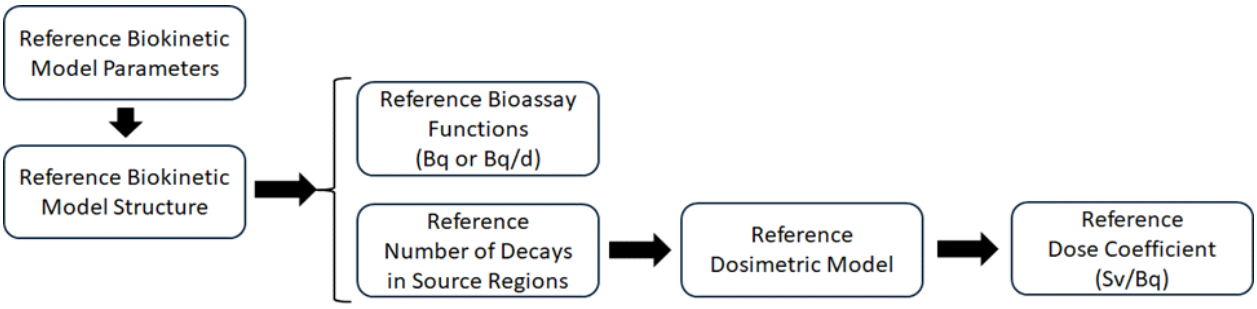

Figure 11: Flow diagram that depicts the implementation of the ICRP methodology in INTDOSKIT.

2.2.2 Biokinetic and dosimetric modelling for the inhalation of radon and long-lived radionuclides in underground uranium mines using INTDOSKIT.

The models for radon progeny isotopes i.e., Po, Pb and Bi were taken from ICRP publication 137 (systemic), ICRP publication 130 (HRTM) and ICRP publication 100 (HATM). During the dose calculation, the first step done was to set up a working directory from which the required

data from files could be read. This was accomplished using the inbuilt R-function setwd(). This function takes as argument the directory path on the computer. Next, the INTDOSKIT libraries i.e., biokinetic functions, dosecalc functions, const-and-lists functions and deposition_model functions were sourced into the main program using another inbuilt R-function source(); this function requires four arguments i.e., the path to the script to be sourced and three Boolean variables i.e., local, echo and verbose. During sourcing of the R-scripts containing the libraries these Boolean variables were set to TRUE, FALSE and FALSE respectively. Another user defined library "Dissolution_parameters_Rn_progeny.r" was also prepared and sourced into the main program. This library contains useful data about radon progeny that is required in the dose calculations; this data includes data on radon progeny dissolution/absorption parameters, dose conversion factors, equilibrium factor, unattached fraction, breathing rate of reference worker and activity concentrations of both attached and unattached radon progeny particles. Additionally, another in built library "readr" was imported during dose calculations. This library contains functions that provide a fast and reliable way to read tabular data into the program.

The biokinetic model definitions were prepared in text files that were imported in the according R-scripts. In these text files for model definitions, the first line represented the number of compartments for the biokinetic model, the second line contained the compartment names, the third line contained the names of the dosimetric source regions while subsequent lines contained information about the transfer of material from one compartment to the other and where necessary information about the probability distribution for the parameter (transfer coefficient).

This was followed by loading the model definitions into the RStudio environment to build a list of models. The systemic models of the parent and progeny radionuclides were loaded using the user defined read_model () function. The argument to this function is the file path containing the model definition. The generic ICRP model definitions for the HRTM and HATM were also read using the same function after which the models were coupled together using another user defined function connect_models (). The connect_models () accept two objects containing the model definitions that are to be connected and merges them to produce one bigger model. This process was repeated for all the radioactive isotopes in the chain and a vector of models was created and stored in the object listmodels using the built-in concatenate (c()) function of R.

The next step was to load connector files and build a list of connectors that served to link the decays occurring in the compartments of the parent model to those of the corresponding progeny model. This was accomplished using three functions in R i.e., the file() that takes as argument the file containing the linking of the compartments of the parent to those of the progeny, the readLines() that takes as argument the variable containing the connector file and reads its contents line by line and the close() function to close the file after the data has been read from it. The above steps were done for all subsequent progeny nuclides in the chain and a vector of connectors built and stored in the object listconnectors using the c() function of R. Following this step, was the building of a numeric vector of decay constants for the parent and progeny nuclides and a character vector of nuclide names which was made possible with the c() of R and stored in the objects listlambdas and listnames respectively.

Having accomplished this, the next step was to build a chain using the user defined decaychain(). This function takes as arguments the objects listmodels, listlambdas, listnames and listconnectors to form a decaychain. The decays of the last radioactive nuclide in the chain to the stable isotope were added to this chain using the add_decay2stable() that takes as arguments the chain of radioactive nuclides, the name of the last radioactive nuclide, its decay constant and the branching ratio to create a new chain object.

Following this, the next step was to create the initial state vector for the compartment contents at time t=0. This vector was created and its components initialized to zero using the inbuilt

function rep() of RStudio. This function took as arguments the integer value 0 and the length of the compartment names vector from the object chain as its arguments. The data in this vector were assigned to the variable q_0. Another built in function names() was used to assign the compartment names for the chain to the corresponding elements in the q_0 vector.

Upon accomplishing this, the text file that contains reference ICRP deposition fractions in the different HRTM regions was sourced to assign the reference deposition fractions to the various HRTM regions. The time steps for the desired solution were also assigned to the object obs. The next step was to solve the system using the solve_chain() that takes as arguments the chain, the vector, q_0 and the object of time steps obs. The solution was assigned to another object schain.

Lastly, was the assignment of the number of decays to the ICRP dosimetric source regions using the NDECin_ICRPSources(). This function takes as arguments the number of decays as given by the schain object, the element bio2dos from the schain object and the Boolean variable verbose that was set to FALSE as parameters. The names() were then used to assign the nuclide names to the decays in the compartments. This was followed by the reading of the S-Coefficients from their respective CSV files using the function Read_SMatrix(), followed by dose calculations. First the doses were initialized to 0 and for each nuclide in the schain object, the calc_doses() was used to calculate the doses. This function takes the number of decays as well as the male and female S-Coefficients as its arguments and outputs the equivalent dose coefficients (Sv/Bq) to the male and female target tissues and the sex averaged effective dose coefficient (Sv/Bq). In this work, the ICRP approach for calculating doses to reference workers was closely followed.

Figure 12 shows the basic workflow for setting up and solving a biokinetic model, the respective INTDOSKIT functions that were implemented in the biokinetic functions library are also indicated on the right side of each box.

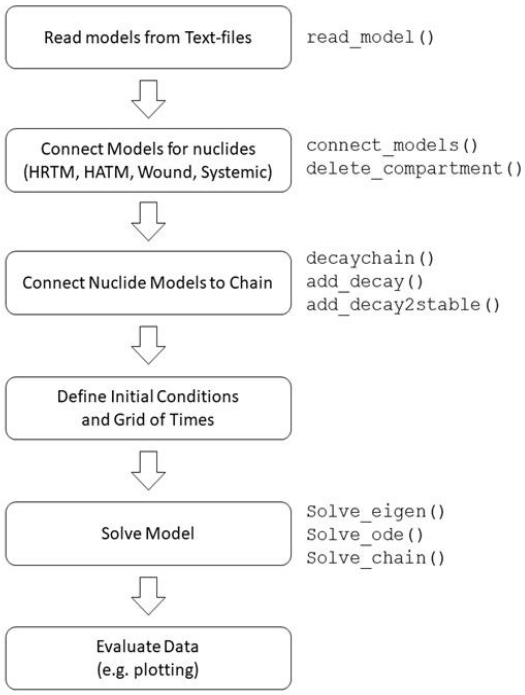

Figure 12: Workflow for the implementation and solution of a biokinetic model using INTDOSKIT (Source: Breustedt et al., 2025).

To calculate the radiation weighted S-Coefficients, the SAF values from ICRP publication 133 for the reference male and female phantoms were read from their respective electronic files using the INTDOSKIT function read_SAF(); this data was stored in the variables SAF_AM and SAF_AF for the adult male and adult female reference phantoms respectively. The function read_SAF() takes as argument the names of the files with SAF for alpha, electrons and photons, the masses of the source and target organs for the reference male and female phantoms, the number of source and target regions, the vector of names for the ICRP source and target regions and the adult male and female reference phantoms. The next step was to read the nuclear decay data for the nuclides that was taken from ICRP publication 107 (ICRP, 2008). This data is available in electronic form in the DECDATA software of ICRP. The INTDOSKIT function read_nuclide() was used to read this data into the RStudio environment. This function requires three arguments i.e., the radiation file name, the beta file name and the isotope name. The nuclear decay data for each nuclide was stored in the variable that was given the name of the respective nuclide. This was followed by building a vector of the list of candidate organs and tissues to be included in the soft tissues for both adult male and female. The inbuilt R function c() was used to accomplish this task. The vector containing the names of candidate organs to be included in the soft tissues was assigned to the variables OT_Inh_AM and OT_Inh_AF for the male and female reference phantoms respectively.

Having accomplished this, the S-Coefficients for both male and female reference computational phantoms were then calculated using the INTDOSKIT function SCoeff_calc_List_OT(). This function requires four arguments i.e., the SAF, the nuclide data, the object of candidates to be include in the soft tissues and a Boolean variable verbose that was set to FALSE. Upon calculation of the S-Coefficients, they were saved in the objects SMaleI and SFemaleI for adult male and adult female values respectively. For permanent storage of the S-Coefficients, this data was saved in files with a CSV format where they can be retrieved and reused in future calculations. This was done with the help of the INTDOSKIT function Save_SMatrix(). This function requires two arguments i.e., the object that contains the calculated S-Coefficients and the file path to which the calculated values can be stored.

For inhalation of radon progeny, the above steps were repeated to calculate dose coefficients for the inhalation of unattached and attached polonium and lead progeny as well as the attached polonium, lead and bismuth progeny particles. The total dose resulting from the inhalation of unattached radon progeny was calculated as the sum of doses from the unattached polonium and lead progeny particles while that from the inhalation of attached radon progeny was calculated as the total dose from the inhalation of attached polonium, lead and bismuth progeny. Finally, the dose resulting from the inhalation of radon progeny was calculated as the sum of doses from the unattached and attached progeny particles.

Since the dose to the lungs from the inhalation of radon progeny mainly comes from alpha particles emitted during their decay, the historical quantity potential alpha energy concentration (PAEC) of the radon progeny mixture is used as a measure of concentration that was an indicator of dose and risk. The historical unit of PAEC that was used in the mining industry is the working level month (WLM), which is defined as the cumulative exposure from breathing an atmosphere at a concentration of 1 working level for a working month of 170 h. A working level in this context is defined as any combination of (short-lived) radon progeny activity that results in the emission of 1.30E+08 MeV of alpha energy i.e., a PAEC of 1.30E+08 MeV/m^3 (ICRP 2017). Therefore, for consistency, it was required to convert the dose to the units the mining industry is accustomed to i.e., from Sv/Bq to mSv/WLM and for comparison purposes with ICRP data, it was necessary to convert the dose to the SI units which are mSv/(mJh/m^3). The conversion was done by using equation (2.17) that relates dose to intake as follows.

$$I_i = C_i . B . t \ldots\ldots\ldots\ldots\ldots\ldots\ldots\ldots (2.17)$$

Where I_i is the intake of activity of the radon progeny for a subject exposed to 1 WL (Bq); C_i is the activity concentration of radon progeny radionuclide i corresponding to a radon progeny mixture of 1 WL (Bq/m^3); B is the breathing rate of exposed subject (m^3/h) and t is the exposure period (h).

$$1\ \text{WLM} = 3.54\ \text{mJh/m}^3$$

The effective dose per WLM from the inhalation of short-lived radon progeny is calculated by combining the intakes, I_i with the effective dose coefficients (Sv/Bq) for the individual radon progeny. Equation (2.18) was used to accomplish this task;

$$E = \sum_j f_{p,j} \sum_{j=1}^{3} I_{j,i} . e_{j,i} \ldots\ldots\ldots\ldots (2.18)$$

Where the index j corresponds to the aerosol mode of the activity size distribution, j=1, 2, and 3 for the unattached, nucleation and accumulation modes respectively, $f_{p,j}$ is the fraction of PAEC associated with mode j. The index i corresponds to the inhaled progeny i.e., i=1, 2, 3 corresponds to Po-218, Pb-214 and Bi-214 respectively. The symbol $e_{j,i}$ is the effective dose coefficient (Sv/Bq) for inhalation of progeny i with an activity size distribution for mode j. The intakes $I_{j,1}$, $I_{j,2}$ and $I_{j,3}$ are the intakes for Po-218, Pb-214 and Bi-214 which result in an exposure of 1WLM for either the unattached progeny (j=1) or the attached progeny (j=2). E is the effective dose coefficient (Sv/WLM). Figure 13 shows the basic workflow for the calculation of S-Coefficients using INTDOSKIT software. The respective functions that were implemented in the dosimetric functions library of INTDOSKIT are shown on the right side of each box.

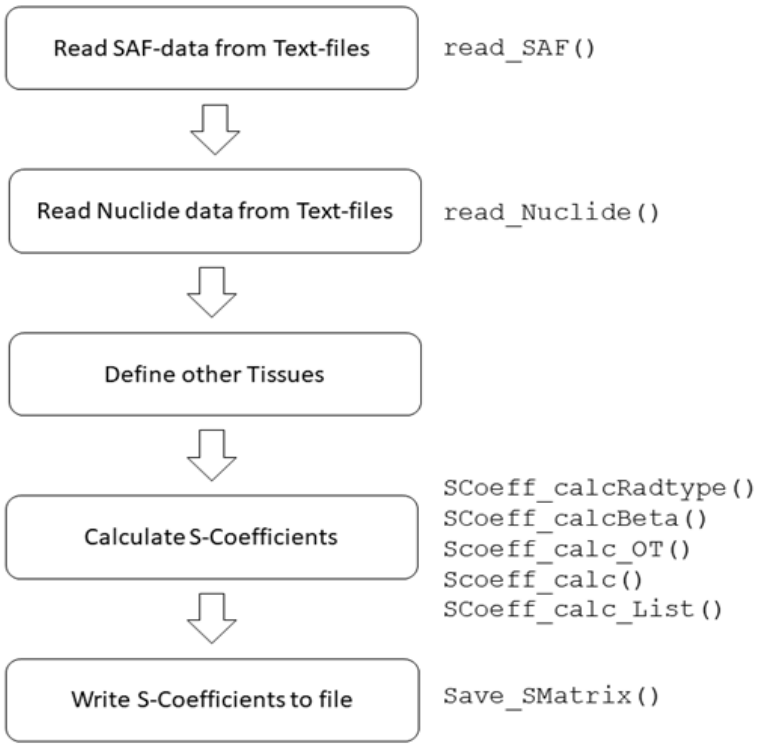

Figure 13: Workflow for the calculation of S-coefficients using INTDOSKIT (Source: Breustedt et al., 2025).

Figure 14 shows the basic workflow for the calculation of internal doses using INTDOSKIT software. The appropriate functions are given at the right of each box.

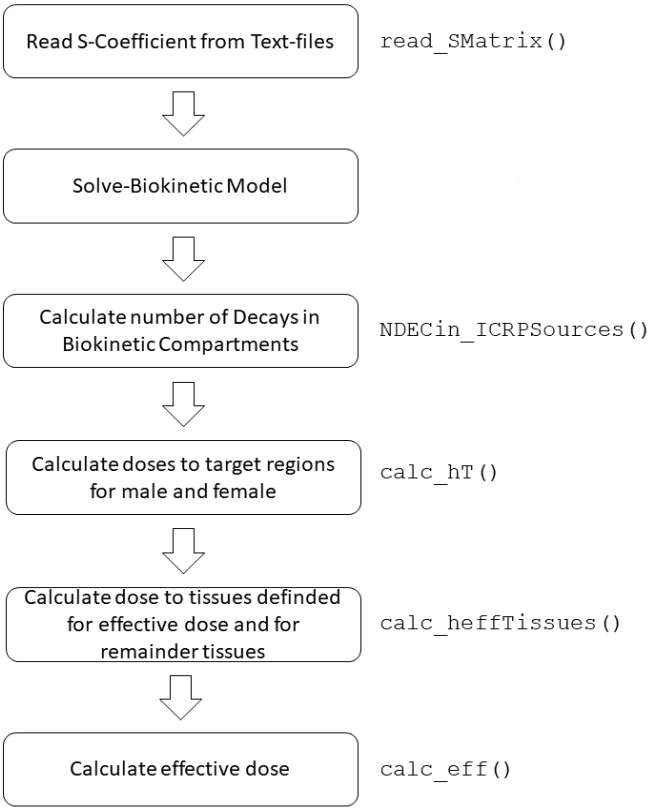

Figure 14: Workflow for dose calculation using INTDOSKIT (Source: Breustedt et al., 2025).

2.2.3 Validation of INTDOSKIT dose calculations

Results for the validation of INTDOSKIT software are presented here. By comparison of calculated results to the reference data provided by ICRP, INTDOSKIT was successfully validated for the intake of single radionuclides such as Pu-239, I-131, Co-60, S-35, Ba-133 and Am-241. The tool was also validated on the modelling of decay chains for NORM radionuclides contained in the three natural decay series of U-238, Th-232 and U-235: these included U-238, U-234, Th-230, Ra-226, Pb-210 and Po-210 of the U-238 decay series; Th-232, Ra-228, Th-228 and Ra-224 of the Th-232 decay series; U-235, Pa-231 and Ac-227 of the U-235 decay series. INTDOSKIT was tested and validated for the three common intake modes of injection, ingestion and inhalation for each of the above nuclides.

A fast test of the implementation of the models was performed by calculation of the total balance of the activity in the model and the results were in good agreement with the physical decay curves of the selected radionuclides. Errors in implementing the model, which can produce sinks and sources could be identified and corrected using this simple check. The tool was then validated against the data taken from the ICRP OIR dataviewer software and the model predictions were in good agreement with the ICRP data i.e., a percentage deviation of less than 2% for single radionuclides and less than 10% for decay chains. One must keep in mind that the dataset of ICRP is given with a precision of only one significant figure.

As a first example for the validation of the tool, results for the inhalation of Pu-239 are presented in Figure 16 and Figure 17. The biokinetic model for the inhalation of Pu-239 is a combination of the ICRP generic models i.e., the HATM and HRTM as well as the element specific systemic model of plutonium. Retention and excretion curves for the inhalation of Pu-239 (default parameters with AMAD of 5 µm and solubility class M) are represented in Figure 16 and

Figure17 respectively. In the plots, the circles (dots) represent ICRP data while the coloured lines represent the calculated data using INTDOSKIT software. From the plots, it can be observed that the calculated values of INTDOSKIT are in good agreement with the ICRP data. Pu-239 deposited in the lungs is rapidly cleared by the two competing processes of absorption into blood and particle transport to the HATM followed by absorption into blood from the HATM. The inhaled Pu-239 that reaches the systemic circulation is mainly deposited in the liver and skeleton. Most Pu-239 is excreted in faeces in the first 10 days, but this rate rapidly diminishes. After 10 days, the Pu-239 continues to be steadily excreted from the body via urine.

Dose calculation results for inhalation of Pu-239, showed that the largest dose is received by the liver followed by bone surface. It was also observed that the female organ doses are higher than the male doses; something that can be attributed mainly to the lower organ masses for female as opposed to the male. The effective dose for the inhalation of Pu-239 was also in good agreement with the ICRP data.

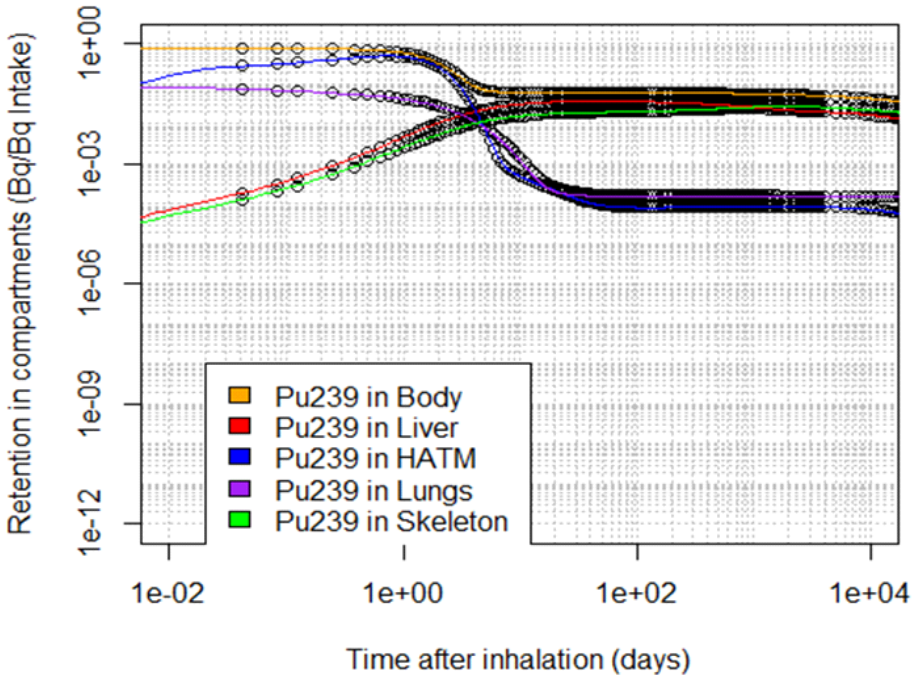

Figure 15: Retention functions after inhalation of Pu-239

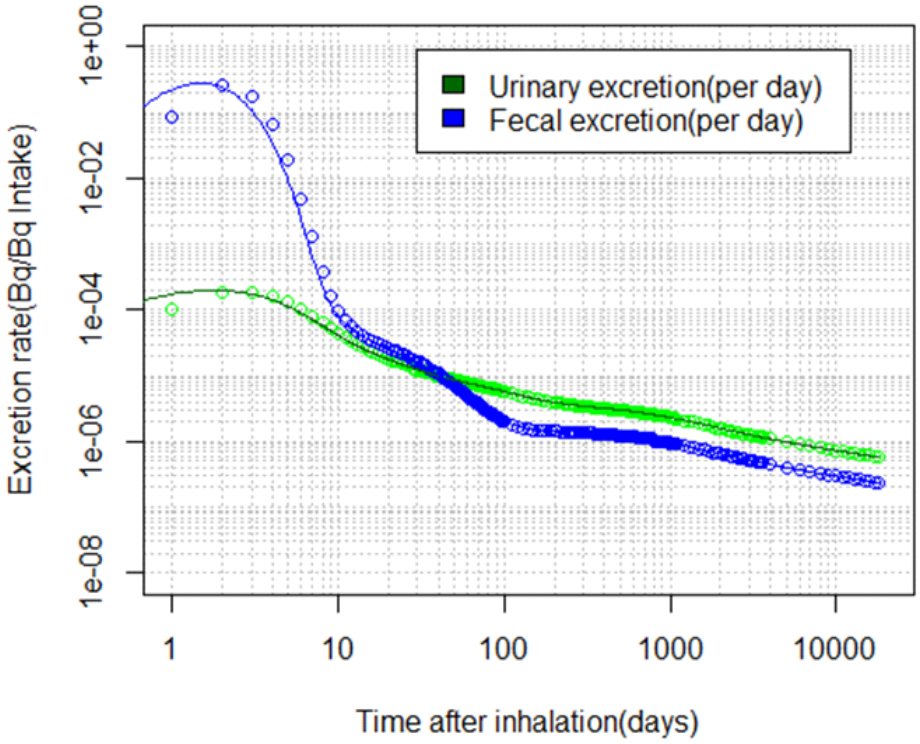

Figure 16: Excretion functions after inhalation of Pu-239.

For the modelling of decay chains, the results for the inhalation of radon gas and radon progeny are presented in Table 6 and Table 7 respectively. From the modelling results in Table 6, inhaled radon gas is mainly deposited in tissues with a high fat content such as the bone marrow, breast and adipose, while for inhalation of radon progeny, the organ that receives the highest dose is the lung followed by liver and bone surface. Most of the dose to the lung is attributed to progeny while for the systemic organs, majority of the dose comes from radon gas. Dose coefficients for the inhalation of radon gas and its progeny are in good agreement with the ICRP data.

Table 6: Validation of results calculated with INTDOSKIT against ICRP data for inhalation of radon gas.

Organ/Tissue	**INTDOSKIT (Sv/Bq)**		**ICRP (Sv/Bq)**		**Male Deviation (%)**	**Female Deviation (%)**
	Male	**Female**	**Male**	**Female**		
Bone marrow	9.2E-10	1.2E-09	9.0E-10	1.2E-09	2	0
Colon	1.1E-10	1.7E-10	1.1E-10	1.6E-10	0	6
Lung	1.0E-09	1.2E-09	1.0E-09	1.2E-09	0	0
Stomach	1.1E-10	1.6E-10	1.1E-10	1.5E-10	0	6
Breast	1.4E-09	7.7E-11	1.4E-09	7.6E-11	0	1
Gonads	9.1E-11	1.2E-10	9.1E-11	1.2E-10	0	0
Urinary bladder	9.8E-11	1.5E-10	9.1E-11	1.4E-10	7	7
Oesophagus	1.1E-10	1.6E-10	1.1E-10	1.5E-10	0	6
Liver	2.5E-10	3.2E-10	2.5E-10	3.2E-10	0	0
Thyroid	1.0E-10	1.6E-10	1.0E-10	1.5E-10	0	6

Bone surface	4.9E-10	6.6E-10	4.9E-10	6.5E-10	0	1
Brain	9.7E-11	1.5E-10	9.0E-11	1.4E-10	7	7
Salivary glands	9.7E-11	1.5E-10	9.0E-11	1.4E-10	7	7
Skin	8.4E-11	1.2E-10	8.4E-11	1.2E-10	0	0
Adrenals	1.1E-10	1.6E-10	1.1E-10	1.5E-10	0	6
Gall bladder	9.8E-11	1.5E-10	9.1E-11	1.4E-10	7	7
Heart	1.0E-10	1.6E-10	1.0E-10	1.5E-10	0	7
Kidneys	8.0E-10	9.4E-10	8.0E-10	9.4E-10	0	0
Muscle	9.6E-11	1.5E-10	8.9E-11	1.4E-10	8	7
Oral mucosa	1.0E-10	1.5E-10	9.4E-11	1.4E-10	6	7
Pancreas	1.1E-10	1.5E-10	1.1E-10	1.5E-10	0	0
Prostate	9.8E-11	0	9.1E-11	0	8	0
Small intestine	1.2E-10	1.7E-10	1.1E-10	1.6E-10	9	6
Spleen	1.3E-10	1.5E-10	1.3E-10	1.5E-10	0	0
Thymus	9.8E-11	1.5E-10	9.1E-11	1.4E-10	7	7
Uterus	0	1.5E-10	0	1.4E-10	0	7
e (50)	4.4E-10		4.4E-10		0	

The results presented in Table 6 compare the organ dose coefficients (Sv/Bq) for radon gas inhalation calculated by INTDOSKIT with those established by ICRP for both male and female subjects. Overall, the comparison shows good agreement between INTDOSKIT and ICRP data, with deviations typically less than 10%. For several organs, including bone marrow, colon, lung, gonads, liver, skin, kidney and spleen, the deviations are either zero or very small, demonstrating the high accuracy of INTDOSKIT. For example, lung exposure values are identical between INTDOSKIT and ICRP for both males and females, with no deviation, indicating excellent validation.

Small deviations are observed for organs such as the urinary bladder, brain, salivary glands, gall bladder and others, where the deviation reaches 9% for both sexes. These small differences suggest that INTDOSKIT slightly overestimates the dose in these cases compared to ICRP. Interestingly, for several organs, such as the colon, stomach, oesophagus, thyroid, adrenal glands and heart, the deviations are higher for women (around 6-7%), while there is no deviation for men. This suggests that the INTDOSKIT calculations may slightly overestimate doses for females compared to the ICRP data.

In contrast, certain organs such as bone marrow, lungs, gonads, liver, skin and kidneys show no deviation between INTDOSKIT and ICRP for either sex, further supporting the accuracy of the software in these cases. The fact that some deviations are consistent between males and females, such as for urinary bladder and brain, suggests a systematic bias that affects both sexes equally. Overall, despite minor differences, particularly for females, the validation shows that INTDOSKIT provides a reliable reproduction of the ICRP dose coefficients for radon gas inhalation.

Table 7: Validation of results calculated with INTDOSKIT against ICRP data for inhalation of radon progeny.

Organ/Tissue	**INTDOSKIT (mSv/(mJh/m^3))**	**ICRP (mSv/(mJh/m^3))**	**Male Deviation (%)**	**Female Deviation (%)**

	Male	**Female**	**Male**	**Female**		
Bone marrow	4.5E-03	5.6E-03	4.3E-03	5.4E-03	5	4
Colon	4.2E-03	4.7E-03	4.0E-03	4.5E-03	5	4
Lung	2.5E+01	2.6E+01	2.4E+01	2.6E+01	4	0
Stomach	7.2E-03	7.8E-03	6.9E-03	7.6E-03	4	3
Breast	2.3E-03	2.7E-03	2.2E-03	2.6E-03	5	4
Gonads	1.7E-03	3.5E-03	1.8E-03	3.6E-03	-6	-3
Urinary bladder	1.9E-03	2.3E-03	1.9E-03	2.3E-03	0	0
Oesophagus	6.1E-03	7.4E-03	5.8E-03	7.1E-03	5	4
Liver	1.3E-02	1.7E-02	1.3E-02	1.7E-02	0	0
Thyroid	3.4E-03	4.3E-03	3.3E-03	4.1E-03	3	5
Bone surface	1.2E-02	1.4E-02	1.2E-02	1.4E-02	0	0
Brain	2.1E-03	2.4E-03	2.0E-03	2.4E-03	5	0
Salivary glands	2.1E-03	2.5E-03	2.1E-03	2.5E-03	0	0
Skin	1.4E-03	1.9E-03	1.4E-03	1.9E-03	0	0
Adrenals	3.8E-03	4.4E-03	3.7E-03	4.2E-03	3	5
Gall bladder	2.2E-03	2.5E-03	2.2E-03	2.4E-03	0	4
Heart	4.2E-03	5.6E-03	4.0E-03	5.4E-03	5	4
Kidneys	5.3E-02	6.2E-02	5.4E-02	6.4E-02	-2	-3
Muscle	1.9E-03	2.2E-03	1.8E-03	2.2E-03	6	0
Oral mucosa	2.8E-03	3.5E-03	2.7E-03	3.4E-03	4	3
Pancreas	3.8E-03	4.5E-03	3.7E-03	4.4E-03	3	2
Prostate	1.9E-03	0	1.9E-03	0	0	0
Small intestine	4.4E-03	5.1E-03	4.3E-03	5.0E-03	2	2
Spleen	5.2E-03	6.3E-03	5.1E-03	6.2E-03	2	2
Thymus	2.9E-03	3.5E-03	2.8E-03	3.4E-03	4	3
Uterus	0	2.2E-03	0	2.2E-03	0	0
e (50)		3.17		3.14		1

The results in Table 7 compare the organ dose coefficients (mSv/ (mJh/m³)) for radon progeny inhalation calculated by INTDOSKIT with the ICRP values for both male and female subjects and show good agreement between the two. Many organs, including the urinary bladder, liver, bone surface, salivary glands, skin and prostate, show no deviation (0%) for both males and females, indicating excellent agreement. Other organs, such as the lungs, colon, stomach, heart and breast, show small deviations of between 3% and 5%, confirming a high degree of accuracy. Some organs, such as the kidneys and gonads, show small negative deviations, with INTDOSKIT underestimating ICRP values by 2-6%, while others, such as the brain and muscles, show small positive deviations of around 5-6%.

There are also some gender differences. For example, the lungs show no deviation in women but a 4% deviation in men, while organs such as the thyroid, adrenal glands and gall bladder show slightly higher deviations in women (around 4-5%) than in men (3%). Despite these variations, the uterus shows no deviation, indicating that INTDOSKIT accurately reflects doses to female reproductive organs. The overall committed effective dose coefficient, e (50), is within 1% of the ICRP values, indicating that the cumulative dose calculations are reliable.

Overall, INTDOSKIT provides accurate and consistent estimates of radiation doses due to radon progeny inhalation, with deviations generally less than 5%.

3. DOSE CALCULATIONS FOR SELECTED SCENARIOS

This chapter presents the internal doses to body organs and tissues of underground miners that were calculated using INTDOSKIT software for the two selected exposure scenarios in the RadoNorm project i.e., wet drilling with good ventilation (Job 1) and dry drilling with poor ventilation (Job 4) for the intake of both radon progeny and long-lived radionuclides in the uranium ore dust.

3.1 Formation of radon progeny aerosols

It is difficult to characterize aerosol parameters in mines due to the highly variable conditions, different mining methods that use diesel or electric-powered equipment, different ventilation rates, and the type of heating used during the winter months (ICRP, 2017). Radon progeny aerosols form in two steps. First, the radon gas decays. Then, the freshly formed radionuclides rapidly react (in less than one second) with trace gases and vapours. They grow by cluster formation to form particles about 1 nm in size. These particles are referred to as unattached particles. These unattached particles can attach to existing aerosol particles within one to 100 seconds to form attached particles (Marsh et al., 2008; 2012). This process is shown in Figure 17.

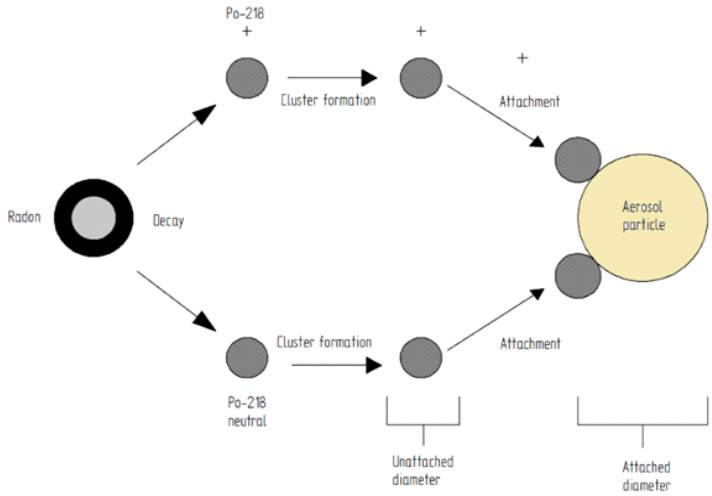

Figure 17: Basic processes of short-lived radon progeny generation in the air defining both the unattached and attached fractions (Source: Skubacz and Wolosczcuk, 2019).

Marsh et al. (2012) reported that the activity size distribution of particles attached to a mine can be described by a lognormal distribution with an AMAD between 100 and 400 nm. Additionally, Butterweck et al. (1992) suggest that the activity size distribution of attached particles in mines can be described by a lognormal distribution with an AMAD between 130 and 350 nm. Skubacz and Woloszczuk (2019) reported that the size range of attached progeny particles is 50–500 nm. Postendörfer et al. (2000) performed experimental studies and observed negligible differences in the activity size distributions of individual progeny attached to aerosol particles. They concluded that, for simplicity and dosimetric purposes, the aerosol distribution of each radon progeny can be assumed to be the same.

Regarding unattached aerosols, Marsh et al. (2008) suggests an activity size distribution with an AMTD of 0.8 nm and a GSD of 1.3 across all mine conditions. However, Skubacz and Woloszczuk (2019) recommend a size range of 0.5–5 nm. For the purposes of dose calculation

and simplicity, the ICRP adopted a unimodal distribution with an AMTD of 1.0 nm and a GSD of 1.3, as well as a unit density and a unit shape factor, for all exposure scenarios involving unattached radon progeny (ICRP, 2017). Two additional aerosol parameters of interest in dose calculations for radon progeny are the equilibrium factor (F), which is a measure of the relationship between radon gas activity and its progeny, and the unattached fraction (f_p), which is the fraction of radon progeny not attached to atmospheric aerosols (Makumbi et al., 2024a).

It has been observed that particles to which radon progeny are attached can have a trimodal size distribution. The three modes are nucleation (ultrafine particles formed by condensation processes and chemical reactions), accumulation (fine particles formed by various processes), and coarse (coarse particles formed mainly by mechanical processes). In mines, however, only the accumulation mode is assumed (ICRP, 2017; Hu et al., 2020). It is assumed that inhalation leads to hygroscopic growth, causing the attached particles to increase by a factor of two in the respiratory tract upon inhalation. This process is represented by a parameter known as the hygroscopic growth factor (Marsh et al., 2008, 2012; Hu et al., 2020).

3.2 Dose calculations for inhalation of radon progeny

The dose calculations for inhalation of radon progeny for the two intake scenarios i.e., wet drilling with good ventilation (Job 1) and dry drilling with poor ventilation (Job 4) are presented in this section. The two scenarios were defined in the RadoNorm project with aerosol characteristics as shown below.

3.2.1 Exposure conditions: Wet drilling with good ventilation

Table 8 shows the appropriate aerosol parameters for a mine with wet drilling and good ventilation (Job 1). In this scenario, the size of the unattached fraction is primarily influenced by the ambient aerosol particle concentration. In a mine, this concentration is usually low because the total number of particles is high, accounting for less than 3% of the PAEC (Marsh et al., 2012). The relative size distribution of the unattached radon progeny cluster depends on the concentrations of water vapor and trace gases, as well as the electric charge distribution of the radionuclides in the ambient air (ICRP, 2017). Postendörfer (2001) observed that, under normal humidity and radon concentration conditions, the activity size distribution of unattached radon progeny in a mine can be approximated by three lognormal distributions. This observation was based on measured AMTD values of 0.6 nm, 0.85 nm, and 1.3 nm, as well as a GSD of 1.2. However, the fraction with an AMTD value of 1.3 nm was never recorded in areas of high radon concentration/humidity.

While the size of unattached radon progeny in the lungs is assumed to be constant, some ambient aerosols are hygroscopic and grow instantaneously by a given factor upon inhalation (Marsh and Birchall, 2009). Since the relative humidity in mines is high and mine aerosols are likely less hygroscopic, Marsh et al. (2008) assumed a hygroscopic growth factor (hgf) of 1.5 for typical mines. For modelling purposes, d_{th} is assumed to increase instantaneously by the hgf as the particle enters the respiratory tract. As a result, the density will also change (Marsh et al., 2012).

3.2.2 Exposure conditions: Dry drilling with poor ventilation

Postendörfer reconstructed the working conditions in the former WISMUT uranium mines prior to 1955 for dry drilling. Thus, the central values of the activity size distribution for dry drilling are based on his work (Marsh et al., 2008). For this job type, the attached mode was reported to be very broad, with an AMAD of 560 nm and a GSD of 4.0. This led to the conclusion that the attached progeny for dry drilling consists mainly of hydrophobic silica (Marsh et al., 2008; 2012). Table 8 shows the appropriate aerosol parameters for a poorly ventilated dry drilling mine (Job 4).

Table 8: Aerosol parameters for selected scenarios in the RadoNorm project

Exposure scenario	**Mode[a]**	**Aerosol fraction of PAEC[b]**	**AMTD[c]/AMAD[d] (nm)**	**σ_g[e]**	**hgf[f]**	**F[g]**
Job 1	u	0.03	1	1.3	1.0	0.20
	a	0.97	350	2.0	1.5	
Job 4	u	0.01	1	1.3	1.0	0.60
	a	0.99	560	4.0	1.0	

Source: Marsh, 2022

[a] Modes u and a represent unattached and attached modes respectively.

[b] Aerosol fraction of potential alpha energy concentration (PAEC)

[c] Aerosol size given in terms of activity median thermodynamic diameter (AMTD)

[d] Aerosol size given in terms of activity median aerodynamic diameter (AMAD)

[e] σ_g Geometric standard deviation

[f] Hygroscopic growth factor

[g] Equilibrium factor

[h] The particle density and shape factor of the attached mode for wet drilling were assumed to be 1.4 g/cm^3 and 1.1 whereas for dry drilling the values were assumed to be 2.5 g/cm^3 and 1.5 respectively.

[i] The particle density and shape factor of unattached progeny were both assumed to be unity.

Table 9: Calculated doses (mSv/ (mJh/m^3)) from inhalation of radon progeny for selected scenarios in the RadoNorm project.

	Job 1		**Job 4**	
Organ/Tissue	**Male**	**Female**	**Male**	**Female**
Bone marrow	5.23E-03	6.55E-03	7.47E-03	9.35E-03
Colon	5.03E-03	5.55E-03	7.14E-03	7.88E-03
Lung	2.75E+01	2.98E+01	3.98E+01	4.30E+01
Stomach	1.51E-02	1.59E-02	2.15E-02	2.27E-02
Breast	2.64E-03	3.04E-03	3.79E-03	4.37E-03
Gonads	1.92E-03	4.13E-03	2.75E-03	5.90E-03
Urinary bladder	2.21E-03	2.73E-03	3.16E-03	3.89E-03
Oesophagus	1.04E-02	1.22E-02	1.49E-02	1.76E-02
Liver	1.48E-02	1.92E-02	2.11E-02	2.74E-02
Thyroid	4.00E-03	5.15E-03	5.72E-03	7.37E-03
Bone surface	1.35E-02	1.66E-02	1.94E-02	2.38E-02

Brain	2.68E-03	3.15E-03	3.85E-03	4.53E-03
Salivary glands	2.71E-03	3.47E-03	3.90E-03	5.01E-03
Skin	1.70E-03	2.29E-03	2.48E-03	3.33E-03
Adrenals	4.45E-03	5.20E-03	6.33E-03	7.40E-03
ET of HRTM	4.00E+01	4.63E+01	6.15E+01	7.11E+01
Gall bladder	2.67E-03	3.04E-03	3.81E-03	4.34E-03
Heart	4.80E-03	6.25E-03	6.87E-03	8.96E-03
Kidneys	5.95E-02	7.04E-02	8.50E-02	1.01E-01
Lymphatic nodes	3.65E-03	4.35E-03	5.32E-03	6.31E-03
Muscle	2.13E-03	2.58E-03	3.05E-03	3.69E-03
Oral mucosa	4.91E-03	6.59E-03	7.19E-03	9.69E-03
Pancreas	4.75E-03	5.68E-03	6.75E-03	8.08E-03
Prostate	2.21E-03	0.00E+00	3.15E-03	0.00E+00
Small intestine	6.01E-03	6.96E-03	8.52E-03	9.86E-03
Spleen	6.13E-03	7.59E-03	8.70E-03	1.08E-02
Thymus	3.22E-03	3.84E-03	4.63E-03	5.53E-03
Uterus	0.00E+00	2.65E-03	0.00E+00	3.77E-03
e (50)	3.80E+00		5.50E+00	

Table 10: Calculated doses (mSv/ (mJh/m^3)) from inhalation of thoron progeny for selected scenarios in the RadoNorm project.

	Job 1		**Job 4**	
Organ/Tissue	**Male**	**Female**	**Male**	**Female**
Bone marrow	4.22E-02	5.47E-02	6.21E-02	8.06E-02
Colon	4.54E-02	5.02E-02	6.70E-02	7.40E-02
Lung	9.32E+00	9.98E+00	1.49E+01	1.59E+01
Stomach	4.22E-02	4.78E-02	6.22E-02	7.05E-02
Breast	1.03E-02	1.01E-02	1.51E-02	1.49E-02
Ovaries	0.00E+00	3.04E-02	0.00E+00	4.48E-02
Testes	1.07E-02	0.00E+00	1.58E-02	0.00E+00
Urinary bladder	7.11E-03	8.83E-03	1.05E-02	1.30E-02
Oesophagus	4.06E-02	4.66E-02	5.99E-02	6.87E-02
Liver	1.32E-01	1.71E-01	1.94E-01	2.52E-01
Thyroid	2.64E-02	3.17E-02	3.88E-02	4.67E-02
Bone surface	1.07E-01	1.40E-01	1.57E-01	2.06E-01
Brain	1.01E-02	1.16E-02	1.49E-02	1.70E-02
Salivary glands	1.02E-02	1.02E-02	1.50E-02	1.50E-02
Skin	8.87E-03	1.26E-02	1.31E-02	1.86E-02
Adrenals	3.48E-02	3.92E-02	5.13E-02	5.78E-02
ET of HRTM	1.62E+01	1.88E+01	2.50E+01	2.89E+01
Gall bladder	1.09E-02	1.05E-02	1.61E-02	1.54E-02
Heart	2.76E-02	3.64E-02	4.06E-02	5.36E-02
Kidneys	3.69E-01	4.36E-01	5.43E-01	6.41E-01
Lymphatic nodes	1.32E-02	1.63E-02	1.94E-02	2.40E-02

Muscle	7.13E-03	8.74E-03	1.05E-02	1.29E-02
Oral mucosa	1.10E-02	1.12E-02	1.62E-02	1.66E-02
Pancreas	3.49E-02	4.17E-02	5.14E-02	6.14E-02
Prostate	1.01E-02	0.00E+00	1.48E-02	0.00E+00
Small intestine	4.39E-02	5.04E-02	6.47E-02	7.43E-02
Spleen	5.78E-02	7.03E-02	8.51E-02	1.04E-01
Thymus	1.05E-02	1.05E-02	1.55E-02	1.55E-02
Uterus	0.00E+00	1.03E-02	0.00E+00	1.52E-02
e (50)	1.36E+00		2.15E+00	

The results of the dose calculations are summarized in Tables 9 and 10. These tables show the calculated radiation doses (mSv/ (mJh/m³)) from the inhalation of radon and thoron progeny for two job types, with values given for both male and female subjects for various organs. For both radon and thoron progeny, Job 4 consistently shows higher radiation doses than Job 1, indicating greater exposure due to factors such as poor ventilation and higher concentrations of airborne progeny in Job 4. For example, lung doses from radon progeny reach 39.8 mSv/ (mJh/m³) for males and 43.0 mSv/ (mJh/m³) for females in Job 4, compared to 27.5 mSv/ (mJh/m³) and 29.8 mSv/ (mJh/m³), respectively, in Job 1. This reflects the fact that dry drilling in Job 4 leads to more airborne progeny particles and a longer residence time before ventilation, resulting in higher inhalation exposures.

Gender differences are evident in both exposure scenarios, with females generally receiving higher doses than males in most organs. For example, for radon progeny exposure, the bone marrow dose is 6.55E-03 mSv/ (mJh/m³) for females compared to 5.23E-03 mSv/ (mJh/m³) for males in Job 1, and similar patterns persist for other organs. This higher susceptibility in females is consistent for both types of work and for thoron progeny. For thoron exposure, the bone marrow dose for females in Job 4 is 8.06E-02 mSv/ (mJh/m³), compared with 6.21E-02 mSv/ (mJh/m³) for males. These results support the need to consider gender differences in radiation protection strategies.

The lungs and the ET region of the respiratory tract receive the highest doses from radon progeny, as is expected for inhalation exposure. For the case of Job 4, the ET region receives up to 71.1 mSv/ (mJh/m³) for females. In contrast, thoron progeny exposure results in significantly lower lung doses, about a factor of three lower than for radon progeny. This difference is mainly due to the nature of radon progeny, which are alpha emitters (Po-218 and Po-214) that emit almost all their energy in the lungs before clearance. Thoron progeny, on the other hand, emit electrons and photons that can be absorbed further away from the source organ, and their longer half-lives allow them to decay even after clearance from the lung. Moreover, the activity concentration of thoron progeny is lower than that of radon progeny explaining the smaller doses from inhalation of thoron progeny.

Following the inhalation of radon progeny, within the lung, the target region receiving the highest dose is the Bronch.sec cells of the BB region, with median dose coefficients of 46.13 mSv/ (mJh/m³) for Job 1 and 86.71 mSv/ (mJh/m³) for Job 4. This high dose can be attributed to the relatively low tissue mass of Bronch.sec cells (8.648E-04 kg) compared to other regions

such as Bchiol.sec (1.949E-03 kg), resulting in higher specific absorption fraction (SAF) values in the Bronch.sec region. In addition, alpha radiation from short-lived polonium isotopes, with its limited penetration, predominantly affects cells close to the source region. Although Bronch.bas cells have a smaller tissue mass (4.324E-04 kg), their greater distance from the source region (35-50 µm) results in lower doses compared to Bronch.sec cells.

In contrast, the AI region receives the lowest dose due to its larger mass (1.1 kg), resulting in lower SAF values. This lower dose is also influenced by the deposition mechanisms of radon progeny in the lung, where larger attached progeny particles that constitute a greater percentage of the aerosol particles are deposited mainly in the upper and central airways, leading to lower particle deposition in deeper lung regions such as the AI.

Outside the lungs, the kidneys receive the highest dose for both types of work, with values of 5.95E-02 mSv/ (mJh/m^3) for Job 1 and 8.50E-02 mSv/ (mJh/m^3) for Job 4. The brain receives the lowest dose with 2.68E-03 mSv/ (mJh/m^3) for Job 1 and 3.85E-03 mSv/ (mJh/m^3) for Job 4.

While radon progeny primarily affects the lungs and respiratory tract, thoron progeny shows higher doses to systemic organs such as the liver, kidneys and bone surface, particularly at Job 4, where doses to the kidneys reach 6.41E-01 mSv/ (mJh/m^3) for females. This is due to the longer half-lives and different decay patterns of thoron progeny, resulting in higher radiation burdens in organs outside the lungs.

The total effective dose, e(50), further underlines the gender differences, with females receiving higher effective doses than males in both scenarios. For radon progeny, the effective dose for females in Job 4 is 5.50 mSv/ (mJh/m^3) compared to 3.80 mSv/ (mJh/m^3) for males. Similarly, for thoron progeny, females receive 2.15 mSv/ (mJh/m^3) compared to 1.36 mSv/ (mJh/m^3) for males. These results emphasise the need for tailored radiation protection measures that consider both the nature of the work and gender differences in dose sensitivity.

3.3 Dose calculations for inhalation of uranium ore dust

For the inhalation of uranium ore dust, the dose was calculated by assuming activity ratios of 0.04 and 0.05 for Th-232/U-238 and U-235/U-238 respectively; additionally, the aerosol parameters and dissolution/absorption parameters for the long-lived radionuclides in the uranium ore dust for Job 1 and Job 4 are given in Table 11 and Table 12 respectively while the dissolution/absorption parameters are presented in Table 13. The dose coefficients for the inhalation of uranium ore dust can be calculated using equation 3.1 (Marsh, 2022).

$$D_{organ} = D_{U238} + k_1 . D_{U235} + k_2 . D_{Th232} \ldots\ldots\ldots\ldots\ldots . (3.1)$$

Where k_1 and k_2 are the activity ratios of U-235 to U-238 and Th-232 to U-238 respectively. D_{organ} is the organ dose coefficient; $D_{U\text{-}238}$ (Sv/Bq) and $D_{U\text{-}235}$(Sv/Bq) are the dose coefficients from the U-238 and U-235 chains respectively and $D_{Th\text{-}232}$ is the dose from the Th-232 chain (Sv/Bq).

The committed dose coefficient to an organ per unit intake of U-238 (Sv/Bq) is then multiplied by the intake of U-238. This intake is calculated from the gross alpha activity exposure as shown in equation 3.2 (Marsh et al., 2012).

$$I_{U238} = \frac{G.B}{U_{alpha}} \ldots\ldots\ldots\ldots\ldots\ldots\ldots\ldots\ldots\ldots\ldots\ldots\ldots\ldots\ldots\ldots\ldots (3.2)$$

Where B is the breathing rate (m^3/h) and U_{alpha} is the total number of alpha disintegrations from uranium ore dust per disintegration of U-238. Assuming activity ratios of U235/U238 is 0.053 (Marsh et al., 2012; Castellani et al., 2013) and Th232/U238 is 0.04; 25% and 10% of Rn-222 and Rn-220 gas escapes from the ore particles respectively, it was calculated that U_{alpha} per disintegration of U-238 is 7.55. A similar value of U has also been reported by other researchers (Marsh et al., 2012; Marsh, 2022).

Table 11: Aerosol parameters for long-lived radionuclides in uranium ore dust for underground mines with Job 1(Source: Marsh et al., 2012).

Parameter	Value
Particle size, AMAD (μm)	7.0
Particle dispersion, GSD	2.5
Particle density, ρ (g/cm^3)	3.0
Particle shape factor, χ	1.5

Table 12: Aerosol parameters for long-lived radionuclides in uranium ore dust for underground mines with Job 4 (Source: Marsh et al., 2012).

Parameter	Value
Particle size, AMAD (μm)	4.7
Particle dispersion, GSD	2.0
Particle density, ρ (g/cm^3)	3.0
Particle shape factor, χ	1.5

Table 13: Dissolution/absorption parameters for long-lived radionuclides in underground mines (Source: Marsh et al., 2012).

Nuclide	Rapid dissolution fraction, $f_r(d^{-1})$	Rapid dissolution rate, $s_r(d^{-1})$	Slow dissolution rate, $s_s(d^{-1})$	Absorption fraction from HATM
U-234, U-235, U-238	0.22	0.78	0.0014	0.0044
Ra-224, Ra-226, Ra-228	0.11	7.3	0.00041	0.000055
Th-230, Th-232	0.14	4.6	0.00068	0.028
Pb-210	0.26	3.9	0.001	0.052
Other	0.18	4.1	0.00087	0.02

Table 14: Doses from the inhalation of uranium ore dust (mSv/ (kBqh/m^3)) for selected scenarios in the RadoNorm project.

	Job 1		Job 4	
Organ/Tissue	Male	Female	Male	Female
Bone marrow	3.17E-04	3.95E-04	4.47E-04	5.50E-04
Colon	4.01E-05	5.11E-05	5.70E-05	7.12E-05
Lung	3.95E-03	4.34E-03	5.70E-03	6.21E-03
Stomach	4.14E-05	5.18E-05	5.83E-05	7.12E-05
Breast	4.92E-05	5.89E-05	7.12E-05	8.42E-05
Gonads	1.10E-04	1.17E-04	1.55E-04	1.62E-04

Urinary bladder	4.98E-05	6.02E-05	7.12E-05	8.42E-05
Oesophagus	4.21E-05	5.24E-05	5.89E-05	7.12E-05
Liver	3.43E-04	4.53E-04	4.86E-04	6.28E-04
Thyroid	4.47E-05	5.44E-05	6.34E-05	7.77E-05
Bone surface	2.59E-03	3.30E-03	3.56E-03	4.60E-03
Brain	4.92E-05	5.96E-05	7.12E-05	8.42E-05
Salivary glands	4.92E-05	6.02E-05	7.12E-05	8.42E-05
Skin	5.18E-05	6.41E-05	7.12E-05	9.06E-05
Adrenals	4.34E-05	5.37E-05	6.09E-05	7.77E-05
Gall bladder	4.92E-05	5.96E-05	7.12E-05	8.42E-05
Heart	4.53E-05	5.50E-05	6.41E-05	7.77E-05
Kidneys	5.37E-04	6.34E-04	7.77E-04	9.06E-04
Muscle	4.98E-05	6.02E-05	7.12E-05	8.42E-05
Oral mucosa	5.18E-05	6.34E-05	7.12E-05	9.06E-05
Pancreas	4.27E-05	5.24E-05	6.02E-05	7.12E-05
Prostate	4.92E-05	0.00E+00	7.12E-05	0.00E+00
Small intestine	4.01E-05	5.05E-05	5.70E-05	7.12E-05
Spleen	5.63E-05	7.12E-05	7.77E-05	9.71E-05
Thymus	4.98E-05	6.02E-05	7.12E-05	8.42E-05
Uterus	0.00E+00	5.89E-05	0.00E+00	8.42E-05
e (50)	8.42E-04		1.17E-03	

The results in Table 14 show the calculated radiation doses (mSv/ (kBqh/m^3)) from inhalation of uranium ore dust for different work scenarios in the RadoNorm project, comparing male and female subjects at different organs. Job 4 consistently shows higher doses than Job 1, reflecting the higher exposure levels in this scenario. For example, lung doses in Job 4 reach 5.70E-03 mSv/ (kBqh/m^3) for males and 6.21E-03 mSv/ (kBqh/m^3) for females, compared with 3.95E-03 mSv/ (kBqh/m^3) and 4.34E-03 mSv/ (kBqh/m^3), respectively, in Job 1. This pattern of higher exposure in Job 4 can be attributed to the smaller aerosol sizes in this scenario, which are more likely to be deposited in the lower regions of the lung and absorbed more rapidly than the larger aerosols found in Job 1.

Females generally receive higher doses than males in most organs, which is consistent with findings in other inhalation scenarios. For example, in the bone marrow, females receive 5.50E-04 mSv/ (kBqh/m^3) for Job 4, compared with 4.47E-04 mSv/ (kBqh/m^3) for males. Organs such as the bone surface and kidneys show particularly high doses, with kidney doses reaching 9.06E-04 mSv/ (kBqh/m^3) for females in Job 4.

The effective dose, e (50), follows the same trend, with females receiving higher doses than males, reaching 1.17E-03 mSv/ (kBqh/m^3) for females compared to 8.42E-04 mSv/ (kBqh/m^3) for males in Job 4. These results emphasise the higher exposure risk associated with Job 4 and underline the importance of considering gender differences when assessing the radiological impact of uranium ore dust inhalation in occupational settings. Further uncertainty and sensitivity studies on these calculated doses are discussed in subsequent chapters.

4. UNCERTAINTY AND SENSITIVITY ANALYSIS

This chapter explains the types and sources of uncertainty in internal dose assessment. Additionally, it discusses the methodologies for uncertainty and sensitivity analysis for dose coefficients and the criteria that were used to assign probability distributions to the model parameters. The chapter also presents the probability distributions that were derived and selected for the various model parameters in this work and the reasoning behind these choices. Lastly, the chapter is concluded with the discussion of how the Monte Carlo simulation technique with random sampling was implemented in INTDOSKIT software to perform the uncertainty and sensitivity analysis on the doses for the intake of radon progeny and long-lived radionuclides in underground uranium mines, which were calculated and presented in the previous chapter.

4.1 Uncertainty and Variability and factors contributing to parameter uncertainty in internal dosimetry

Uncertainty refers to a lack of knowledge about a particular parameter value when the value itself is fixed but unknown with precision (Puncher and Burt, 2013). In Bayesian inference, uncertainty is expressed as a probability, and in classical statistics, it is expressed as a confidence interval (Puncher and Harrison, 2012a). Variability, on the other hand, refers to the natural range and frequency of a parameter value in a population of interest. Variability and uncertainty are sometimes referred to as aleatory and epistemic uncertainty, respectively (Puncher and Harrison, 2012b; Li et al., 2015; Paquet et al., 2016).

The variability of biokinetics within a population often contributes to uncertainty in central estimates of biokinetic quantities. This is because such variability makes it difficult to identify the central tendency of these properties in the population due to the small number of observations generally available, as well as the fact that subjects in biokinetic studies are often not randomly selected. According to Paquet et al. (2016), variability in the biokinetics of radionuclides, drugs, or chemicals in humans is due to physiological factors and environmental modulating effects, such as age, sex, pregnancy, lactation, exercise, disease, stress, smoking, and diet.

It is important to distinguish between uncertainty and variability. More precisely, in certain cases, it is important to consider variability as a component of uncertainty (Puncher and Harrison, 2012b). Harrison and Day (2008) argue that, in the context of dose and risk assessment, uncertainty refers to the degree of confidence that can be placed in given parameter values or dose estimates as central values for a population. In this limited sense, variability refers to quantitative differences between members of the population in question and is therefore biological variability. Therefore, it can be concluded that uncertainty affects the distribution of the mean, whereas variability only affects its location. Thus, it is crucial to consider the distinct effects of uncertainty and variability in an uncertainty analysis to determine the uncertainty in the population mean dose or cancer risk resulting from the intake of a radionuclide.

Uncertainty in an internal dose assessment based on bioassay data depends on several factors. These include uncertainties associated with measurements used to determine radionuclide

activity in vivo or in a biological sample; uncertainties in the exposure scenario used to interpret bioassay results; and uncertainties in biokinetic and dosimetric models used to interpret bioassay results (Harrison et al., 2001; Paquet et al., 2016). Some uncertainties due to measurement techniques and subjective behaviour can be reduced; however, those due to natural human variability can be quantified but are difficult to reduce. Paquet et al. (2016) reported that the ICRP has made considerable efforts to revise and improve its models, making them more physiologically realistic. The ICRP models are now sophisticated enough to calculate absorbed doses to organs and tissues for scientific purposes and in fields such as toxicology, pharmacology, and medicine.

Several authors have presented the sources and levels of uncertainty in internal dosimetry (Leggett, 2001, 2003; Harrison et al., 2001; Leggett et al., 2007; Paquet et al., 2016; ICRP, 2017; Li, 2018; Breustedt et al., 2018; Kwon et al., 2020). The main factors identified by these authors are outlined below.

Uncertainties in the exposure scenario: These include the uncertainty in (i) the time and route of intake, (ii) the uncertainty in the particle size distribution of the inhaled radionuclide aerosols, (iii) the uncertainty in the physico-chemical form of the inhaled radionuclide and (iv) the influence of background radiation.

Uncertainties in biokinetic models: These include (i) uncertainties in the structure of a biokinetic model, (ii) uncertainties due to the type of information used to construct biokinetic models, (iii) uncertainties associated with the application of human data, (iv) uncertainties in interspecies extrapolation of biokinetic data, (v) uncertainties due to inter-element extrapolation of biokinetic data, and (vi) uncertainties in central estimates due to within-population variability.

Uncertainties in dosimetric models: These include (i) the energy and intensity of the nuclear and atomic radiation emitted by the radionuclide and any radioactive progeny, (ii) the interaction coefficients of the emitted radiation in tissues, (iii) the elemental composition of body tissues, (iv) the geometry and density of body organs, and (v) parameters describing the spatial relationship between the source and target regions.

4.2 Methodologies for parameter uncertainty and sensitivity analysis

4.2.1 Monte Carlo methods

Monte Carlo methods use simulation to find solutions to mathematical and statistical problems (Everitt, 1995). In a Monte Carlo analysis, a value is randomly selected from each input distribution. This set of random variables defines a scenario that serves as the input for the model, and the model's outputs are then calculated (Morgan and Henrion, 1990). The resulting simulated distribution of outputs is then used to evaluate the uncertainty caused by the input uncertainty. Monte Carlo simulations can also be used in sensitivity analyses to identify important input parameters.

Due to the increased availability of powerful yet inexpensive computers, Monte Carlo methods are arguably the most widely used method for uncertainty analysis today. Monte Carlo methods often use simple random sampling but can also use more sophisticated methods, such as stratified sampling and Latin hypercube sampling, for greater efficiency. In stratified sampling,

the range of possible output values can be divided into n sub-intervals, each of which is sampled a predetermined number of times. This ensures that each sub-interval is represented in the sample for that input. In Latin hypercube sampling (LHS), each interval of each simulation is sampled only once (NCRP, 2009).

Internal dosimetry typically involves solving a series of ordinary differential equations derived from the compartmental structure of the biokinetic model. This is done to obtain the activity in the different model compartments. Then, dose calculations are performed using the conventional ICRP dosimetric approach (ICRP, 2015). One can also perform parameter uncertainty analysis on the calculated doses using Monte Carlo methods. First, one assigns probability distributions to the values of the input parameters for the model of interest. These probability distributions can account for correlations between parameters (Puncher and Harrison, 2012a). Then, the model is solved, and doses are calculated through multiple iterations using sampled parameters from the assigned probability distributions instead of ICRP reference values (Puncher et al., 2008; NCRP, 2009). The resulting output from this approach is a distribution of doses that can be characterized using a statistical summary.

However, dosimetrists should exercise caution, as the reliability of such analyses depends on the quality of the available data and the analyst's judgment (Puncher and Harrison, 2012a). Second, care must be taken to ensure that the number of simulations is large enough to converge on a solution, especially when using random sampling in Monte Carlo, and that reliable software is used for sampling. Additionally, correlations between model parameters must be adequately considered. Finally, aleatory and epistemic uncertainties should be distinguished.

4.2.2 Bayes' theorem

Bayes' theorem is a mathematical rule that explains how to adjust existing beliefs considering new evidence. It provides a framework for scientists to combine new data with their existing knowledge or expertise (NCRP, 2009). Bayes' theorem is based on probability theory and serves as a common language for expressing uncertainties in model parameters, model structure, and quantities of interest, such as those related to dose or activity. In the Bayesian approach, initial (prior) distributions are first assigned to model parameters, competing model structures, and/or intake values. These prior distributions are then updated to incorporate information from measured data. These updated probability distributions are called posterior distributions (Puncher et al., 2013). The mathematical representation of Bayes' theorem is given by equation (4.1).

$$P\left(X/M\right) = \frac{P\left(M/X\right).P(X)}{P(M)} \ldots\ldots\ldots\ldots\ldots\ldots\ldots\ldots\ldots\ldots\ldots\ldots (4.1)$$

Where; P(X/M) is read as the probability of X given M and is called the posterior distribution; P(M/X) is called the likelihood function and P(X) is the prior probability of X.

In Bayes' theorem, the posterior distributions (e.g., biokinetic model parameter values) are proportional to the prior distributions assigned to the parameter values, multiplied by the probability distributions for the measurements given the parameter values. This is called the likelihood function (NCRP, 2009). Miller et al. (2001) stated that Bayesian methods have the advantage of providing direct visualization of the relationship between uncertainties in model

input parameters and model predictions. However, they require a higher level of expertise and computer code than is commonly used, which is a disadvantage.

Birchall et al. (2016) demonstrated that calculating the posterior distribution can be numerically challenging. However, there are conventional methods for addressing this issue, such as Markov chain Monte Carlo (MCMC) and weighted likelihood Monte Carlo sampling (WeLMoS). According to Birchall et al. (2016), applying MCMC is extremely computationally intensive and time-consuming for a large cohort. Fortunately, the WeLMoS method addresses these limitations and is ideally suited to cases where the uncertainties in the posterior parameter values are relatively large.

The WeLMoS method is particularly suited to situations with a single intake regime. However, the work history of some subjects may consist of several separate and independent unknown intakes. This makes the method difficult to apply to such situations due to the multidimensionality of the probability distribution for intake. If the method were extended without modification, it would likely suffer from convergence problems. Such a situation would require approximating multiple intakes into a single intake regime, known as a complex intake regime (CIR) (Puncher et al., 2012; Birchall et al., 2016).

Another drawback of Bayes' theorem is the lack of guidance on choosing a prior distribution (Miller et al., 2001). While assigning prior probability distribution functions to model parameters can be based on data analysis (i.e., fitting probability distribution curves to existing data), it relies on subjective judgment about the state of knowledge relating to specific model parameters (Miller et al., 2001; NCRP, 2009). Miller et al. (2001) argue that the prior probability distribution has little effect on the inferred result when a large amount of measurement data is available.

4.3 Assignment of probability distributions to model parameters

The main challenge for dosimetrists performing parameter uncertainty analyses using Monte Carlo methods is assigning appropriate probability distributions to the model parameters of interest. Dosimetrists often use simple, common-sense rules based on judgment to assign probability distributions. For example, a uniform distribution is used when a parameter varies between a minimum and maximum value, and all values within this range are considered equally likely (Birchall and James, 1994). A triangular distribution may be used when values near the middle of the possible range are considered more likely than values near the extremes (Morgan and Henrion, 1990). When minimum and maximum values cannot be defined, it is appropriate to use unbounded distributions (e.g., normal and lognormal). Bounded or truncated distributions must be used if the parameter has physical limits (e.g., a parameter representing a fraction is always greater than zero and less than one). When a parameter value is expected to vary by more than an order of magnitude, a distribution defined on a logarithmic scale is often best, e.g., log-uniform, log-triangular, or lognormal (NCRP, 2009).

According to the NCRP (2009), subjectively derived prior distributions may reflect the opinion of one expert or a panel of experts. Selecting a probability function based on judgment often describes the degree of belief that the parameter's values are within a certain range, rather than describing the statistical frequency of measured values.

4.4 Assignment of Probability distributions to HRTM parameters

Specific parameter values can be entered into the HRTM to generate more realistic dose estimates than those obtained using ICRP reference values (Bolch et al., 2001, 2003; Fritsch, 2006; Marsh and Birchall, 2009). The uncertainties of these values can be grouped into the following categories:

i) Uncertainties in the HRTM parameters for the particle deposition model

ii) Uncertainties in HRTM parameters for the particle transport model

iii) Uncertainties in the HRTM parameters for the particle dissolution/absorption model

iv) Uncertainties in HRTM parameters for the dosimetry model

4.4.1 Probability distributions for HRTM particle deposition parameters

Skubacz and Wołoszczuk (2019) demonstrated that the dose received by the respiratory tract from radon progeny depends heavily on the size distribution of the aerosols, breathing mode, and breathing rate. Since the dose depends heavily on breathing mode, it is typically higher for mouth breathing than for nose breathing at the same rate. Uncertainties in the parameters of the particle deposition model fall into four categories: uncertainties in the aerosol parameters, the fraction of air inhaled through the nose, the deposition efficiencies of aerosols in different HRTM regions, and the anatomical and physiological parameters of the subjects.

4.4.1.1 Aerosol parameters

The probability distributions assigned to the radon progeny aerosol parameters were primarily based on the work of Marsh (2022), who compiled and analyzed measured data from various studies conducted in mines (Butterweck et al., 1992; Birchall and James, 1994; Postendörfer and Reineking, 1999). Aerosol parameter values are presented for the two exposure scenarios defined by epidemiologists in the RadoNorm project (Deffner, personal communication). These scenarios and their respective distributions were adopted for this study. Tables 15 and 16 present the probability distributions assigned to the aerosol parameters for inhaling radon progeny by underground miners under Jobs 1 and 4, respectively.

Table 15: Radon progeny aerosol parameter probability distributions for Job 1.

Parameter description	**Central value**	**Probability distribution**		
		Form	**A[e]**	**B[f]**
Unattached fraction[a], f_p	0.03[c]	uniform	0.005	0.07
Unattached aerosol size, AMTD (nm)	1.0[d]	lognormal	1	1.3
Unattached hygroscopic growth factor, hgf	1.0[c]	constant		
Unattached particle density, ρ (g/cm^3)	1.0[d]	constant		
Unattached shape factor, χ	1.0[d]	constant		
Attached fraction, (1-f_p)	0.97[c]			
Attached aerosol size, AMAD (nm)	350[b]	uniform	235	460
Attached dispersion	2.0[b]	uniform	1.8	3.0
Attached hygroscopic growth factor, hgf	1.5[b]	uniform	1.0	2.0
Attached particle density, ρ(g/cm^3)	1.4[c]	constant		

Attached shape factor, χ	1.1[c]	constant		
Equilibrium factor (F)	0.2[b]	uniform	0.1	0.5

[a] Expressed as a fraction of total PAEC of the radon progeny mixture.

[b] Data taken from Marsh, 2022.

[c] Data taken from Marsh et al., 2012.

[d] Data taken from ICRP, 2017.

[e] Minimum value of uniform distribution/ geometric mean of lognormal distribution.

[f] Maximum value of uniform distribution/ geometric standard deviation for lognormal distribution.

Table 16: Radon progeny aerosol parameter probability distributions for Job 4.

Parameter description	**Central value**	**Probability distribution**		
		Form	**A[d]**	**B[e]**
Unattached fraction[a], f_p	0.01[g]	uniform	0.005	0.02
Unattached aerosol size, AMTD (nm)	1.0[b]	lognormal	1	1.3
Unattached hygroscopic growth factor, hgf	1.0[c]	constant		
Unattached particle density, ρ (g/cm^3)	1.0[b]	constant		
Unattached shape factor, χ	1.0[b]	constant		
Attached fraction, (1-f_p)	0.99[c]			
Attached aerosol size, AMAD (nm)	560[c]	lognormal	560	4.0
Attached hygroscopic growth factor, hgf	1.0[c]	constant		
Attached particle density, ρ(g/cm^3)	2.5[c]	constant		
Attached shape factor, χ	1.5[c]	constant		
Equilibrium factor (F)	0.6[g]	uniform	0.4	0.8

Expressed as a fraction of total PAEC of the radon progeny mixture.

[b] Data taken from ICRP, 2017.

[c] Data taken from Marsh et al., 2012.

[d] Minimum value of uniform distribution/ geometric standard deviation for lognormal distribution.

[e] Maximum value of uniform distribution/ geometric standard deviation for lognormal distribution

[g] Data taken from Marsh, 2022.

Various authors (Duport and Edwardson, 1984; Duport and Horvath, 1989; Bigu, 1990) have carried out particle size measurements for aerosols in underground uranium mines with wet drilling. Marsh et al. (2012) summarized these findings and adopted a value of 7 µm to represent an aerosol of long-lived radionuclides in underground mines, with a possible range of values between 4 and 14 µm. According to Duport and Edwardson (1984), the dispersion of aerosols for this mining method ranges from 3 to 5, whereas the ICRP (1994), recommends using the default value of 2.5. Based on this information, the activity size distribution of aerosols containing long-lived radionuclides in underground mines with wet drilling was assigned a lognormal distribution with a median value of 7 µm and a geometric standard deviation (GSD) of 1.4. The dispersion distribution assigned to this job type was uniform, ranging from a minimum of 2.5 to a maximum of 5.0, based on the range of possible values presented by Duport and Edwardson (1984).

The probability distributions for the aerosol parameters for dry drilling were obtained from the data analyzed by Marsh et al. (2012), who examined measurements carried out by Postendorfer

(2001). For this job type, Marsh et al. (2012) recommends an average AMAD value of 4.7 µm, with possible values ranging from 4 µm to 6 µm, and an average aerosol dispersion of 2.0, with possible values ranging from 1.6 to 2.8. Based on this information, both parameters were assigned a uniform probability distribution with minimum and maximum values of 3 µm and 6 µm, respectively, for the particle size of the aerosol, and values ranging from 1.6 to 2.8 for the aerosol dispersion. Additionally, ICRP HRTM defaults (ICRP, 1994) were assumed for particle density and shape factor, and the probability distributions for these two parameters were adopted from the work of Fritsch (2006). The aerosol parameters and their respective probability distributions for long-lived radionuclides in uranium ore dust are presented in Tables 17 and 18 for Jobs 1 and 4, respectively.

Table 17: Aerosol parameter probability distributions for inhalation of uranium ore dust under Job 1 conditions.

Parameter description	**Central value**	**Probability distribution**			
		Form	**A[c]**	**B[d]**	**C[e]**
Particle size, AMAD (µm)	7[a]	lognormal	7	1.4	
Particle dispersion, GSD	2.5[a]	uniform	2.5	5.0	
Particle density, ρ (g/cm^3)	3.0[b]	triangular	1.0	10.0	3.0
Particle shape factor, χ	1.5[b]	triangular	1.1	1.9	1.5

[a]Data taken from Marsh, 2012.

[b]Data taken from Fritsch, 2006.

[c] Minimum value for a uniform/triangular distribution or median for the lognormal distribution.

[d] Maximum value for a uniform/triangular distribution or GSD for the lognormal distribution.

[e] Mode for a triangular distribution.

Table 18: Aerosol parameter probability distributions for inhalation of uranium ore dust under Job 4 conditions.

Parameter description	**Central value**	**Probability distribution**			
		Form	**A[c]**	**B[d]**	**C[e]**
Particle size, AMAD (µm)	4.7[a]	uniform	3.0	6.0	
Particle dispersion, GSD	2.0[b]	uniform	1.6	2.8	
Particle density, ρ (g/cm^3)	3.0[f]	triangular	1.0	10.0	3.0
Particle shape factor, χ	1.5[f]	triangular	1.1	1.9	1.5

[a]Data taken from Marsh, 2012.

[b]Data taken from Pöstendorfer, 2006.

[c] Minimum value for a uniform/triangular distribution or median for the lognormal distribution.

[d] Maximum value for a uniform/triangular distribution or GSD for the lognormal distribution.

[e] Mode for a triangular distribution.

[f]Data taken from Fritsch, 2006.

4.4.1.2 Fraction of air breathed through the nose (F_n)

The nose is considered a more effective filter than the mouth. Therefore, the dose delivered to the lungs is sensitive to the fraction of ventilatory airflow passing through the nose (Marsh and Birchall, 2009). The breathing patterns of 30 healthy young adults were studied. Twenty of the subjects were normal augmenters who switched to oronasal breathing at a ventilation rate of 2.1 m³/h during the transition from light to heavy exercise. Five subjects were pure nose breathers who continued to breathe through the nose, even during vigorous exercise. Four

subjects were habitual mouth breathers who breathed oronasal at all levels of exercise. The remaining subject showed no consistent pattern (Niinima et al., 1980, 1981).

Ruzer et al. (1995) reported that, on average, a driller spends 10% of his time resting, 80% performing light exercise, and 10% performing heavy exercise. Marsh and Birchall (2009) combined this information and assigned a triangular probability distribution to this parameter with a minimum value of 0.3 and an apex at 1.

4.4.1.3 Subject anatomical and physiological parameters

The anatomical and physiological characteristics of subjects that introduce uncertainties in the HRTM deposition model have been presented elsewhere (ICRP, 1994; Bolch et al., 2001; Fritsch, 2006). According to Fritsch (2006), the deposition model requires the following parameters: tracheobronchial tree diameters (d_x), dead space volumes for the endotracheal tube (ET) region (VD_ET), bronchi (VD_BB), bronchioles (VD_bb), total dead space (VD), tidal volume (V_T), ventilation rate (B), volumetric flow rate (V_f), and functional residual capacity (FRC). These parameters can be calculated as a function of the subject's age and height (Bolch et al., 2001; Fritsch, 2006).

Bolch et al. (2001) calculated VD, VD_(ET), VD_(BB), VD_(bb), and tracheal diameter (d_0) as functions of subject height (H_t). Fritsch (2006) calculated BB (d_9) and bb (d_{16}) diameters as functions of d_0. He assigned normal probability distributions to these diameters, with standard deviations of 0.1, 0.1, and 0.2 for d_0, d_9 and d_{16} respectively. In their studies, these authors used the calculated values of d_0, d_9, and d_{16} to derive the corresponding scaling factors for the subject's airway dimensions relative to the reference man's dimensions when calculating aerodynamic and thermodynamic deposition efficiencies.

Ventilation rates can be calculated by considering the amount of oxygen required according to basal metabolic rate and activity level (Layton, 1993; Bolch et al., 2001; Fritsch, 2006; Marsh and Birchall, 2009). The ICRP (1994) defines a standard worker as someone who breathes only through their nose, sits for one-third of their workday, and performs light exercise for the rest of their workday. The ICRP also considers habitual mouth breathers, for whom the nasal breathing fraction is 0.7 and 0.4 while sitting and performing light activity, respectively. Fritsch (2006) used this information to assign uniform probability distributions to the default activity level values. The probability distributions assigned to the subject's anatomical and physiological parameters are shown in Table 19.

Table 19: Probability distributions for subject parameters of the HRTM deposition model.

Parameter description and calculation	Distribution type	A[e]	B[f]
Age (***A***, years)	Constant	30	
Body height ($\boldsymbol{H_t}$, cm)	Normal[b]	176.70	6.70
Body mass index (***BMI***, kg/m^2) $\boldsymbol{W_t = H_t^2 . BMI}$	Lognormal[b]	24.89	1.17
Fraction breathed through nose (F_n)	Triangular[c]	0.30	1.00[d]
Airway diameter (cm)			
Trachea: $\boldsymbol{d_o = (0.00902 . H_t + 0.06225) . Ed_o}$			

$\boldsymbol{Ed_o}$ **relative error**	Normal[a]	1.00	0.10
Bronchi: $\boldsymbol{d_9 = (0.00049.H_t + 0.07930).Ed_9}$			
$\boldsymbol{Ed_9}$ relative error	Normal[a]	1.00	0.10
Bronchioles: $\boldsymbol{d_{16} = (0.0002.H_t + 0.04917).Ed_{16}}$			
$\boldsymbol{Ed_{16}}$ **relative error**	Normal[a]	1.00	0.20
Anatomical dead spaces (ml): $\boldsymbol{V_D = 8.72 \exp(0.0162H_t).E_{VD}}$			
$\boldsymbol{E_{VD}}$ relative error	Lognormal[b]	1.00	1.17
$\boldsymbol{V_D(ET) = 18.37.d_o^2}$ $\boldsymbol{V_D(BB) = V_D(bb) = 0.5[V_D - V_D(ET)]}$			
Functional residual capacity (ml): $\boldsymbol{FRC = 23.48H_t + 9.0A - 1093 + E_{FRC}}$			
$\boldsymbol{E_{FRC}}$ residual error	Normal[b]	0.00	600.00
Vital Capacity (ml) $\boldsymbol{VC = 61.0H_t - 28.0A - 4650 + E_{VC}}$			
$\boldsymbol{E_{VC}}$ residual error term	Normal[b]	0.00[b]	560.00
Ventilation rate (ml/min): $\boldsymbol{V_E = V_Q.V_{O2}}$ $\boldsymbol{V_{O2} = (0.694.BMR.H_{oxy}).B_{mult}}$			
Ventilatory equivalent ratio $\boldsymbol{VQ}$ distribution	Lognormal[b]	26.40	1.16
Basal metabolic rate (MJ/d): $\boldsymbol{BMR = 0.063W_t + 2.896 + E_{BMR}}$			
$\boldsymbol{E_{BMR}}$ residual error on BMR	Normal[b]	0.00	0.6702
Amount of O_2 required to produce 1 kJ (L) $\boldsymbol{H_{oxy}}$	Uniform[b]	0.0476	0.0529
Basal multiplication factor ($\boldsymbol{B_{mult}}$):			
Resting	Uniform[b]	1.00	1.10
Sitting	Uniform[b]	1.10	1.40
Light exercise	Uniform[b]	2.00	5.00
Heavy exercise	Uniform[b]	5.50	8.50
Breathing frequency (min^{-1}) Sitting $\boldsymbol{B_f = 12E_{Bf}}$ Light exercise $\boldsymbol{B_f = 20E_{Bf}}$ Heavy exercise $\boldsymbol{B_f = 26E_{Bf}}$			
$\boldsymbol{E_{Bf}}$ relative error	Lognormal[a]	1.00	1.25
Standard worker			
Fraction of sitting during 8 h (remaining light exercise)	Uniform[a]	0.21	0.41
Nose breather			
Sitting fraction breathed through the nose	Uniform[a]	0.90	1.00
Light exercise: Fraction breathed through the nose	Uniform[a]	0.90	1.00
Mouth augmenter			
Sitting fraction breathed through the nose	Uniform[a]	0.60	0.80
Light exercise: fraction breathed through the nose	Uniform[a]	0.30	0.50
Heavy worker			

Fraction of light exercise during 8 h (remaining heavy exercise)	Uniform[a]	0.78	0.98
Nose breather			
Light exercise: fraction breathed through the nose	Uniform[a]	0.90	1.00
Heavy exercise: fraction breathed through the nose	Uniform[a]	0.30	0.50
Mouth augmenter			
Light exercise: fraction breathed through the nose	Uniform[a]	0.20	0.40
Heavy exercise: fraction breathed through the nose	Uniform[a]	0.20	0.40

[a]Data obtained from Fritsch, 2006.

[b]Data obtained from Bolch et al., 2001.

[c] Data obtained from Marsh and Birchall, 2009.

[d] Parameter assigned a triangular distribution with the vertex representing both the maximum value and mode of the distribution.

[e] Minimum value for a uniform/triangular distribution or mean for the normal distribution or geometric mean for the lognormal distribution.

[f] Maximum value for a uniform/triangular distribution or standard deviation for the normal distribution or geometric standard deviation for the lognormal distribution.

4.4.1.4 Aerosol deposition efficiencies of different HRTM regions

The ICRP (1994) provides mathematical expressions for calculating the aerodynamic and thermodynamic filtration efficiencies of the various HRTM regions. These efficiencies are calculated according to equations (4.2) through (4.7).

$$\eta_{ae} = 0.5\left[1 - {}^{1}/_{(aR^{p}+1)}\right] \text{..... (4.2)}$$

$$\eta_{th} = 0.5[1 - \exp(-aR^{p})] \text{..... (4.3)}$$

$$\eta_{ae} = 1 - {}^{1}\Big/_{\left(aR_{th}^{p}+1\right)} \text{..... (4.4)}$$

$$\eta_{th} = 1 - \exp(-\alpha R^{p}) \text{..... (4.5)}$$

$$\eta_{ae} = 1 - \exp(-aR^{p}) \text{..... (4.6)}$$

$$\eta_{th} = 1 - \exp(-aR^{p}) \text{..... (4.7)}$$

Where a and p are constants and R varies with aerosol size and subject characteristics. Equations (4.2) and (4.3) apply to particle deposition in ET_1, equations (4.4) and (4.5) to particle deposition in ET_2, and equations (4.6) and (4.7) to particle deposition in the thoracic region. In each region of the HRTM, the total deposition is a combination of the two independent equations.

Fritsch (2006) demonstrated that these uncertainties can be addressed by multiplying the fitting parameters a_i in Tables 12 and 13 of ICRP Publication 66 (ICRP, 1994) by the random variables $C_{ae(j)}$ and $C_{th(j)}$ for the aerodynamic and thermodynamic deposition mechanisms, respectively, in each HRTM region. These random variables are assigned lognormal distributions with a mean of one and a GSD equal to the square root of c_j (Table 14 of ICRP Publication 66). These distributions are summarized in Table 20.

Table 20: Probability distributions for the aerosol deposition efficiencies in different HRTM regions.

Parameter	Distribution	Median	GSD
$C_{ae}(ET_1)$	lognormal	1.00	1.82

$C_{ae}(ET_2)$	lognormal	1.00	1.82
$C_{ae}(BB)$	lognormal	1.00	1.58
$C_{ae}(bb)$	lognormal	1.00	1.58
$C_{ae}(AI)$	lognormal	1.00	1.30
$C_{th}(ET_1)$	lognormal	1.00	1.18
$C_{th}(ET_2)$	lognormal	1.00	1.18
$C_{th}(BB)$	lognormal	1.00	1.23
$C_{th}(bb)$	lognormal	1.00	1.23
$C_{th}(AI)$	lognormal	1.00	1.23

4.4.2 Probability distributions for HRTM particle transport parameters

The ICRP derived particle transport rates in the HRTM from several studies using laboratory animals and an element of expert judgment (Bolch et al., 2003; Puncher and Burt, 2013). The ICRP's key assumption in their derivation is that variability in particle transport within the HRTM varies by a factor of three around the reference value. Thus, the uncertainty in these rates can be represented by a lognormal distribution with a median equal to the ICRP reference value and a GSD of 1.73 (Puncher and Burt, 2013).

However, Puncher and Burt (2013) stated that material moves from the AI region to the bb region and thoracic lymph nodes (LN_{TH}) by processes different from those governing particle transport from the BB and bb airways. The former is facilitated by macrophages in the AI region, while the latter is facilitated by mucociliary transport along the airway walls. Based on this, Puncher (2014a) proposed that the variability in the clearance rate from the alveolar region (ALV) to the bb region could be represented by a lognormal distribution with a median equal to the ICRP reference value and a GSD of 3.2, while the clearance rate from the ALV to the interstitium (INT) could be represented by a lognormal distribution with a median equal to the ICRP reference value and a GSD of 4.5. Due to the slow rate, the variability in the rate from the interstitium to the thoracic lymph nodes was represented by a lognormal distribution with a median equal to the ICRP reference value and a GSD of 3.0.

The particle transport rates relevant to uncertainties in the calculated lung dose from radon progeny inhalation are the rates from BB to ET_2 and from ET_2 to the alimentary tract. The other rates are considered too slow to significantly alter the calculated lung dose since it is assumed that the deposited material decays in situ. The probability distributions associated with these rates are shown in Table 21.

Table 21: Probability distributions for the particle transport rates of the HRTM

From	**To**	**Reference value[a] (d^{-1})**	**Distribution**	**Median**	**GSD**
bb	BB	0.2	lognormal[b]	1.00	1.73
BB	ET_2	10	lognormal[b]	1.00	1.73
ET_2	Oesophagus	100	lognormal[b]	1.00	1.73
ET_1	ET_2	1.5	lognormal[b]	1.00	1.73
ET_1	Environment	0.6	lognormal[b]	1.00	1.73
BBseq	LN_{TH}	0.001	lognormal[b]	1.00	1.73

bb_{seq}	LN_{TH}	0.001	lognormal[b]	1.00	1.73
ETseq	LNET	0.001	lognormal[b]	1.00	1.73
ALV	bb	0.002	lognormal[c]	0.002	4.50
ALV	INT	0.001	lognormal[c]	0.001	3.20
INT	LN_{TH}	0.00003	lognormal[c]	0.00003	3.00

[a] The reference value was obtained from ICRP publication 130 (ICRP, 2015).

[b] The uncertainty on these correlated parameters was introduced by multiplying the ICRP reference value with a value obtained from a random variable sampled from a lognormal probability distribution with a median of 1.0 and GSD of 1.73.

[c] Data taken from Puncher (2014a).

4.4.3 Probability distributions for HRTM target cell parameters

It is assumed that the depth and thickness of the target cell layer are correlated with epithelial thickness. Here, epithelial thickness is used to introduce a correlation between target cell layer depth and thickness (Marsh and Birchall, 2009). The ICRP (1994) adopted a reference value of 55 µm for the epithelial thickness of the BB region of the HRTM, based on data from Mercer et al. (1991). However, a lower value for this parameter was reported in the measurements of Harley et al. (1996).

Harley et al. (1996) reported a mean basal cell depth of 27 µm in airway generations 3 to 6. However, the HRTM assumes a uniform distribution of basal cells in a 15 µm layer at a depth of 35 µm (i.e., a mean depth of 43 µm) in the BB region. This assumption is consistent with the data of Mercer et al. (1991).

Marsh and Birchall (2009) used this information to assume a rectangular distribution of BB epithelial thickness ranging from 30 to 75 µm to reflect intra and inter-subject variability with the lower value being consistent with the data of Harley et al. (1996). These authors also based the distribution of epithelial thickness in the BB region on the data of Mercer et al. (1991), which reflects intra and inter-subject variation. Furthermore, Marshall and Birchall (2009) derived the probability distribution for mucus sol thickness from measurements reported in ICRP Publication 66 (ICRP, 1994). The assumed probability distributions for these parameters in this work are given in Table 22.

Table 22: Probability distributions for the HRTM target cell parameters

Description of parameter	**HRTM reference value (µm)**	**Probability distribution**		
		Form	**A[d]**	**B[e]**
Bronchial epithelium thickness (E_{BB})[a]	55	uniform	30µm	75µm
Bronchial basal cell layer depth[b]	35	$35E_{BB}/55$		
Bronchial basal cell layer thickness	15	$15E_{BB}/55$		
Bronchial secretory cell layer depth[c]	10	$10E_{BB}/55$		
Bronchial secretory cell layer thickness	30	$30E_{BB}/55$		

Bronchial mucus (gel) thickness	5	lognormal	4µm	2
Bronchial mucus (sol) thickness	6	normal	6µm	1µm
Bronchiolar epithelium thickness (E_{bb})[a]	15	uniform	8µm	22µm
Bronchiolar secretory cell layer depth[c]	4	$4E_{bb}/15$		
Bronchiolar secretory cell layer thickness	8	$8E_{bb}/15$		
Bronchiolar mucus (gel) thickness	2	lognormal	1.6µm	2
Bronchiolar mucus (sol) thickness	4	normal	4µm	1µm

[a] Parameter not used directly in the model but are used to introduce correlation between model parameters which are functions of them.

[b] Depth of basal cell layer is defined here as in ICRP Publication 66 as the distance from the luminal surface of the epithelium (excluding cilia) to the beginning of the basal cell layer.

[c] Depth of secretory cell layer is defined here as in ICRP Publication 66 as the distance from the luminal surface of the epithelium (excluding cilia) to the beginning of the secretory cell layer.

[d] Minimum value of uniform distribution / mean of normal distribution/geometric mean of lognormal distribution.

[e] Maximum value of uniform distribution/standard deviation of normal distribution/ geometric standard deviation of lognormal distribution.

4.4.4 Probability distributions for HRTM dissolution/absorption parameters

The HRTM dissolution/absorption parameters relevant to dose calculation are;

i) Dissolution parameters, i.e., the fraction of rapidly dissolving material, f_r, the dissolution rate of the rapid fraction, s_r, and the dissolution rate of the slow fraction, s_s.

ii) Bound state parameters such as the fraction of bound material, f_b, and the absorption rate of bound material into blood, s_b.

Studies have been conducted to determine the absorption parameters of unattached and attached radon progeny in the lungs after inhalation, and the results have been published in the literature (Butterweck et al., 2002; Marsh and Bailey, 2013). The ICRP (2017) assigns independent parameters to polonium, lead, and bismuth as radon progeny and assumes that lead progeny binds to the respiratory tract. Additionally, the ICRP assumes common kinetics for radon progeny formed in the HRTM and independent kinetics for the absorption of material cleared from the HRTM to the alimentary tract by mucociliary transport into the blood (ICRP, 2015; 2017).

Furthermore, ICRP assumes only a fast component with biological half-lives of 5.5 hours for polonium isotopes and 17 hours for bismuth isotopes, with no bound state. A fast absorption rate with a biological half-life of 10 minutes is assumed for 10% of lead isotopes; with the remaining fraction being absorbed at a rate with a biological half-life of 9.8 hours. Retention in the airway walls is assumed to have a biological half-life of 9.8 hours for the bound state (Hu et al., 2020). Table 23 shows the dissolution/absorption parameters for radon progeny published in ICRP Publication 137 (ICRP, 2017).

The probability distributions for the absorption parameters of lead as radon progeny were derived from several measurement results (Booker et al., 1969; Hursh et al., 1969; Hursh and Mercer, 1970; Marsh and Birchall, 2013). For lead progeny, values of the rapid dissolution fraction ranged from 0.06 (Booker et al., 1969) to 0.35 (Greenhalgh et al., 1982). Other

researchers reported values of 0.2 (James et al., 1997) and 0.1 (Greenhalgh et al., 1978; Marsh and Bailey, 2013; ICRP, 2017). Based on this information, a uniform probability distribution was adopted for this parameter, ranging from a minimum of 0.06 to a maximum of 0.12. The rapid absorption rate for lead progeny has been reported in the literature to range from 58 d^{-1} (Greenhalgh et al., 1982) to 1,000 d^{-1} (Butterweck et al., 2002). Other reported values include 67 d^{-1} (Booker et al., 1969; Hursh et al., 1969; Hursh and Mercer, 1970; Greenhalgh et al., 1982), 100 d^{-1} (Greenhalgh et al., 1978; Marsh and Bailey, 2013; ICRP, 2017), and 250 d^{-1} (James et al., 1997). Since these values differ by more than an order of magnitude, it was best to describe this parameter's probability distribution as lognormal, with a median value of 100 d^{-1} (the ICRP reference value) and a GSD of 3.20.

The values reported in the literature for the slow dissolution rate of lead as radon progeny range from 1.3 d^{-1} (Hursh et al., 1969) to 1.8 d^{-1} (James et al., 1997). Other reported values include 1.4 d^{-1} (Booker et al., 1969; Hursh and Mercer, 1970; Bianco et al., 1973) and 1.7 d^{-1} (Greenhalgh et al., 1982; Booker et al., 1969; Marsh and Bailey, 2013; ICRP, 2017). Since these values vary minimally within a well-defined range, it was necessary to assign a uniform probability distribution to this parameter with minimum and maximum values of 1.3 and 1.8, respectively. Published values in the literature for the parameter that defines the rate of transfer of lead ions from the bound state to blood range from 0.5 d^{-1} (Boudène et al., 1977) to 5.7 d^{-1} (Chamberlain et al., 1978). Other reported values include 1.7 d^{-1} (Greenhalgh et al., 1982; Butterweck et al., 2002; Marsh and Bailey, 2013; ICRP, 2017). Due to the large variation in this value, the parameter was assigned a lognormal distribution with a median equal to the ICRP reference value (1.7 d^{-1}) and a GSD of 1.73. The variation in the fraction of lead absorbed from the alimentary tract into the bloodstream was modelled using a regression of the fractional absorption value of ingested lead and the rapid dissolution fraction (f_r).

Most of the experimental evidence on the absorption characteristics of radon progeny relates to short-lived lead progeny, such as Pb-214 and Pb-212. Specifically, experimental evidence on binding to the respiratory tract only relates to lead. Furthermore, dosimetric calculations of past radon progeny intake assumed that all radon progeny (Po-218, Pb-214, and Bi-214) had the same absorption characteristics, based on information about lead (Marsh and Bailey, 2013; Makumbi et al., 2024a). Consequently, there is limited data on the absorption of bismuth and polonium in animals and humans.

The ICRP has now published different absorption parameters for short-lived radon progeny, assuming no binding to the epithelium for bismuth and polonium. Furthermore, the published data suggest assignment to type F absorption (ICRP, 2017; Makumbi et al., 2024a). Therefore, probability distributions for the absorption parameters of bismuth and polonium progeny had to be derived in this work. Based on this information, the rapid dissolution fraction was assigned a uniform probability distribution ranging from 0.7 to 1.0 for both bismuth and polonium. The rapid dissolution rate for each progeny was assigned a lognormal probability distribution, setting the median equal to the ICRP reference value and the GSD to 3.2. The probability distributions assigned to the short-lived radon progeny are given in Table 23.

Table 23: Probability distributions for dissolution/absorption parameters for radon progeny.

Nuclide	Parameter	Reference value[a]	Probability distribution	A[b]	B[c]
Polonium	f_r	1.00	uniform	0.70	1.00
	s_r	3.00	lognormal	3.00	3.20
	s_s	0.00	constant		
	f_b	0.00	constant		
	s_b	0.00	constant		
	f_A	0.10	$0.10*f_r$[d]		
Lead	f_r	0.10	uniform	0.06	0.12
	s_r	100.00	lognormal	100.00	3.20
	s_s	1.70	uniform	1.30	1.80
	f_b	0.50	uniform	0.25	0.70
	s_b	1.70	lognormal	1.70	1.73
	f_A	0.20	$0.20*f_r$[d]		
Bismuth	f_r	1.00	uniform	0.70	1.00
	s_r	1.00	lognormal	1.00	3.20
	s_s	0.00	constant		
	f_b	0.00	constant		
	s_b	0.00	constant		
	f_A	0.05	$0.05*f_r$[d]		

[a]Data taken from ICRP, 2017.

[b]Minimum value for a uniform distribution and median value for a lognormal distribution.

[c]Maximum value for a uniform distribution and GSD for a lognormal distribution.

[d]The probability distribution for f_A parameter is derived from a correlation with f_r i.e., uncertainty is introduced on this parameter by multiplying the ICRP reference value for ingestion of the element with the sampled value of the f_r parameter from its respective probability distribution during Monte Carlo simulation.

Absorption parameters for long lived radionuclides in uranium ore dust were estimated by Marsh et al. (2012) based on the findings from two studies (Duport et al., 1991; Beckova and Malatova, 2008) and are presented in Table 13 of chapter 3. In their study, Duport et al. (1991), investigated the influence of the ore grade, particle size and pH of the solution on the absorption rates. The authors expressed their results as undissolved fractions which were functions of time with two components i.e., the rapid component and the slow component. For U-238, the rapid dissolved fraction was approximately 25% indicating assignment to Type M with no observable effect on size in total dissolution over 40 days for particles in size ranges 7-10, 3-7, 1-3 and less than 1 μm for the high-grade ore.

For medium and low-grade ores, measurements were done for 12 days but only for particle sizes of at least 37μm. The rapidly dissolved fraction results for U-238 were approximately

0.33 and 0.5 respectively for low and medium grade ores. Another study by Beckova and Malatova (2008), measured the dissolution of U-238, U-234 and Th-230 in simulated serum ultra-filtrate of uranium ore dust collected on personal air filters in a uranium mine in Czech Republic for 26 days. The retention was represented by a two-component exponential function representing both the rapid and slow dissolution. The results for parameter values of U-238 were $f_r = 0.14$, $s_r = 0.49\ d^{-1}$ and $s_s = 0.004d^{-1}$ indicating assignment to Type M. However, due to alpha recoil phenomena, the dissolution of U-234 was relatively faster with parameter values $f_r = 0.18$, $s_r = 0.49\ d^{-1}$ and $s_s = 0.006d^{-1}$.

Based on the above information it was assumed reasonable to assign a triangular probability distribution to the rapid dissolution fraction of uranium isotopes characterized by a minimum value of 0.14, maximum value of 0.33 with mode at 0.22. Owing to the small range of values within the same order of magnitude, the rapid dissolution rate was assigned a uniform probability distribution with a minimum value of 0.49 and a maximum value of 0.78. The probability distribution assigned to the slow dissolution rate was also uniform with a minimum value of 0.0014 and maximum value of 0.006.

Studies were conducted to determine the absorption parameters for Th-230 and Th-232 isotopes in uranium ore dust (Duport et al., 1991; Reif et al., 1994; Chen et al., 1995; Beckova and Malatova, 2008; Marsh et al., 2012). Results from two of these studies showed that no dissolution of Th-230 was detected hence indicating assignment to Type S. Duport et al. (1991), obtained rapid dissolution fractions of 0.15 and 0.01 for Th-230 and Th-232 respectively. The value of 0.15 for Th-230 indicates assignment to Type M while that of Th-232 indicates assignment to Type S. Reif et al. (1994), measured the dissolution rates in simulated lung fluid of thorium residues from two different uranium mill tailings in USA for 100 days. Dissolution parameters calculated for one sample were $f_r = 0.0$ and $s_s = 0.00064\ d^{-1}$ indicating assignment to Type S while for the other sample, the calculated values were $f_r = 0.3$, $s_r = 0.23d^{-1}$ and $s_s = 0.0041d^{-1}$ indicating assignment to Type M.

Using the above data, it was decided to assign the rapid dissolution fraction for thorium isotopes a lognormal distribution characterized by a median value of 0.06 and GSD of 2.34; the 95% confidence interval for this distribution ranges from 0.01 to 0.33 since this parameter varies by an order of magnitude. The median and GSD of the above distribution were arrived at as follows; First, it is known that the lower limit of the 95% confidence interval for the lognormal distribution is given by the quotient of the median and the square of the GSD value. Hence, Assuming the distribution is characterised by a median value x and GSD value z; this quotient was then assigned to the lowest value available in the literature for this parameter (0.01).

It is also known that the higher limit of the 95% confidence interval for a lognormal distribution is given by the product of the median and square of the GSD value; this product was assigned to the highest value for this parameter available in the above literature (0.30). The mathematical translation of the above statements led to two simultaneous equations as follows.

$$\frac{x}{z^2} = 0.01 \dots\dots\dots (i)$$

$$x.z^2 = 0.30 \dots\dots (ii)$$

Making x the subject in both equations (i) and (ii) and solving for z gave a value of 2.34 which is the GSD for the distribution. This value when substituted back in either equation gives a value of 0.06 for x which is the median value for the distribution.

The probability distribution assigned to the rapid dissolution rate was lognormal with a median value of 1.03d^{-1} and GSD of 2.11; this was because this parameter varied by an order of magnitude while a uniform distribution was assigned to the slow dissolution rate with a minimum value of 0.00041 and maximum value of 0.00068 due to the limited range of variation for this parameter.

Duport et al. (1991) reported fractions of Ra-226 that was absorbed rapidly to be 0.12 and 0.07 for high grade and low to medium grade ores respectively. These fractional values differ by an order of magnitude and point to an indication of assignment to Type M and S for high grade and low to medium grades respectively for radium isotopes. In the absence of more specific data, one can conclude that absorption parameters for radium isotopes lie between solubility Type M and S for long lived isotopes of radium in uranium ore dust. Therefore, the probability distribution that was assigned to this parameter was a lognormal distribution with a median value of 0.09 and GSD of 1.14; these values were arrived at using a similar approach as described for its thorium counterpart.

Probability distributions for the rapid dissolution rate and the slow dissolution rate were derived from the values published by Marsh et al. (2012) and ICRP (2017) for Type M and Type S parameters of radium. According to ICRP (2017), the rapid dissolution rate of radium is 3 d^{-1} for both Type M and Type S solubility, while Marsh et al. (2012) gives a value of 7.32 d^{-1} for this parameter. Published values for the slow dissolution rate are 0.00041 d^{-1} (Marsh et al., 2012) while ICRP (2017) recommends the use of 0.005 d^{-1} for Type M and 0.0001 d^{-1} for Type S. Hence, the assigned probability distribution to the rapid dissolution rate was a uniform distribution with a minimum value of 3 d^{-1} and a maximum value of 7.32 d^{-1} considering the limited range of variation for this parameter. Because values for the slow dissolution rate varied by over an order of magnitude, it was assigned a lognormal probability distribution with a median value of 0.00041 and GSD of 2.76.

Values of the rapid dissolution fraction for Pb-210 in uranium ore dust reported in Canadian mines were 0.28 for high grade ore and less than 0.01 for low and medium grade ores (Duport et al., 1991). These values differ by an order of magnitude and indicate assignment to Type M for the high-grade ore and Type S for the low and medium grade ores. Using the above information and the data of Marsh et al. (2012), this parameter was assigned a lognormal distribution with a median value of 0.06 and GSD of 2.30; the 95% confidence interval for this parameter ranges from 0.01 to 0.12. The median and GSD values for the distribution were arrived at using a similar approach for thorium and radium described above.

In the absence of more specific data, it was necessary to combine the data presented by Marsh et al. (2012) and ICRP (2017) to derive probability distribution for the rapid and slow absorption rates. Considering its variation over a very short interval, the rapid dissolution rate for Pb-210 was assigned a uniform probability distribution with a minimum value of 3 d^{-1} (ICRP, 2017) and a maximum value of 3.91 d^{-1} (Marsh et al., 2012). The probability distribution assigned to the slow dissolution rate was lognormal with a median value of 0.001 (Marsh et al., 2012) and GSD of 2.7 owing to the variation of this parameter value by at least an order of magnitude. Since lead isotopes are known to bind to the epithelium, the probability distributions assigned to the bound fraction and the transfer rate from the bound state to blood were the same as those for lead as radon progeny.

Since the absorption parameters of other long-lived radionuclides (Po-210, Th-228, Pa-231 and Ac-227) in the uranium ore dust were obtained as the arithmetic averages of the above values, a similar approach was taken to derive their probability distributions. The first step was to determine the range of possible values for each of these parameters. This was achieved by calculating the arithmetic averages of the corresponding minimum and maximum parameter values for the parameters of the nuclides discussed earlier. For the case of those parameters whose probability distributions were described by uniform and triangular distributions, the minimum and maximum values to be used in the calculation of the arithmetic averages could be directly obtained from the values that characterise these distributions while for parameters having a lognormal distribution, it was necessary to first derive the minimum and maximum values to be used in the calculation of the arithmetic values from the 95% confidence interval for these parameters.

Arithmetic averages for the rapid dissolution fraction ranged between 0.06 and 0.26 while those for the rapid dissolution rate ranged from 1.68 d^{-1} to 4.14 d^{-1}. For the slow dissolution rate, parameter values ranged from 0.0005 d^{-1} to 0.0043 d^{-1}. Since the rapid dissolution fraction values varied by at least an order of magnitude, this parameter was assigned a lognormal distribution with a median value of 0.18 (Marsh et al., 2012) and a GSD of 1.47; the 95% confidence interval for this parameter is between 0.08 and 0.39. The slow dissolution rate was also assigned a lognormal distribution with a median value of 0.00089 d^{-1} and GSD of 1.77: the 95% confidence interval for this parameter ranges between 0.00028 d^{-1} and 0.0028 d^{-1}. On the other hand, the rapid dissolution rate was assigned a uniform distribution with a minimum value of 1.68 d^{-1} and maximum value of 4.14 d^{-1}.

Table 24: Probability distributions for absorption/dissolution parameters[a,b] of long-lived radionuclides in uranium ore dust.

Nuclides	**Parameter**	**Reference value[c]**	**Probability distribution**	**A[d]**	**B[e]**	**C[f]**
U-234, U-235, U-238	f_r	0.22	triangular	0.14	0.33	0.22
	s_r	0.78	uniform	0.49	0.78	
	s_s	0.0014	uniform	0.0014	0.006	
	f_b	0.00	constant			
	s_b	0.00	constant			
	f_A	0.02	$0.02*f_r$[g]			
Ra-226, Ra-224, Ra-228	f_r	0.11	lognormal	0.09	1.14	
	s_r	7.30	uniform	3.00	7.32	
	s_s	0.00041	lognormal	0.00041	2.76	
	f_b	0.00	constant			
	s_b	0.00	constant			

	f_A	0.20	$0.20*f_r^g$		
Th230, Th232	f_r	0.14	lognormal	0.06	2.34
	s_r	4.56	lognormal	1.03	2.11
	s_s	0.00068	uniform	0.00041	0.00068
	f_b	0.00	constant		
	s_b	0.00	constant		
	f_A	0.0005	$0.0005*f_r^g$		
Pb-210	f_r	0.26	lognormal	0.06	2.30
	s_r	3.90	uniform	3.00	3.91
	s_s	0.001	lognormal	0.001	2.70
	f_b	0.50	uniform	0.25	0.70
	s_b	1.70	lognormal	1.70	1.73
	f_A	0.20	$0.20*f_r^g$		
Other	f_r	0.18	lognormal	0.18	1.47
	s_r	4.1	uniform	1.68	4.14
	s_s	0.00089	lognormal	0.00089	1.77
	f_b				
	s_b				
	f_A	0.11	$0.11*f_r^g$		

[a]Values of f_r=0.18, s_r=4.1d^{-1}, s_s=0.00089d^{-1} and f_A=0.02 were assumed for other long-lived radionuclides in the uranium ore dust. These values are the arithmetic mean of those given in Table 21.

[b]Values given in Table 21 for thorium, radium and lead are based on the data of Duport et al. (1991), Beckova and Malatova (2008), Marsh et al. (2012) and ICRP (2017).

[c]Reference parameter values were taken from ICRP (2017).

[d]Minimum value for a uniform/triangular distribution and median value for a lognormal distribution.

[e]Maximum value for a uniform/triangular distribution and GSD for a lognormal distribution.

[f] Mode for the triangular distribution.

[g]The probability distribution for f_A parameter is derived from a correlation with f_r i.e., uncertainty is introduced on this parameter by multiplying the ICRP reference value for ingestion of the element with the sampled value of the f_r parameter from its respective probability distribution during Monte Carlo simulation.

4.5 Probability distributions for HATM particle transport parameters

For particle transport within the HATM, the distributions describing uncertainties in transfer rates were taken from Kwon et al. (2020), who derived transfer rate probability distributions from the uncertainty factors (UF) proposed by Leggett et al. (2007). A lognormal distribution with the median given by the ICRP reference value was assumed in the study by Kwon et al. (2020). These probability distributions are presented in Table 25.

Table 25: Probability distributions for HATM particle transport rates

From	To	Distribution	A[c]	B[d]
Oral cavity	Oesophagus-fast	lognormal	6480	1.52[a]
Oral cavity	Oesophagus-slow	lognormal	720	1.52[a]
Oesophagus-fast	Stomach	lognormal	12343	1.52[a]
Oesophagus-slow	Stomach	lognormal	2160	1.52[a]
Stomach	Small intestine	lognormal	20.57	1.28[b]
Small intestine	Right colon	lognormal	6.00	1.28[b]
Right-colon	Left colon	lognormal	2.00	1.28[b]
Left colon	Rectosigmoid colon	lognormal	2.00	1.28[b]
Rectosigmoid colon	Faeces	lognormal	2.00	1.28[b]

[a] Derived from the proposed UF of 2 for the 95% confidence interval.

[b] Derived from the proposed UF of 1.5 for the 95% confidence interval.

[c] Geometric mean for the lognormal probability distribution.

[d] Geometric standard deviation for a lognormal distribution.

4.6 Probability distributions for systemic model particle transport parameters

The systemic models that are considered in this study for long lived radionuclides are models of elements in the three natural decay series of U-238, Th-232, and U-235. Probability distributions for uranium isotopes were taken from the study done by Puncher and Burt (2013). In this study, the decision on which rate constants to vary was guided by the following considerations (Puncher and Burt, 2013).

(i) Consideration of the weighted equivalent organ doses that contribute most to the effective dose among systemic tissues. For actinide elements, for example, these rates included those governing uptake and retention by the skeleton and liver, uptake into long-term soft tissue compartments (ST_2), and loss from the blood to the urinary bladder.

(ii) Since data describing uranium's biological behaviour in humans is sparse, distributions for rate constants that reproduce the observed range of organ content in available human data sets were selected.

(iii) The selection of distributions was also constrained to ensure that the median values of the simulated bioassay predictions were close to the values calculated using the undisturbed model at different times after intake.

4.6.1 Excretion

To account for variability in the urinary excretion of actinide isotopes among individuals, Puncher and Burt (2013) multiplied the transfer rate from blood to the urinary bladder by three above or below the standard value. They achieved this adjustment by applying a random variable derived from a lognormal distribution with a median of 1 and GSD of 1.73. For alkaline earth isotopes, they introduced variability in the transfer rate from blood to the colon by scaling the rate with a random variable from a lognormal distribution with a median of 1 and a GSD of 1.6 (Puncher, 2014a). Similarly, the rate from blood to the urinary bladder for alkaline earth elements was modified using a random variable drawn from the same distribution (median of 1, GSD of 1.6) (Puncher, 2014a). In the present study, the same lognormal distributions

proposed by Puncher and Burt (2013) for actinide isotopes and the distributions reported by Puncher (2014a) for alkaline earth isotopes were used.

4.6.2 Uptake to the skeleton from blood

All transfer rates from blood to bone surfaces were varied simultaneously under the assumption of complete (100%) correlation among them. This was achieved by applying a scaling factor that was randomly selected from a lognormal distribution with a median of 1 and GSD of 1.3 (Puncher and Burt, 2013; Puncher, 2014b; Puncher and Harrison, 2012a). This sampling method was chosen because it accurately captured the differences in bone retention of alkaline earth elements among individuals, as inferred from human radium retention data (Schlenker et al., 1982) and whole-body strontium retention data compiled by Apostoaei and Miller (2004). The same methodology was applied in this work to model the transfer rates from the skeleton to blood for actinides and alkaline earth elements found in uranium ore dust.

4.6.3 Rates within the skeleton

Under the assumption of full (100%) correlation, all transfer rates from bone surfaces were varied collectively, allowing for a ninefold increase or decrease from the central estimate. This was achieved by applying a shared scaling factor drawn from a lognormal distribution with a median of 1 and GSD of 3 (Puncher and Burt, 2013; Puncher, 2014b). Similarly, transfer rates from bone volume were varied by up to a factor of two above and below their respective reference values. Due to differing physiological mechanisms between exchangeable and non-exchangeable bone volumes, their rate variations were considered uncorrelated. Rates from the exchangeable bone volume were varied together using a common scaling factor drawn from a lognormal distribution with a median of 1 and GSD of 1.4 (Puncher and Burt, 2013; Puncher, 2014b).

A comparable method was applied to the non-exchangeable bone volume, using a scaling factor from a lognormal distribution with a median of 1 and a GSD of 1.4. This approach reflects the range of variation observed in plasma levels of biochemical markers associated with bone resorption in adults (Puncher and Burt, 2013; Puncher, 2014b). The assignment was further informed by the work of Harrison et al. (2007), who developed a similar method for uranium, considered a physiological analog of radium (ICRP, 2015).

In their work, Puncher and Harrison (2012a) applied a uniform scaling approach, varying all rates from bone surfaces to bone volumes by up to a factor of three above or below the reference value. They did the same for rates leading to bone marrow. In their Monte Carlo simulations, they used a common factor, S, to scale rates from bone surfaces and a separate factor, V, to scale rates from bone volume. Both S and V were drawn from lognormal distributions with a median of 1 and a GSD of 1.73. The authors justified using a variation factor greater than two to account for parameter uncertainty and variability in bone turnover rates among individuals. The present study adopted these distributions, as recommended by Puncher and Burt (2013), to evaluate uncertainty in model transfer rates for actinides and long-lived alkaline earth radionuclides present in uranium ore dust.

4.6.4 Rate from blood to liver

Following the approach recommended by Puncher and Burt (2013), the transfer rate from blood to the liver was modelled using a lognormal distribution with a median equal to the ICRP reference value and GSD of 1.4. This method was chosen based on a similar study by Harrison

et al. (2007). However, Puncher and Harrison (2012b) assumed that this rate could vary by a factor of three above or below the central estimate. In their Monte Carlo simulations, they implemented this variability by multiplying the rates by a scaling factor, L, drawn from a lognormal distribution with a median of 1 and a GSD of 1.73, for Pu-239 and Am-241 specifically. In the present study, the distribution proposed by Harrison et al. (2007) was applied to all long-lived alkaline earth isotopes, and the distribution described by Puncher and Harrison (2012b) was applied to actinide isotopes.

4.6.5 Rates to gonads

Due to the limited data regarding the distribution of plutonium and americium in gonads, Puncher and Harrison (2012b) used information about systemic plutonium levels in testes of former Mayak workers, as reported by Suslova et al. (2002). They also used data about americium in four U.S. workers, as provided by McInroy et al. (1989). Based on these sources, they modelled gonadal uptake rates by applying a common variation factor, G, to the rates for both ovaries and testes. They sampled this factor from a lognormal distribution with a median of 1 and GSD of 1.7. The present study employed the same distributions used by Puncher and Harrison (2012b) to model actinide behaviour in uranium ore dust.

4.6.6 Long-term retention in massive soft tissues

Puncher and Burt (2013) modelled the variation in the uptake rate from blood to the massive soft tissue compartment (ST_2) for U-238, and Puncher (2014a) modelled it for Ra-226. In both cases, the rate was assigned a lognormal distribution, with the median set to the ICRP reference value and GSD of 1.73. This study adopted the same distribution for this parameter across all actinide and alkaline earth isotopes present in uranium ore dust.

The probability distributions for the systemic model parameters of the long-lived radionuclides that were used in this study are presented in Table 26.

Table 26: Probability distributions for selected systemic model parameters.

Pathway	**Distribution**	**Median**	**GSD/Distribution of scaling factor**	**Nuclides**	**Remarks**
Rates from blood to skeleton					
Blood->CS/TS	Lognormal	ICRP value	~LN (1, 1.3)	U-238[a]; Ra-226[b]; Am-241[c]	Correlated parameters
Blood1->CV/TV	Lognormal	ICRP value	~LN (1, 1.3)	Am-241[c]	Correlated parameters
Rates from bone surfaces to bone volume					
CS->CV	Lognormal	ICRP value	~LN (1, 1.73)	Am-241[c]	Correlated parameters
TS->TV	Lognormal	ICRP value	~LN (1,1.73)	Am-241[c]	Correlated parameters
Rates from bone surface to bone marrow					
CS->CM	Lognormal	ICRP value	~LN (1, 1.4)	Am-241[c]	Correlated parameters

TS->TM	Lognormal	ICRP value	~LN (1, 1.73)	Am-241[c]	Correlated parameters
Rate from bone surfaces					
CS/TS->Other	Lognormal	ICRP value	~LN (1, 3)	U-238[a]; Ra-226[b]	Correlated parameters
Rates from exchangeable bone volume					
EXCH CV/TV->Other	Lognormal	ICRP value	~LN (1, 1.4)	U-238[a]; Ra-226[b]	Correlated parameters
Rates from nonexchangeable bone volume					
NONEXCH CV/TV->Other	Lognormal	ICRP value	~ LN (1, 1.4)	U-238[a]; Ra-226[b]	Correlated parameters
Rate to soft tissues					
Blood->ST2	Lognormal	ICRP value	1.7	U-238[a]	Uncorrelated parameter
	Lognormal	ICRP value	1.6	Ra226[b]	Uncorrelated parameter
Rate to liver from blood					
Blood->Liver1	Lognormal	ICRP value	1.4	U-238[a]	Uncorrelated parameter
Rates from liver					
Liver->Blood	Lognormal	ICRP value	1.4	Am-241[c]	Uncorrelated parameter
Rate to gonads					
Blood->gonads	Lognormal	ICRP value	~LN (1, 1.73)	Am-241[c]	Correlated parameters
Rate from blood to bladder					
Blood->UBC	Lognormal	ICRP value	1.73	U-238[a]	Uncorrelated parameter
	Lognormal	ICRP value	1.6	Ra-226[b]	Uncorrelated parameter
Rate from blood to upper large intestine					
Blood->Right colon contents	Lognormal	ICRP value	1.6	Ra-226[b]	Uncorrelated parameter

[a] Data taken form Puncher and Burt, 2013.

[b] Data taken from Puncher, 2014a.

[c] Data taken from Puncher and Harrison, 2012b.

~LN (a, b) - parameter assigned a lognormal distribution with median value of a and geometric standard deviation b.

CS:Cortical surface; CV:Cortical volume; CM: Cortical marrow; TM: Trabecular marrow; EXCH CV: Exchangeable cortical volume; EXCH TV: Exchangeable trabecular volume; NONEXCH CV: Nonexchageable cortical volume; NONEXCH TV: Nonexchangeable trabecular volume; ST2: Soft tissues with long term retention; UBC: Urinary bladder contents.

4.7 Extension of INTDOSKIT for uncertainty and sensitivity analysis

The methodology for implementing Monte Carlo simulation for uncertainty and sensitivity analysis in the RadoNorm project followed a structured approach. The primary objective was

to explore uncertainties and sensitivities in model outputs, in radiation dose. This was achieved by randomly sampling parameter values from their respective probability distributions, considering correlations between parameters.

For each iteration, the dose coefficients for committed equivalent dose to the organs of interest and the effective dose were calculated. The result is then a sample of the distribution of the dose coefficients, whose properties can be studied to get information about either the uncertainty (if all parameters of the model were sampled from the according distributions) or the sensitivity to parameters or groups thereof (if only these were sampled). This established method has been used by many authors (Klein et al., 2010; Puncher, 2012b; Puncher and Burt, 2013; Puncher 2014a, b; Li et al., 2015; Spielmann et al., 2020).

Figure 18 presents a graphical representation of the Monte Carlo simulation concept that was used in this work.

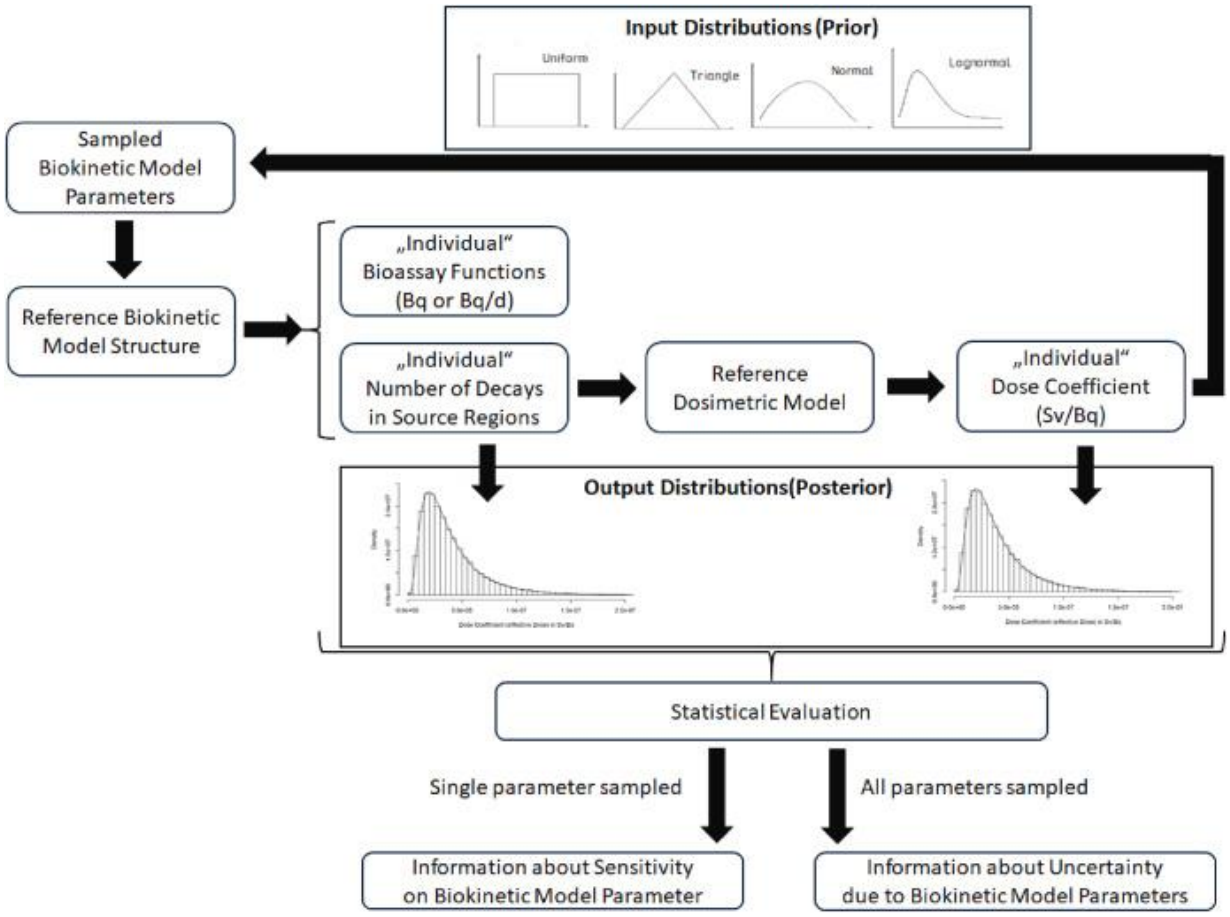

Figure 18: Graphical representation of the Monte Carlo method used in this work.

For this study the INTDOSKIT toolkit has been extended with functions that allow performing the Monte Carlo simulations. The methods have been successfully tested and validated against results of other authors (Puncher and Burt, 2013) for a scenario of ingestion of U-238 (Makumbi et al., 2024b).

A key challenge in Monte Carlo simulation with random sampling was to determine the appropriate number of iterations for convergence. To address this, a central limit theorem approach was used. The theorem ensures that for a sufficiently large sample, the mean is normally distributed regardless of the underlying data distribution (Heijungs, 2020). Based on

the authors' experience, 500 runs were considered an appropriate sample size to achieve a reasonable SD for the dose distribution, balance accuracy and computational efficiency. This sample size ensured that the SD converged adequately without excessive computational time. This was done to come up with an SD value that could be used to solve equation (4.8) for the required number of runs to ensure convergence of the solution.

The first step in implementing the central limit theorem was to select the desired confidence level and associated z-statistic. In this case, it was the 95% confidence level with 1.96 as the associated z-statistic.

i) The second step was to solve for the number of iterations, n as seen in equation (4.8).

$$z = (\bar{x} - \mu)/(s / \sqrt{n}) \ldots\ldots\ldots \quad (4.8)$$

Where $\bar{x} - \mu$ is the desired level of precision i.e., 0.01 in this case, s is the sample standard deviation, n is the required number of iterations and z is the chosen z-statistic.

ii) Once the required number of iterations had been determined, the Monte Carlo simulations were repeated approximately n times to achieve the desired accuracy.

Monte Carlo simulations were conducted using the INTDOSKIT computational tool to estimate organ-specific doses following radionuclide inhalation. To ensure statistical convergence and a comprehensive exploration of the probabilistic input space, a total of 50,000 iterations were performed per simulation.

Posterior distributions were generated for each organ and tissue by sampling respiratory deposition, biokinetic and dosimetric parameter distributions. Essential summary statistics were calculated to characterise these distributions, including mean, median, standard deviation (SD), geometric mean (GM), geometric standard deviation (GSD) and various percentiles (2.5^{th}, 5^{th}, 25^{th}, 75^{th}, 95^{th} and 97.5^{th}). These were calculated using functions from the EnvStats package in R.

Uncertainty in the estimated doses for each organ or tissue was quantified using the uncertainty factor (UF), which is defined as the square root of the ratio between the 97.5^{th} and 2.5^{th} percentiles. This metric provides a consistent, percentile-based measure of dispersion that is particularly useful for comparing variability across different anatomical targets.

$$UF = \sqrt{\left(\frac{P_{97.5}}{P_{2.5}}\right)} \ldots\ldots\ldots\ldots . \quad (4.9)$$

To model the posterior data further, probability distributions were fitted to each organ/tissue dataset using maximum likelihood estimation (MLE), which was implemented through the fitdistrplus package in R. This package supports the fitting of various distributions, such as lognormal, gamma, Weibull and normal, and includes tools for graphical diagnostics, including histograms, box plots, quantile–quantile (Q–Q) plots, probability–probability (P–P) plots and cumulative distribution function (CDF) visualisations.

The suitability of the fitted distributions was evaluated using the Kolmogorov–Smirnov (K–S) test, which was applied using the ks.test() function from base R, as well as model-specific diagnostic functions from the fitdistrplus package. These tests helped to assess whether the selected probability models had captured the empirical behaviour of the posterior distributions appropriately.

To determine whether simulation outputs from different scenarios (e.g., Job Type 1 versus Job Type 4) were statistically distinct, non-parametric hypothesis tests were applied. Specifically, the Kolmogorov–Smirnov test was used to assess differences in the empirical distribution functions and the Mann–Whitney U test (implemented via wilcox.test() in base R) was used to detect differences in central tendency without making a normality assumption.

These analytical steps, taken together, provided a robust statistical framework for quantifying uncertainty and comparing the distributional properties of internal dose estimates across multiple simulation conditions.

4.6.7 New Functions implemented in INTDOSKIT

Before implementing the Monte Carlo simulation concept in INTDOSKIT, several functions had to be written to support its implementation. In addition, these functions served to speed up the Monte Carlo runs by facilitating the use of parallel computing in the code. A brief description of these functions is given in the text below.

1. sample_params_RADONORM_JTx

The sample_params_RADONORM_JTx' function generates and returns a set of sampled properties for the HRTM and particle properties with options to sample various subsets of these properties. The subscript x on JT could be replaced by 1 or 4 for Job 1 and Job 4 respectively. A detailed breakdown of the function is given below.

i) Function definition and parameters

sample_params_RADONORM_JTx<-function(sample_sprop=TRUE, sample_pprop=TRUE, sample_aprop=TRUE) gives the function definition with three optional boolean parameters i.e., 'sample_pprop' whereby if TRUE allows the sampling of the HRTM parameters for the subject such as dead space volumes of the ET, BB and bb HRTM regions and the functional residual capacity (FRC) from their assigned respective probability distributions. 'sample_pprop' whereby if TRUE, allows for sampling of the aerosol properties such as particle size, dispersion, density, shape factor and hygroscopic factor from their respective probability distributions, 'sample_aprop' whereby if TRUE, allows for the sampling of activity properties such as tidal volume (V_T), breathing frequency (f_R) and fraction of air breathed through the nose (F_n) from their respective probability distributions.

ii) Initialization of reference variables

Within the function body, the subject properties and activity properties for sitting and light exercise were initialized with the ICRP reference values for an adult male, ICRP reference male seated and ICRP reference male performing light exercise respectively. These parameters could be sourced from the INTDOSKIT library for the deposition model. The attached and unattached radon progeny particle properties were initialized with the reference particle properties obtained from literature (Marsh et al., 2012; Marsh, 2022).

iii) Setting default values for particle properties

Furthermore, in the function body, default values for both the attached and unattached progeny particles were set for the particle size, GSD, hygroscopic growth factor, density and shape factor for the two job types.

iv) Sample HRTM parameters from their probability distributions

The next step within the function body was to sample subject properties. If 'sample_sprop' is TRUE, the random variable is assigned to various properties of 'tsprop' using chosen probability distributions i.e., VD(ET), VD(BB), VD (bb) and FRC get values sampled from their respective probability distributions. If sample_aprop is TRUE, random values are assigned to various properties for light exercise and sitting as follows; for light exercise, the tidal volume (V_T), breathing frequency (f_R) and fraction breathed through nose (F_noseNB) get values sampled from their respective probability distributions followed by calculation of the breathing rate (B) from the sampled values of V_T and f_R. A similar approach for light exercise was done for sitting. On the other hand, if 'sample_pprop' is TRUE, random values are assigned to particle properties such as particle size, hygroscopic growth factor, GSD, density and shape factor. However, if no probability distribution was assigned to any of the above parameters, the ICRP default values would be used in the calculation.

v) Returning results

The function returns a list of the sampled or default particle sizes and GSDs along with updated respiratory and particle property objects.

In summary, this function initializes reference values, modifies certain particle properties to new defaults, samples values for various properties based on the provided boolean parameters and returns a list of the modified and sampled parameters.

2. sample_parameters_Jobtypex()

This function generates and returns a list of parameters sampled from various probability distributions as explained in the following text.

i) Function definition

sample_parameters_Jobtypex<-function (). The function 'sample-parameters_Jobtypex' is defined without any arguments. The x on Jobtype can be replaced with 1 or 4 for sampling of parameters for either Job 1 or Job 4.

ii) Sampling parameters

The dissolution and absorption parameters for radon progeny as well as the unattached fraction were sampled from their respective probability distributions and in case no probability distribution was assigned to a parameter, the ICRP reference value was maintained for this parameter. The parameters for the absorption fraction from the HATM to blood were varied using the ICRP approach i.e., as a product of the ICRP reference value for the ingestion of the radionuclide and the sample rapid dissolution fraction for the radionuclide.

iii) Returning the list of parameters

Lastly, after the sampling of the parameters had been done, this function returns a list containing all the sampled and calculated parameters.

In summary, the 'sample_parameters_Jobtypex' function samples various parameters from their respective probability distributions and performs some basic calculations for the fraction of radionuclide absorbed from HATM to blood. Afterwards, it packages them into a list. This list of sampled parameters can then be used as input for further calculations.

3. read_deposition_data

The 'read_deposition_data' function was designed to read a CSV file containing deposition data. The function takes a file path as input and returns the data as a data frame. Its detailed explanation follows below.

i) Function definition

read_deposition_data<-function (file_path). The function is defined with a single argument 'file_path' which is the path to the CSV file to be read.

ii) Reading the CSV file

The function uses the 'read.csv' function to read the csv file located at 'file-path'. The sep= ";" argument specifies that the CSV file uses a semicolon (';') as delimiter between values rather than the default comma (',').

iii) Return the data

The 'read.csv' function returns a data frame containing the data from the CSV file, which is then returned by the 'read_deposition_data' function.

In summary, the 'read_deposition_data' function reads a semicolon delimited CSV file and returns its contents as a data frame. This function can be used to easily load deposition data from a file into a data frame for further processing.

4. calculate_deposition_fractions

The 'calculate_deposition_fractions' computes various deposition fractions for a particular radionuclide inhalation based on given parameters and updates the provided list 'q' with these values. The detailed description is given below.

i) Function definition

Calculate_deposition_fractions<-function (q, nrun, f_r, cf, dum1, dum2, sp). The function 'calculate_deposition_fractions' was defined with the following arguments i.e. q, which is a list or data frame to be updated with the calculated deposition fractions; nrun which is the current run index; f_r which is the rapid dissolution fraction for the given radionuclide; cf which is a correction factor; dum1 which is a data frame containing deposition data for light exercise; dum2 which is a data frame containing deposition data for sitting and sp which is a split factor for deposition.

ii) Calculating deposition fractions

The function calculates various deposition fractions and updates the 'q' list with these calculated values. Deposition fractions for ET_1, ET_2, BB, bb and ALV for both rapid and slow dissolution compartments were calculated.

iii) Returning the updated list

The function returns the updated list 'q' containing the calculated deposition fractions.

In summary, the 'calculate_deposition_fractions' function took in various parameters and updates a provided list or data frame with deposition fractions for different regions and states.

5. update_tcoeff

The function 'update_tcoeff' updated the values in a specific part of the 'element$tcoeff' matrix based on the input parameters 'f_b', 's_r', 's_s' and 's_b'.

i) Function definition

update_tcoeff<-function (element, f_b, s_r, s_s, s_b). The function 'update_tcoeff' was defined with several arguments i.e., 'element' which is an object containing a matrix 'tcoeff' of transfer coefficients that needed to be updated; 'f_b' which is a numeric factor of the sampled bound fraction for the radionuclide of interest; 's_r', 's_s' and 's_b' which are numeric values used in the update calculations for different components.

ii) Update

Prior to the process of updating the 'tcoeff' matrix starts by defining component groups i.e., 3 groups were identified which include 'r_components' which were simply the components to be updated with '(1-f_b) *s_r'; 's_components 'which are components to be updated with '(1-f_b) *s_s' and 'b-components' which are components to be updated with 's_b'.

The next step was to define pairs of components where each 'r_component' or 's_component' had a corresponding 'b_component'. These pairs were updated with 'f_b*s_r' and 'f_b*s_s' respectively. Having accomplished this, the updating was done whereby for each component in the 'r_components', the value in the 'Blood' column of the 'element$tcoeff' matrix was updated to '(1-f_b)*s_r', while for each component in 's_components', the value in 'Blood' column of the 'element$tcoeff' matrix was updated to '(1-f_b)*s_s'; for each component in the 'b_components', the value in the 'Blood' column of the 'element$tcoeff' matrix is updated to 's_b', while for each pair in the 'pairs' list, the function updated the value in the 'element$tcoeff' matrix using '$f_b$*$s_r$' if the 'r_components' starts with "r" and 'f_b*s_s' if it starts with "s".

iii) Return

The function returns the updated 'element' object.

In summary, this function first categorizes components into 'r_components', 's_components' and 'b_components'. It directly updates the values for these components in the 'Blood' column of the 'element$tcoeff' matrix and then it updates specific pairs of components with values computed from 'f_b', 's_r' and 's_s'. This approach ensures the 'element$tcoeff' matrix is updated in a structured and efficient manner based on provided parameters.

6. calculate_total_doses

The function 'calculate_total_doses' was designed to calculate and sum up radiation doses from a decay chain of radionuclides, considering both male and female biokinetic compartments. The description of this function is given below.

i) Function definition

Calculate_total_doses<-function (schain, SK_male, SK_female). This function calculated the total doses for a series of nuclides in a decay chain, distributing the decays into biokinetic compartments and summing up the doses for each nuclide. The first argument

for this function is ‘schain’ which is an object representing the decay chain. This object contains ‘nuclides’ which is a list of nuclide names in the chain; ‘NDEC’ which is a list containing the number of decays for each nuclide, ‘bio2dos’ which is a list mapping the biokinetic compartments to dosimetric source regions for each nuclide. The other arguments ‘SK_male’ and ‘SK_female’ are also lists containing the values of the S-coefficients for adult male and adult female respectively for each nuclide.

ii) Dose calculation

Dose calculation starts with initialization. Within this function, two empty lists are initialized i.e., decays to store the number of decays in ICRP source regions and ‘doses’ to store the calculated doses. Next, the function loops through each nuclide in the decay chain and for each nuclide, it calculates the number of decays in ICRP source regions using the ‘NDECin_ICRPSources’ function and stores the result in the ‘decays’ list. Upon completion of this step, the function then again loops through each nuclide to calculate doses. For each nuclide, it calculates doses using the ‘calc_doses’ function, which takes the male and female dose conversion coefficients and the distributed decays and stores the result in the ‘doses’ list. Lastly, the function initializes ‘dosissumme’ with the dose values from the first nuclide in the chain. It then loops through the remaining nuclides summing up the doses for each component (‘effD’, ‘hT_male’, ‘hT_female’, ‘heffT_male’, ‘heffT_female’).

iii) Return the result

The function returns ‘dosissumme’, which contains the total summed doses for all nuclides in the decay chain.

In summary, ‘calculate_total_doses’ function accomplishes the dose calculation process in five steps i.e., initialization, decays calculation, dose calculation, summation and output. Using this approach ensures that the number of decays and corresponding dose calculations are systematically handled providing a comprehensive dose assessment for the decay chain.

7. add_noise

The ‘add_noise’ function introduces randomness into a given model by replacing elements of a matrix (‘tcoeff’) with values drawn from specified probability distributions. This randomness is controlled by additional model parameters that define the type and characteristics of the distributions. Below is a description of the function’s operation.

i) Function definition

The ‘add_noise’ function was used to add noise to the elements of a model’s ‘tcoeff’ matrix by replacing each element with a sample from a specified distribution. This is useful for simulating variations or uncertainties in model parameters. The function definition is.

add_noise<-function (model). The function requires a single argument ‘model’ which is an object containing several components such as ‘tcoeff’, a matrix of transfer coefficients that is to be modified with random samples; ‘compnames’ which are the names of the compartments (used to iterate over the rows and columns of ‘tcoeff’); ‘disttype’ which is a matrix specifying the type of distribution to use for each element in ‘tcoeff’; ‘distwidth’ which is a matrix specifying a parameter (like standard deviation or width) for the distribution. Other parameters such as ‘distparam’ and ‘distparam2’ apply for distributions that need more parameters (e.g., uniform and triangular distributions).

ii) Randomization

The function starts by creating a copy of the input model to avoid modifying the original model directly. The function then iterates over each element of the 'tcoeff' matrix using nested loops. For each element, the function checks the type of distribution specified in the 'disttype' matrix and samples a new value accordingly. If the distribution type is 'lognormal', it calls the 'sample_realistic_lognormal' function with the current value as median and width as GSD. If the distribution type is 'normal', it calls the 'sample_realistic_normal' function. If the distribution type is 'uniform', it uses the 'runif' function to sample a value between 'distwidth' (as minimum) and 'distparam' (as maximum) while if the distribution type is 'triangular', it uses a triangular distribution function (assumed to be 'rtriangle').

iii) Return the modified model

After all elements have been processed, the function returns the modified model.

In summary, the function adds noise to the elements of a model's matrix of transfer coefficients by replacing the element of interest with a sample from a specified distribution. This process is accomplished in four (4) steps i.e., model copy, nested looping, distribution sampling and return. The function is designed to handle multiple types of distributions and additional types can be added by extending the 'if' statements. This function was very useful for simulating the effects of parameter uncertainties in models and provided a more robust analysis through stochastic modelling.

8. solve_chain

The 'solve_chain' function was designed to solve a chain of radioactive decays using a numerical solver for ordinary differential equations (ODE). It takes the initial quantities of nuclei, simulates their decay over time, and returns the activities of the nuclides in the chain. Below is a detailed description of the function.

i) Function definition

This function was used to solve a chain of radioactive decays and split the results into separate values for each member nuclide, converting the number of nuclei to activities. The function definition is as follows.

solve_chain<-function (chain, initial, times). The first argument is chain which is an object containing the information about the decay chain such as 'tcoeff' which is a matrix of transfer coefficients for the decay chain, 'compnames' which consists of the compartment names with nuclide prefixes; 'isotopes' which is a string with nuclide names separated by '%'; 'lambdas' which contains decay constants for the nuclides; 'bio2dos'which performs the biokinetic to dosimetric mapping; 'initial' which gives the initial number of nuclei in compartments and 'times' which provides the time points for which the solution is required.

ii) Solving the decay chain

The function starts with solving the system of ODE representing the decay chain using the 'solve_ode' function. The result is stored in 'solchain', after which the nuclides are extracted from the 'isotopes' string and various variables are initialized for later use. Next, the function loops through 'compnames' to determine the number of compartments for each nuclide and to strip the nuclide prefixes from compartment names. Further, the 'bio2dos'

mapping is adjusted to use the compartment names without nuclide prefixes. The function continues by processing each nuclide separately to convert the solution from the number of nuclei to activities and to calculate the balance of activities over time. Finally, the total activity balance for the whole system is calculated by the sum of the balances for all nuclides.

iii) Return the results

The function returns a list containing the nuclide names, solution activities, activity balances, number of decays and biokinetic to dosimetric mapping.

In summary, the function solve_chain solves the decay chain under the following steps; ODE solution (solves the decay chain using 'solve_ode'), extract and initialize (extracts nuclides and initializes necessary variables), dimension calculation (determines the number of compartments for each nuclide and prepares compartment names), mapping setup (adjusts biokinetic to dosimetric mapping), nuclide processing (converts the solution from number of nuclei to activities and calculates the activity balance for each nuclide), total balance (computes the total system activity balance), return results (returns a comprehensive list of the solution, balances and mappings). This function is useful for modelling the behavior of a decay chain over time, providing detailed insights into the activities of individual nuclides and their overall contributions to the system.

4.6.8 Batch processes and parallel computing

Simulations were run in batches, this allowed running multiple simulations in parallel and that the CPU-load could be distributed to multiple machines. A 'run-batch' function was developed to run a series of simulations, utilizing the 'sample_params_RADONORM_JTx' function to generate sampled parameters for each run and then performing deposition calculations using these parameters.

Below is a detailed breakdown of how this function works.

i) Function definition and parameters

run_batch<-function (nruns_per_core, start_run); whereby nruns_per_core is the number of simulation runs to execute and start_run is a parameter (though not used in the function body, is intended for tracking/offset purposes in a broader context).

ii) Initialization and loop through runs

An empty list 'results' is initialized to store the results of each run. A for loop iterates from 1 to 'nruns_per_core', performing the following steps in each iteration;

Sampling parameters: The 'sample_params_RADONORM_JTx' function is called to generate sampled parameters. The returned values are extracted into local variables for particle properties, subject properties and activity properties.

Deposition calculations: Depositions for both attached and unattached particle progeny inhalation were calculated using the function HRTMDEP_depositionsGSD() from the deposition model library of INTDOSKIT. Attached and unattached depositions were calculated for both light exercise and sitting activities and the total depositions for each aerosol mode summed up from each activity.

Storing results: The results of the current run ('nrun') are stored in the results list. Each entry in results contains four sublists i.e., 'ale', 'asi', 'ule' and 'usi'. Each sublist includes; the total deposition values, the summed total deposition, the sampled particle size and GSD and the associated respiratory properties.

Returning results: After completion of all runs, the function returns the results list containing the deposition results and sampled parameters for each run.

In summary, the run_batch() function systematically performs multiple simulation runs, sampling parameters for each run, calculating particle depositions for different activity levels and particle types and storing results in a structured list. The use of sampled parameters ensures variation in the simulations, providing a comprehensive set of results based on the specified number of runs_per_core. In order to speed up the calculation of the deposition fractions. It was necessary to perform parallel computing on the run_batch function.

Finally, R-Scripts were set up that run a large number of simulations in parallel across multiple cores, collect the results and write these to output files as explained in the steps below.

i) Set up and configuration

In this step, it was required to define the desired number of iterations, the number of cores and the number of runs on each core. Assignments statements were used to assign values to the number of runs and number of cores to the variables nruns and ncores respectively, while the ceiling () function in R was used to calculate the number of runs to be handled by each core; this was assigned to the variable nruns_per_core. The argument to the function ceiling was the quotient of nruns and ncores. Having accomplished this, the next step was to create a cluster object with the specified number of cores using the makeCluster () function with ncores as its argument. The created cluster was assigned to the variable cl. The set up and configuration step was concluded by exporting all required variables and functions to each worker in the cluster so they can have access to all the needed resources. This was made possible with the help of the clusterExport () function that took on as its arguments, the cluster variable cl and a list of required variables and functions.

ii) Running simulations

The function parLapply () was used to execute the run_batch () function in parallel across all cores. Each core executed the 'run_batch' function with 'nruns_per_core' iterations, starting at a different run number. The arguments for this function were the cluster variable, the vector of cores, the function run_batch, number of cores and the number of runs per core. The output of this function was assigned to the variable results.

iii) Collecting and saving results

The stopCluster () function was used to stop the cluster and free up the resources after the simulations. The argument for this function was the cluster variable cl. Having accomplished this, it was necessary to combine the results from all cores into a single list. This was done using the do.call () function. The arguments to this function were the concatenate function and the results variable. The next step after this was the setting up of output files. Four output files were created, one for each type of deposition

calculation i.e., ‘ale’, ‘asi’, ‘ule’ and ‘usi’ for collecting results for deposition fractions for attached radon progeny during light exercise, attached radon progeny during sitting, unattached radon progeny during light exercise and unattached radon progeny during sitting. The files were created using the file () function of R with two arguments i.e., the directory specifying the file path and the method of opening the file which was assigned a default value ‘wt’. Headers were written to these files using the cat () function of R. Once the files had been created, the next step was to write the results to the files using a combination of for loop and the cat () function whereby each result in ‘all_results’ was written to the corresponding file. The results were formatted as semi-colon-separated strings. Lastly, after completing the writing, the output files were closed using the close () function of R. This function uses the file name as its argument.

In summary, using parallel computing, the above approach efficiently handled a large number of simulations, distributing the workload across multiple CPU cores. The results were then systematically collected, combined and written to files for further use/analysis of the full distributions calculated.

5. UNCERTAINTY AND SENSITIVITY ANALYSIS FOR SELECTED SCENARIOS

This chapter presents the results of the uncertainty and sensitivity analysis for the intake of radon progeny and uranium ore dust by underground miners. The statistical summaries of the results and discussions are also presented.

5.1 Analysis of the datasets from the Monte Carlo simulations

This section gives an overview on the evaluations of the datasets generated by the Monte Carlo simulations. The datasets consist of samples of the distributions of the dose coefficients for organs of interest and effective dose.

5.1.1 Convergence of the simulations

During the Monte Carlo simulations, the convergence of the final dataset with 50,000 repetitions was tested by recalculating the GSD of the distributions after every 500th run. As an example, Figure 19 shows the GSD of the distribution of the committed equivalent lung dose coefficient (Job 1) against the number of iterations. As expected, the values of the first 2,000 runs show a larger fluctuation with GSD values ranging from 1.585 to 1.6300. After 2500 runs, the fluctuations are within ±0.2% of the GSD of the dataset of 1.58. Similar results were seen for the other dose distributions over all scenarios investigated in this study. Therefore, it was concluded that 50,000 runs ensured the desired convergence of the simulations.

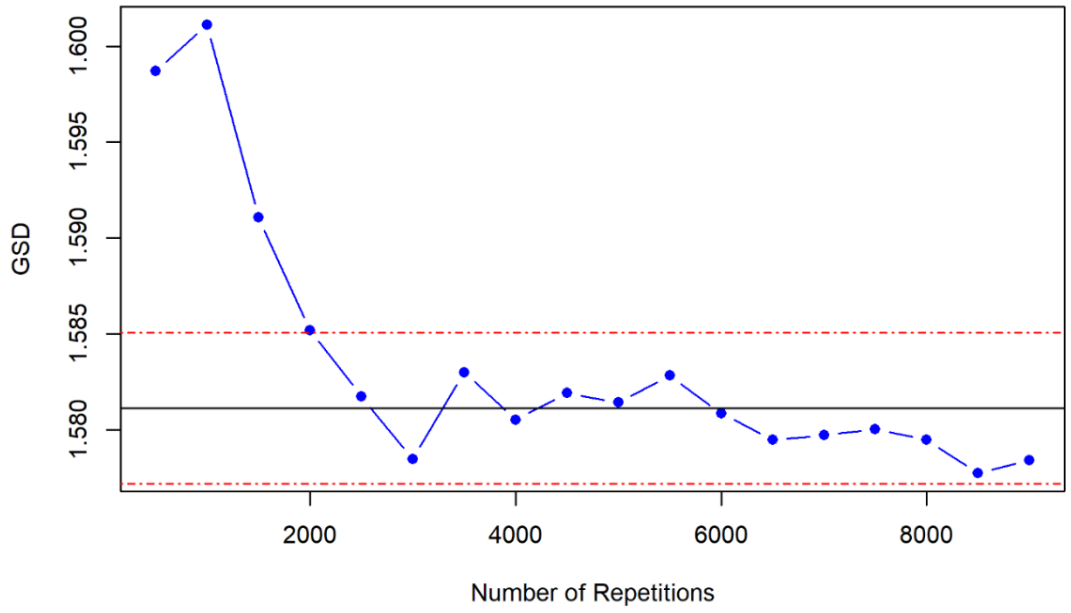

Figure 19: Test for convergence of the dataset

5.1.2 Characterisation of the distributions of the dose coefficients

For the description of the distributions in the datasets some statistical parameters were calculated. These include the quantiles (2.5% = X2.5, 5%=X5.0, 25%=X25, 50% = X50(Median), 75%=X75, 95%=X95 and 97.5% = X97.5), minimum (Min) and maximum value (Max), the arithmetic mean and standard deviation (SD), the geometric mean (GM) and standard deviation (GSD). Additionally, the uncertainty factor (UF) was calculated. For the

distributions in the datasets all values were tabulated together with the undisturbed value calculated using the reference parameters. In this subsection we will use the scenario of ingestion of U-238 (Makumbi et al., 2024b) to demonstrate the analyses of the distributions. An example for table of the statistical parameters is given below as Table 27. In this table the values for the various statistical parameters following inhalation of radon progeny by underground miners performing Job 1 are presented.

The results presented in Table 27, reveal that the average committed effective dose coefficient is approximately 1.3 times greater than the reference value provided by ICRP, indicating an average increase of 30%. In contrast, the median value aligns with the ICRP estimate, suggesting that the central tendency remains consistent with the reference. The highest simulated dose coefficient is notably elevated, reflecting substantial uncertainty at the upper range, while the lower limit, though less extreme, still indicates a considerable level of variability. The increased mean is indicative of positive skewness in the assumed lognormal distribution of the model parameters.

This skewness implies that larger values within the distribution are disproportionately influencing the mean, producing an asymmetry where high dose values occur more frequently than in a symmetric (normal) distribution. This emphasizes the impact of outliers on the average dose estimate. The broad uncertainty interval spanning from the 2.5^{th} to the 97.5^{th} percentile is covering nearly two orders of magnitude and demonstrates a high degree of uncertainty in the dose coefficients attributable to uncertainties in the model parameters. These findings suggest that for conservative radiation safety assessments, it may be appropriate to adopt values exceeding the ICRP reference.

Therefore, while the ICRP reference value remains a valid benchmark for protection, incorporating additional statistical metrics and considering the overall shape of the distribution could lead to improved protective strategies. Potential enhancements could include adopting higher percentiles (e.g., 75^{th} or 95^{th}), using the mean as a reference point, or refining model parameters to reduce skewness, thereby supporting more robust radiation protection measures.

Furthermore, the average committed equivalent dose coefficients across most organs surpass the ICRP reference values, with ratios ranging between 1.24 and 1.40. In comparison, median dose coefficients closely resemble the ICRP values, with ratios typically between 0.99 and 1.02, indicating that while the mean dose is elevated, the median or typical dose remains in close agreement with the reference.

The GSD values for most organs fall consistently between 2.08 and 2.14, pointing to a comparable level of uncertainty in the dose distributions. These elevated GSD values are characteristic of a lognormal distribution and reflect significant dispersion. Ratios comparing the 97.5^{th} percentile to the ICRP reference are considerably high (ranging from 3.64 to 4.32), indicating that the upper range of dose coefficients can be markedly higher than ICRP benchmarks. Conversely, ratios of ICRP to the 2.5^{th} percentile (3.62 to 4.43) reveal that the lower tail of the distribution is substantially below the ICRP values.

On average, the mean to ICRP ratios for most organs hover around 1.32, suggesting that average dose levels are approximately 32% higher than the ICRP reference. Meanwhile, the median-to-ICRP ratios remain close to 0.99, highlighting a skewed distribution with a longer tail extending toward higher dose values.

Table 27: Statistical summary of the organ and tissue doses (Sv/Bq) following ingestion of uranium by workers (Source: Makumbi et al., 2024b).

Organ	ICRP	Mean	SD	GM	GSD	UF	Min	X2.5	X5.0	X25	X50	X75	X95	X97.5	Max
effective	3.08E-08	4.04E-08	3.02E-08	3.2E-08	1.98669	4.832855	2.86E-09	8.35E-09	1.02E-08	1.99E-08	3.21E-08	5.13E-08	9.86E-08	1.21E-07	4.4E-07
Bone-Marrow	3.87E-08	5.21E-08	3.8E-08	4.15E-08	1.968114	4.734675	3.46E-09	1.1E-08	1.35E-08	2.6E-08	4.18E-08	6.66E-08	1.25E-07	1.53E-07	5.46E-07
Colon	1.93E-08	2.54E-08	2.11E-08	1.92E-08	2.117483	5.661	1.29E-09	4.48E-09	5.57E-09	1.14E-08	1.91E-08	3.22E-08	6.59E-08	8.26E-08	3.25E-07
Lung	1.53E-08	2.01E-08	1.68E-08	1.52E-08	2.1275	5.781683	9.29E-10	3.48E-09	4.35E-09	9.01E-09	1.51E-08	2.55E-08	5.23E-08	6.55E-08	2.58E-07
Stomach	1.97E-08	2.6E-08	2.18E-08	1.96E-08	2.132473	5.812881	1.19E-09	4.47E-09	5.59E-09	1.16E-08	1.95E-08	3.3E-08	6.78E-08	8.49E-08	3.34E-07
Breast	2.43E-08	3.2E-08	2.69E-08	2.41E-08	2.135827	5.835695	1.44E-09	5.48E-09	6.85E-09	1.43E-08	2.4E-08	4.06E-08	8.35E-08	1.05E-07	4.12E-07
Testes	2.4E-08	3.16E-08	2.66E-08	2.38E-08	2.135623	5.834944	1.43E-09	5.42E-09	6.78E-09	1.41E-08	2.38E-08	4.02E-08	8.26E-08	1.03E-07	4.08E-07
Urinary Bladder	2.49E-08	3.28E-08	2.76E-08	2.47E-08	2.134891	5.829827	1.49E-09	5.63E-09	7.05E-09	1.46E-08	2.47E-08	4.17E-08	8.57E-08	1.07E-07	4.23E-07
Oesophagus	1.99E-08	2.62E-08	2.19E-08	1.98E-08	2.128015	5.781599	1.21E-09	4.53E-09	5.66E-09	1.17E-08	1.97E-08	3.33E-08	6.82E-08	8.54E-08	3.36E-07
Liver	7.33E-08	9.09E-08	6.65E-08	7.25E-08	1.972668	4.731786	6.03E-09	1.92E-08	2.34E-08	4.53E-08	7.3E-08	1.16E-07	2.21E-07	2.67E-07	8.47E-07
Thyroid	2.18E-08	2.87E-08	2.41E-08	2.16E-08	2.134449	5.825599	1.3E-09	4.93E-09	6.17E-09	1.28E-08	2.16E-08	3.65E-08	7.5E-08	9.4E-08	3.7E-07
Bone-Surface	1.4E-07	1.96E-07	1.54E-07	1.53E-07	2.02501	5.083	1.22E-08	3.85E-08	4.75E-08	9.43E-08	1.53E-07	2.48E-07	4.89E-07	6.03E-07	2.06E-06
Brain	2.46E-08	3.24E-08	2.71E-08	2.44E-08	2.128972	5.787993	1.49E-09	5.59E-09	6.99E-09	1.45E-08	2.44E-08	4.11E-08	8.43E-08	1.06E-07	4.16E-07
Salivary-Glands	2.43E-08	3.21E-08	2.69E-08	2.42E-08	2.132612	5.816595	1.46E-09	5.51E-09	6.89E-09	1.43E-08	2.41E-08	4.07E-08	8.36E-08	1.05E-07	4.13E-07
Skin	2.42E-08	3.19E-08	2.68E-08	2.4E-08	2.135159	5.832377	1.44E-09	5.46E-09	6.83E-09	1.42E-08	2.39E-08	4.05E-08	8.32E-08	1.04E-07	4.11E-07
Remainder	3.52E-08	4.45E-08	3.21E-08	3.58E-08	1.944007	4.576876	3.46E-09	9.73E-09	1.19E-08	2.26E-08	3.59E-08	5.66E-08	1.07E-07	1.29E-07	4.45E-07

SD: Standard deviation; GM: Geometric mean; GSD: Geometric standard deviation; UF: Uncertainty factor; Min: minimum value; X2.5: 2.5th percentile; X5.0: 5th percentile; X25: 25th percentile; X50: 50th percentile; X75: 75th percentile; X95: 95th percentile; X97.5: 97.5th percentile; Max: maximum value.

Histograms and density functions of the distributions of the committed effective dose coefficient were plotted. The distribution of the committed effective dose coefficient, e (50) was well fitted by a lognormal distribution with a GM of 3.2E-08 Sv/Bq and a GSD of 2.0. The distributions show a skewness with a long tail to the right.

The fitditrplus package of R (Dellignette-Muller and Dutang, 2015) was used to fit "Normal", "Lognormal" and "Gamma" distributions to the dataset. To test, which distribution could best be used to describe the distribution, probability plots (QQ-Plots and PP-Plots) of the distributions were made. While the QQ-Plots compare the quantiles of the distributions the PP-Plots compare the cumulative densities of the distributions. Figures 20 and 21 show the QQ-plot and PP-Plot of the distribution of committed effective dose coefficient in the U-238 ingestion scenario. While the QQ-Plots show that none of the distributions is fitting the data really well, the PP-plots indicate that the lognormal distribution is best to describe the posterior distributions in the dataset.

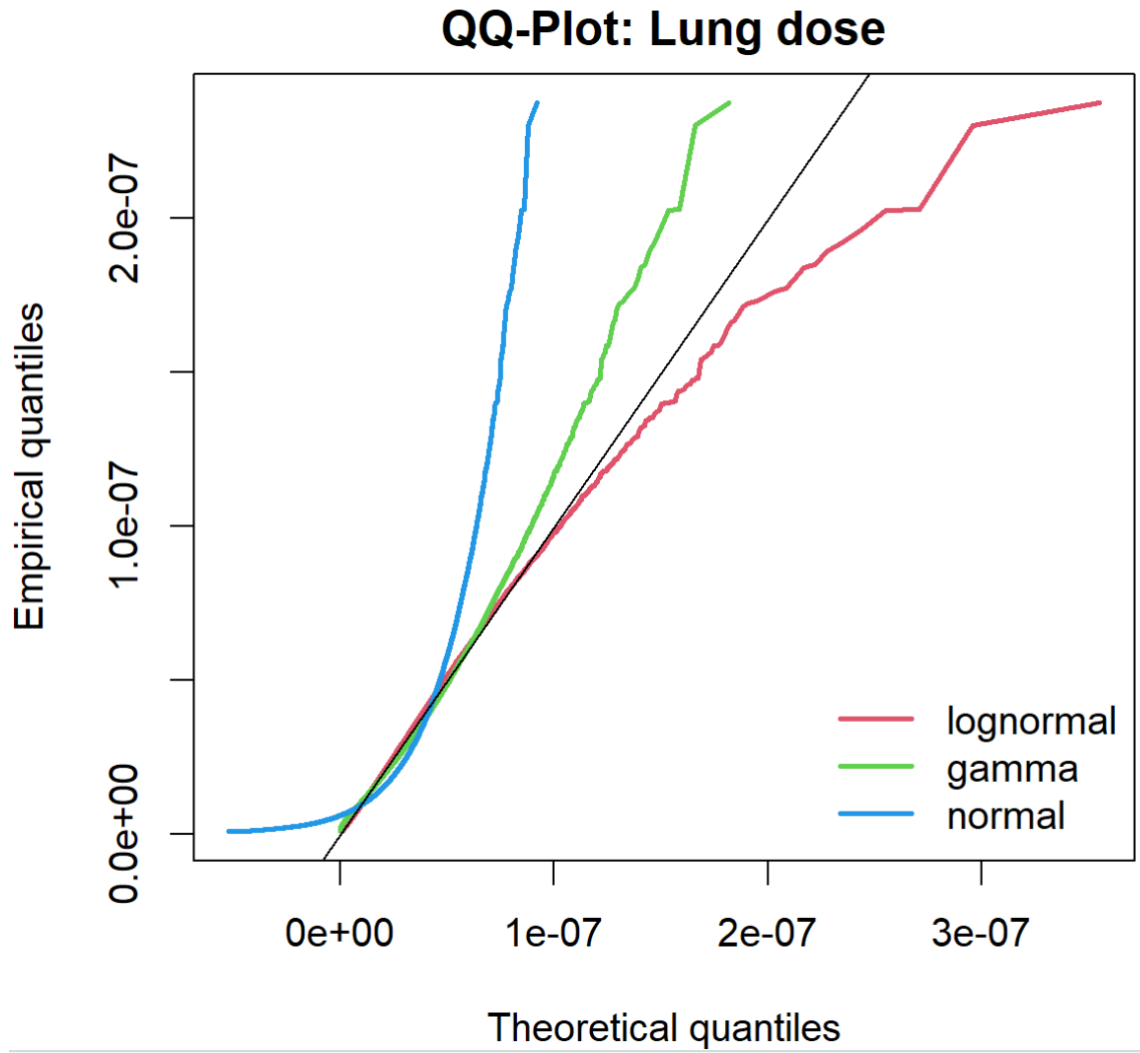

Figure 20: Fitting of probability distributions using a QQ-plot to the posterior dataset of the effective dose coefficient following U-238 ingestion.

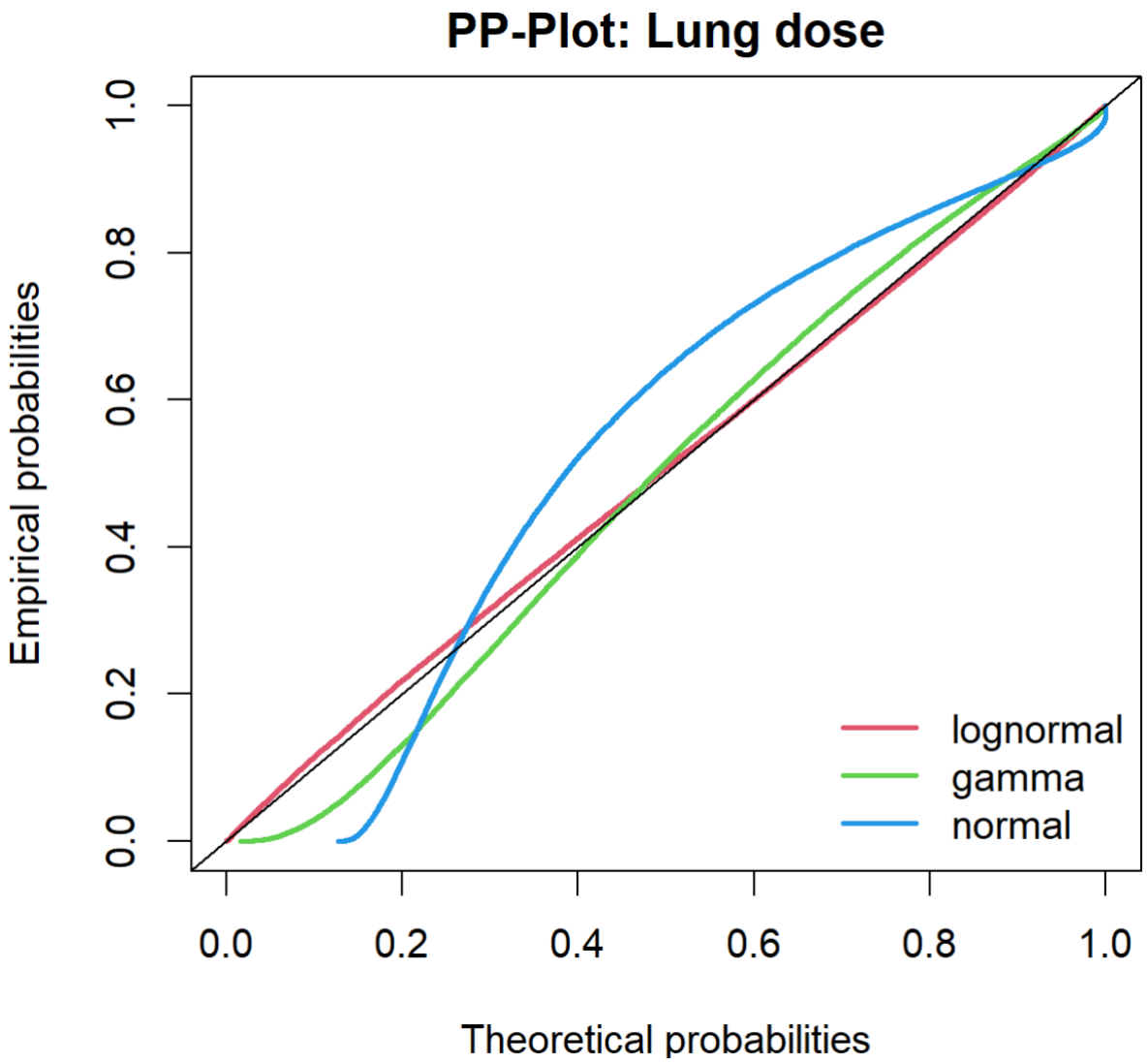

Figure 21: Fitting of probability distributions using a PP- plot to the effective dose coefficient dataset following ingestion of U-238

Therefore, lognormal probability distributions were fitted to the posterior dataset in INTDOSKIT using maximum likelihood estimation (MLE). This was confirmed by the Kolmogorov-Smirnov (K–S) test, which accepted the lognormal fits.

As an illustration for this kind of analysis, Figure 22 shows the histogram of the distribution of effective dose for the ingestion of U-238 together with a fit of the log-normal distribution. The fit was validated using a Kolmogorov-Smirnov (K-S) statistic of 0.00522, representing the greatest deviation between the empirical cumulative distribution function (CDF) of the observed data and the CDF of the proposed model. Since this value is well below the threshold of 0.01, it reflects an excellent agreement between the model and the data.

The K-S test was selected due to its nonparametric characteristics, its sensitivity to differences between distributions, its adaptability to various sample sizes, straightforward interpretability, uniformly distributed test statistic, and its broad applicability across multiple distribution types (Aslam, 2019; Lanzante, 2021; Cardoso and Galeno, 2023). Alternative methods such as the Chi-square goodness-of-fit, Anderson-Darling, and Shapiro-Wilk tests were deemed unsuitable

due to certain drawbacks, including poor performance with small datasets, restrictions to normal distributions, and limited efficiency when dealing with continuous variables (Surucu, 2008; Ghasemi and Zahediasl, 2012; Rana and Singhal, 2015; Luong, 2018; Khatun, 2021; Hagel et al., 2024).

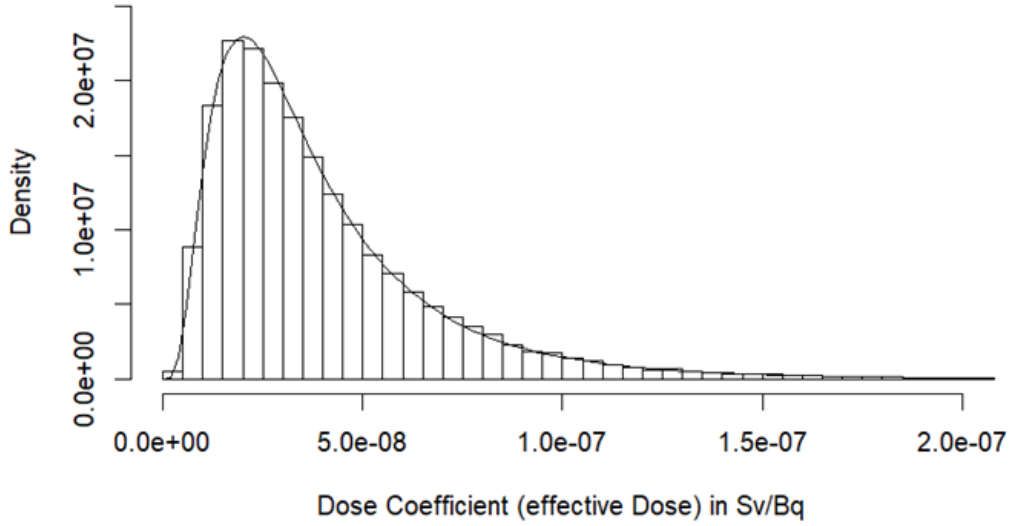

Figure 22: Frequency distribution plot of the effective dose coefficient following ingestion intake of U-238. The histogram shows the dataset, the black line is the fit of a lognormal distribution with GM of 3.2E-08 Sv/Bq and GSD of 2.0 (Source: Makumbi et al., 2024b).

For a graphical representation of the dataset, boxplots for the distributions of the committed effective and equivalent dose coefficients were plotted. Figure 23 shows the boxplots for the dose coefficients in the U-238 ingestion scenario.

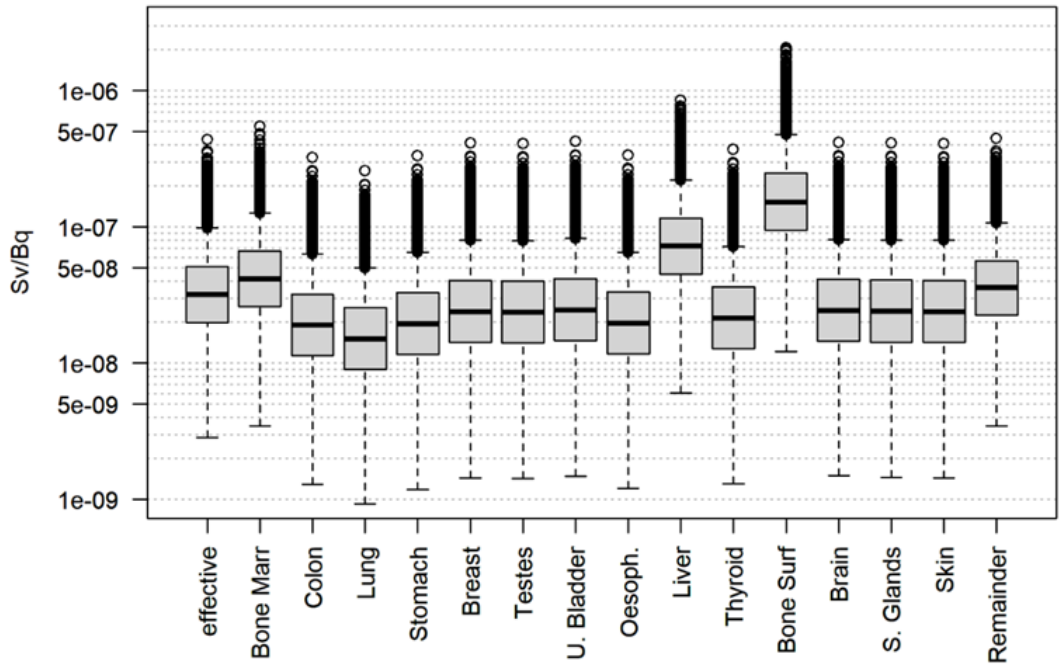

Figure 23: Boxplots of the distribution of the dose coefficients for committed effective and equivalent dose coefficients to the organs following ingestion of U-238.

Bone Marr: Bone marrow; U. Bladder: Urinary bladder; Oesoph: Oesophagus; Bone Surf: Bone surface; S. Glands: Salivary glands.

The following sections present the main findings for the scenarios studied in this project. A full set of tables and graphs for the datasets is provided in the Annex at the end of this report.

5.2 Uncertainty and sensitivity analysis for radon progeny inhalation in underground mines

The tabulated results of the global uncertainty analysis for the inhalation of radon progeny in underground mines are summarised in Appendix A (Table A1 and Table A2 for Job 1 and Job 4 respectively). Results and main findings are summarized in this subsection.

A global uncertainty analysis was conducted to evaluate uncertainties of the committed equivalent lung dose coefficients resulting from the inhalation of radon progeny in underground mining scenarios. For Job 1, the GM dose coefficient is 47.05 mSv/ (mJh/m³), with GSD of 1.58. The 95% confidence interval (CI) ranges from 18.59 to 104.74 mSv/ (mJh/m³) and the uncertainty factor (UF) is 2.37. For Job 4, the GM increases to 61.87 mSv/ (mJh/m³) (GSD = 1.56), with a CI ranging from 24.83 to 133.09 mSv/ (mJh/m³) and UF of 2.32.

Right-skewed distributions are evident in both scenarios, as indicated by mean values slightly exceeding their corresponding medians. This reflects the influence of extreme values, which are typical of skewed distributions such as the lognormal distribution for most model parameters used in the Monte Carlo simulations.

The highest uncertainty occurs in the AI region (UF = 3.32 for Job 1 and 3.13 for Job 4), while the lowest lung dose uncertainty occurs in the Bchiol.sec and Bronch.bas regions for Job 1 (UF = 2.49) and in the Bchiol.sec region for Job 4 (UF = 2.29). Outside of the lung, the kidneys exhibit the greatest uncertainty (UF = 2.88 for Job 1 and 2.75 for Job 4) while the St.stem region is associated with the lowest systemic uncertainty (UF = 2.53 for Job 1 and 2.32 for Job 4).

In Job 1, the mean dose coefficient of 52.01 mSv/ (mJh/m³) is 2.2 times higher than the ICRP reference value of 24.00 mSv/ (mJh/m^3) given in Table 7, while the median is 48.48 mSv/ (mJh/m³), which is higher than the ICRP reference value by a factor of 2. The 97.5th percentile (Q_U) of 104.74 mSv/ (mJh/m³) indicates considerable variation in higher dose outcomes, while the 2.5th percentile (Q_L) of 18.59 mSv/ (mJh/m³) suggests more limited uncertainty in the lower range. In Job 4, the mean rises to 67.98 mSv/ (mJh/m³) (2.8 times the ICRP value) and the median to 63.73 mSv/ (mJh/m³) (2.7 times higher). Meanwhile, Q_U extends to 133.09 mSv/ (mJh/m³), highlighting greater uncertainty at the upper end, although the Q_L value of 24.83 mSv/ (mJh/m³) closely approximates the ICRP benchmark.

The significant deviation of the medians from the ICRP reference values for the two job types can be attributed to the non-linear relationship between dose coefficients and model parameters. This is because the representative values used in the Monte Carlo simulations were not always the same as the mean or median values of the parameter probability distributions. Another possible factor is the choice of probability distributions. While the selection of probability distributions was demonstrated to have a relatively minor effect on the central values and ranges of calculated dose distributions when constant variance in parameter uncertainties was assumed (Klein et al., 2010; Puncher and Harrison, 2012), this was not applicable to this study. The

discrepancy between the median dose values obtained and the ICRP reference values can therefore be explained.

The wide uncertainty range (Q_L to Q_U), which is about an order of magnitude, reflects significant variation in the calculated dose coefficients due to uncertainties in the model parameters. For conservative safety assessments, it may therefore be prudent to consider values higher than the ICRP reference. While the ICRP reference value can still be used as a protective measure, incorporating additional statistical measures and considering distributional characteristics could enhance protection. This can be achieved by making adjustments to the reference value based on higher percentiles (e.g., the 75^{th} or 95^{th}), adopting the mean as the reference value, or revising biokinetic model parameters/biokinetic model structure to reduce the degree of skewness (Makumbi et al., 2024b).

These results underline the importance of considering both dose distribution and uncertainty when assessing the health risks associated with radon progeny inhalation. The variation in dose coefficients highlight the complexity of modelling dose distributions in the respiratory and systemic organs, particularly in high-risk occupational environments such as underground mines.

An overview and the comparison of the results from the Monte Carlo simulation for the two exposure scenarios is presented by the boxplots of the distributions of the different organs and target regions in Figure 24. The boxplots indicate that the uncertainties in the two scenarios are rather large and of comparable size, which can be seen in the similar values of GSD and UF in the two scenarios.

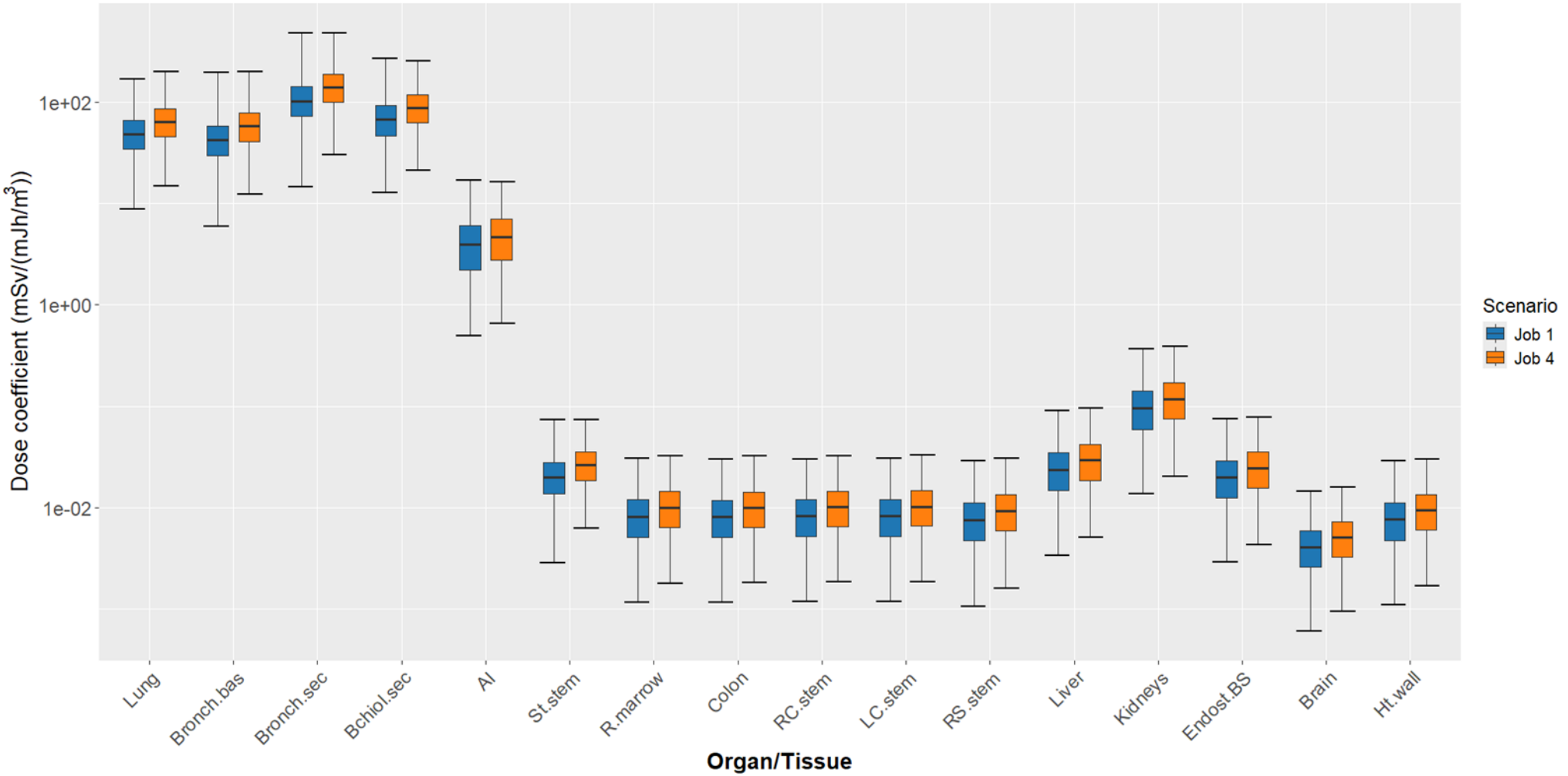

Figure 24: Boxplots showing the comparison of doses from the uncertainty analysis due to inhalation of radon progeny in underground mines under Job 1 and Job 4 exposure conditions.

Figures 25 and 26 present Q-Q and P-P plots, respectively, to visually assess how well the sample data of committed equivalent dose to the lungs fits three theoretical distributions: normal, gamma, and lognormal for Job 1. The Q-Q plot (Figure 25) presents the empirical quantiles of the data against the theoretical quantiles of each distribution. The diagonal reference line represents a perfect fit; the closer the plotted points are to this line, the better the fit of the distribution. The normal distribution (blue line) deviates significantly from the reference line, especially in the tails, indicating that the data are skewed or have heavier tails than would be expected under normality. In contrast, the gamma (green line) and lognormal (red line) distributions are more closely aligned with the reference line, especially in the central region of the data. While both still show some deviation in the upper quantiles, the lognormal better captures the upper tail, suggesting the presence of high value outliers. The gamma distribution, on the other hand, provides a better fit in the lower to middle quantiles. Similar observations can be made for Job 4 (Figure 28 and 29 for Q-Q plot and P-P plot respectively).

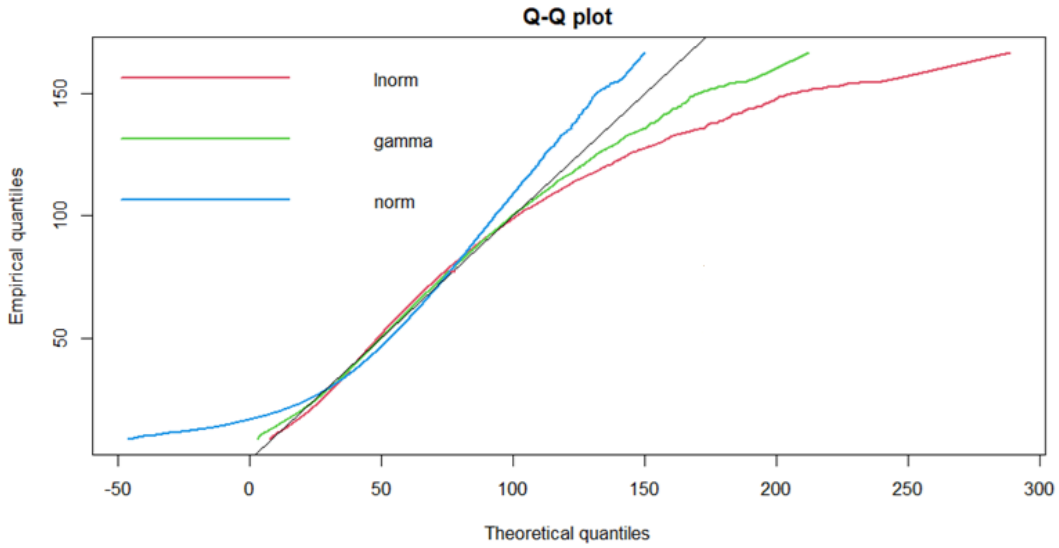

Figure 25: Fitting of probability distributions using a QQ-plot to the posterior dataset of committed equivalent lung dose coefficient following inhalation of radon progeny in underground mines under Job 1 conditions.

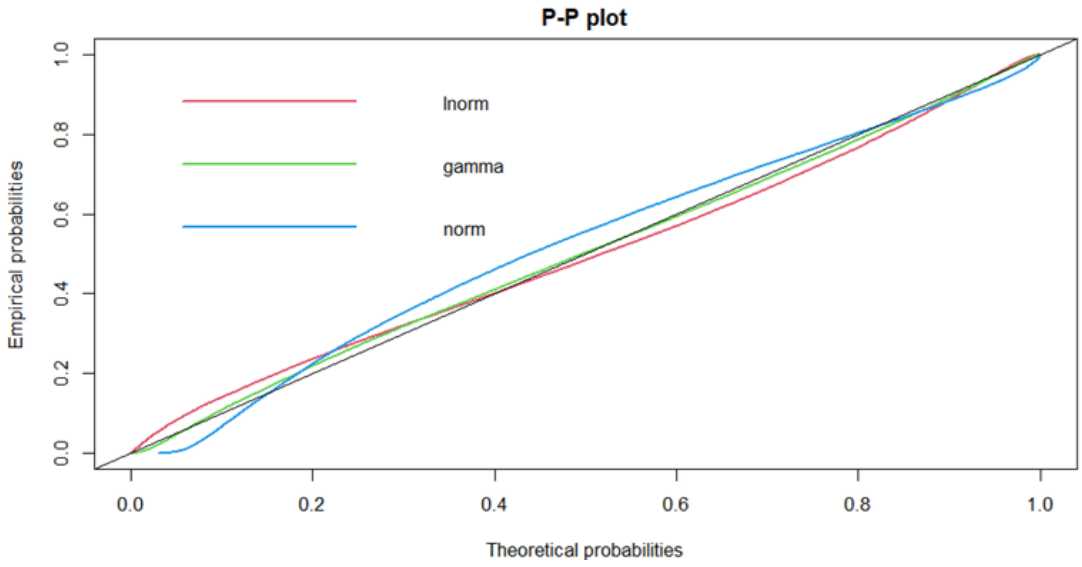

Figure 26: Fitting of probability distributions using a PP-plot to the posterior dataset of the committed equivalent lung dose coefficient following inhalation of radon progeny in underground mines under Job 1 conditions.

For both types of work, the committed equivalent lung dose coefficient follows a lognormal distribution. For the case of Job 1, the GM is 47.05 mSv/ (mJh/m³) with a GSD of 1.58 as shown in Figure 25, while the 95% confidence interval (CI) ranges from 18.59 mSv/ (mJh/m³) to 104.74 mSv/ (mJh/m³) and the UF is 2.37. For Job 4, the GM is 61.87 mSv/ (mJh/m³), the GSD is 1.56 as shown in Figure 28, and the 95% CI ranges from 24.83 mSv/ (mJh/m³) to 133.09 mSv/ (mJh/m³), with a UF of 2.32.

Figures 27 and 30 show histograms and fits of normal, lognormal, and gamma distributions to the committed equivalent lung dose coefficients for Job 1 and Job 4 respectively. From these figures, lognormal distributions can be used to describe the distributions in this study since most physiological data is described by this type of distribution (Spielmann et al., 2020).

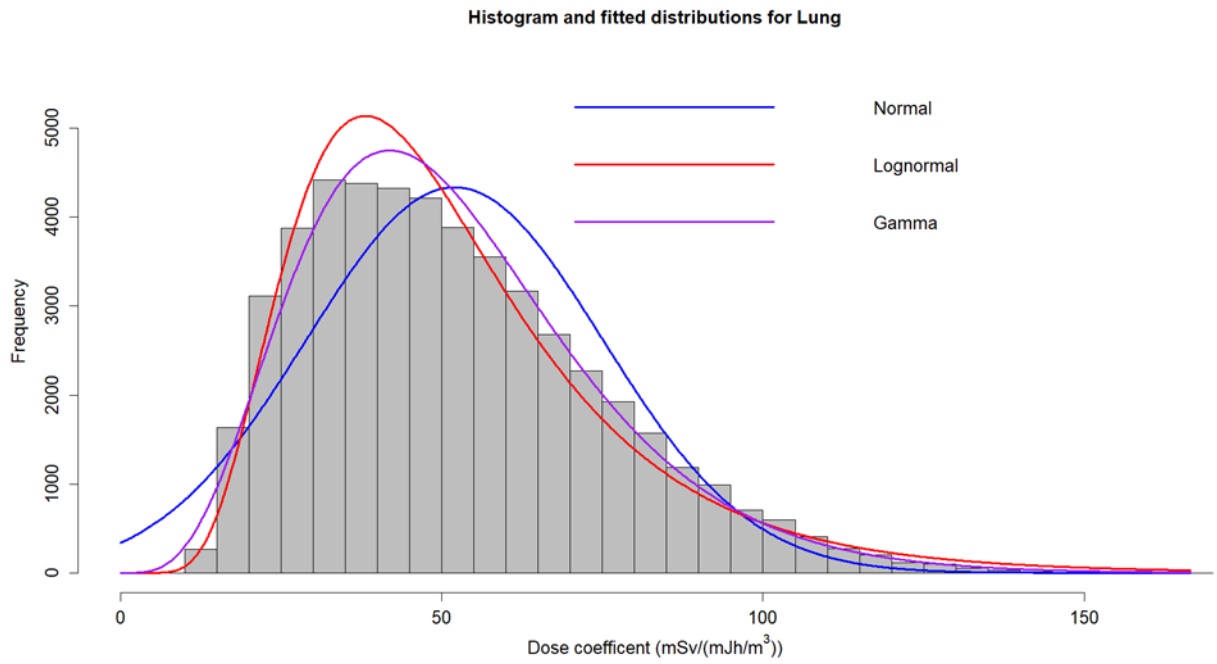

Figure 27: Fitting probability distributions to the committed equivalent lung dose coefficient for the inhalation of radon progeny under Job 1 exposure conditions.

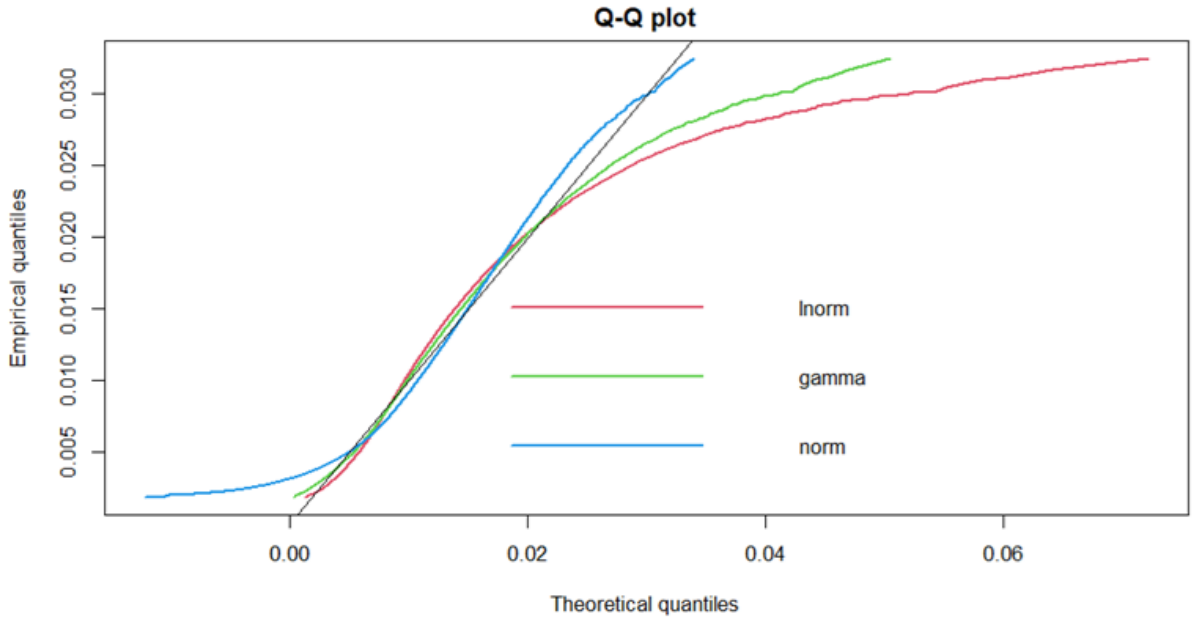

Figure 28: Fitting of probability distributions using a QQ-plot to the posterior dataset of the equivalent lung dose coefficient following inhalation of radon progeny in underground mines under Job 4 conditions.

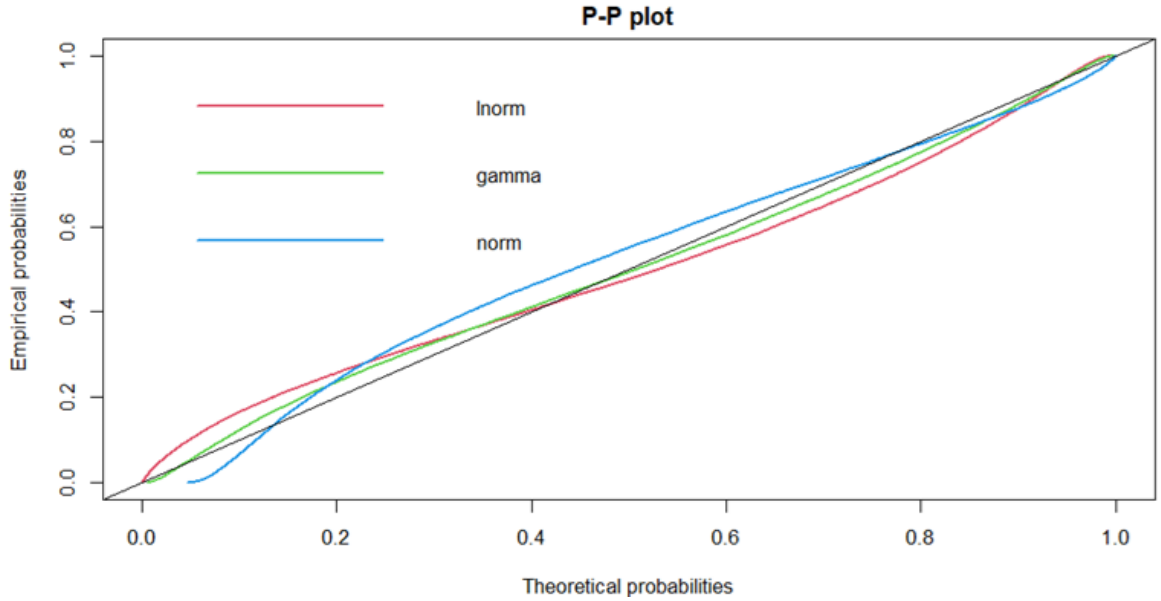

Figure 28: Fitting of probability distributions using a PP-plot to the posterior dataset of the committed equivalent lung dose coefficient following inhalation of radon progeny inhalation in underground mines under Job 4 conditions.

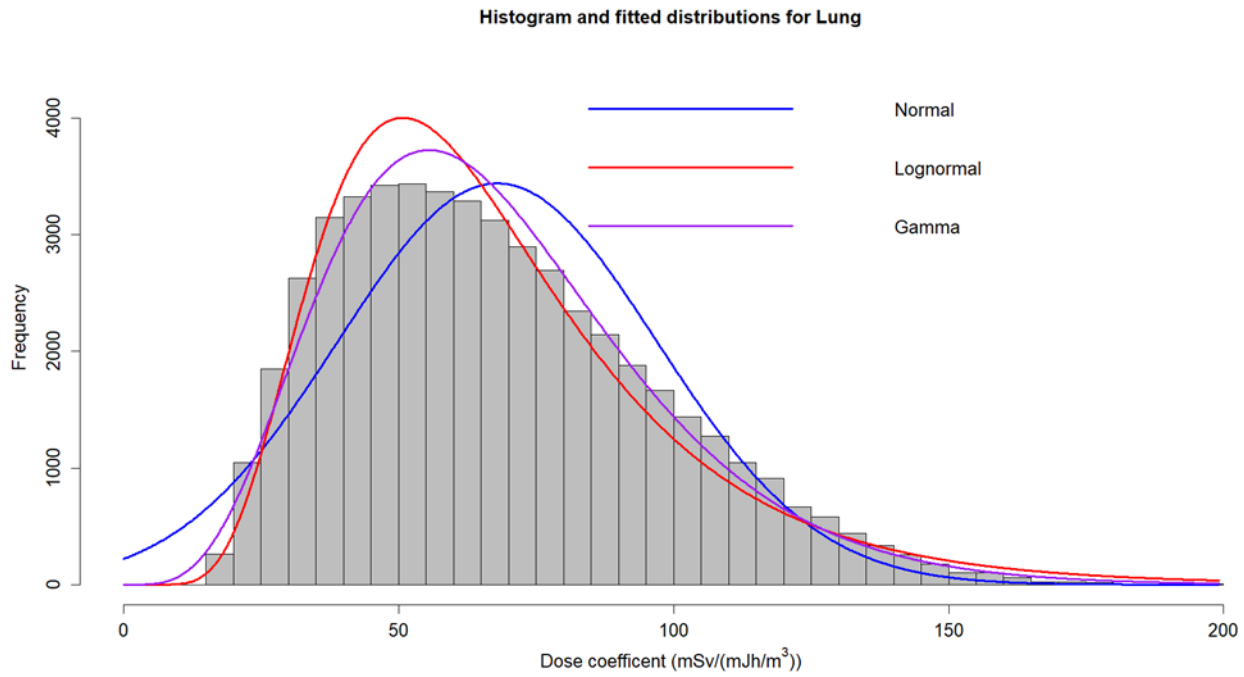

Figure 30: Fitting probability distributions to the committed equivalent lung dose coefficient for inhalation of radon progeny under Job 4 exposure conditions.

Table 28 gives a statistical summary of the results from the uncertainty analysis of the committed equivalent dose coefficients for the various target regions of the lung for both Job 1 and Job 4 exposure conditions.

Table 28: Statistical summary of the posterior distribution of the committed equivalent lung dose coefficient (mSv/ (mJh/m^3)) for the inhalation of radon progeny in underground mines.

	Job 1					**Job 4**				
	Lung	**Bronch.bas**	**Bronch.sec**	**Bchiol.sec**	**AI**	**Lung**	**Bronch.bas**	**Bronch.sec**	**Bchiol.sec**	**AI**
GM	47.05	40.98	100.26	65.13	3.57	61.87	56.07	135.47	85.05	4.29
Median	48.45	41.85	102.34	66.92	3.91	63.73	57.42	138.77	87.93	4.69
Mean	52.01	45.77	111.97	72.82	4.34	67.98	61.82	149.34	93.23	5.12
GSD	1.58	1.61	1.61	1.62	1.93	1.56	1.57	1.57	1.55	1.87
Q_L	18.59	15.75	38.51	24.38	0.92	24.83	22.47	29.87	34.18	1.17
Q_U	104.74	97.96	239.55	154.08	10.18	133.09	125.15	302.34	179.43	11.48
UF	2.37	2.49	2.49	2.51	3.32	2.32	2.36	2.36	2.29	3.13

GM: geometric mean; Q_L: 2.5th percentile; Q_U: 97.5th percentile; UF: Uncertainty factor

5.2.1 Hypothesis testing to compare the uncertainty analysis results for Job 1 and Job 4.

The primary objective of hypothesis testing was to assess whether there were significant differences in organ-specific radiation dose coefficients between the two underground mining job types. The null hypothesis (H_0) was that the dose distributions (or their medians, assuming similarly shaped distributions) were similar in both job scenarios and the alternative hypothesis (H_1) was that the dose distributions for the two groups were not similar in both job scenarios.

However, because Monte Carlo simulations revealed that the dose data were positively skewed and could best be described by lognormal or gamma distributions, parametric methods such as the Welch t-test were deemed inappropriate (West, 2021). Hence, the Mann–Whitney U test was employed, as it is robust when comparing independent, non-normally distributed samples. Secondly, this distribution-free test compares the ranks of values between groups and is particularly well-suited to skewed datasets, which are common in radiation dose modelling (Nachar, 2008; Schober and Vetter, 2020; Tai et al., 2022).

This study involved 50,000 dose samples in each group (Job 1 and Job 4), resulting in an expected U-statistic[1] under the null hypothesis of 1.25E+09; calculated as the mean of the product of the number of iterations in the Monte Carlo simulations for the two job types. The value of 1.25E+09 represents the midpoint of the U distribution under the null hypothesis, if the two groups have the same underlying distribution. Therefore, deviations from this value indicate differences in distributions.

From the data presented in Table 29, the observed U-statistics were much lower than 1.25 billion across all organs (e.g., 8.441089E+08 for the lungs) and the p-values were all 0 ($p<1.0E-16$). Since the p-values are less than the limiting value of 0.05 for all organs and tissues, there was overwhelming evidence to reject the null hypothesis. The confidence intervals for the differences in medians were all negative, confirming the earlier notion of higher dose coefficients in Job 4 compared to Job 1. The largest differences were observed in the respiratory tract, particularly in Bronch.sec, with a median difference of up to −38 mSv/ (mJh/m³). Even systemic organs such as the kidneys, liver and brain showed significant dose increases, albeit to a lesser extent.

These results clearly confirm that Job 4 poses significantly higher radiation exposure risks than Job 1. The statistical evidence decisively supports the conclusion that the two job types are not equivalent in terms of exposure levels. These findings are also presented in form of a forest plot in Figure 29.

Table 29: Hypothesis testing results from the Mann-Whitney U test of committed equivalent dose coefficients (Job1 - Job 4) following radon progeny inhalation in underground mines.

Organ	U-statistic	p-value	Lower CI	Upper CI	Conclusion
Lung	8.441089E+08	0	-1.627531E+01	-1.563076E+01	Reject H_0
Bronch-bas	8.000256E+08	0	-1.635339E+01	-1.572746E+01	Reject H_0
Bronch-sec	8.165637E+08	0	-3.811601E+01	-3.662982E+01	Reject H_0
Bchiol-sec	8.616237E+08	0	-2.086583E+01	-1.996313E+01	Reject H_0
AI	1.054938E+09	0	-8.120807E-01	-7.421513E-01	Reject H_0
St-stem	8.698039E+08	0	-6.307882E-03	-6.021458E-03	Reject H_0

[1] The parameter U represents a test statistic used to determine whether there is a significant difference between two independent samples.

R-marrow	9.967009E+08	0	-1.986989E-03	-1.855644E-03	Reject H_0
Colon	9.918619E+08	0	-1.989495E-03	-1.858328E-03	Reject H_0
RC-stem	9.905315E+08	0	-2.012250E-03	-1.888697E-03	Reject H_0
LC-stem	9.889507E+08	0	-2.050828E-03	-1.917849E-03	Reject H_0
RS-stem	1.000913E+09	0	-1.817771E-03	-1.696854E-03	Reject H_0
Liver	1.000499E+09	0	-5.704884E-03	-5.340373E-03	Reject H_0
Kidneys	1.002141E+09	0	-2.292444E-02	-2.148859E-02	Reject H_0
Endost-BS	9.967420E+08	0	-4.839645E-03	-4.523037E-03	Reject H_0
Brain	9.773504E+08	0	-1.036001E-03	-9.760035E-04	Reject H_0
Ht-wall	9.938810E+08	0	-1.869726E-03	-1.753668E-03	Reject H_0

In conclusion, the Mann–Whitney U test clearly showed that there were significant differences in radiation dose coefficients between Jobs 1 and 4. Workers in Job 4 received substantially higher doses, primarily due to poorer environmental conditions and higher radon levels. These results highlight the urgent need for effective ventilation, dust suppression and exposure control measures to protect the health of underground miners.

Having accomplished this, the next step was to perform a sensitivity analysis to determine which of the parameters/ groups of parameters contributes most to the calculated committed equivalent lung dose coefficients for both exposure scenarios.

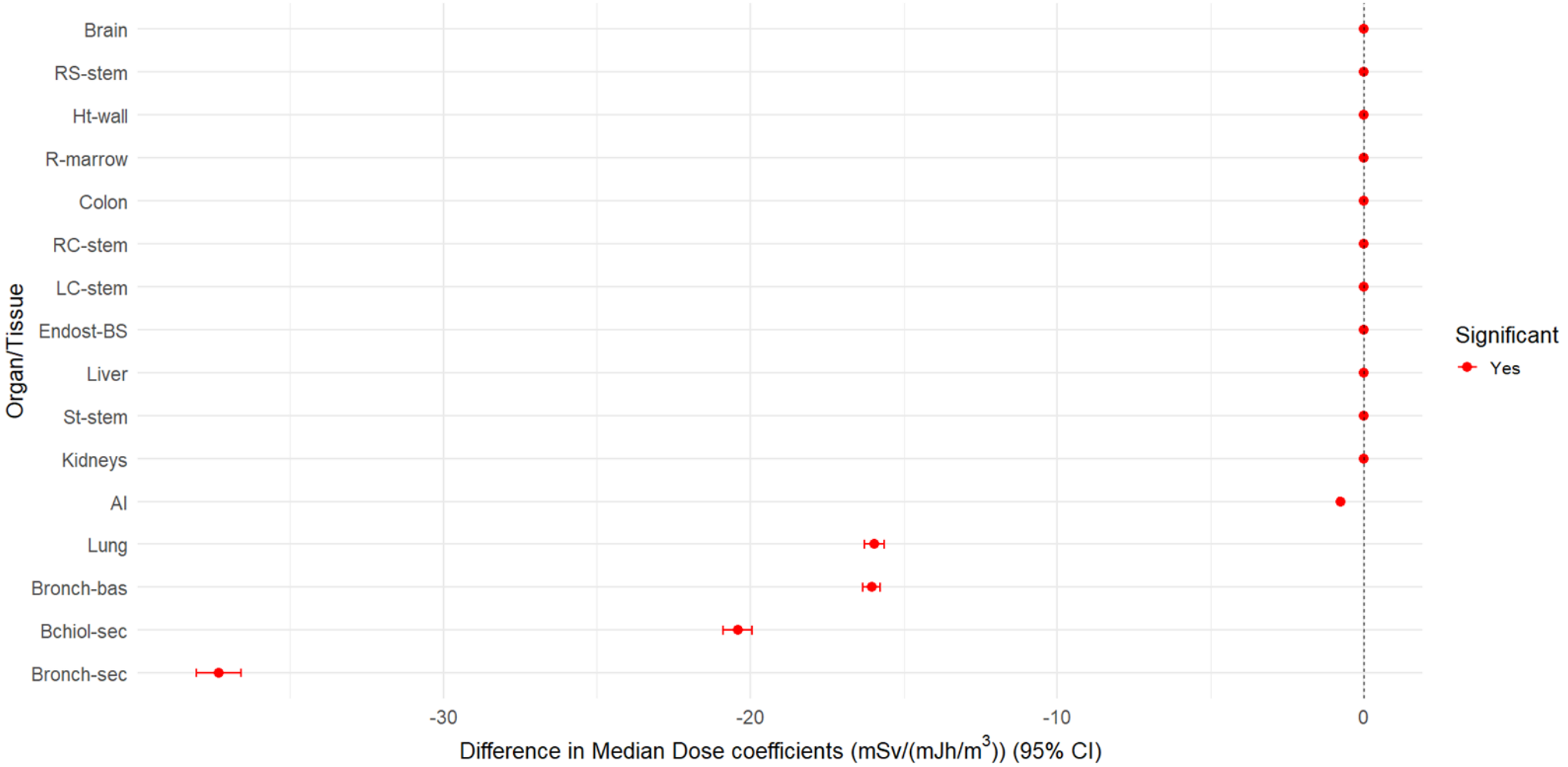

Figure 29: Forest plot showing the comparison of committed equivalent dose coefficients (Job 1 - Job 4) using the Mann-Whitney U test following inhalation of radon progeny in underground mines.

5.3. Sensitivity of the committed equivalent lung dose coefficient to parameter groups due to inhalation of radon progeny in underground mines.

5.3.1 Sensitivity of lung dose to the activity parameters

Table 30 presents the results for the sensitivity analysis of the committed equivalent lung dose coefficient to the activity parameters. From Table 30, the committed equivalent lung dose coefficient resulting from the inhalation of radon progeny in underground mining environments is highly sensitive to activity parameters. These physiological factors determine the quantity and characteristics of air and thus of radioactive aerosols inhaled, thereby directly influencing deposition patterns, dose distribution and the total radiation burden delivered to lung tissues. Their role is even more critical in physically demanding jobs, where elevated respiratory activity can significantly increase the inhaled dose.

The results of the Monte Carlo simulations to assess the contribution of these parameters to the overall uncertainty in the committed equivalent lung dose coefficient indicate that the greatest uncertainty occurs when all parameters are varied simultaneously (UF = 2.37 for Job 1 and 2.32 for Job 4). However, focusing exclusively on activity parameters still results in a substantial UF (2.26 and 2.30 for Jobs 1 and 4, respectively), emphasizing their dominant influence particularly in Job 4, where they account for almost all the uncertainty.

The physical relevance of these parameters is underscored by their mechanistic links to inhalation dynamics. For instance, increased tidal volume and breathing frequency common in high-exertion roles such as hewing amplify radon progeny intake, resulting in higher lung doses. The nasal fraction also matters; nasal breathing partially filters out aerosols, whereas mouth breathing allows greater penetration of radon progeny into the lungs. Therefore, changes in breathing patterns due to exertion or environmental factors (e.g., heat or poor ventilation as is the case in Job 4) increase uncertainty.

Notably, the lower UF observed when only 'Other parameters' parameters are varied (1.26 for Job 1 and 1.05 for Job 4) demonstrate that, although other inputs contribute to the dose, activity parameters are more influential. However, dose outcomes are also affected by environmental differences, such as variations in radon progeny concentration and aerosol characteristics between jobs. This confirms that, although activity parameters are important, they must be considered in the context of job-specific environmental exposures.

Table 30: Statistical summary of results for the uncertainty analysis of the committed equivalent lung dose coefficient (mSv/(mJh/m^3)) to activity parameters due to inhalation of radon progeny in underground mines.

Statistical parameter	**All parameters**		**Other parameters**		**Activity parameters**	
	Job 1	**Job 4**	**Job 1**	**Job 4**	**Job 1**	**Job 4**
Median	48.44	63.73	38.43	47.03	40.69	61.81
Mean	52.01	67.98	38.44	47.02	43.09	65.96
GM	47.05	61.87	38.17	47.00	39.34	60.05
Q_L	18.59	24.83	29.92	44.70	16.13	24.35
Q_U	104.74	133.09	47.63	49.30	82.68	129.30
SD	23.00	28.98	4.56	1.25	17.95	28.12
GSD	1.58	1.56	1.13	1.03	1.55	1.56
UF	2.37	2.32	1.26	1.05	2.26	2.30

5.3.2 Sensitivity of lung doses to the aerosol parameters

Aerosol parameters have a significant impact on particle deposition in the respiratory tract and consequently on dose estimates for radon progeny inhalation in underground mining environments. Monte Carlo simulations were used to assess the sensitivity of the committed equivalent lung dose coefficient to aerosol parameters for Jobs 1 and 4. Table 31 presents the results for the sensitivity of the committed equivalent lung dose coefficient to the aerosol parameters.

In Job 1, the presence of smaller, less stable particles and fluctuating unattached fractions significantly impacts dose variation due to aerosol parameters. This is reflected in a GSD of 1.12 and UF of 1.25). When all other parameters except aerosols ('Other parameters') are varied, the UF increases to 1.56, indicating interactive effects and highlighting the importance of aerosol behavior in dose assessments. By contrast, Job 4 exhibits a highly stable aerosol environment with minimal sensitivity to variation in the aerosols (both GSD and UF = 1.01). In this case, most of the dose uncertainty originates from 'Other parameters', with a UF of 2.32 that matches the overall UF.

Despite higher radon progeny activity concentrations, the consistent aerosol properties in Job 4 lead to narrower dose ranges and more predictable lung doses. The unattached fraction remains the primary aerosol variable, but its impact is relatively minor compared to the influence of activity parameters and exposure conditions. These findings suggest that, in Job 1, aerosol parameters alone contribute less to the overall uncertainty in the committed equivalent lung dose coefficient, while in Job 4, their contribution is negligible.

Table 31: Statistical summary of results for the sensitivity analysis of the committed equivalent lung dose coefficient (mSv/ (mJh/m³)) to aerosol parameters due to inhalation of radon progeny in underground mines.

Statistical parameter	**All parameters**		**Other parameters**		**Aerosol parameters**	
	Job 1	**Job 4**	**Job 1**	**Job 4**	**Job 1**	**Job 4**
Median	48.44	63.73	42.52	63.28	37.27	45.62
Mean	52.01	67.98	45.16	67.45	37.18	45.61
GM	47.05	61.87	41.14	61.32	36.93	45.61
Q_L	18.59	24.83	16.75	24.52	29.04	44.96
Q_U	104.74	133.09	87.15	132.29	45.55	46.26
SD	23.00	28.98	19.04	28.90	4.31	0.41
GSD	1.58	1.56	1.56	1.56	1.12	1.01
UF	2.37	2.32	1.56	2.32	1.25	1.01

5.3.3Sensitivity of lung doses to the subject parameters

Results for the sensitivity of the committed equivalent lung dose coefficient to subject parameters are presented in Table 32. Subject parameters influence aerosol deposition by modulating airflow dynamics within the respiratory tract. From Table 32, the sensitivity analysis results for Job 1 show that varying only the subject parameters yielded a median lung dose of 34.75 mSv/(mJh/m³), which is well below 48.44 mSv/ (mJh/m^3) obtained when all parameters were varied and lower than 47.29 mSv/ (mJh/m^3) observed when subject parameters were fixed ('Other parameters'). A comparable pattern emerged in Job 4, where the median dose was 46.50 mSv/ (mJh/m^3) for subject-only variation versus 63.73 mSv/ (mJh/m^3) for all

parameters varied and 62.44 mSv/ (mJh/m^3) for 'Other parameters'. These lower median, mean and GM values suggest that subject parameters contribute minimally to central dose estimates.

Uncertainty metrics reinforce this finding. For instance, in Job 1, the standard deviation (SD)[2], and UF for subject-only variation were low at 1.10 mSv/ (mJh/m^3) and 1.06 respectively, compared to 23.00 mSv/ (mJh/m^3) and a UF of 2.37 for all parameter variation. Similar trends were observed in Job 4, with an even lower UF of 1.04 for subject parameters. These results confirm that 'Other parameters' are the main sources of dose uncertainty, particularly in settings involving high exposure, such as Job 4.

Interestingly, subject parameters had a slightly greater impact at the lower end of the dose distribution. For example, in Job 1, Q_L was 32.78 mSv/ (mJh/m^3) for subject-only variation, which is notably higher than 18.59 mSv/ (mJh/m^3) and 18.42 mSv/ (mJh/m^3) observed for all parameters and 'Other parameters'. This suggests that subject parameter variation slightly increases minimum dose estimates. However, these parameters had little effect on Q_U values, which remained low in contrast to the much higher extremes observed for 'Other parameters'. From a physiological perspective, this is to be expected, given that V_D affects upper-airway deposition and therefore contributes minimally to total dose.

Table 32: Statistical summary of results for the sensitivity analysis of the committed equivalent lung dose coefficient (mSv/ (mJh/m³)) to subject parameters due to inhalation of radon progeny in underground mines.

Statistical parameter	**All model parameters**		**Other parameters**		**Subject parameters**	
	Job 1	**Job 4**	**Job 1**	**Job 4**	**Job 1**	**Job 4**
Median	48.44	63.73	47.29	62.44	34.77	46.51
Mean	52.01	67.98	50.75	66.51	34.75	46.50
GM	47.05	61.87	46.00	60.55	34.73	46.49
Q_L	18.59	24.83	18.42	24.42	32.78	44.56
Q_U	104.74	133.09	101.48	130.27	36.66	48.41
SD	23.00	28.98	22.24	28.32	1.10	1.11
GSD	1.58	1.56	1.57	1.56	1.03	1.02
UF	2.37	2.32	2.35	2.31	1.06	1.04

5.3.4 Sensitivity of lung doses to the absorption parameters

Absorption parameters describe the rate at which inhaled radioactive particles, particularly radon progeny, transfer from the respiratory tract to the bloodstream. Sensitivity analysis results presented in Table 33, show that the median lung dose when absorption parameters are varied alone is 33.81 mSv/ (mJh/m³) for Job 1, which is substantially lower than the 48.44 mSv/ (mJh/m^3) observed when all parameters are varied. Similarly, Job 4 exhibits a comparable pattern i.e., 45.71 mSv/ (mJh/m^3) for absorption only variation versus 63.73 mSv/ (mJh/m^3) for all-parameter variation. This trend reflects the limited sensitivity of lung dose estimates to variation in the absorption rates.

[2] As a measure of variation, SD determines how much the data values deviate from the mean or the closeness of a particular data structure from the mean (Mbaji et al., 2023).

Uncertainty metrics further support this observation. For both jobs, the SD is extremely low i.e., 0.15 mSv/ (mJh/m^3) for Job 1 and 0.19 mSv/ (mJh/m^3) for Job 4. The GSD and UF are both 1.01 in each case, indicating that the dose outcome remains almost constant regardless of absorption rate fluctuation. The narrow percentile range, particularly in Job 1 (Q_L = 33.59 mSv/ (mJh/m^3), Q_U = 34.04 mSv/ (mJh/m^3)), highlights the stability and predictability of dose estimates based on absorption parameters alone.

However, when all parameters except absorption are varied, the uncertainty profile closely mirrors that of the full-parameter simulation. In Job 1, the median dose for 'Other parameters' is 47.55 mSv/ (mJh/m^3), with a UF of 2.35 nearly identical to the UF of 2.37 for the full-parameter simulation. Job 4 shows a similar result (UF = 2.31 for 'Other parameters' versus 2.32 for all parameters). These results clearly indicate that the dominant sources of uncertainty lie outside the absorption domain. While these parameters are biologically significant for internal dosimetry, they demonstrate minor variation and influence on lung dose uncertainty for the case of radon progeny inhalation.

Table 33: Statistical summary of results for the sensitivity analysis of the committed equivalent lung dose coefficient (mSv/ (mJh/m³)) to absorption parameters due to inhalation of radon progeny in underground mines.

Statistical parameter	**All parameters**		**Other parameters**		**Absorption parameters**	
	Job 1	**Job 4**	**Job 1**	**Job 4**	**Job 1**	**Job 4**
Median	48.44	63.73	47.55	63.29	33.81	45.71
Mean	52.01	67.98	50.97	67.51	33.81	45.71
GM	47.05	61.87	46.19	61.44	33.81	45.71
Q_L	18.59	24.83	18.45	24.71	33.59	45.43
Q_U	104.74	133.09	102.18	132.22	34.04	46.00
SD	23.00	28.98	22.34	28.79	0.15	0.19
GSD	1.58	1.56	1.57	1.56	1.01	1.01
UF	2.37	2.32	2.35	2.31	1.01	1.01

5.3.5 Sensitivity of lung doses to the particle transport parameters

The movement and deposition of inhaled radioactive aerosols within the respiratory tract is governed by particle transport parameters. The sensitivity analysis results (see Table 34) for Job 1 show that, the committed equivalent lung dose coefficient associated with variation in these parameters is notably lower at a median of 33.54 mSv/ (mJh/m³) compared to 48.44 mSv/ (mJh/m^3) when all parameters are varied. Similarly, in Job 4, the median dose is 45.34 mSv/ (mJh/m^3) for particle transport variation alone versus 63.73 mSv/ (mJh/m^3) for the full parameter scenario. These substantial differences highlight the limited contribution of particle transport to overall dose sensitivity.

Uncertainty metrics support this interpretation. The SD for particle transport in Job 1 is just 0.21mSv/ (mJh/m^3), with a GSD and UF of 1.01 indicating extremely tight dose distributions. Job 4 shows slightly broader but still low uncertainty (SD = 0.40 mSv/ (mJh/m^3), GSD = 1.01, UF = 1.02). These values confirm that, although particle transport parameters are integral to deposition modelling, they have a minimal effect on propagated uncertainty under job-specific conditions.

Conversely, when all parameters except particle transport are varied ('Other parameters'), the uncertainty is close to that of the full-parameter case. For instance, Job 1 exhibits a UF of 2.36 and 2.37 for all parameters, whereas Job 4 maintains a UF of 2.32 in both instances. This highlights that most dose uncertainty arises from other sources. Despite their biophysical relevance, sensitivity analysis results show that variation in particle transport parameters alone introduces minor variation to estimates of committed equivalent lung dose coefficient.

Table 34: Statistical summary of results for the sensitivity of the committed equivalent lung dose coefficient (mSv/ (mJh/m³)) to particle transport parameters for the inhalation of radon progeny in underground mines.

Statistical parameter	**All parameters**		**Other parameters**		**Particle transport parameters**	
	Job 1	**Job 4**	**Job 1**	**Job 4**	**Job 1**	**Job 4**
Median	48.44	63.73	48.55	63.84	33.54	45.35
Mean	52.01	67.98	52.15	68.08	33.54	45.34
GM	47.05	61.87	47.25	61.96	33.54	45.34
Q_L	18.59	24.83	18.74	24.84	33.15	44.59
Q_U	104.74	133.09	104.60	133.53	33.91	46.08
SD	23.00	28.98	22.91	29.03	0.21	0.40
GSD	1.58	1.56	1.58	1.56	1.01	1.01
UF	2.37	2.32	2.36	2.32	1.01	1.02

Table 35 gives a summary of the sensitivity of the committed equivalent lung dose coefficient to the various parameter groups for Job 1.

Table 35: Statistical summary of the comparison of the sensitivity of the committed equivalent lung dose coefficient (mSv/ (mJhm³)) to parameter groups due to inhalation of radon progeny in underground mines under Job 1 exposure conditions.

Parameters	**Median**	**Mean**	**GM**	**SD**	**GSD**	**UF**
All	48.44	52.01	47.05	23.00	1.58	2.37
Activity	40.69	43.09	39.04	17.95	1.55	2.26
Aerosol	37.27	37.18	36.93	4.31	1.12	1.25
Subject	34.77	34.75	34.73	1.10	1.03	1.06
Absorption	33.81	33.81	33.81	0.15	1.01	1.01
Particle transport	33.54	33.54	33.54	0.21	1.01	1.01

From Table 35 and Figure 30, the sensitivity analysis of the committed equivalent lung dose coefficient for radon progeny inhalation in underground mines under Job 1 exposure conditions shows that activity and aerosol parameters contribute most to dose variation and uncertainty. This is evidenced by higher values of SD, GSD and UF.

Conversely, parameters related to absorption, particle transport and subject characteristics have minimal effects, as shown by their consistently low SD and UF values, indicating very stable dose estimates with low uncertainty. This can mainly be attributed to the short half-lives of the radon progeny (less than 30 minutes) causing them to decay mainly at their deposition sites before being cleared by the competing processes of either absorption to blood or particle transport to the alimentary tract.

This suggests that biological variation and particle movement in the lung do not significantly influence dose results for inhalation of radon progeny. From a health perspective, the lower sensitivity of these factors may reduce the complexity of risk assessment for workers, but the substantial influence of activity and aerosol parameters underlines the need for careful monitoring and control of radon progeny concentrations and aerosol properties to minimise radiation exposure and associated health risks in underground mining environments. Similar analysis is presented for Job 4 in Table 36 and Figure 30.

Table 36: Statistical summary of the comparison of the sensitivity analysis of the committed equivalent lung dose coefficient (mSv/ (mJhm^3)) to parameter groups due to inhalation of radon progeny in underground mines under Job 4 exposure conditions.

Parameters	**Median**	**Mean**	**GM**	**SD**	**GSD**	**UF**
All	63.73	67.98	61.87	28.98	1.56	2.32
Activity	61.81	65.96	60.05	28.12	1.56	2.30
Aerosol	45.62	45.61	45.61	0.41	1.01	1.01
Subject	46.51	46.50	46.49	1.11	1.02	1.04
Absorption	45.71	45.71	45.71	0.19	1.01	1.01
Particle transport	45.35	45.34	45.34	0.40	1.01	1.02

From the results presented in Table 36 as well as Figure 30, it again can be observed that "activity parameters" contribute the most to the variation in the committed equivalent lung dose coefficient for the inhalation of radon progeny in underground mines for both exposure scenarios. Therefore, it was deemed necessary to investigate which of these "activity parameters" contribute most to the overall variation in the committed equivalent lung dose coefficient for the inhalation of radon progeny under both exposure conditions. The results are presented in the following subsections.

The sensitivity analysis results of committed equivalent dose coefficients for other organs and tissues due to variation in different parameter groups are presented in Annex B at the end of this report (see Table B1 to Table B10).

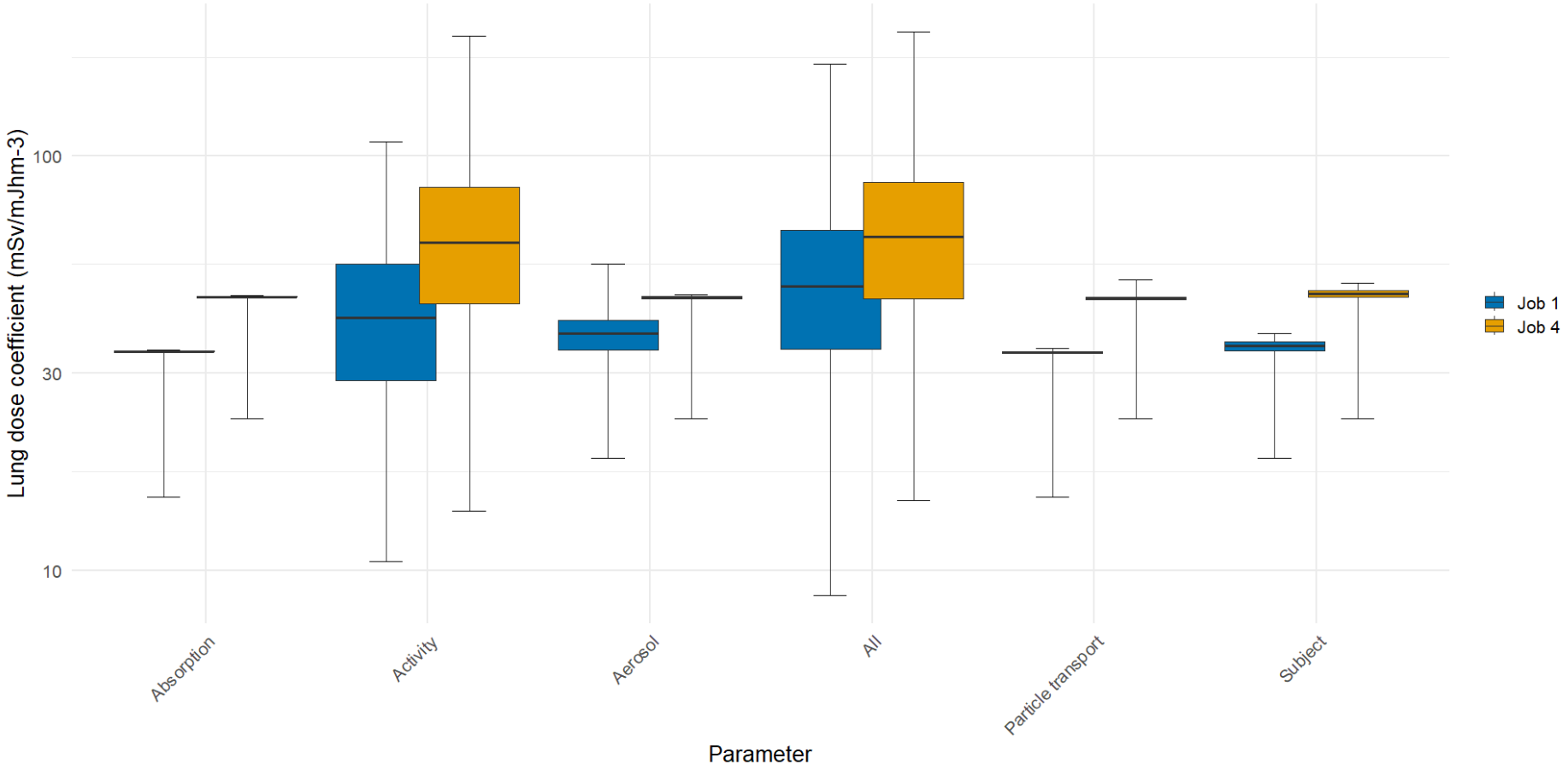

Figure 30: Grouped boxplots showing the sensitivity of committed equivalent lung dose coefficient (mSv/ (mJh/m³)) to parameter groups due to inhalation of radon progeny in underground mines.

5.4. Sensitivity of the committed equivalent lung dose coefficient to activity parameters of the HRTM for inhalation of radon progeny in underground mines.

5.4.1 Sensitivity of lung dose to tidal volume

From Table 37, the sensitivity analysis of the committed equivalent lung dose coefficient shows that tidal volume has a significant influence on exposure. Its values are consistently higher than those for 'Other parameters'. For instance, the results for Job 1 show that the median and mean values for tidal volume (43.32 mSv/ (mJh/m^3) and 43.53 mSv/ (mJh/m^3)) are higher than those for 'Other activity' parameters (33.25 mSv/ (mJh/m^3) and 33.46 mSv/ (mJh/m^3)). A similar pattern is observed for Job 4, where tidal volume values (57.92 mSv/ (mJh/m^3) and 58.13 mSv/ (mJh/m^3)) exceed 'Other activity' parameters.

The GM, GSD and UF follow the same trend, emphasising the influence of tidal volume on the committed equivalent lung dose coefficient. The results suggest that increased depth of breathing increases the risk of exposure, particularly in physically demanding or poorly ventilated environments. This suggests that tidal volume alone makes a significant contribution to the committed equivalent lung dose coefficient when compared to 'Other activity' parameters.

Table 37: Statistical summary of the sensitivity of the committed equivalent lung dose coefficient (mSv/ (mJh/m^3)) to tidal volume for the inhalation of radon progeny in underground mines.

Statistical parameter	**Activity parameters**		**Other activity parameters**		**Tidal volume**	
	Job 1	**Job 4**	**Job 1**	**Job 4**	**Job 1**	**Job 4**
Median	40.69	61.81	33.25	50.60	43.32	57.92
Mean	43.09	65.96	33.46	51.61	43.53	58.13
GM	39.34	60.05	32.62	49.98	40.73	54.63
Q_L	16.13	24.35	21.06	30.49	19.23	26.55
Q_U	82.68	129.30	47.67	79.06	68.58	90.37
SD	17.95	28.12	7.42	13.01	15.01	19.41
GSD	1.55	1.56	1.26	1.29	1.46	1.44
UF	2.26	2.30	1.51	1.61	1.89	1.85

5.4.2 Sensitivity of lung dose to breathing frequency

Basing on the results presented in Table 38, the sensitivity analysis of the committed equivalent lung dose coefficient shows that breathing frequency has a smaller effect on the committed equivalent lung dose coefficient compared to activity parameters and 'Other activity' parameters.

For both Job 1 and Job 4, the median and mean values for breathing frequency are consistently lower. For Job 1, the values (32.01 mSv/ (mJh/m^3) and 32.04 mSv/ (mJh/m^3)) are significantly lower than those for activity parameters (40.69 mSv/ (mJh/m^3) and 43.09 mSv/ (mJh/m^3)) and 'Other activity' parameters (44.92 mSv/ (mJh/m^3) and 45.39 mSv/ (mJh/m^3)). A similar trend can be observed for Job 4. The GM also confirms the lower effect of breathing frequency.

Variation metrics, including SD, GSD and UF (6.66 mSv/ (mJh/m^3), 1.24 and 1.43 respectively), indicate that dose contributions from breathing frequency are more stable and predictable. This suggests that breathing frequency alone contributes less to committed equivalent lung dose coefficient when compared to 'Other activity' parameters.

Table 38: Statistical summary of the results from the sensitivity analysis of the committed equivalent lung dose coefficient (mSv/ (mJh/m³)) to breathing frequency due to inhalation of radon progeny in underground mines.

Statistical parameter	**Activity parameters**		**Other activity parameters**		**Breathing frequency**	
	Job 1	**Job 4**	**Job 1**	**Job 4**	**Job 1**	**Job 4**
Median	40.69	61.81	44.93	67.72	32.01	43.30
Mean	43.09	65.96	45.39	69.20	32.04	43.34
GM	39.34	60.05	42.36	64.49	31.33	42.31
Q_L	16.13	24.35	19.75	29.76	21.10	28.23
Q_U	82.68	129.30	75.21	119.64	42.99	58.22
SD	17.95	28.12	16.07	25.02	6.66	9.09
GSD	1.55	1.56	1.47	1.47	1.24	1.24
UF	2.26	2.30	1.95	2.01	1.43	1.44

5.4.3 Sensitivity of lung dose to fraction of air breathed through the nose

According to the results presented in Table 39, the sensitivity analysis of the committed equivalent lung dose coefficient highlights the role of the nasal fraction in reducing lung exposure compared to activity and 'Other activity' parameters. For Job 1, the median and mean dose values for the nasal fraction are consistently lower, indicating its effectiveness in filtering radioactive particles. For instance, the median and mean values (34.77 mSv/ (mJh/m^3) and 34.89 mSv/ (mJh/m^3)) are significantly lower than those for activity parameters (40.69 mSv/ (mJh/m^3) and 43.09 mSv/ (mJh/m^3)) and 'Other activity' parameters (39.37 mSv/ (mJh/m^3) and 41.71 mSv/ (mJh/m^3)).

The variation metrics confirm this trend. For instance, the nasal fraction has SD, GSD and UF values indicating greater stability. For instance, the SD for Job 1 is 0.84 mSv/ (mJh/m^3), significantly lower than the activity parameters (17.95 mSv/ (mJh/m^3)). Similarly, the UF for the nasal fraction is much lower, reinforcing its predictability.

For Job 4, although the parameter values increase, they remain lower than the values associated with the activity parameters. This suggests that poor air quality in Job 4 likely prompts miners to breathe through their mouths, bypassing the natural filtration system of nasal breathing. Consequently, more radon progeny can penetrate deeper into the lungs, exposing sensitive lung tissues to increased radiation and thereby elevating the risk of lung cancer.

These findings suggest that nasal fraction alone has a minor contribution to the committed equivalent lung dose coefficient in Job 1 and minimal contribution in Job 4.

Table 39: Statistical summary of the results from the sensitivity analysis of the committed equivalent lung dose coefficient (mSv/ (mJh/m³)) to fraction of air breathed through the nose due to inhalation of radon progeny in underground mines.

Statistical parameter	**Activity parameters**		**Other activity parameters**		**Nasal fraction**	
	Job 1	**Job 4**	**Job 1**	**Job 4**	**Job 1**	**Job 4**

Median	40.69	61.81	39.37	52.73	34.77	52.83
Mean	43.09	65.96	41.71	55.76	34.89	53.79
GM	39.34	60.05	38.05	51.05	34.88	53.48
Q_L	16.13	24.35	15.56	21.32	33.70	45.76
Q_U	82.68	129.30	79.94	105.84	36.63	66.39
SD	17.95	28.12	17.44	22.88	0.84	5.87
GSD	1.55	1.56	1.55	1.54	1.02	1.11
UF	2.26	2.30	2.27	2.23	1.04	1.21

5.4.4 Sensitivity of lung dose to time fraction spent in each activity

From Table 40, the sensitivity analysis of the committed equivalent lung dose coefficient shows that the time fraction has a stable and predictable effect on lung exposure, with consistently lower dose coefficients and reduced uncertainty compared to activity and 'Other activity' parameters.

For both Job 1 and Job 4, the median and mean values for the time fraction are significantly lower. For Job 1, the median and mean values (33.68 mSv/ (mJh/m^3) and 33.69 mSv/ (mJh/m^3)) are lower than those for activity parameters (40.69 mSv/ (mJh/m^3) and 43.09 mSv/ (mJh/m^3)). Similarly, for Job 4, the values for the time fraction (45.54 mSv/ (mJh/m^3) and 45.55 mSv/ (mJh/m^3)) remain lower than those for the activity parameters (61.81 mSv/ (mJh/m^3) and 65.96 mSv/ (mJh/m^3)).

The time fraction also shows lower uncertainty, as indicated by its lower SD, GSD and UF values. For Job 1, the SD is 2.63 mSv/ (mJh/m^3), significantly lower than for the activity parameters (17.95 mSv/ (mJh/m^3)). These results suggest that while time fraction has a minimal effect on lung dose coefficients, prolonged exposure combined with high intensity activity could increase risks.

Table 40: Statistical summary of the results from the sensitivity analysis of the committed equivalent lung dose coefficient (mSv/ (mJh/m³) to the fraction of time spent in each activity due to inhalation of radon progeny in underground mines.

Statistical parameter	**Activity parameters**		**Other activity parameters**		**Time fraction**	
	Job 1	**Job 4**	**Job 1**	**Job 4**	**Job 1**	**Job 4**
Median	40.69	61.81	40.82	61.78	33.69	45.55
Mean	43.09	65.96	42.93	65.70	33.68	45.54
GM	39.34	60.05	39.32	60.03	33.58	45.39
Q_L	16.13	24.35	16.32	24.61	29.35	39.40
Q_U	82.68	129.30	81.12	125.88	38.02	51.71
SD	17.95	28.12	17.52	27.36	2.63	3.75
GSD	1.55	1.56	1.54	1.55	1.08	1.09
UF	2.26	2.30	2.23	2.26	1.14	1.15

From the results presented in Figure 31 and Table 41, the sensitivity of activity parameters, including breathing frequency, tidal volume, nasal fraction and time fraction, to the committed equivalent lung dose coefficient for inhalation of radon progeny in underground mines can be

analysed in terms of statistical variation and health implications. The activity parameters, which summarises the variations in all these individual parameters, has a median of 40.69 mSv/ (mJh/m^3) and a mean of 43.09 mSv/ (mJh/m^3), with a relatively high SD (17.95 mSv/ (mJh/m^3)), a GSD of 1.55 and UF of 2.26. This indicates moderate variability and sensitivity, suggesting that the combined effect of these parameters significantly influences the lung dose coefficients.

Breathing frequency shows much lower variation compared to total activity, with a median of 32.01 mSv/ (mJh/m^3) and a mean of 32.04 mSv/ (mJh/m^3), along with a low SD (6.66 mSv/ (mJh/m^3)), GSD (1.24) and UF (1.43). This stability suggests that breathing frequency, while relevant, contributes less to the uncertainty in the calculated value of the lung dose coefficient. However, during strenuous activities, elevated breathing frequencies could contribute significantly to increased radon progeny deposition, highlighting their importance in high impact scenarios.

The nasal fraction is the least variable parameter, with a median of 34.77 mSv/ (mJh/m^3), mean of 34.89 mSv/ (mJh/m^3) and exceptionally low SD (0.84 mSv/ (mJh/m^3)), GSD (1.02) and UF (1.04). This stability indicates a minimal contribution to lung dose variability compared to the activity parameters. The role of the nasal fraction is limited under normal conditions, as most air inhalation occurs through the nose; however, mouth breathing during intense exercise could alter radon progeny deposition, especially in deeper lung regions.

Tidal volume shows a median of 43.32 mSv/ (mJh/m^3) and a mean of 43.53 mSv/ (mJh/m^3), with a relatively high SD (15.01 mSv/ (mJh/m^3)), GSD (1.46) and UF (1.89), making it the most sensitive parameter among the individual components. This high uncertainty is closely related to activity parameters, highlighting the important role of tidal volume in influencing radon progeny deposition in the lung. Larger tidal volumes during strenuous work greatly increase the risk of exposure, making this parameter critical in assessing lung dose coefficients.

The fraction of time spent in each activity has a median of 33.69 mSv/ (mJh/m^3) and a mean of 33.68 mSv/ (mJh/m^3), with low variation as indicated by the SD (2.63 mSv/ (mJh/m^3)), GSD (1.08) and UF (1.14). This stability reflects the low sensitivity observed for breathing frequency and nasal fraction. While the time fraction alone has minimal impact, longer durations in radon-rich environments could increase exposure, especially when combined with high tidal volumes and increased activity levels.

In comparison, the activity parameters reflect the cumulative variation of all individual parameters and is moderately sensitive to dose coefficients. Among the activity parameters, it was observed that tidal volume has the highest variation and hence sensitivity, making it the most influential in determining radon progeny deposition and associated health risks. Breathing frequency, nasal fraction and time fraction are less variable parameters but still play an important role under certain conditions such as strenuous exercise or prolonged exposure. These findings highlight the need for targeted control measures, such as reducing physical exertion in high radon zones and managing exposure duration, to minimise health risks to underground miners.

A similar trend can be observed for Job 4 (see Figure 31 and Table 42). The sensitivity of the activity parameters i.e., breathing frequency, tidal volume, nasal fraction and time fraction to

the committed equivalent lung dose coefficient for inhalation of radon progeny in underground mines can be assessed from their statistical summary, with comparisons made to the overall activity parameters, which includes all variations. The activity row has the highest median (61.81mSv/ (mJh/m^3)) and mean (65.96 mSv/ (mJh/m^3)) values, along with the greatest variation, as indicated by its SD (28.12 mSv/ (mJh/m^3)), GSD of 1.56, and UF of 2.30. This highlights the cumulative effect of all the individual parameters, making it moderately sensitive to variations in lung dose coefficients.

Breathing frequency shows much less variation compared to total activity, with a median of 43.34 mSv/ (mJh/m^3), a mean of 43.30 mSv/ (mJh/m^3), and low SD (9.09 mSv/ (mJh/m^3)), GSD (1.24), and UF (1.44). This suggests that breathing frequency is less sensitive to dose coefficients, although an increase in breathing frequency during exercise can increase radon progeny deposition and is therefore important in high activity scenarios.

The nasal fraction shows moderate stability with a median of 52.83 mSv/ (mJh/m^3) and a mean of 53.79 mSv/ (mJh/m^3), together with a relatively low SD (5.87 mSv/ (mJh/m^3)), GSD (1.11) and UF (1.21). These values indicate limited sensitivity compared to total activity. While nasal breathing dominates normal breathing, mouth breathing during exercise could alter radon progeny deposition patterns, making the nasal fraction relevant under certain conditions.

Tidal volume is more variable and closer to "activity parameters". With a median of 57.92 mSv/ (mJh/m^3), a mean of 58.13 mSv/ (mJh/m^3) and a higher SD (19.41 mSv/ (mJh/m^3)), GSD (1.44) and UF (1.85), tidal volume has a significant effect on radon progeny deposition. Larger tidal volumes during exertion contribute to deeper deposition of radon progeny in the lung, increasing exposure and lung dose coefficients, making this parameter highly sensitive.

Time fraction is the most stable parameter with a median of 45.55 mSv/ (mJh/m^3), mean of 45.54 mSv/ (mJh/m^3) and very low uncertainty (SD of 3.75 mSv/ (mJh/m^3), GSD of 1.09 and UF of 1.15). Although it has limited sensitivity on its own, prolonged exposure times in high radon areas may amplify the effects of other parameters, such as tidal volume and breathing frequency, on lung dose coefficients.

Compared to activity parameters, tidal volume shows the greatest similarity in uncertainty and sensitivity; while breathing frequency, nasal fraction and time fraction show less uncertainty and sensitivity. The combined variation in the activity parameters highlights the importance of understanding how these individual factors interact to influence lung dose coefficients. From a health perspective, high tidal volumes and prolonged exposure times pose the greatest risks, highlighting the need for strategies such as reducing physical exertion and limiting time spent in high radon environments to reduce the risk of lung cancer in miners.

The comparison of the two job types as presented in Table 41 (Job 1) and Table 42 (Job 4), shows noticeable differences in the statistical summaries of the activity parameters and their uncertainty. In both cases, the activity parameters show the highest variation, reflecting the combined effects of all the individual parameters. For Job 1 the median (40.69 mSv/ (mJh/m^3)), mean (43.09 mSv/ (mJh/m^3)) and SD (17.95 mSv/ (mJh/m^3)) are lower than for Job 4 where the median is 61.81 mSv/ (mJh/m^3), the mean is 65.96 mSv/ (mJh/m^3) and SD increases

significantly to 28.12 mSv/ (mJh/m^3). The GSD and UF are slightly higher for Job 4 (1.56 and 2.30 respectively), indicating a higher variability and uncertainty in the data set for Job 4.

Breathing frequency shows minimal variation in both tables, with medians of 32.01mSv/ (mJh/m^3) and 43.34 mSv/ (mJh/m^3) in Table 41 and Table 42 respectively. The SD is slightly higher in Table 42 (9.09 mSv/ (mJh/m^3) compared to 6.66 mSv/ (mJh/m^3)), but the GSD (1.24) and UF (1.43-1.44) remain consistent, indicating a similar level of sensitivity in both cases, despite the higher central tendency in the dataset for Job 4.

For the nasal fraction, Table 42 shows higher values for all metrics, with a median of 52.83 mSv/ (mJh/m^3) compared to 34.77 mSv/ (mJh/m^3) in Table 41. However, the uncertainty remains low in both cases, as indicated by the small SD (0.84 mSv/ (mJh/m^3) in Table 41 versus 5.87 mSv/ (mJh/m^3) in Table 42), GSD (1.02-1.11) and UF (1.04-1.21). This suggests that the nasal fraction remains a relatively stable parameter in both data sets.

Table 41: Statistical summary of the comparison of the sensitivity of the committed equivalent lung dose coefficient (mSv/ (mJh/m^3)) to activity parameters for the inhalation of radon progeny in underground mines under Job 1 conditions.

Parameters	**Median**	**Mean**	**GM**	**SD**	**GSD**	**UF**
Activity	40.69	43.09	39.04	17.95	1.55	2.26
Breathing frequency	32.01	32.04	31.33	6.66	1.24	1.43
Nasal fraction	34.77	34.89	34.88	0.84	1.02	1.04
Tidal volume	43.32	43.53	40.73	15.01	1.46	1.89
Time fraction	33.69	33.68	33.58	2.63	1.08	1.14

Table 42: Statistical summary of the comparison of the sensitivity of the committed equivalent lung dose coefficient (mSv/ (mJh/m^3)) to activity parameters for the inhalation of radon progeny in underground mines under Job 4 conditions.

Parameters	**Median**	**Mean**	**GM**	**SD**	**GSD**	**UF**
Activity	61.81	65.96	60.05	28.12	1.56	2.30
Breathing frequency	43.34	43.30	42.31	9.09	1.24	1.44
Nasal fraction	52.83	53.79	53.48	5.87	1.11	1.21
Tidal volume	57.92	58.13	54.63	19.41	1.44	1.85
Time fraction	45.55	45.54	45.39	3.75	1.09	1.15

The sensitivity analysis results of committed equivalent dose coefficients for other organs and tissues due to variation in activity parameters are presented in Annex C at the end of this report (see Table C1 to Table C8).

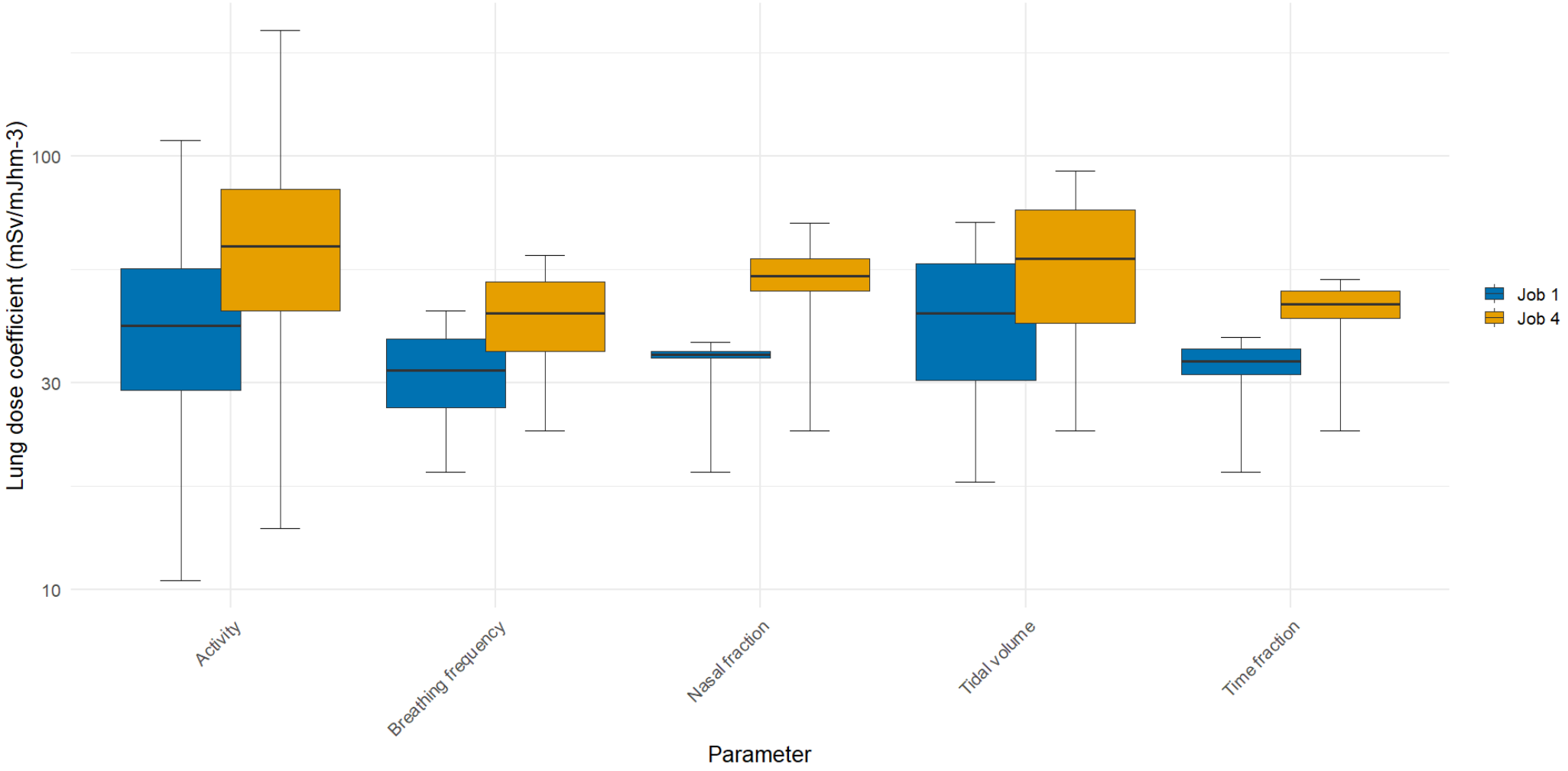

Figure 31: Boxplots showing the sensitivity of the committed equivalent lung dose coefficient (mSv/ (mJh/m^3)) to activity parameters due to inhalation of radon progeny in underground mines.

5.3 Uncertainty and sensitivity analysis of doses for the inhalation of uranium ore dust in underground mines

5.3.1 Uncertainty analysis of committed dose coefficients for the inhalation of uranium ore dust in underground mines

The global uncertainty analysis results for uranium ore dust inhalation in underground mines are summarized in Appendix D1 for Job 1 and Appendix D2 for Job 4. In both cases, the committed equivalent lung dose coefficient follows a lognormal distribution. For Job 1, the GM is 2.97E-02 mSv/ (kBqh/m^3), with a GSD of 2.28, as illustrated in Figure 32. The 95% confidence interval (CI) ranges from 6.07E-03 mSv/ (kBqh/m^3) to 1.50E-01 mSv/ (kBqh/m^3), with UF of 4.97. For Job 4, the GM is 4.41E-02 mSv/ (kBqh/m^3), with a GSD of 2.28, as shown in Table 39. The 95% CI spans from 8.84E-03 mSv/ (kBqh/m^3) to 2.10E-01 mSv/ (kBqh/m^3), and the UF is 4.88.

For both job types, the highest uncertainty within the lung is again observed in the AI region, with UF of 6.15 for Job 1 and 5.97 for Job 4. Conversely, the lowest uncertainty is found in Bronch.bas, where UFs are 4.52 for Job 1 and 4.50 for Job 4. Within the lung, the Bchiol.sec cells in the bb region receive the highest dose, with median dose coefficients of 3.46E-02 mSv/ (kBqh/m^3) for Job 1 and 5.22E-02 mSv/ (kBqh/m^3) for Job 4. In contrast, the AI region receives the lowest dose due to its larger mass (1.1 kg), which leads to lower specific absorbed fractions (SAFs). This reduced dose is also influenced by aerosol deposition mechanisms in the lung, as larger particles primarily settle in the upper and central airways, limiting deposition in deeper regions such as the AI.

Outside the lungs, the bone receives the highest dose for both job types, with values of 5.25E-02 mSv/ (kBqh/m^3) for Job 1 and 7.93E-03 mSv/ (kBqh/m^3) for Job 4. In contrast, the colon receives the lowest dose, with dose coefficients of 1.85E-04 mSv/ (kBqh/m^3) for Job 1 and 2.76E-04 mSv/ (kBqh/m^3) for Job 4. Among systemic organs, the highest uncertainty is observed in St.stem for Job 1 (UF = 5.85) and for Job 4 (UF = 5.59). The brain exhibits the lowest uncertainty, with UF of 3.23 for Job 1 and 3.31 for Job 4.

The posterior distribution data for both job types exhibit significant variation, particularly in lung dose coefficients. For Job 1, the lung dose data show an SD of 4.03E-02 mSv/ (kBqh/m^3), with a mean of 4.17E-02 mSv/ (kBqh/m^3), which is slightly higher than the median of 2.96E-02 mSv/ (kBqh/m^3). This difference suggests a right-skewed distribution. The GM of 2.97E-02 mSv/ (kBqh/m^3), being close to the median, further supports the assumption of a lognormal distribution. The Bchiol.sec region exhibits substantial variation, with a high SD of 4.75E-02 mSv/ (kBqh/m^3). The right-skewed nature of this distribution is evident as the mean exceeds the median, indicating uneven data spread with a tail extending toward higher values.

A similar pattern is observed for Job 4, where lung dose coefficients show high variation, with SD of 5.73E-02 mSv/ (kBqh/m^3). The mean (6.14E-02 mSv/ (kBqh/m^3)) is slightly higher than the median (4.43E-02 mSv/ (kBqh/m^3)), indicating a right-skewed distribution. The Bchiol-sec region again exhibits the highest variation, with an SD of 6.76E-02 mSv/ (kBqh/m^3) and a strong right-skew. The uncertainty analysis for both job types reveal consistent trends in lung

and systemic organ dose variation. Within the lung, the highest uncertainties occur in the AI region, while the Bchiol.sec of the bb region receive the highest doses.

Outside the lung, bone consistently exhibits the highest dose and uncertainty. These findings emphasize the need to consider both dose distribution and uncertainty when evaluating health risks associated with uranium ore dust inhalation. The uncertainty in dose coefficients highlight the complexity of modelling dose distributions in respiratory and systemic organs, particularly in high-risk occupational environments such as underground mines.

The uncertainty analysis results for the committed equivalent dose coefficients to the lung and its target regions, comparing both job types, reveal significant differences in magnitude, uncertainty, and potential health effects, as presented in Table 39 and Figure 32. Across all lung regions, Job 4 consistently shows higher doses than Job 1. For instance, the GM lung dose for Job 4 is 4.41E-02 mSv/ (kBqh/m^3), approximately 41% higher than the 2.97E-02 mSv/ (kBqh/m^3) observed for Job 1.

Similar trends are observed in target regions such as Bronch.bas, Bronch.sec, Bchiol.sec, and AI, where GM values for Job 4 are 35% to 42% higher than those for Job 1. The median values are close to the GMs, confirming a symmetric lognormal distribution of doses. However, the mean values are even more pronounced for Job 4, with the mean lung dose reaching 6.14E-02 mSv/ (kBqh/m^3), approximately 42% higher than the 4.17E-02 mSv/ (kBqh/m^3) observed for Job 1. This suggests that Job 4 is associated with a greater number of high dose cases, potentially increasing health risks for workers in this category.

Statistical variation, measured by the GSD, is similar between the two job types, with values ranging from 2.2 to 2.3 across most regions. However, the AI region exhibits slightly greater variation, with GSD values of 2.6 for Job 1 and 2.5 for Job 4, indicating increased uncertainty in dose predictions for this region. When analysing interquartile ranges (Q_L-Q_U), Job 4 shows wider uncertainty intervals, suggesting that some workers in this category may receive exceptionally high doses. For instance, the lung Q_U for Job 4 is 2.10E-01 mSv/ (kBqh/m^3), compared to 1.50E-01 mSv/ (kBqh/m^3) for Job 1, with similar trends observed in other regions.

Additionally, the UF is slightly higher for Job 4, particularly in the AI region, further indicating greater variation in dose estimates. This increased uncertainty may stem from differences in exposure scenarios or biological factors, underscoring the importance of tailored risk assessments to ensure accurate dose evaluation and worker protection.

The health implications of these findings are significant. Higher radiation doses in Job 4 conditions indicate an increased risk of radiation-induced damage to critical lung regions, particularly Bronch.bas and AI. The AI region, essential for gaseous exchange, receives particularly high doses in Job 4, with a GM of 3.67E-02 mSv/ (kBqh/m^3) and a mean of 5.57E-02 mSv/ (kBqh/m^3). Prolonged exposure at these levels could elevate the risk of lung fibrosis, chronic inflammation, and lung cancer.

Although doses in Job 1 are lower, risks remain a concern, especially for workers at the higher end of the dose distribution. Additionally, the wider dose ranges and higher average values in Job 4 emphasize the need for more stringent protective measures. These could include enhanced

ventilation systems, improved personal protective equipment (PPE), and more frequent dose monitoring to better safeguard workers from radiation exposure.

In conclusion, the analysis highlights the increased health risks faced by Job 4 workers due to higher radiation doses and greater exposure variation. This underscores the need for targeted measures to minimize exposure, particularly in high-risk lung regions. Additionally, effective risk communication and the implementation of personalized protective strategies are essential to mitigate the long-term health effects of uranium ore dust exposure and ensure worker safety.

Table 41: Statistical summary of the posterior distribution of the committed equivalent lung dose coefficient (mSv/ (kBqh/m³)) for the inhalation of uranium ore dust in underground mines.

	Job 1					**Job 4**				
	Lung	**Bronch.bas**	**Bronch.sec**	**Bchiol.sec**	**AI**	**Lung**	**Bronch.bas**	**Bronch.sec**	**Bchiol.sec**	**AI**
GM	2.97E-02	2.91E-02	2.75E-02	3.46E-02	2.46E-02	4.41E-02	4.25E-02	4.03E-02	5.18E-02	3.67E-02
Median	2.96E-02	2.92E-02	2.77E-02	3.46E-02	2.47E-02	4.43E-02	4.28E-02	4.09E-02	5.22E-02	3.75E-02
Mean	4.17E-02	3.93E-02	3.77E-02	4.88E-02	3.77E-02	6.14E-02	5.72E-02	5.52E-02	7.25E-02	5.57E-02
GSD	2.28E+00	2.17E+00	2.23E+00	2.29E+00	2.54E+00	2.28E+00	2.18E+00	2.23E+00	2.29E+00	2.54E+00
Q_L	6.07E-03	6.41E-03	5.67E-03	6.97E-03	3.97E-03	8.84E-03	9.02E-03	8.06E-03	1.02E-02	5.84E-03
Q_U	1.50E-01	1.31E-01	1.28E-01	1.78E-01	1.50E-01	2.10E-01	1.83E-01	1.79E-01	2.48E-01	2.08E-01
UF	4.97E+00	4.52E+00	4.76E+00	5.05E+00	6.15E+00	4.88E+00	4.50E+00	4.72E+00	4.93E+00	5.97E+00

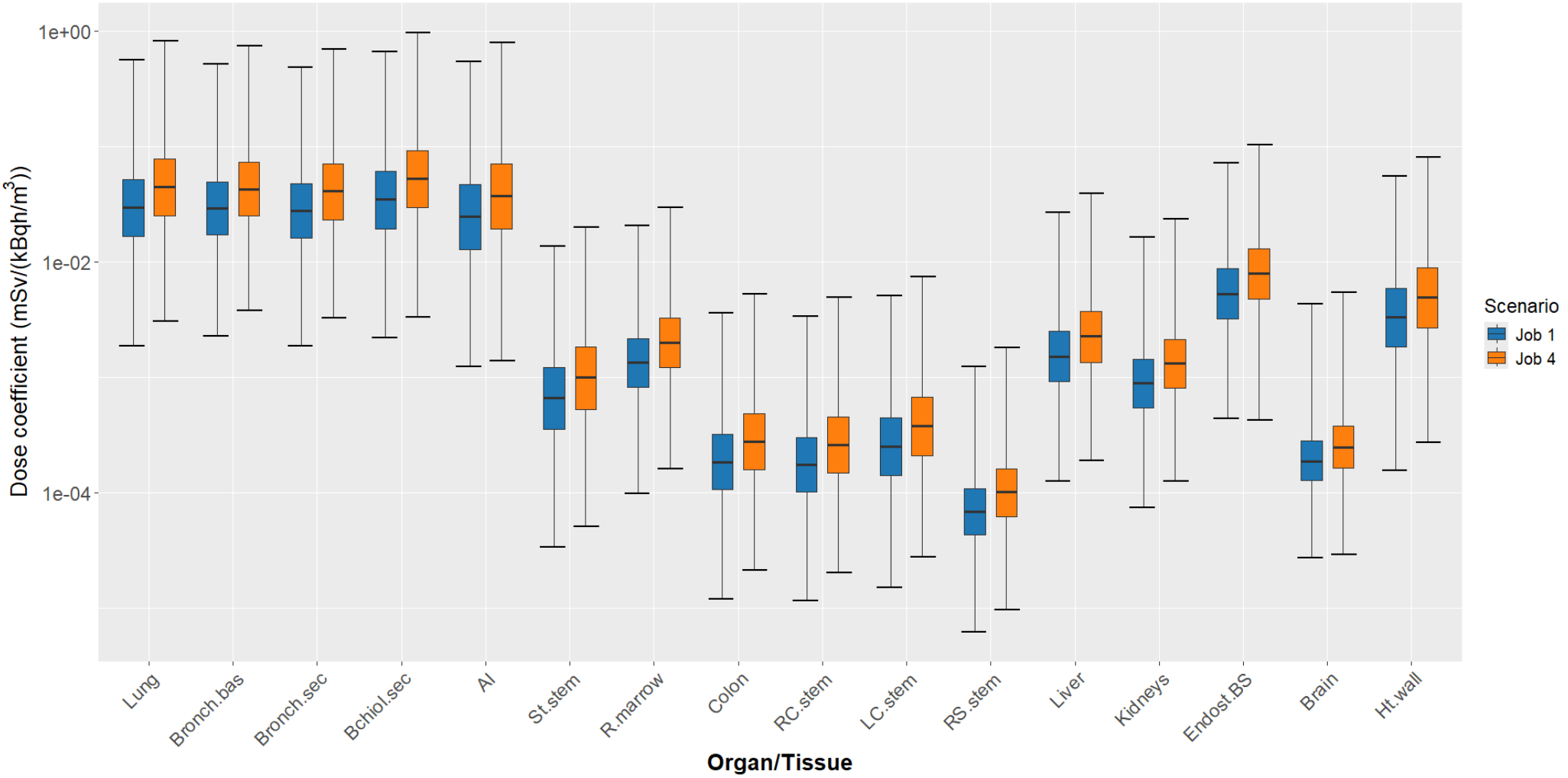

Figure 32: Boxplots for the global uncertainty analysis of dose coefficients (mSv/ (kBqh/m³)) for the inhalation of uranium ore dust by underground miners.

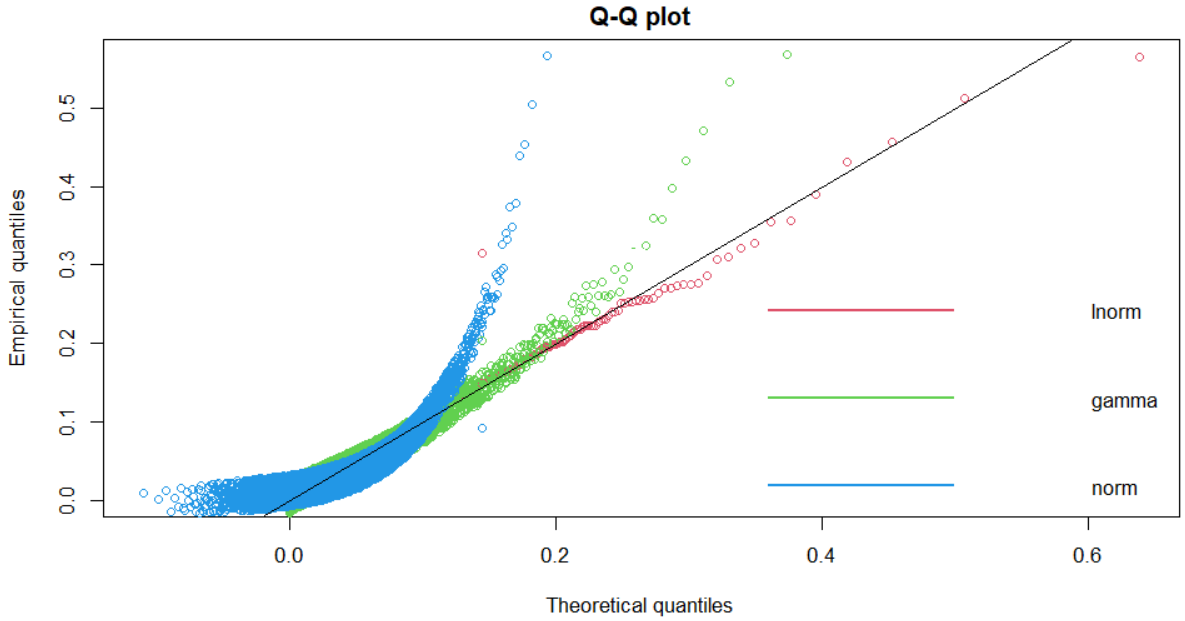

Figure 33: Fitting probability distributions using QQ plot to the posterior dataset of the committed equivalent lung dose coefficient following inhalation of uranium ore dust in underground mines under Job1 exposure conditions.

The Q-Q and P-P plots presented in Figure 33 and Figure 34 provide complementary visual assessments of how well three theoretical distributions i.e., lognormal, gamma, and normal fit the data set for Job 1. Both plots use different aspects of distribution comparison. The Q-Q plot evaluates how the quantiles of the empirical data match those of the theoretical distributions, while the P-P plot compares cumulative probabilities.

In the Q-Q plot, the lognormal distribution (red dots) shows the closest fit to the 45-degree reference line, especially through the middle of the data. Although there are small deviations at the extremes, overall, the lognormal distribution closely mirrors the empirical quantiles, suggesting that it is the most accurate representation of the data. The gamma distribution (green dots) performs moderately well, aligning with the diagonal in the mid-range but deviating in the tails, indicating a reasonable but imperfect fit. In contrast, the normal distribution (blue dots) diverges significantly, especially in the lower quantiles, underestimates the empirical values, and fails to capture the skewness and tail behaviour, making it an unsuitable model for these data.

Similarly, the P-P plot confirms these findings through cumulative probability comparisons. The lognormal distribution again shows the best fit to the diagonal with minimal deviation, reinforcing its suitability as the primary model. The gamma distribution has a moderate fit, but deviates significantly at the tails, indicating its limited ability to accurately capture extreme values. The normal distribution has a pronounced S-shaped deviation, systematically over and underestimating parts of the empirical distribution, further demonstrating its inadequacy.

Together, the Q-Q and P-P plots provide strong visual and statistical support for selecting the lognormal distribution as the most appropriate model. The gamma distribution can serve as a secondary option, while the normal distribution should be eliminated. These findings, while visually compelling, should ideally be corroborated by formal goodness-of-fit tests to strengthen the conclusions and guide further modelling decisions. Similar plots for Job 4 are given in Appendix E (Figure E1 ad Figure E2).

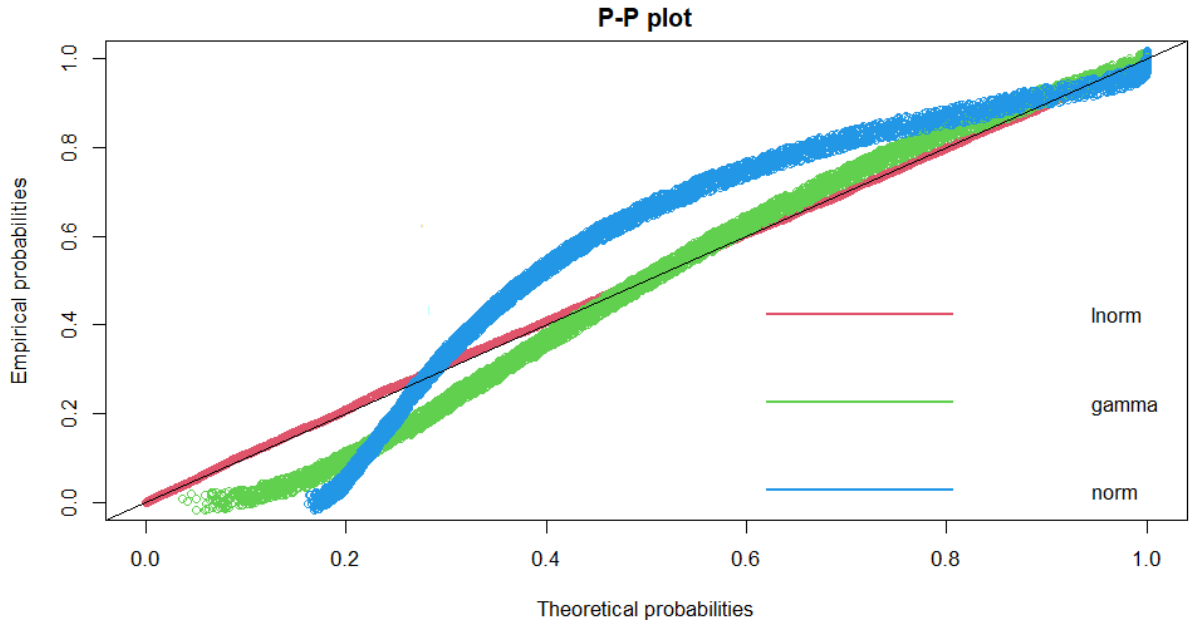

Figure 34: Fitting probability distributions using a PP plot to the posterior dataset of the committed equivalent lung dose coefficient following inhalation of uranium ore dust in underground mines under Job 1 conditions.

The histograms in Figure 35 and Figure 36 show the frequency distributions of the lung dose coefficients with three fitted probability distributions i.e., normal (blue), lognormal (red) and gamma (purple) for Job 1 and Job 4 respectively. The shape of the histograms suggests highly right-skewed distributions, characterised by a peak at lower values and a long tail extending to higher values. This skewness indicates that the data are not symmetrically distributed, which is an important consideration when choosing an appropriate probabilistic model.

The normal distribution, shown in blue, does not appear to be an appropriate fit to the data. As the normal distribution is symmetric, it struggles to accommodate the skewed nature of the dataset, leading to noticeable discrepancies, particularly in the peak region and the long tail. In contrast, the lognormal and gamma distributions, both of which are inherently right-skewed, provide a much better fit. The lognormal distribution closely follows the peak of the histograms and fits the overall shape of the data well, making it a strong candidate for modelling these datasets. Similarly, the gamma distribution also captures the right skew, although its fit near the peak is not as precise as the lognormal.

Overall, the lognormal distribution appears to provide the best representation of the observed data, particularly in the highest frequency region and along the extended tail. The gamma distribution is also a reasonable choice, although its effectiveness depends on the specific parameterisation. The poor fit of the normal distribution highlights the need to consider skewed distributions when modelling dose coefficients, as radiation dose response data often exhibit asymmetric characteristics due to variations in exposure and biological response. Therefore, from a statistical modelling perspective, the lognormal or gamma distributions would be more appropriate choices to represent these datasets.

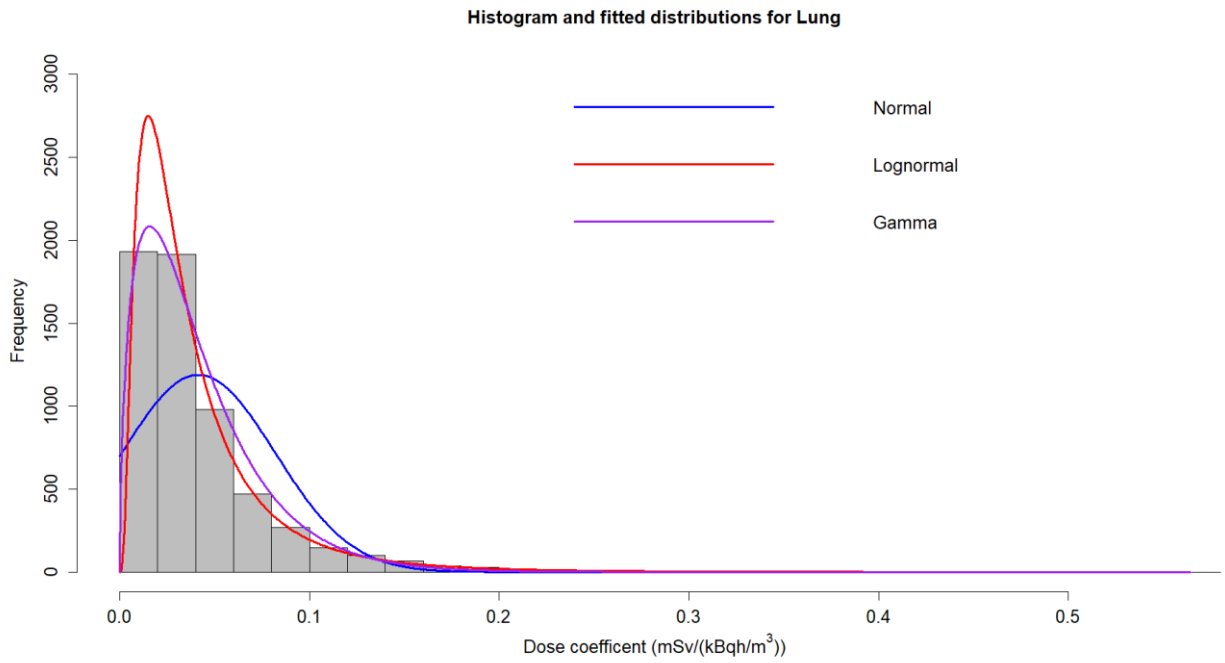

Figure 35: Fitting probability distributions to the committed equivalent lung dose coefficient (mSv/ (kBqh/m³)) for the inhalation of uranium ore dust under Job 1 exposure conditions.

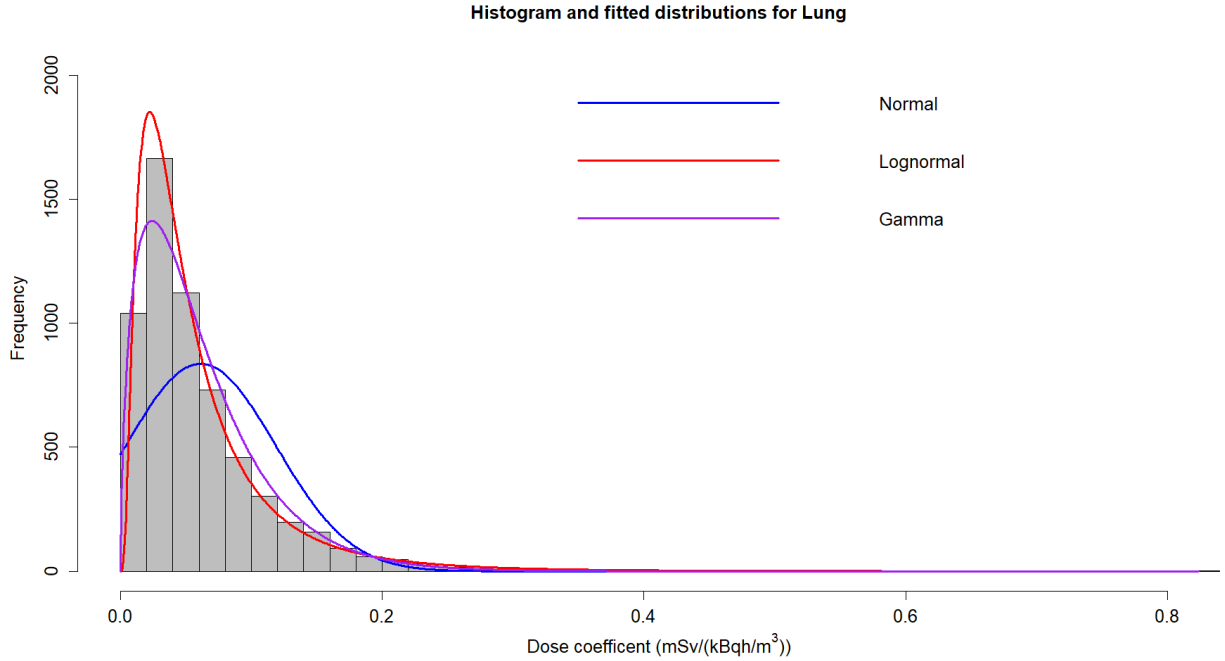

Figure 36: Fitting probability distributions to the committed equivalent lung dose coefficient (mSv/ (kBqh/m³)) for the inhalation of uranium ore dust under Job 4 exposure conditions.

5.3.1 Hypothesis testing to compare the uncertainty analysis results for Job 1 and Job 4.

A Mann–Whitney U test was used to statistically compare the dose coefficients derived from 6,000 Monte Carlo simulation iterations for each job type, between two occupational exposure scenarios involving the inhalation of uranium ore dust i.e., Job 1 and Job 4. For each organ or

tissue, the null hypothesis (H_0) was that the median dose coefficients for the two job types were equal.

The results presented in Table 40 strongly reject the null hypothesis for all analysed organs, with p-values far below 0.05, ranging from 5.0E-114 to 7.0E-188. This indicates extremely strong evidence of a difference in dose coefficients. The U-statistic values reflect a significant deviation from what would be expected under H_0, which further supports this conclusion. Notably, all confidence intervals for the median differences (Job 1–Job 4) are negative, suggesting that Job 4 consistently results in higher dose coefficients than Job 1.

These results are visualised in Figure 37, which presents a forest plot of median dose coefficient differences with 95% confidence intervals for each organ. The figure shows that all the statistically significant results (in red) are below zero, clearly demonstrating the consistent direction and magnitude of the differences. Organs and tissues such as the lungs, Bronch.bas, Bronch.sec, Bchiol.sec and AI tissue show particularly pronounced differences, which aligns with their known sensitivity to inhaled radioactive particles.

From a health perspective, these differences are significant. The elevated dose coefficients for Job 4 suggest a higher potential radiation dose burden and, consequently, a greater risk of stochastic effects, such as lung cancer. The dose differentials for high-risk tissues such as the lung (CI: −0.0216 to −0.0181 mSv/(kBqh/m^3)) and associated target regions i.e., Bronch.bas, Bronch.sec, Bchiol.sec and AI highlight the necessity of stricter exposure controls or revised dose modelling assumptions for Job 4. Even tissues with relatively small numerical differences, such as the colon or stem cells, achieved statistical significance, likely due to the large sample size and the precision of the simulations.

In conclusion, the statistical results in Table 40 and clear visualisation in Figure 37 provide strong, consistent evidence that Job 4 is associated with significantly higher internal doses across all assessed tissues. These findings reinforce the need for targeted radiological protection measures and exposure mitigation strategies tailored to the higher risk job category as well as potentially revised dose limits.

Table 42: Hypothesis testing results from the Mann-Whitney U test of committed equivalent dose coefficients (Job 1 - Job 4) following uranium ore dust inhalation in underground mines.

Organ	U-statistic	p-value	Lower CI	Upper CI	Conclusion
Lung	1.320807E+07	5.312399E-141	-2.157676E-02	-1.807613E-02	Reject H_0
Bronch-bas	1.319143E+07	5.741463E-142	-1.940542E-02	-1.634631E-02	Reject H_0
Bronch-sec	1.326228E+07	7.046735E-188	-1.896619E-02	-1.592418E-02	Reject H_0
Bchiol-sec	1.312389E+07	6.383443E-146	-2.581743E-02	-2.156079E-02	Reject H_0
AI	1.369899E+07	5.216545E-114	-1.986034E-02	-1.607183E-02	Reject H_0
St-stem	1.360100E+07	3.639075E-119	-5.024554E-04	-4.165558E-04	Reject H_0
R-marrow	1.260386E+07	3.317406E-178	-8.749150E-04	-7.578900E-04	Reject H_0
Colon	1.315738E+07	5.921767E-144	-1.316543E-04	-1.107343E-04	Reject H_0
RC-stem	1.311201E+07	1.270710E-146	-1.232943E-04	-1.036233E-04	Reject H_0
LC-stem	1.332259E+07	1.911371E-134	-1.836279E-04	-1.546160E-04	Reject H_0
RS-stem	1.234397E+07	1.465897E-195	-4.268370E-05	-3.700644E-05	Reject H_0
Liver	1.266616E+07	3.635825E-174	-1.014931E-03	-8.605167E-04	Reject H_0
Kidneys	1.257654E+07	5.429653E-180	-5.663961E-04	-4.900621E-04	Reject H_0

Endost-BS	1.258818E+07	3.139940E-179	-3.627666E-03	-3.135904E-03	Reject H_0
Brain	1.347965E+07	1.036792E-125	-8.037052E-05	-6.713774E-05	Reject H_0
Ht-wall	1.353197E+07	7.240094E-123	-2.384750E-03	-2.005934E-03	Reject H_0

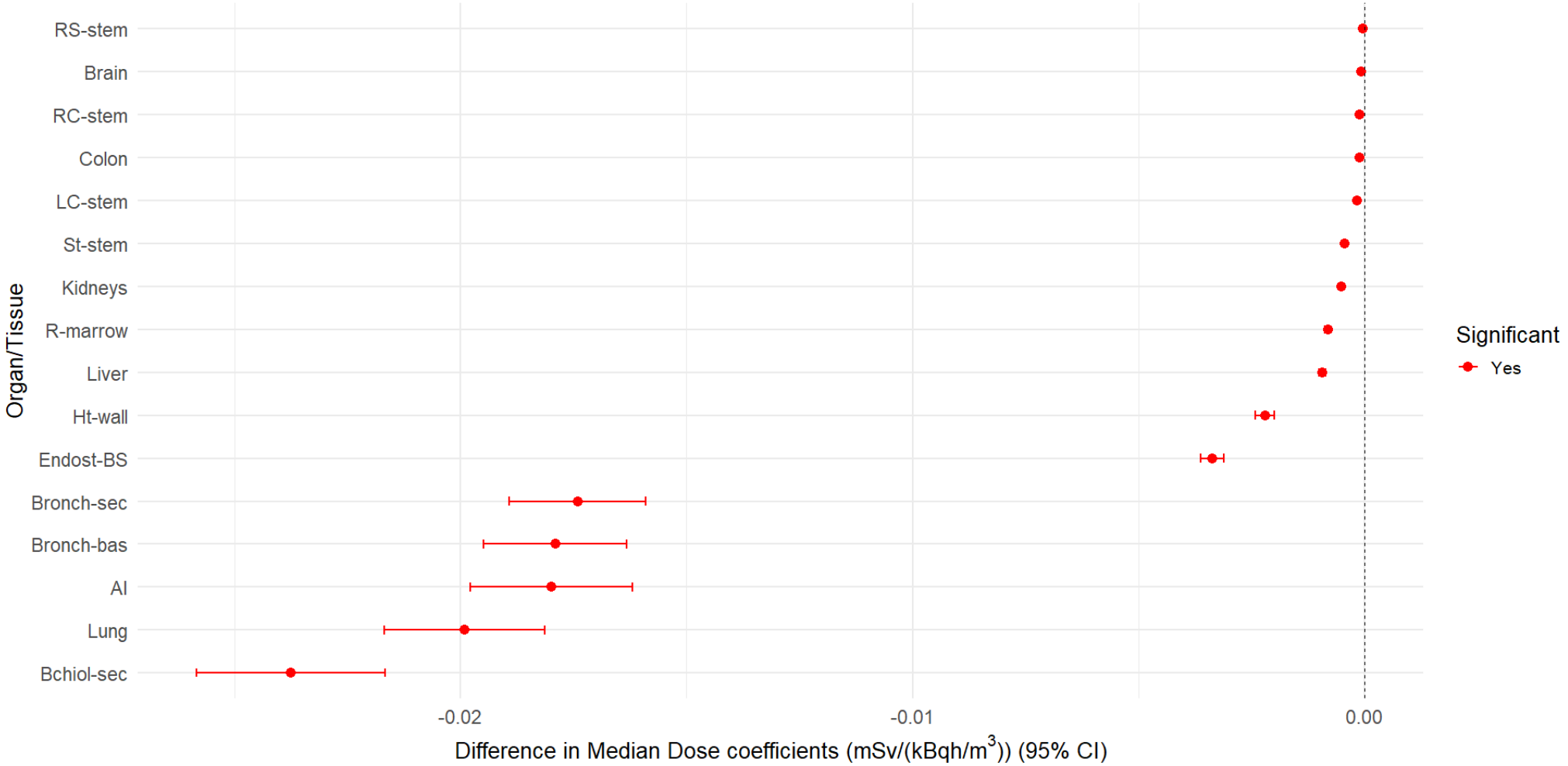

Figure 37: Forest plot showing the comparison of committed equivalent dose coefficients (Job 1-Job 4) using the Mann-Whitney U test from inhalation uranium ore dust in underground mines.

5.3.2 Sensitivity analysis of doses from the inhalation of uranium ore dust

5.3.2.1 Sensitivity of the committed equivalent lung dose coefficient to absorption parameters for uranium ore dust inhalation.

From Table 41, the comparison of the committed equivalent lung dose coefficients between Jobs 1 and 4 across different parameter categories i.e., “all parameters”, “other parameters” and absorption parameters shows significant differences in exposure levels and sensitivity to dose variations. In all categories, Job 4 has consistently higher dose values than Job 1, indicating a higher radiation exposure for Job 4 workers.

For “all parameters”, taking into account all exposure factors, the median dose coefficient is 4.49E-02 mSv/ (kBqh/m^3) for Job 4 and 3.07E-02 mSv/ (kBqh/m^3) for Job 1, with mean values of 6.09E-02 mSv/ (kBqh/m^3) and 4.29E-02 mSv/ (kBqh/m^3), respectively. The SD is high (6.09E-02 mSv/ (kBqh/m^3) for Job 4 and 4.12E-02 mSv/ (kBqh/m^3) for Job 1), reflecting considerable variation in the exposure conditions. The GSD of 2.27 and UF of 4.9 for Job 4 and GSD of 2.26 and UF of 4.70 for Job 1 indicate that the overall dose estimates have a high degree of uncertainty and sensitivity to variations in external exposure conditions.

For “other parameters”, excluding absorption, the dose coefficients remain comparable to the “all parameters” category, with a median of 4.25E-02 mSv/ (kBqh/m^3) for Job 4 and 2.97E-02 mSv/ (kBqh/m^3) for Job 1. The means are 6.12E-02 mSv/ (kBqh/m^3) and 4.14E-02 mSv/ (kBqh/m^3), respectively, and the SD is slightly lower for Job 4 (5.91E-02 mSv/ (kBqh/m^3)) but slightly higher for Job 1 (4.20E-02 mSv/ (kBqh/m^3)) compared to the “all parameter” category. The GSD for Job 1 increases to 2.28, while it is 2.26 for Job 4, indicating increased uncertainty in the dose estimates for Job 1. The UF is 4.96 for Job 1 and 4.54 for Job 4, confirming that these parameters have a strong influence on lung dose variation and should be a focus of exposure assessment.

For absorption parameters, the difference between Job 1 and Job 4 is less pronounced, with median values of 4.57E-02 mSv/ (kBqh/m^3) and 3.14E-02 mSv/ (kBqh/m^3), and mean values of 4.64E-02 mSv/ (kBqh/m^3) and 3.18E-02 mSv/ (kBqh/m^3), respectively. Unlike the other two categories, the SD (1.54E-02 mSv/ (kBqh/m^3) for Job 1 and 2.25E-02 mSv/ (kBqh/m^3) for Job 4) is significantly lower and the GSD is only 1.09 for both jobs, indicating minimal uncertainty. The UF is only 1.02, suggesting that absorption parameters contribute little to dose uncertainty. These results indicate that absorption parameters have the lowest sensitivity to lung dose variations, meaning that “other parameters” other than absorption drive most of the uncertainty in dose estimates.

The comparison between the three parameter categories shows that “all parameters” and “other parameters” have the highest sensitivity to dose uncertainty, as indicated by their high SD, GSD and UF values. In contrast, the absorption parameters have the least effect on dose variation, suggesting that once uranium ore dust is inhaled, its absorption follows a predictable pattern. These findings emphasise the need for radiation protection measures that prioritise the reduction of exposure conditions rather than relying on physiological differences in absorption. Strategies such as improved ventilation, enhanced personal protective equipment (PPE) and frequent monitoring should be implemented, particularly for workers in Job 4, who have significantly higher lung dose coefficients.

Table 43: Sensitivity of absorption parameters on the committed equivalent lung dose coefficient (mSv/ (kBqh/m³)) for the inhalation of uranium ore dust in underground mines.

Statistical parameter	All parameters		Other parameters		Absorption	
	Job 1	**Job 4**	**Job 1**	**Job 4**	**Job 1**	**Job 4**
Median	3.07E-02	4.49E-02	2.97E-02	4.25E-02	3.14E-02	4.57E-02
Mean	4.29E-02	6.10E-02	4.14E-02	6.12E-02	3.18E-02	4.64E-02
GM	3.08E-02	4.35E-02	2.94E-02	4.38E-02	3.15E-02	4.58E-02
Q_L	6.53E-03	8.50E-03	5.88E-03	1.01E-02	3.07E-02	4.47E-02
Q_U	1.45E-01	2.08E-01	1.44E-01	2.09E-01	3.20E-02	4.66E-02
SD	4.12E-02	6.09E-02	4.20E-02	5.91E-02	1.54E-02	2.25E-02
GSD	2.26E+00	2.27E+00	2.28E+00	2.26E+00	1.09E+00	1.09E+00
UF	4.70E+00	4.94E+00	4.96E+00	4.54E+00	1.02E+00	1.02E+00

5.3.2.2 Sensitivity of committed equivalent lung dose coefficient to particle transport parameters for uranium ore dust inhalation.

Table 42 shows the comparison of the committed equivalent lung dose coefficients between Job 1 and Job 4 for "all parameters", "other parameters" and particle transport parameters provides insight into the role of particle transport in radiation exposure. As noted earlier, Job 4 has consistently higher dose values than Job 1 in all categories, indicating greater exposure to uranium ore dust. However, the degree of uncertainty and sensitivity differs between the parameter categories.

For "all parameters" considering all exposure factors, the median lung dose is 4.49E-02 mSv/ (kBqh/m^3) for Job 4 and 3.07E-02 mSv/ (kBqh/m^3) for Job 1, with means of 6.09E-02 mSv/ (kBqh/m^3) and 4.29E-02 mSv/ (kBqh/m^3), respectively. The high SD and UF indicate considerable uncertainty in the exposure conditions. This suggests that lung dose is highly sensitive to changes in total exposure.

For "other parameters", which exclude particle transport parameters the dose coefficients increase significantly. The median dose rises to 5.90E-02 mSv/ (kBqh/m^3) for Job 4 and 3.94E-02 mSv/ (kBqh/m^3) for Job 1, an increase of 31% to 32% compared to the "all parameters" category. Mean and SD values follow similar trends, while UFs decrease, indicating that the removal of particle transport parameters reduces overall dose uncertainty and makes estimates more predictable.

For particle transport parameters, which focus on clearance and redistribution of inhaled uranium dust, dose values are lower and show less variation compared to the other categories. The median dose is 3.47E-02 mSv/ (kBqh/m^3) for Job 4 and 2.30 mSv/ (kBqh/m^3) for Job 1, with mean values also significantly lower. The GSD and UF values are reduced, showing that particle transport plays a minor role in the overall dose uncertainty compared to external exposure conditions.

The results indicate that external exposure factors such as dust concentration and ventilation could have the greatest influence on lung dose uncertainty, while particle transport parameters contribute less to dose uncertainty. Therefore, radiation protection measures should focus on reducing airborne uranium dust concentrations, improving ventilation and ensuring proper use of respiratory protective equipment, rather than targeting internal lung transport mechanisms.

By controlling the most variable and influential factors, radiation protection strategies can be more effective in minimising lung dose risks, particularly for underground mine workers.

Table 44: Sensitivity of the committed equivalent lung dose (mSv/ (kBqh/m³)) to particle transport parameters for the inhalation of uranium ore dust in underground mines.

Statistical parameter	**All parameters**		**Other parameters**		**Particle transport**	
	Job 1	**Job 4**	**Job 1**	**Job 4**	**Job 1**	**Job 4**
Median	3.07E-02	4.49E-02	3.94E-02	5.90E-02	2.30E-02	3.47E-02
Mean	4.29E-02	6.10E-02	4.73E-02	6.91E-02	2.80E-02	4.22E-02
GM	3.08E-02	4.35E-02	3.90E-02	5.84E-02	2.34E-02	3.53E-02
Q_L	6.53E-03	8.50E-03	1.10E-02	1.84E-02	7.98E-03	1.23E-02
Q_U	1.45E-01	2.08E-01	1.21E-01	1.74E-01	7.55E-02	1.13E-01
SD	4.12E-02	6.09E-02	3.28E-02	4.57E-02	2.32E-02	3.45E-02
GSD	2.26E+00	2.27E+00	1.87E+00	1.79E+00	1.79E+00	1.79E+00
UF	4.70E+00	4.94E+00	3.32E+00	3.08E+00	3.08E+00	3.03E+00

5.3.2.3 Sensitivity of committed equivalent lung dose coefficient to particle deposition parameters for uranium ore dust inhalation.

The results in Table 43 highlight the sensitivity of the committed equivalent lung dose coefficient to variations in particle deposition parameters for uranium ore dust inhalation in underground mines. A key observation is that for both types of work, the dose coefficients increase when particle deposition parameters are specifically considered. This indicates that particle deposition plays an important role in determining lung dose sensitivity.

When comparing the results for "all parameters", "other parameters" and "particle deposition", the lung dose coefficients are lowest for "other parameters" and highest when only "particle deposition" is considered. This trend is evident for both job types. For example, for Job 1 the mean dose coefficient increases from 3.47E-02 mSv/ (kBqh/m³) for "other parameters" to 3.60E-02 mSv/ (kBqh/m³) for "particle deposition", and for Job 4 it increases from 5.14E-02 mSv/ (kBqh/m^3) to 5.41E-02 mSv/ (kBqh/m^3). A similar pattern can be seen in the mean values, where Job 1 increases from 3.59E-02 mSv/ (kBqh/m^3) to 4.07E-02 mSv/ (kBqh/m^3) and Job 4 from 5.35E-02 mSv/ (kBqh/m^3) to 5.95E-02 mSv/ (kBqh/m^3). This upward trend shows that the particle deposition parameters contribute significantly to the lung dose and cannot be ignored in dose assessment.

The uncertainty in the dose estimates further support the sensitivity of lung dose to particle deposition. The SD and interquartile range (Q_L-Q_U) are consistently higher for particle deposition than for “other parameters”, indicating greater uncertainty when considering the effects of particle deposition. For example, in Job 1 the SD increases from 1.82E-02 mSv/ (kBqh/m^3) for "other parameters" to 2.57E-02 mSv/ (kBqh/m^3) for "particle deposition", while in Job 4 it increases from 2.64E-02 mSv/ (kBqh/m^3) to 3.65E-02 mSv/ (kBqh/m^3). The upper quantile (Q_U) values show a similar trend, with Job 4 reaching the highest observed value of 1.29E-01 mSv/ (kBqh/m^3) for particle deposition. In addition, the UF is significantly higher for "all parameters" (4.70 for Job 1 and 4.94 for Job 4), reflecting the overall uncertainty in dose estimates.

These results have important health implications, as higher lung dose coefficients indicate an increased risk of radiation exposure, particularly for Job 4 workers. The strong influence of particle deposition suggests that control of airborne particle size and concentration through improved ventilation, respiratory protection and exposure monitoring is critical in reducing radiation doses.

Furthermore, the observed uncertainty highlights the need for detailed site-specific dose assessments rather than relying on generalised exposure models. Overall, these results reinforce the importance of considering particle deposition parameters in lung dose calculations to ensure accurate risk assessment and effective radiation protection measures in underground uranium mines.

Table 45: Sensitivity of the committed equivalent lung dose coefficient (mSv/ (kBqh/m^3)) to particle deposition parameters for the inhalation of uranium ore dust in underground mines.

Statistical parameter	**All parameters**		**Other parameters**		**Particle deposition**	
	Job 1	**Job 4**	**Job 1**	**Job 4**	**Job 1**	**Job 4**
Median	3.07E-02	4.49E-02	3.47E-02	5.14E-02	3.60E-02	5.41E-02
Mean	4.29E-02	6.10E-02	3.59E-02	5.35E-02	4.07E-02	5.95E-02
GM	3.08E-02	4.35E-02	3.41E-02	5.10E-02	3.53E-02	5.21E-02
Q_L	6.53E-03	8.50E-03	1.83E-02	2.78E-02	1.16E-02	1.94E-02
Q_U	1.45E-01	2.08E-01	5.62E-02	8.21E-02	8.95E-02	1.29E-01
SD	4.12E-02	6.09E-02	1.82E-02	2.64E-02	2.57E-02	3.65E-02
GSD	2.26E+00	2.27E+00	1.36E+00	1.34E+00	1.71E+00	1.68E+00
UF	4.70E+00	4.94E+00	1.75E+00	1.72E+00	2.78E+00	2.59E+00

Table 46: Statistical summary of the comparison of the sensitivity of the committed equivalent lung dose coefficient (mSv/ (kBqh/m³)) to different parameter groups for the inhalation of uranium ore dust in underground mines under Job 1 exposure conditions.

Parameters	Median	Mean	GM	SD	GSD	UF
All parameters	3.07E-02	4.29E-02	3.08E-02	4.12E-02	2.26E+00	4.70E+00
Absorption	3.14E-02	3.18E-02	3.15E-02	1.54E-02	1.09E+00	1.02E+00
Particle deposition	3.60E-02	4.07E-02	3.53E-02	2.57E-02	1.71E+00	2.78E+00
Particle transport	2.30E-02	2.80E-02	2.34E-02	2.32E-02	1.79E+00	3.08E+00

Table 47: Statistical summary of the comparison of the sensitivity of the committed equivalent lung dose coefficient (mSv/ (kBqh/m³)) to different parameter groups for the inhalation of uranium ore dust in underground mines under Job 4 exposure conditions.

Parameters	Median	Mean	GM	SD	GSD	UF
All parameters	4.49E-02	6.10E-02	4.35E-02	6.09E-02	2.27E+00	4.94E+00
Absorption	4.57E-02	4.64E-02	4.58E-02	2.25E-02	1.09E+00	1.02E+00
Particle deposition	5.41E-02	5.95E-02	5.21E-02	3.65E-02	1.68E+00	2.59E+00
Particle transport	3.47E-02	4.22E-02	3.53E-02	3.45E-02	1.79E+00	3.03E+00

The sensitivity of the committed equivalent lung dose coefficients to different groups of parameters i.e., absorption, particle transport and particle deposition highlighting the different influences of these factors on the radiation exposure of underground miners inhaling uranium ore dust is presented in Table 44 and Table 45 for Job 1 and 4 respectively. Comparison of the job types across these categories provides insights into dose variability, uncertainty and key determinants of lung dose.

The "all parameters" category, which takes all exposure factors into account, shows the highest overall lung dose values. The median dose is 4.49E-02 mSv/ (kBqh/m^3) for Job 4 and 3.07E-02 mSv/ (kBqh/m^3) for Job 1, with means of 6.09E-02 mSv/ (kBqh/m^3) and 4.29E-02 mSv/ (kBqh/m^3), respectively. The GSD of 2.26-2.27 and the UF of 4.70-4.94 indicate considerable uncertainty, suggesting that several interacting factors contribute to the lung dose uncertainty.

The absorption category, which focuses on uranium dissolution and retention in lung tissue, has median dose values (4.57E-02 mSv/ (kBqh/m^3) for Job 4 and 3.14E-02 mSv/ (kBqh/m^3) for Job 1) similar to the "all parameters" category. However, the mean values (4.64E-02 mSv/ (kBqh/m^3) and 3.18E-02 mSv/ (kBqh/m^3)) are significantly lower. The GSD (1.09) and UF (1.02) are the lowest of all categories, indicating minimal variation. This suggests that absorption processes are highly predictable and contribute little to lung dose uncertainty.

The particle transport category, which describes how inhaled uranium ore dust is removed and redistributed in the human body, gives lower lung dose values compared to "all parameters" and "other parameters". The median dose is 3.47E-02 mSv/ (kBqh/m^3) for Job 4 and 2.30E-02 mSv/ (kBqh/m^3) for Job 1, with mean values of 4.22E-02 mSv/ (kBqh/m^3) and 2.80E-02 mSv/ (kBqh/m^3). The UF (3.03-3.08) and GSD (1.79) are higher than for absorption but lower than for "all parameters", indicating moderate uncertainty in dose estimates due to transport mechanisms. This suggests that although particle transport contributes to dose uncertainty, it does not dominate the total variation in lung dose.

The particle deposition category, which governs the deposition of uranium particles in the respiratory tract, gives the highest lung dose values among the individual parameter groups. The median dose is 5.41E-02 mSv/ (kBqh/m^3) for Job 4 and 3.60E-02 mSv/ (kBqh/m^3) for Job 1, with mean values of 5.95E-02 mSv/ (kBqh/m^3) and 4.07E-02 mSv/ (kBqh/m^3), respectively. The GSD (1.68-1.71) and UF (2.59-2.78) are slightly lower than for particle transport, suggesting that deposition patterns are more predictable but still significantly influence lung dose variation.

Of the parameter groups, absorption has the least sensitivity to lung dose variation, with minimal uncertainty, making it a stable factor in dose estimation. Particle transport and deposition play a more important role in dose uncertainty, with deposition having the strongest effect on increasing dose values while the greatest uncertainties are associated with particle transport parameters as indicated by their highest GSD and UF values for both job types. However, it should be noted that overall, external exposure conditions (such as uranium ore dust concentration and ventilation efficiency) drive the greatest variation in lung dose, while particle-related processes (transport and deposition) mainly influence the internal lung distribution patterns.

These findings emphasise the need for radiation protection measures that focus on reducing airborne uranium dust concentrations, improving workplace ventilation and ensuring the proper use of respiratory protective equipment. By targeting the most influential parameters such as particle transport, radiation protection strategies can be more effective in minimising lung dose risks to underground miners.

The relative sensitivity of the committed equivalent lung dose coefficient to the various exposure and biokinetic model parameter groups is also presented using grouped boxplots as shown in Figure 38. The sensitivity analysis results of the systemic organ and tissue dose coefficients to various parameter groups following inhalation of uranium ore dust in underground mines are presented in Annex F at the end of this report.

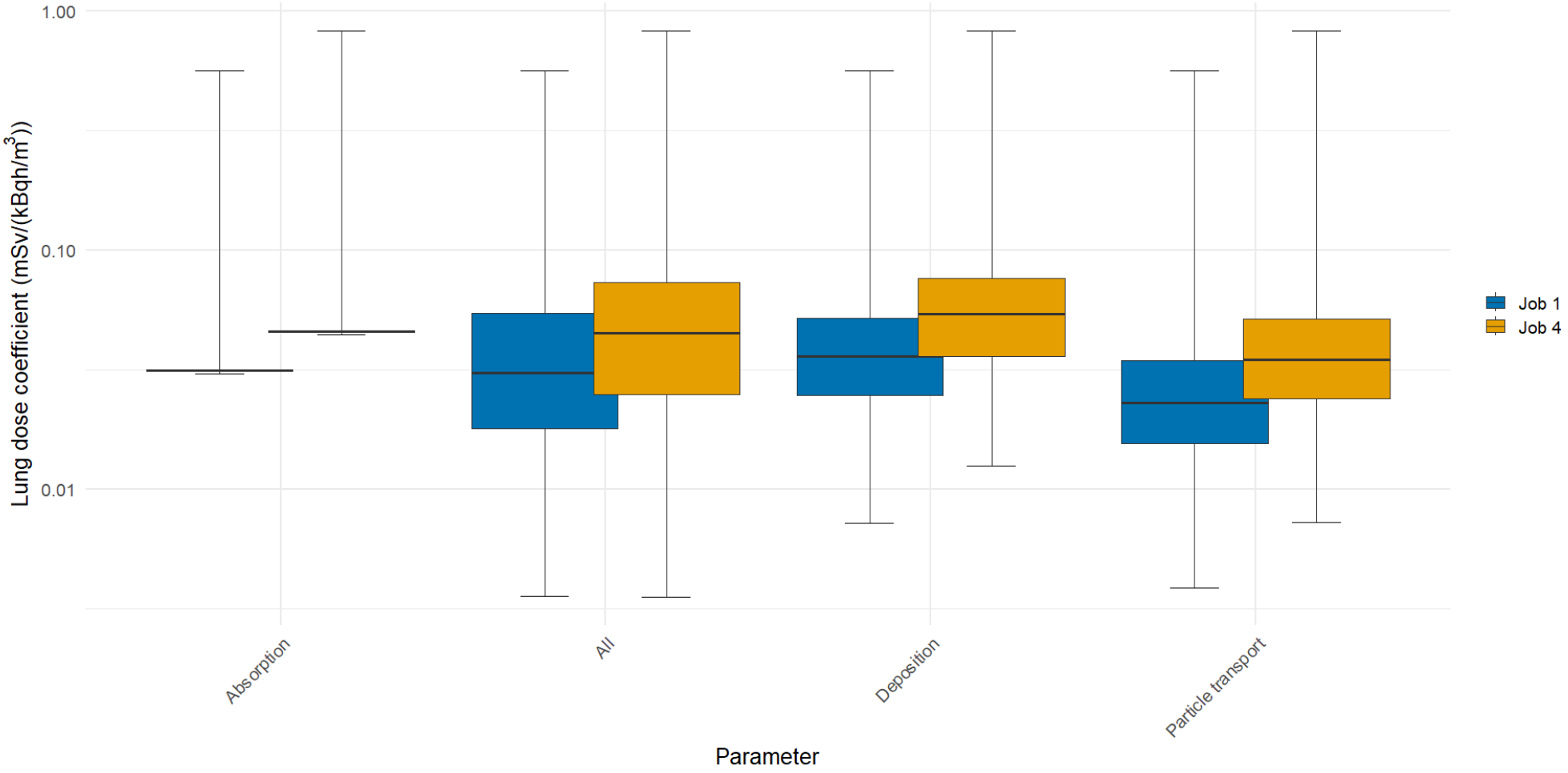

Figure 38: Grouped boxplots showing the sensitivity of the committed equivalent lung dose coefficients (mSv/ (kBqh/m³)) to parameter groups from the inhalation of uranium ore dust in underground mines.

This chapter presented the results from the Monte Carlo simulation from the inhalation of radon progeny and uranium ore dust by underground miners. A parameter uncertainty analysis was performed using the latest biokinetic and dosimetric models published by ICRP to determine the posterior distributions of committed equivalent organ and tissue dose coefficients for the inhalation of radon progeny and long-lived radionuclides in uranium ore dust. The study focused on two exposure scenarios: Job 1 (wet drilling with good ventilation) and Job 4 (dry drilling with poor ventilation). The resulting dose distributions were approximately lognormal, and their main parameters have been presented.

For radon progeny inhalation, the committed equivalent lung dose coefficient for Job 1 has a GM of 47.05 mSv/ (mJh/m³) and a GSD of 1.58, while Job 4 has a GM of 61.87 mSv/ (mJh/m³) and a GSD of 1.56. The dose for Job 4 exceeds that of Job 1 by a factor of 1.3-1.6, while their GSD and UF values remain comparable. The 95% confidence interval (CI) for Job 1 ranges from 18.59 mSv/ (mJh/m^3) to 104.74 mSv/ (mJh/m³), while for Job 4 it ranges from 24.83 mSv/ (mJh/m^3) to 133.09 mSv/ (mJh/m³).

Within the lung, the AI region has the greatest uncertainty, while Bronch.sec receive the highest dose in both exposure scenarios. Among the systemic organs, the kidneys receive the highest dose and also have the greatest uncertainty. Across all lung regions, workers in Job 4 consistently receive higher doses than workers in Job 1 by a factor of 1.3-1.6, indicating an increased risk of radiation induced lung cancer.

Sensitivity analysis shows that particle deposition parameters, especially “activity parameters”, have the greatest influence on lung dose calculations. These parameters account for most of the GSD in Job 1 and almost all of the GSD in Job 4. Among them, tidal volume has the most significant effect. Reducing the uncertainty in lung dose estimates requires more accurate measurements of “activity parameters”, including respiratory rate, nasal fraction, tidal volume and time spent in each activity. These factors need to be carefully considered in lung dose estimates for radon progeny inhalation in underground mines.

For uranium ore dust inhalation, the committed equivalent lung dose coefficient also follows a lognormal distribution. Under Job 1 exposure conditions, the GM is 3.08E-02 mSv/ (kBqh/m³), with a GSD of 2.26 and a 95% CI of 6.53E-03 mSv/ (kBqh/m^3) to 1.45E-01 mSv/ (kBqh/m³). The UF for this scenario is 4.70. For Job 4, the GM increases to 4.35E-02 mSv/ (kBqh/m³), with a GSD of 2.27, a 95% CI of 8.50E-03 mSv/ (kBqh/m^3) to 2.08E-01 mSv/ (kBqh/m³), and a UF of 4.94.

As with radon progeny inhalation, the greatest uncertainty is observed in the AI region, with UF values of 6.11 for Job 1 and 6.12 for Job 4. However, in contrast to radon progeny, Bchiol.sec rather than Bronch.sec receive the highest dose. Among the systemic organs, the bone receives the highest dose, while the uncertainties are greatest in St. Stem (UF = 5.48) for Job 1 and in Ht.wall (UF = 5.67) for Job 4. Overall, the doses from Job 4 exceed those from Job 1 by a factor of 1.4.

The sensitivity analysis shows that the particle deposition parameters contribute most to the lung dose, while the particle transport parameters are responsible for the highest uncertainties and variabilities. This is expected due to the long half-lives of these radionuclides and their moderate to slow solubility characteristics, which significantly influence their absorption and transport dynamics.

6. CONCLUSIONS AND RECOMMENDATIONS

6.1 Conclusions

This study conducted a comprehensive uncertainty analysis of internal radiation dose estimates resulting from the inhalation of radon progeny and long-lived radionuclides in uranium ore dust. The latest biokinetic and dosimetric models published by ICRP were used for this analysis. The investigation focused on two distinct job types in the mining industry, based on historical data from the former Wismut uranium mines: Job 1, involving wet drilling with good ventilation; and Job 4, involving dry drilling with poor ventilation. The study aimed to determine the posterior distributions of committed equivalent organ and tissue doses, and to evaluate the associated health risks.

The committed equivalent lung dose coefficients for radon progeny inhalation followed lognormal distributions in both job types. Workers in Job 4 consistently received higher doses than those in Job 1, with GM doses of 61.87 mSv/(mJh/m³) and 47.05 mSv/(mJh/m³), respectively representing a difference of approximately 1.3 to 1.6 times. Despite this disparity in magnitude, GSD were similar, at around 1.56–1.58. The 95% confidence intervals further demonstrated this difference, ranging from 18.59 to 104.74 mSv/ (mJh/m³) for Job 1 and from 24.83 to 133.09 mSv/ (mJh/m³) for Job 4. Within the lungs, Bronch.sec received the highest doses in both scenarios, suggesting that they are most susceptible to radon-induced malignancies. The AI region exhibited the greatest uncertainty, and the kidneys received the highest dose among systemic organs, underlining their importance in occupational health assessments.

Similarly, inhaling uranium ore dust produced lognormal dose distributions, with Job 4 again being associated with higher exposure levels. The GM for Job 1 was 3.08E-02 mSv/ (kBqh/m³), compared to 4.35E-02 mSv/ (kBqh/m³) for Job 4. The respective uncertainty factors were 4.70 and 4.94, and the 95% confidence intervals ranged from 6.53E-03 to 1.45E-01 mSv/ (kBqh/m³) for Job 1 and from 8.50E-03 to 2.08E-01 mSv/ (kBqh/m³) for Job 4. Unlike with radon progeny, the Bchiol.sec received the highest doses with uranium ore dust exposure. The systemic organ receiving the highest dose was bone, while the greatest uncertainties were observed in the red marrow (R.marrow) for Job 1 and the heart wall (Ht.wall) for Job 4. Notably, the kidneys also received significant doses in uranium ore dust inhalation. Although not classified as highly radiosensitive, the kidneys are particularly vulnerable to the chemical toxicity of uranium, especially when inhaled in particulate form. Uranium accumulates in renal tissue where it can cause nephrotoxic effects, making exposure to uranium in occupational settings a dual radiological and chemical concern.

Sensitivity analysis across both exposure types indicated that particle deposition parameters, especially activity parameters such as tidal volume, breathing frequency, nasal fraction and time spent on specific activities, were the primary drivers of dose uncertainty. Tidal volume had the greatest influence, as deeper breaths enhance particle deposition in the lungs. In the case of exposure to uranium ore dust, particle transport parameters contributed most to uncertainty due to the radionuclides' long biological half-lives and slow solubility, which affect their absorption and transport within the body.

A statistical comparison using the Mann–Whitney U test confirmed that Job 1 and 4 involved significantly different exposure profiles and dose distributions for radon progeny and uranium ore dust. The p-values were below 0.05 for all organs and tissues in both cases, indicating that

the dose coefficients differ between the two job types. This strongly supports the need for job-specific radiological protection strategies. Furthermore, the lung dose coefficients for both job types were significantly higher than the ICRP reference value of 24.00 mSv/ (mJh/m³), exceeding it by more than a factor of two for radon progeny inhalation. This suggests that standardised values may underestimate actual occupational exposure, particularly in poorly ventilated environments such as those encountered in Job 4.

The analysis also showed that replacing Job 4 conditions with Job 1 conditions could reduce lung dose coefficients by around 36%, emphasising the importance of proper ventilation and dust suppression measures. These findings emphasise the need to refine operational and regulatory strategies for occupational radiation protection. Key interventions include improving ventilation in underground mines, enforcing the consistent use of respiratory protective equipment in areas with high exposure, and optimising work-rest cycles to minimise time spent in conditions that require high respiratory effort, as this can increase the internal dose.

To track fluctuations in radon progeny concentrations and enable timely protective responses, continuous air monitoring should also be implemented. From a regulatory standpoint, there is a strong case for revising the reference dose coefficients and exposure action levels to reflect the wide uncertainty ranges identified in this study. Using higher percentiles of dose distributions, such as the 75^{th} or 95^{th}, or mean values from probabilistic simulations could provide more realistic and protective guidelines. Improving biokinetic models with scenario-specific activity parameters would further enhance the accuracy of dose assessments.

This study therefore provides valuable insights into the uncertainty and risks associated with the inhalation of radioactive materials in uranium mining environments. It shows that job-specific conditions have a substantial effect on internal dose and health risk, with Job 4 workers facing significantly higher exposure and uncertainty. The results therefore support targeted improvements in mine ventilation, protective equipment standards, real-time exposure monitoring and regulatory dose models, with the aim of ensuring safer and healthier conditions for underground miners. Recognising the chemical toxicity of uranium, particularly its nephrotoxic effects on the kidneys, adds further urgency to the implementation of robust occupational health measures in environments where airborne uranium ore dust is present.

6.2 Recommendations

The recommendations presented here are derived from a detailed analysis of the health risks associated with exposure to radon progeny in underground mining environments. The analysis focused particularly on the variability and uncertainties in dose assessments. These recommendations are crucial for mitigating critical health risks, particularly to the lungs and kidneys, arising from prolonged exposure to radon progeny and uranium ore dust. Sensitivity and uncertainty analyses revealed that certain organs, notably the bronchial regions of the lung and kidneys, are at greater risk due to the high UF associated with dose estimates. Given the potential for severe health outcomes such as lung cancer, chronic obstructive pulmonary disease (COPD) and kidney toxicity, the aim of these recommendations is to reduce exposure and improve safety protocols. Enhanced monitoring, improved ventilation, more stringent regulatory standards and the use of protective equipment were identified as crucial measures to mitigate these risks. Furthermore, the recommendations emphasise the need for personalised protective strategies and ongoing research to refine risk assessments and improve occupational safety practices. The goal is to minimise long-term health impacts, ensure safer working

conditions and better protect the wellbeing of miners exposed to radon progeny and uranium ore dust by implementing these strategies.

1. ***Enhanced monitoring and surveillance***
   Special attention should be given to organs and tissues with the highest UF, particularly Bronch.bas and Bronch.sec. Regular and detailed monitoring of radon of radon progeny levels in these tissues is critical. Additionally, it is necessary to implement regular checks focusing on the respiratory system for miners, especially in environments with high radon progeny exposure, to detect early signs of lung cancer, cumulative obstructive pulmonary disease (COPD) or other respiratory illnesses.
2. ***Improved ventilation and environmental controls***
   To reduce radon progeny concentration in underground environments, it is necessary to improve ventilation systems, particularly in areas where high concentrations are expected. This is crucial in minimizing radon exposure especially in confined or poorly ventilated spaces which are typical for Job 4 conditions. Additionally, it is necessary to implement additional environmental controls such as air filtration systems, to further reduce airborne radon progeny in high-risk zones.
3. ***Stringent regulatory standards***
   Given the variability and high uncertainty in certain tissues, regulatory bodies should consider reviewing and possibly tightening the safety standards for radon progeny exposure. This could involve lowering permissible exposure limits or adopting more conservative risk models. Additionally, it would be prudent to introduce stricter exposure limits and safety protocols for miners who are identified as more vulnerable due to existing health conditions or prolonged exposure to high-risk areas.
4. ***Personal Protective Equipment (PPE)***
   For miners in high-risk areas, the mandatory use of advanced PPE such as respirators that can effectively filter radon progeny should be enforced. It is also necessary to conduct regular evaluations of PPE to ensure its effectiveness in protecting against radon progeny. Upgrades or replacements should be implemented where necessary to maintain safety.
5. ***Education and Training***
   Increased awareness and education among miners regarding the risks associated with radon progeny exposure, especially in tissues with high UF should be considered. Training should emphasize the importance of using PPE and adhering to safety protocols. Furthermore, it is important to equip safety officers and health professionals with the knowledge to recognize early symptoms of radon related diseases and effectively manage exposure risks.
6. ***Further research and data collection***
   Efforts should be made to conduct additional studies to further refine the uncertainty analysis, focussing on understanding the factors contributing to high uncertainty in specific tissues. This will help in developing more accurate risk assessments. Additionally, it is necessary to implement long term studies to track the health outcomes of workers exposed to radon progeny over extended periods, particularly in tissues with high UF.
7. ***Personalized protective strategies***
   Development of personalized protective strategies based on individual susceptibility, such as genetic predisposition to lung diseases, which could influence the impact of radon progeny exposure should be encouraged.

8. ***Immediate interventions in high-risk areas***
   Focus should be directed to immediate intervention efforts on areas identified as having the highest radon progeny concentrations and UF. This could involve increased monitoring, rapid implementation of environmental controls and enhanced worker protection protocols.
9. ***Adopt safer mining practices***
   The adoption of safe mining practices should be prioritized. These may include, discouraging the use of dry drilling with poor ventilation in mining since it is associated with relatively higher doses as compared to wet drilling with good ventilation.

   The author believes that by implementing these recommendations, it is possible to significantly reduce the health risks associated with radon progeny exposure in occupational settings, thereby protecting workers long term health and wellbeing.

7. REFERENCES

1. Almeida, A., Loy, A., Hofmann, H. (2018). ggplot2 compatible Quantile-Quantile plots in R. The R journal, 10(2), 248-261. https://doi.org/10.32614/RJ-2018-051
2. Aslam, M. (2019). Introducing Kolomogorov-Smirnov tests under uncertainty: an application to radioactive data. ACS Omega Publications, 5(1), 914-917. https://doi.org/10.1021/acsomega.9b03940
3. Bailey, M. R., & Puncher, M. (2007). Uncertainty analysis of the ICRP human respiratory tract model applied to interpretation of bioassay data for depleted uranium. Health Protection Agency, UK. https://assets.publishing.service.gov.uk/media/5a7e0faded915d74e33efcd6/HpaRpd023.pdf
4. Beckova, V., & Malatova, I. (2008). Dissolution behaviour of 238U, 234U and 230Th deposited on filters from personal dosemeters. Radiation Protection Dosimetry, 129(4), 469-472. https://doi.org/10.1093/rpd/ncm455
5. Birchall, A., & James, A. C. (1994). Uncertainty analysis of the effective dose per unit exposure from radon progeny and its implication for ICRP risk-weighting factors. Radiation Protection Dosimetry, 53(1-4), 133-140. https://doi.org/10.1093/rpd/53.1-4.133
6. Birchall, A., Puncher, M., & Vostrotin, V. (2016). The Mayak Worker Dosimetry System (MWDS-2013): Treatment of uncertainty in model parameters. Radiation Protection Dosimetry, 176(1-2), 144-153. https://doi.org/10.1093/rpd/ncw248
7. Bolch, W. E., Farfan, E. B., Huh, C., Huston, T. E., & Bolch, W. E. (2001). Influences of parameter uncertainties within the ICRP 66 respiratory tract model: Particle deposition. Health Physics, 81(4), 378-394. https://doi.org/10.1097/00004032-200110000-00003
8. Bolch, W. E., Huston, T. E., Farfan, E. B., Vernetson, W. G., & Bolch, W. E. (2003). Influences of parameter uncertainties within the ICRP-66 respiratory tract model: Particle clearance. Health Physics, 84(4), 421-435. https://doi.org/10.1097/00004032-200304000-00002
9. Breustedt, B., Blanchardon, E., Castellani, C. M., Etherington, G., Franck, D., Giussani, A., Hofmann, W., Lebacq, A. L., Li, W. B., Noßke, D., & Lopez, M. A. (2017). EURADOS work on internal dosimetry. Annals of ICRP, 47(3-4), 75-82. https://doi.org/10.1177/0146645318756232
10. Breustedt, B., Chavan, N., & Makumbi, T. (2025). An R Code for calculation of dose coefficients and studying their uncertainties. Health Physics.192(2):50-60 http://dx.doi.org/10.1097/HP.0000000000001833
11. Breustedt, B., Giussani, A., & Noßke, D. (2018). Internal dose assessment - Concepts, models and uncertainties. Radiation Measurements, 115, 49-54. https://doi.org/101016/jradmeas201806013

12. Brudecki, K., Li, W. B., Meisenberg, O., Tschiersch, C., Hoeschen, C., & Oeh, U. (2014). Age-dependent inhalation doses to members of the public from indoor short-lived radon progeny. Radiation Environment Biophysics, 53, 535-549. https://doi.org/10.1007/s00411-014-0543-8

13. Butterweck, G., Porstendörfer, J., Reineking, A., & Kesten, J. (1992). Unattached fraction and the aerosol size distribution of the radon progeny in a natural cave and mine atmospheres. Radiation Protection Dosimetry, 45(1-4), 167-170. https://doi.org/10.1093/rpd/45.1-4.167

14. Butterweck, G., Schuler, Ch., Vezzu, G., Müller, R., Marsh, J. W., Thrift, S., & Birchall, A. (2002). Experimental determination of the absorption rate of unattached radon progeny from respiratory tract to blood. Radiation Protection Dosimetry, 102(4), 343-348. https://doi.org/10.1093/oxfordjournals.rpd.a006103

15. Cardoso, D.O., & Galeno, T.D. (2023). Online evaluation of the Kolmogorov-Smirnov test on arbitrarily large samples. Journal of Computational Science, 67, 101959. https://doi.org/10.1016/j.jocs.2023.101959

16. Deffner, V. (2022, October 06). Personal conversation.

17. Delignette-Muller, M. L., & Dutang, C. (2015). fitdistrplus: An R Package for Fitting Distributions. Journal of Statistical Software, 64(4), 1–34. https://doi.org/10.18637/jss.v064.i04.

18. Duport, P., Robertson, R., Ho, K. & Horvath, F. (1991). Flow through dissolution of uranium-thorium ore dust, uranium concentrate, uranium dioxide and thorium alloy in simulated lung fluid. Radiation Protection Dosimetry, 38(1-3), 121-133. https://www.doi.org/10.1093/rpd/38.1-3.121

19. Everitt, B. S. (1995). The Cambridge dictionary of statistics in medical sciences. Cambridge University Press, New York. ISBN-13:978-0521479288

20. Fritsch, P. (2006). Uncertainties in aerosol deposition within the respiratory tract using the ICRP 66 model: A study in workers. Health Physics Society, 114-126. https://doi.org/10.1097/01.hp.0000174810.12283.18

21. Ghasemi, A., & Zahediasl, S. (2012). Normality tests for statistical analysis. A guide for non-statisticians. International Journal of Endocrinology Metabolism, 10(2), 486-489. https://doi.org/10.5812/ijem.3505

22. Hagel, M.L, Trutzenberg, F., & Eid, M. (2024). Applying the robust Chi-squared goodness-of-fit test to multilevel multitrait-multimethod models: a Monte Carlo simulation study on statistical performance. Psychology International, 6, 462-491. https://doi.org/10.3390/psycholint6020029

23. Harley, N., Cohen, B. S., & Robbins, E. S. (1996). The variability in radon decay product bronchial dose. Environment International, 22, 959-964. https://doi.org/10.1016/S0160-4120(96)00208-5

24. Harrison, J. D., & Day, P. (2008). Radiation doses and risks from internal emitters. Journal of Radiological Protection, 28, 137-159. https://doi.org/10.1088/0952-4746/28/2/R01

25. Harrison, J. D., Leggett, R. W., Lloyd, D, Phipps, A. W., & Scott, B.R. (2007). Po-210 as a poison. Journal of Radiological Protection. 27(1),17-40. https://doi.org/10.1088/0952-4746/27/1/001

26. Harrison, J.D., Leggett, R.W., Noßke, D., Paquet, F., Phipps, A.W., Taylor, D.M., & Metivier, H. (2001). Reliability of the ICRPs dose coefficients for members of the public, II. Uncertainties in the absorption of ingested radionuclides and the effect on dose estimates. Radiation Protection Dosimetry. 95, 295-308. https://doi.org/10.1093/oxfordjournals.rpd.a006554

27. Hernandez, A., Endesfelder, D., Einbeck, J., Puig, P., Bebadjaoud, M.A, Higueras, M., Ainsbury, E., Gruel, G., Oestreicher, U., Barrios, L., & Barquinero, J.F. (2023). Biodose tools: an R shiny application for biological dosimetry. International Journal of Radiation Biology, 99(9), 1378-1390. https://www.doi.org/10.1080/09553002.2023.2176564

28. Hu, J., Iwaoka, K., Hosoda, M., & Tokonami, S. (2020). Lung dose estimation of ^{222}Rn and ^{220}Rn progeny based on IMBA Professional Software. Radiation Environment and Medicine, 9(1), 21-27. https://doi.org/10.51083/radiatenvironmed.9.1_21

29. IAEA. (2011). IAEA annual report 2010. International Atomic Energy Agency, Vienna, Austria.

30. ICRP. (1991). 1990 recommendations of the international commission on radiological protection. ICRP Publication 60. Annals of the ICRP, 21(1-3).

31. ICRP. (1993). Protection against ^{222}Rn at home and at work. ICRP Publication 65. Annals of the ICRP 23(2).

32. ICRP. (1994). Human respiratory tract model for radiological protection. ICRP Publication 66. Annals of the ICRP, 24(1-3).

33. ICRP. (1995). Age-dependent doses to members of the public from intake of radionuclides - Part 4 Inhalation Dose Coefficients. ICRP Publication 71. Annals of the ICRP, 25 (3-4).

34. ICRP. (2006). Human Alimentary Tract Model for Radiological Protection. ICRP Publication 100. Annals of the ICRP, 36 (1-2).

35. ICRP. (2007). The 2007 recommendations of the international commission on radiological protection. ICRP Publication 103. Annals of the ICRP, 37 (2-4).

36. ICRP. (2008). Nuclear decay data for dosimetric calculations. ICRP Publication 107. Annals of the ICRP, 38(3).

37. ICRP. (2009). Application of the commission's recommendations for the protection of people in emergency exposure situations. ICRP Publication 109. Annals of the ICRP, 39 (1).

38. ICRP. (2015). Occupational intakes of radionuclides: Part 1. ICRP Publication 130. Annals of the ICRP, 44(2).

39. ICRP. (2016). The ICRP computational framework for internal dose assessment for reference adults: specific absorbed fractions. ICRP Publication 133. Annals of the ICRP, 45(2), 1-74.

40. ICRP. (2017). Occupational intakes of radionuclides: Part 3. ICRP Publication 137. Annals of the ICRP, 46(3/4).

41. ICRP. (2019). Occupational intakes of radionuclides: Part4. ICRP Publication 141. Annals of the ICRP, 48(2/3).

42. ICRP. (2022). Occupational intakes of radionuclides: Part 5. ICRP Publication 151. Annals of the ICRP, 51 (1–2).

43. Joyce, P.J., Goronovski, A., Tkaczyk, A.H. & Bjorklund A. (2017). A framework for including enhanced exposure to naturally occurring radioactive materials (NORM) in LCA. International Journal of Life Cycle Assessment, 22, 1078-1095. https://doi.org/10.1007/s11367-016-1218-2

44. Khatun, N. (2021). Applications of normality test in statistical analysis. Open Journal of Statistics, 11, 113-122. https://doi.org/10.4236/ojs.2021.111006

45. Klein, W., Breustedt, B., & Urban, M. (2010). Analysis of the variability of biokinetic model parameters due to inter-individual variation. Health Physics, 99(4):577-580. https://doi.org/10.1097/HP.0b013e318/db9eec

46. Klein, W., Breustedt, B., Manfred, U. (2010). Analysis of the variability of biokinetic model parameters due to inter-individual variation. Health Physics. https://doi.org/10.1097/HP.0b013e3181db9eec

47. Kwon, T., Chung, Y., Yoo, J., Ha, W., & Cho, M. (2020). Uncertainty quantification of bioassay functions for the internal dosimetry of radioiodine. Journal of Radiation Research, 61(6), 860-870. https://doi.org/10.1093/jrr/rraa081

48. Lamart, S., Griffiths, N.M., Tchitchek, N., Angulo, J.F., Van der Meeren, A. (2017). Analysis, methodology and development of a statistical tool for biodistribution data from internal contamination with actinides. Journal of Radiological Protection, 37(1), 296-308. https://www.doi.org/10.1088/1361-6498/37/1/296

49. Lanzante, J.R. (2021). Testing for differences between two distributions in the presence of serial correlation using the Kolmogorov-Smirnov and Kuiper's tests. International Journal of Climatology, 1-10. https://doi.org/10.1012/joc.7196

50. Layton. (1993). Metabolically consistent breathing rates for use in dose assessments. Health Physics, 64, 23-26. https://doi.org/10.1097/00004032-199301000-00003

51. Leggett, R. W. (2001). Reliability of the ICRP's dose coefficients for members of the public: I. Sources of uncertainty in the biokinetic models. Radiation Protection Dosimetry, 95(3), 199-213. https://doi.org/10.1093/oxfordjournals.rpd.a006543

52. Leggett, R. W. (2003). Reliability of the ICRP's dose coefficients for members of the public: III. Plutonium as a case study of uncertainties in the systemic biokinetics of radionuclides. Radiation Protection Dosimetry, 106(2), 103-120. https://doi.org/10.1093/oxfordjournals.rpd.a006340

53. Leggett, R. W., Harrison, J., & Phipps, A. (2007). Reliability of the ICRP's dose coefficients for members of the public: IV. Basis of the human alimentary tract model and uncertainties in model predictions. Radiation Protection Dosimetry, 123(2), 156-170. https://doi.org/10.1093/rpd/ncl104

54. Leggett, R. W., Marsh, J. W., Gregoratto, D., & Blanchardon, E. (2013). A generic biokinetic model for noble gases with application to radon. Journal of Radiological Protection, 33, 413-432. https://doi.org/10.1088/0952-4746/33/2/413

55. Li, W. B. (2018). Internal dosimetry: A review of progress. Health Physics, 53(2), 72-99. https://doi.org/10.5453/jhps.53.72

56. Li, W. B., Klein, W., Blanchardon, E., Puncher, M., Leggett, R. W., Oeh, U., Breustedt, B., Noßke, D., & Lopez, M. A. (2015). Parameter uncertainty analysis of a biokinetic model of cesium. Radiation Protection Dosimetry, 163(1), 37-57. https://doi.org/10.1093/rpd/ncu055

57. Luong, A. (2018). Asymptotic results for goodness-of-fit tests using a class of generalized spacing methods with estimated parameters. Open Journal of Statistics, 8, 731-746. https://doi.org/10.4236/ojs.2018.84048

58. Makumbi, T., Breustedt, B., & Raskob, W. (2024a). Parameter uncertainty analysis of the equivalent lung dose coefficient for the intake of radon in mines: A review. Journal of Environmental Radioactivity, 276(1-4):107446. https://doi.org/10.1016/j.jenvrad.2024.107446

59. Makumbi, T., Breustedt, B., Raskob, W., & Ottenburger, S.S. (2024b). Application of INTDOSKIT tool for assessment of uncertainties on dose coefficients for ingestion of uranium by workers. Radiation Physics and Chemistry. 226(1): 112247. https://doi.org/10.1016/j.radphyschem.2024.112247

60. Makumbi, T., Breustedt, B., Raskob, W., & Ottenburger, S.S. (2025). Parameter uncertainty analysis of the committed equivalent dose coefficients from inhalation of radon progeny in underground uranium mines. Journal of Environmental Radioactivity. 289: 107751. https://doi.org/10.1016/j.jenvrad.2025.107751

61. Marsh, J. W., & Bailey, M. R. (2013). A review of lung-to-blood absorption rates for radon progeny. Radiation Protection Dosimetry, 157(4), 499-514. https://doi.org/10.1093/rpd/nct179

62. Marsh, J. W., & Birchall, A. (2009). Uncertainty analysis of the absorbed dose to regions of the lung per unit exposure to radon progeny in a mine. Health Protection Agency Report. ISBN 978-0-85951-642-6.

63. Marsh, J. W., Bessa, Y., Birchall, A., Blanchardon, E., Hofmann, W., Noßke, D., & Tomasek, L. (2008). Dosimetric models used in the Alpha-Risk Project to quantify

exposure of uranium miners to radon gas and its progeny. Radiation Protection Dosimetry, 1-6. https://doi.org/10.1093/rpd/ncn119

64. Marsh, J. W., Blanchardon, E., Gregoratto, D., Hofmann, W., Karcher, K., Noßke, D., & Tomasek, L. (2012). Dosimetric calculations for uranium miners for epidemiological studies. Radiation Protection Dosimetry, 1-13. https://doi.org/10.1093/rpd/ncr310

65. Marsh, J.W. (2022). Dosimetry Protocol for Miners and Millers [Unpublished report]. United Kingdom Health Security Agency (UKHSA), Oxfordshire OX 11 0RQ, UK.

66. Mbaji, R, M., Benedict, T. J. & Kevin, O. O. (2023). Determinants of estimate difference between geometric measure and standard deviation. Asian Journal of Probability and Statistics, 24(4):23-34. https://doi.org/10.9734/AJPAS/2023/v24i4532

67. McInroy, J.F, Kathren, R.L & Swint, M.J (1989). Distribution of plutonium and americium in whole bodies donated to the United States transuranium registry. Radiation Protection Dosimetry. 1989; 26(1-4): 151-159.

68. Mercer, R. R., Russell, M. L., & Crapo, J. D. (1991). Radon dosimetry based on the depth distribution of nuclei in human and rat lungs. Health Physics, 61, 117-130. https://doi.org/10.1097/00004032-199107000-00013

69. Miller, G., Inkret, W. C., Little, T. T., Martz, H. F., & Schillaci, M. E. (2001). Bayesian prior probability distributions for internal dosimetry. Radiation Protection Dosimetry, 94(4), 347-352. https://doi.org/10.1093/oxfordjournals.rpd.a006509

70. Mirsch, J., Hintz, L., Maier, A., Fournier, C., & Löbrich, M. (2020). An assessment of radiation doses from radon exposure using a mouse model system. International Journal of Radiation Oncology, 108(3), 770-778. https://doi.org/10.1016/j.ijrobp.2020.05.031

71. Morgan, M. G., & Henrion, M. (1990). Uncertainty: A guide to dealing with uncertainty in quantitative risk and policy analysis. Cambridge University Press.

72. Nachar, N. (2008). The Mann-Whitney U: A test for assessing whether two independent samples come from the same distribution. Tutorials for Qualitative Methods for Psychology, 4(1):13-20. https://doi.org/10.20982/tqmp.04.1.p013

73. NCRP. (2009). Uncertainties in internal radiation dose assessment. NCRP Report 164. Bethesda, MD: NCRP.

74. Niinimaa, V., Cole, P., Mintz, S., & Shephard, R. J. (1980). The switching point from nasal to oro-nasal breathing. Respiration Physiology, 42, 61-71. https://doi.org/10.1016/0034-5687(80)90104-8

75. Niinimaa, V., Cole, P., Mintz, S., & Shephard, R. J. (1981). Oronasal distribution of respiratory airflow. Respiration Physiology, 43, 69-75. https://doi.org/10.1016/0034-5687(81)90089-x

76. Paquet, F., Bailey, M. R., Leggett, R. W., & Harrison, J. D. (2016). Assessment and interpretation of internal doses: Uncertainty and variability. Annals of the ICRP, 45(1), 202-214. https://doi.org/10.1177/0146645316633595

77. Pleil, J.D. (2016). QQ-plots for assessing distributions of biomarker measurements and generating defensible summary statistics. Journal of Breath Research, 10(3),1-7. https://doi.org/10.1088/1752-7155/10/3/035001

78. Postendörfer, J. (2001). Physical parameters and dose factors of the radon and thoron decay products. Radiation Protection Dosimetry, 94, 365-373. https://doi.org/10.1093/oxfordjournals.rpd.a006512

79. Postendörfer, J., & Reineking, A. (1999). Radon: Characteristics in air and dose conversion factors. Health Physics, 76(3), 300-305. https://doi.org/10.1097/00004032-199903000-00011

80. Postendörfer, J., Zock, Ch., & Reineking, A. (2000). Aerosol size distribution of the radon progeny in outdoor air. Journal of Environmental Radioactivity, 51(1), 37-48. http://dx.doi.org/10.1016/S0265-931X(00)00043-6

81. Puncher, M. (2014a). Assessing the reliability of dose coefficients for ingestion and inhalation of ^{226}Ra and ^{90}Sr by members of the public. Radiation Protection Dosimetry, 158(1), 8-21. https://doi.org/10.1093/rpd/nct188

82. Puncher, M. (2014b). An assessment of the reliability of dose coefficients for intakes of radionuclides by members of the public. Journal of Radiological Protection, 34, 625-643. https://doi.org/10.1088/0952-4746/34/3/625

83. Puncher, M., & Burt, G. (2013). The reliability of dose coefficients for inhalation and ingestion of uranium by members of the public. Radiation Protection Dosimetry, 157(2), 242-254. https://doi.org/10.1093/rpd/nct134

84. Puncher, M., & Harrison, J. D. (2012a). Assessing the reliability of dose coefficients for inhaled and ingested radionuclides. Journal of Radiological Protection, 32, 223-241. https://doi.org/10.1088/0952-4746/32/3/223

85. Puncher, M., & Harrison, J. D. (2012b). Uncertainty analysis of doses from ingestion of plutonium and americium. Radiation Protection Dosimetry, 148(3), 284-296. https://doi.org/10.1093/rpd/ncr032

86. Puncher, M., Bailey, M. R., & Harrison, J. D. (2008). Uncertainty analysis of doses from inhalation of depleted uranium. Health Physics, 95(3), 300-309. https://doi.org/10.1097/01.hp.0000314645.61534.b7

87. Puncher, M., Birchall, A., & Bull, R. K. (2012). A method for calculating Bayesian uncertainties on internal doses resulting from complex occupational exposures. Radiation Protection Dosimetry, 151(2), 224-236. https://doi.org/10.1093/rpd/ncr475

88. Puncher, M., Birchall, A., & Bull, R. K. (2013). A Bayesian analysis of uncertainties on lung doses resulting from occupational exposures to uranium. Radiation Protection Dosimetry, 156(2), 131-140. https://doi.org/10.1093/rpd/nct062

89. Rana, R., & Singhal, R. (2015). Chi-square test and its application in hypothesis testing. Journal of the Practice of Cardiovascular Sciences, 1(1), 69-71. https://doi.org/10.4103/2395-5414.157577

90. Ruzer, L. S., Nero, A. V., & Harley, N. H. (1995). Assessment of lung deposition and breathing rate of underground miners in Tadjikistan. Radiation Protection Dosimetry, 58, 261-268.

91. Schlenker, R.A, Keane, A.T & Holtzman, R.B. (1982). The retention of Ra-226 in human soft tissue and bone: implications for the ICRP 20 alkaline earth model. Health Physics, 42, 671-693.

92. Schober, P. & Vetter, T. (2020). Non-parametric statistical methods in medical research. Anesthesia & Analgesia, 131(6): 1862-1863. https://doi.org/10.1213/ANE.0000000000005101

93. Skubacz, K., & Woloszczuk, K. (2019). Size distribution of ambient and radioactive aerosols formed by short-lived radon progeny. Journal of Sustainable Mining, 18, 61-66. https://doi.org/10.1016/j.jsm.2019.03.006

94. Skubacz, K., Woloszczuk, K., Grygier, A., & Samolej, K. (2023). Influence of dose conversion factors and unattached fractions on radon risk assessment in operating and show underground mines. International Journal of Environmental Research and Public Health, 20, 5482. https://doi.org/10.3390/ijerph20085482

95. Spielmann, V., Li, W.B., Zankl, M., Ramos, J.C.O., Petoussi-Henss, N. (2020). Uncertainty analysis in internal dose calculations for cerium considering the uncertainties of biokinetic parameters and S values. Radiation and Environmental Biophysics, 59, 663–682 (2020). https://doi.org/10.1007/s00411-020-00872-9

96. Surucu, B. (2008). A power comparison and simulation study of goodness-of-fit tests. Computers and Mathematics with Applications, 56, 1617-1625. https://doi.org/10.1016/j.camwa.2008.03.010

97. Suslova, K.G., Khokryakov, V.F., Tokaskaya, Z.B., Nifatov, A., Krakenbuhl, M.P. & Miller, S.C. (2002). Extrapulmonary organ distribution of plutonium in healthy workers exposed by chronic inhalation at the Mayak production association. Health Physics, 82:432-444. https://doi.org/10.1097/00004032-200204000-00002

98. Tai, K.Y., Dhaliwal, J. & Balasubramaniam, V. (2022). Leveraging Mann-Whitney U test on large scale genetic variation data for analysing malaria genetic markers. Malaria Journal, 21(79): 1-13. https://doi.org/10.1186/s12936-022-04104-x

99. UNSCEAR. (2008). Sources and effects of ionizing radiation. Volume 1 and 2: Report of the United Nations Scientific Committee on the Effects of Atomic Radiation to the General Assembly, 2008.

100. Van der Steen, J. & Van Weers A.W. (2004). Radiation protection in NORM industries. In Proceedings of the 11th International Congress of the International Radiation Protection Association, IRPA11, May 23-24, 2004. Madrid, Spain.

101. Wang, Y., Sun, C., Zhang, L., & Guo, Q. (2021). Optimized method for individual radon progeny measurement based on alpha spectrometry following the Wicke method. Radiation Measurements, 142, 1-8. https://doi.org/10.1016/j.radmeas.2021.106558

102. West, R.M. (2021). Best practices in statistics: Use the Welch t-test when testing the difference between two groups. Annals of Clinical Biochemistry, 58(4):267-269. https://doi.org/10.1177/0004563221992088

103. Castellani, C.M., Marsh, J.W., Hurtgen, C., Blanchardon, E., Berard, P., Giussani, A., & Lopez, M.A. (2013). IDEAS Guideline (Version 2) for the estimation of committed doses from incorporation monitoring data. EURADOS Report 2013-01. Braunschweig. https://eurados.sckcen.be/sites/eurados/files/uploads/Publications/24_EURADOS-Report-2013-01_online-version.pdf

104. Duport, P., Robertson, R., Ho, K. & Horvath, F. (1991). Flow through dissolution of uranium-thorium ore dust, uranium concentrate, uranium dioxide and thorium alloy in simulated lung fluid. Radiation Protection Dosimetry, 38(1-3), 121-133. https://www.doi.org/10.1093/rpd/38.1-3.121

105. Duport, P. (1994). Radiation protection in uranium mining: two challenges. Radiation Protection Dosimetry. 53(1-4):13-19. https://doi.org/10.1093/rpd/53.1-4.13

106. Duport, P. & Edwardson, E. (1984). Characterization of radioactive long-lived dust in uranium mines and mills atmospheres: In H.E Stocker (Ed), Proceedings of the International Conference on Occupational Radiation Safety in Mining. Canadian Nuclear Association. Toronto, Canada.

107. Duport, P. & Horvath, F. (1989). Practical aspects of monitoring and dosimetry of long-lived dust in uranium mines and mills: Determination of the annual limit on intake for uranium/thorium ore dust. Radiation Protection Dosimetry. 26(1/4): 43-48. https://doi.org/10.1093/rpd/26.1-4.43

108. Bigu, J. (1990). Electrical charge characteristics of long-lived radioactive dust. Health Physics. 58(3): 341-350. https://doi.org/10.1097/00004032-199003000-00012

8. APPENDICES

Appendix A: This subsection presents a statistical summary of the results from the uncertainty analysis of organ and tissue doses following inhalation of radon progeny by underground miners performing both Job 1 and Job 4.

Table A1: Summary statistics from the uncertainty analysis of organ and tissue committed equivalent dose coefficients (mSv/ (mJh/m^3)) from inhalation of radon progeny by underground miners performing Job 1.

Organ	Undisturbed	Mean	SD	GM	GSD	UF	Min	X2.5	X5.0	X25	X50	X75	X95	X97.5	Max
Lung	1.50E+01	5.20E+01	2.30E+01	4.70E+01	1.58E+00	2.37E+00	8.70E+00	1.86E+01	2.12E+01	3.41E+01	4.84E+01	6.62E+02	9.52E+01	1.05E+02	1.67E+02
Bronch.bas	2.10E+01	4.58E+01	2.17E+01	4.10E+01	1.61E+00	2.49E+00	5.92E+00	1.57E+01	1.81E+01	2.94E+01	4.18E+01	5.80E+01	8.66E+01	9.80E+01	1.94E+02
Bronch.sec	4.61E+01	1.12E+02	5.32E+01	1.00E+02	1.61E+00	2.49E+00	1.45E+01	3.85E+01	4.42E+01	7.20E+01	1.02E+02	1.42E+02	2.12E+02	2.40E+02	4.77E+02
Bchiol.sec	2.90E+01	7.28E+01	3.43E+01	6.51E+01	1.62E+00	2.51E+00	1.28E+01	2.44E+01	2.83E+01	4.65E+01	6.69E+01	9.29E+01	1.37E+02	1.54E+02	2.69E+02
AI	1.72E+00	4.34E+00	2.56E+00	3.57E+00	1.93E+00	3.32E+00	4.96E-01	9.24E-01	1.09E+00	2.22E+00	3.91E+00	5.99E+00	9.16E+00	1.02E+01	1.69E+01
St.stem	1.30E-02	2.17E-02	1.02E-02	1.93E-02	1.63E+00	2.53E+00	2.84E-03	7.08E-03	8.20E-03	1.38E-02	2.01E-02	2.79E-02	4.09E-02	4.52E-02	7.38E-02
R.marrow	4.45E-03	8.93E-03	4.69E-03	7.70E-03	1.76E+00	2.84E+00	1.17E-03	2.45E-03	2.83E-03	5.10E-03	8.19E-03	1.19E-02	1.78E-02	1.97E-02	3.08E-02
Colon	1.97E-03	8.87E-03	4.62E-03	7.67E-03	1.75E+00	2.80E+00	1.16E-03	2.47E-03	2.86E-03	5.10E-03	8.13E-03	1.18E-02	1.76E-02	1.94E-02	3.01E-02
RC.stem	4.37E-03	8.98E-03	4.66E-03	7.77E-03	1.75E+00	2.79E+00	1.18E-03	2.52E-03	2.91E-03	5.18E-03	8.23E-03	1.20E-02	1.78E-02	1.96E-02	3.03E-02
LC.stem	4.42E-03	9.05E-03	4.69E-03	7.83E-03	1.75E+00	2.79E+00	1.19E-03	2.54E-03	2.94E-03	5.22E-03	8.30E-03	1.21E-02	1.79E-02	1.98E-02	3.05E-02
RS.stem	3.94E-03	8.29E-03	4.38E-03	7.13E-03	1.77E+00	2.86E+00	1.06E-03	2.25E-03	2.60E-03	4.71E-03	7.58E-03	1.11E-02	1.66E-02	1.83E-02	2.91E-02
Liver	5.73E-03	2.60E-02	1.38E-02	2.24E-02	1.77E+00	2.86E+00	3.37E-03	7.04E-03	8.15E-03	1.48E-02	2.38E-02	3.48E-02	5.20E-02	5.75E-02	9.11E-02
Kidneys	5.12E-02	1.05E-01	5.57E-02	8.99E-02	1.78E+00	2.88E+00	1.36E-02	2.80E-02	3.26E-02	5.92E-02	9.56E-02	1.40E-01	2.10E-01	2.32E-01	3.70E-01
Endost.BS	1.15E-02	2.18E-02	1.15E-02	1.88E-02	1.76E+00	2.84E+00	2.89E-03	5.96E-03	6.90E-03	1.24E-02	2.00E-02	2.91E-02	4.34E-02	4.79E-02	7.47E-02
Brain	1.09E-03	4.43E-03	2.27E-03	3.85E-03	1.73E+00	2.75E+00	6.09E-04	1.27E-03	1.46E-03	2.58E-03	4.08E-03	5.89E-03	8.73E-03	9.61E-03	1.44E-02
Ht.wall	4.09E-03	8.35E-03	4.38E-03	7.20E-03	1.76E+00	2.83E+00	1.11E-03	2.29E-03	2.64E-03	4.77E-03	7.66E-03	1.12E-02	1.66E-02	1.83E-02	2.88E-02

SD: Standard deviation; GM: Geometric mean; GSD: Geometric standard deviation; UF: Uncertainty factor; Min: minimum value; X2.5: 2.5th percentile; X5.0: 5th percentile; X25: 25th percentile; X50: 50th percentile; X75: 75th percentile; X95: 95th percentile; X97.5: 97.5th percentile; Max: maximum value; Undisturbed: Reference dose value for the exposure scenario.

Table A2: Summary statistics from the uncertainty analysis of organ and tissue committed equivalent dose coefficients (mSv/ (mJh/m³)) from inhalation of radon progeny by underground miners performing Job 4.

Organ	Undisturbed	Mean	SD	GM	GSD	UF	Min	X2.5	X5.0	X25	X50	X75	X95	X97.5	Max
Lung	2.33E+01	6.80E+01	2.90E+01	6.19E+01	1.56E+00	2.32E+00	1.48E+01	2.48E+01	2.84E+01	4.53E+01	6.37E+01	8.64E+01	1.22E+02	1.33E+02	1.99E+02
Bronch.bas	4.22E+01	6.18E+01	2.72E+01	5.61E+01	1.57E+00	2.36E+00	1.24E+01	2.25E+01	2.57E+01	4.10E+01	5.74E+01	7.81E+01	1.13E+02	1.25E+02	1.99E+02
Bronch.sec	8.67E+01	1.49E+02	6.56E+01	1.35E+02	1.57E+00	2.36E+00	2.99E+01	5.42E+01	6.20E+01	9.91E+01	1.39E+02	1.89E+02	2.73E+02	3.02E+02	4.77E+02
Bchiol.sec	4.71E+01	9.32E+01	3.90E+01	8.51E+01	1.55E+00	2.29E+00	2.12E+01	3.42E+01	3.92E+01	6.24E+01	8.79E+01	1.19E+02	1.66E+02	1.79E+02	2.53E+02
AI	2.44E+00	5.12E+00	2.86E+00	4.29E+00	1.87E+00	3.13E+00	6.57E-01	1.17E+00	1.38E+00	2.74E+00	4.69E+00	7.02E+00	1.05E+01	1.15E+01	1.64E+01
St.stem	2.60E-02	2.79E-02	1.19E-02	2.53E-02	1.57E+00	2.32E+00	6.25E-03	1.01E-02	1.15E-02	1.84E-02	2.62E-02	3.56E-02	5.00E-02	5.43E-02	7.32E-02
R.marrow	7.28E-03	1.09E-02	5.43E-03	9.47E-03	1.72E+00	2.72E+00	1.78E-03	3.12E-03	3.63E-03	6.41E-03	1.01E-02	1.44E-02	2.10E-02	2.30E-02	3.24E-02
Colon	2.87E-03	1.08E-02	5.36E-03	9.45E-03	1.71E+00	2.69E+00	1.81E-03	3.15E-03	3.66E-03	6.42E-03	1.00E-02	1.43E-02	2.08E-02	2.28E-02	3.22E-02
RC.stem	7.25E-03	1.09E-02	5.41E-03	9.58E-03	1.70E+00	2.68E+00	1.85E-03	3.21E-03	3.73E-03	6.52E-03	1.02E-02	1.45E-02	2.11E-02	2.30E-02	3.25E-02
LC.stem	7.37E-03	1.10E-02	5.46E-03	9.67E-03	1.70E+00	2.68E+00	1.86E-03	3.24E-03	3.77E-03	6.59E-03	1.03E-02	1.46E-02	2.12E-02	2.32E-02	3.27E-02
RS.stem	6.38E-03	1.00E-02	5.06E-03	8.75E-03	1.72E+00	2.74E+00	1.61E-03	2.85E-03	3.33E-03	5.91E-03	9.30E-03	1.34E-02	1.95E-02	2.14E-02	3.08E-02
Liver	8.24E-03	3.15E-02	1.59E-02	2.75E-02	1.73E+00	2.74E+00	5.07E-03	8.95E-03	1.04E-02	1.85E-02	2.92E-02	4.20E-02	6.13E-02	6.70E-02	9.59E-02
Kidneys	8.27E-02	1.27E-01	6.43E-02	1.10E-01	1.72E+00	2.75E+00	2.01E-02	3.58E-02	4.16E-02	7.43E-02	1.18E-01	1.69E-01	2.47E-01	2.71E-01	3.88E-01
Endost.BS	1.88E-02	2.65E-02	1.33E-02	2.31E-02	1.73E+00	2.72E+00	4.34E-03	7.59E-03	8.84E-03	1.56E-02	2.46E-02	3.52E-02	5.13E-02	5.61E-02	7.82E-02
Brain	1.70E-03	5.44E-03	2.66E-03	4.79E-03	1.72E+00	2.64E+00	9.49E-04	1.63E-03	1.89E-03	3.28E-03	5.06E-03	7.19E-03	1.04E-02	1.14E-02	1.58E-02
Ht.wall	6.70E-03	1.02E-02	5.08E-03	8.88E-03	1.69E+00	2.71E+00	1.71E-03	2.92E-03	3.40E-03	6.02E-03	9.43E-03	1.35E-02	1.97E-02	2.15E-02	3.02E-02

SD: Standard deviation; GM: Geometric mean; GSD: Geometric standard deviation; UF: Uncertainty factor; Min: minimum value; X2.5: 2.5th percentile; X5.0: 5th percentile; X25: 25th percentile; X50: 50th percentile; X75: 75th percentile; X95: 95th percentile; X97.5: 97.5th percentile; Max: maximum value; Undisturbed: Reference dose value for the exposure scenario.

Appendix B: This subsection presents a statistical summary of the results from the sensitivity of organ and tissue doses to parameter groups following inhalation of radon progeny by underground miners performing both Job 1 and Job 4.

Table B1: Sensitivity of organ and tissue committed equivalent dose coefficients (mSv/ (mJh/m^3)) to activity parameters of the HRTM deposition model for inhalation of radon progeny by underground miners performing Job 1.

Organ	Undisturbed	Mean	SD	GM	GSD	UF	Min	X2.5	X5.0	X25	X50	X75	X95	X97.5	Max
Lung	1.87E+01	4.31E+01	1.79E+01	3.93E+01	1.55E+00	2.26E+00	1.05E+01	1.61E+01	1.83E+01	2.88E+01	4.07E+01	5.50E+01	7.65E+01	8.27E+01	1.08E+02
Bronch.bas	2.72E+01	2.92E+01	1.17E+01	2.68E+01	1.52E+00	2.18E+00	7.40E+00	1.15E+01	1.30E+01	1.99E+01	2.76E+01	3.68E+01	5.09E+01	5.49E+01	7.19E+01
Bronch.sec	5.86E+01	7.14E+01	2.86E+01	6.57E+01	1.52E+00	2.18E+00	1.81E+01	2.83E+01	3.18E+01	4.89E+01	6.75E+01	9.01E+01	1.25E+02	1.34E+02	1.76E+02
Bchiol.sec	3.77E+01	7.45E+01	3.13E+01	6.79E+01	1.56E+00	2.28E+00	1.78E+01	2.75E+01	3.10E+01	4.96E+01	7.04E+01	9.53E+01	1.33E+02	1.44E+02	1.88E+02
AI	1.99E+00	4.43E+00	2.53E+00	3.68E+00	1.90E+00	3.20E+00	5.80E-01	9.86E-01	1.16E+00	2.31E+00	4.05E+00	6.12E+00	9.19E+00	1.01E+01	1.37E+01
St.stem	1.94E-02	2.05E-02	9.63E-03	1.83E-02	1.65E+00	2.51E+00	4.22E-03	6.66E-03	7.59E-03	1.27E-02	1.92E-02	2.69E-02	3.86E-02	4.19E-02	5.57E-02
R.marrow	7.56E-03	1.16E-02	6.07E-03	9.95E-03	1.77E+00	2.84E+00	1.94E-03	3.11E-03	3.59E-03	6.53E-03	1.07E-02	1.56E-02	2.30E-02	2.51E-02	3.37E-02
Colon	3.04E-03	1.38E-02	7.21E-03	1.19E-02	1.77E+00	2.82E+00	2.33E-03	3.74E-03	4.31E-03	7.82E-03	1.28E-02	1.86E-02	2.74E-02	2.98E-02	4.01E-02
RC.stem	9.96E-03	1.39E-02	7.23E-03	1.19E-02	1.77E+00	2.82E+00	2.35E-03	3.77E-03	4.34E-03	7.86E-03	1.28E-02	1.87E-02	2.75E-02	2.99E-02	4.03E-02
LC.stem	1.00E-02	1.39E-02	7.27E-03	1.20E-02	1.77E+00	2.82E+00	2.36E-03	3.79E-03	4.36E-03	7.90E-03	1.29E-02	1.88E-02	2.76E-02	3.01E-02	4.05E-02
RS.stem	9.47E-03	1.34E-02	7.05E-03	1.15E-02	1.78E+00	2.84E+00	2.23E-03	3.60E-03	4.15E-03	7.56E-03	1.24E-02	1.81E-02	2.67E-02	2.91E-02	3.92E-02
Liver	6.32E-03	2.52E-02	1.32E-02	2.16E-02	1.78E+00	2.84E+00	4.20E-03	6.76E-03	7.79E-03	1.42E-02	2.33E-02	3.40E-02	5.01E-02	5.46E-02	7.35E-02
Kidneys	2.45E-02	7.63E-02	4.02E-02	6.55E-02	1.78E+00	2.85E+00	1.26E-02	2.03E-02	2.35E-02	4.29E-02	7.05E-02	1.03E-01	1.52E-01	1.66E-01	2.23E-01
Endost.BS	8.74E-03	1.84E-02	9.64E-03	1.58E-02	1.77E+00	2.84E+00	3.07E-03	4.93E-03	5.69E-03	1.04E-02	1.70E-02	2.48E-02	3.65E-02	3.98E-02	5.36E-02
Brain	1.21E-03	4.26E-03	2.20E-03	3.69E-03	1.75E+00	2.78E+00	7.52E-04	1.18E-03	1.36E-03	2.44E-03	3.94E-03	5.72E-03	8.39E-03	9.14E-03	1.22E-02
Ht.wall	7.20E-03	1.08E-02	5.65E-03	9.27E-03	1.77E+00	2.84E+00	1.80E-03	2.90E-03	3.34E-03	6.08E-03	9.96E-03	1.45E-02	2.14E-02	2.33E-02	3.14E-02

SD: Standard deviation; GM: Geometric mean; GSD: Geometric standard deviation; UF: Uncertainty factor; Min: minimum value; X2.5: 2.5th percentile; X5.0: 5th percentile; X25: 25th percentile; X50: 50th percentile; X75: 75th percentile; X95: 95th percentile; X97.5: 97.5th percentile; Max: maximum value; Undisturbed: Reference dose value for the exposure scenario.

Table B2: Sensitivity of organ and tissue committed equivalent dose coefficients (mSv/ (mJh/m^3)) to activity parameters of the HRTM deposition model for inhalation of radon progeny by underground miners performing Job 4.

Organ	Undisturbed	Mean	SD	GM	GSD	UF	Min	X2.5	X5.0	X25	X50	X75	X95	X97.5	Max
Lung	2.33E+01	6.60E+01	2.81E+01	6.01E+01	1.56E+00	2.30E+00	1.39E+01	2.43E+01	2.76E+01	4.40E+01	6.18E+01	8.39E+01	1.18E+02	1.29E+02	1.95E+02
Bronch.bas	4.22E+01	6.05E+01	2.67E+01	5.49E+01	1.57E+00	2.36E+00	1.21E+01	2.21E+01	2.52E+01	4.02E+01	5.61E+01	7.66E+01	1.11E+02	1.23E+02	2.00E+02
Bronch.sec	8.67E+01	1.46E+02	6.44E+01	1.32E+02	1.57E+00	2.36E+00	2.92E+01	5.34E+01	6.09E+01	9.69E+01	1.35E+02	1.85E+02	2.67E+02	2.96E+02	4.81E+02
Bchiol.sec	4.71E+01	8.94E+01	3.71E+01	8.17E+01	1.54E+00	2.26E+00	2.03E+01	3.34E+01	3.79E+01	6.01E+01	8.45E+01	1.14E+02	1.58E+02	1.71E+02	2.32E+02
AI	2.46E+00	5.22E+00	2.89E+00	4.39E+00	1.86E+00	3.08E+00	6.89E-01	1.23E+00	1.44E+00	2.28E+00	4.78E+00	7.18E+00	1.06E+01	1.17E+01	1.63E+01
St.stem	3.21E-02	3.45E-02	1.51E-02	3.11E-02	1.59E+00	2.37E+00	7.41E-03	1.21E-02	1.37E-02	2.23E-02	3.24E-02	4.45E-02	6.26E-02	6.79E-02	8.84E-02
R.marrow	1.05E-02	1.52E-02	7.58E-03	1.33E-02	1.72E+00	2.70E+00	2.65E-03	4.41E-03	5.10E-03	8.99E-03	1.41E-02	2.03E-02	2.94E-02	3.21E-02	4.35E-02
Colon	3.79E-03	1.83E-02	9.07E-03	1.60E-02	1.71E+00	2.68E+00	3.22E-03	5.35E-03	6.19E-03	1.09E-02	1.70E-02	2.44E-02	3.52E-02	3.84E-02	5.21E-02
RC.stem	1.40E-02	1.84E-02	9.11E-03	1.61E-02	1.71E+00	2.67E+00	3.25E-03	5.41E-03	6.25E-03	1.09E-02	1.71E-02	2.45E-02	3.54E-02	3.87E-02	5.23E-02
LC.stem	1.41E-02	1.85E-02	9.17E-03	1.62E-02	1.71E+00	2.67E+00	3.28E-03	5.45E-03	6.29E-03	1.10E-02	1.72E-02	2.47E-02	3.57E-02	3.89E-02	5.26E-02
RS.stem	1.31E-02	1.75E-02	8.77E-03	1.53E-02	1.72E+00	2.70E+00	3.02E-03	5.07E-03	5.87E-03	1.04E-02	1.63E-02	2.34E-02	3.39E-02	3.70E-02	5.04E-02
Liver	7.90E-03	3.29E-02	1.64E-02	2.87E-02	1.72E+00	2.70E+00	5.67E-03	9.50E-03	1.10E-02	1.94E-02	3.05E-02	4.39E-02	6.36E-02	6.95E-02	9.44E-02
Kidneys	3.31E-02	9.88E-02	4.96E-02	8.61E-02	1.72E+00	2.72E+00	1.68E-02	2.83E-02	3.28E-02	5.81E-02	9.17E-02	1.32E-01	1.91E-01	2.09E-01	2.85E-01
Endost.BS	1.22E-02	2.42E-02	1.20E-02	2.11E-02	1.71E+00	2.69E+00	4.23E-03	7.01E-03	8.11E-03	1.43E-02	2.25E-02	3.23E-02	4.67E-02	5.09E-02	6.87E-02
Brain	1.64E-03	5.87E-03	2.85E-03	5.17E-03	1.69E+00	2.62E+00	1.10E-03	1.78E-03	2.04E-03	3.54E-03	5.46E-03	7.78E-03	1.12E-02	1.22E-02	1.61E-02
Ht.wall	1.00E-02	1.42E-02	7.07E-03	1.24E-02	1.71E+00	2.69E+00	2.46E-03	4.12E-03	4.77E-03	8.39E-03	1.32E-02	1.89E-02	2.74E-02	2.99E-02	4.06E-02

SD: Standard deviation; GM: Geometric mean; GSD: Geometric standard deviation; UF: Uncertainty factor; Min: minimum value; X2.5: 2.5th percentile; X5.0: 5th percentile; X25: 25th percentile; X50: 50th percentile; X75: 75th percentile; X95: 95th percentile; X97.5: 97.5th percentile; Max: maximum value; Undisturbed: Reference dose value for the exposure scenario.

Table B3: Sensitivity of organ and tissue committed equivalent dose coefficients (mSv/ (mJh/m^3)) to aerosol parameters of the HRTM deposition model for inhalation of radon progeny by underground miners performing Job 1.

Organ	Undisturbed	Mean	SD	GM	GSD	UF	Min	X2.5	X5.0	X25	X50	X75	X95	X97.5	Max
Lung	1.87E+01	3.72E+01	4.31E+00	3.69E+01	1.12E+00	1.25E+00	1.87E+01	2.90E+01	3.01E+01	3.40E+01	3.73E+01	4.02E+02	4.40E+01	4.55E+01	5.49E+01
Bronch.bas	2.72E+01	3.18E+01	5.55E+00	3.13E+01	1.20E+00	1.41E+00	1.73E+01	2.13E+01	2.27E+01	2.78E+01	3.17E+01	3.57E+01	4.12E+01	4.26E+01	4.80E+01
Bronch.sec	5.86E+01	7.76E+01	1.37E+01	7.64E+01	1.20E+00	1.42E+00	4.16E+01	5.18E+01	5.52E+01	6.78E+01	7.74E+01	8.72E+01	1.01E+02	1.04E+02	1.18E+02
Bchiol.sec	3.77E+01	5.40E+01	1.08E+01	5.30E+01	1.21E+00	1.45E+00	3.25E+01	3.78E+01	3.94E+01	4.60E+01	5.23E+01	6.04E+01	7.45E+01	7.95E+01	9.93E+01
AI	1.99E+00	2.83E+00	3.60E-01	2.80E+00	1.13E+00	1.25E+00	1.99E+00	2.37E+00	2.39E+00	2.55E+00	2.75E+00	3.03E+00	3.54E+00	3.72E+00	4.42E+00
St.stem	1.51E-02	1.93E-02	3.39E-03	1.90E-02	1.20E+00	1.41E+00	1.06E-02	1.31E-02	1.39E-02	1.69E-02	1.92E-02	2.17E-02	2.52E-02	2.60E-02	2.87E-02
R.marrow	5.22E-03	7.17E-03	6.34E-04	7.14E-03	1.09E+00	1.19E+00	5.22E-03	6.03E-03	6.14E-03	6.70E-03	7.19E-03	7.60E-03	8.20E-03	8.47E-03	9.75E-03
Colon	2.27E-03	7.21E-03	6.31E-04	7.19E-03	1.09E+00	1.18E+00	2.27E-03	6.03E-03	6.15E-03	6.74E-03	7.26E-03	7.67E-03	8.17E-03	8.42E-03	9.65E-03
RC.stem	5.12E-03	7.31E-03	6.38E-04	7.28E-03	1.09E+00	1.18E+00	5.12E-03	6.11E-03	6.23E-03	6.84E-03	7.36E-03	7.79E-03	8.26E-03	8.50E-03	9.73E-03
LC.stem	5.19E-03	7.37E-03	6.44E-04	7.35E-03	1.09E+00	1.18E+00	5.19E-03	6.15E-03	6.28E-03	6.89E-03	7.43E-03	7.86E-03	8.33E-03	8.56E-03	9.80E-03
RS.stem	4.63E-03	6.69E-03	6.01E-04	6.67E-03	1.09E+00	1.19E+00	4.63E-03	5.64E-03	5.74E-03	6.25E-03	6.70E-03	7.08E-03	7.71E-03	7.97E-03	9.20E-03
Liver	6.62E-03	2.09E-02	1.88E-03	2.08E-02	1.09E+00	1.19E+00	6.62E-03	1.76E-02	1.79E-02	1.95E-02	2.09E-02	2.21E-02	2.41E-02	2.49E-02	2.88E-02
Kidneys	6.02E-03	8.38E-02	7.71E-03	8.35E-02	1.10E+00	1.19E+00	6.02E-02	7.08E-02	7.20E-02	7.82E-02	8.37E-02	8.85E-02	9.73E-02	1.01E-01	1.17E-01
Endost.BS	1.35E-02	1.74E-02	1.54E-03	1.74E-02	1.09E+00	1.19E+00	1.35E-02	1.47E-02	1.49E-02	1.63E-02	1.75E-02	1.85E-02	2.00E-02	2.06E-02	2.37E-02
Brain	1.26E-03	3.67E-03	3.25E-04	3.66E-03	1.09E+00	1.18E+00	1.26E-03	3.04E-03	3.10E-03	3.43E-03	3.71E-03	3.94E-03	4.12E-03	4.19E-03	5.22E-03
Ht.wall	4.81E-03	6.55E-03	5.82E-04	6.52E-03	1.09E+00	1.19E+00	4.81E-03	5.51E-03	5.61E-03	6.12E-03	6.56E-03	6.94E-03	7.50E-03	7.76E-03	8.93E-03

SD: Standard deviation; GM: Geometric mean; GSD: Geometric standard deviation; UF: Uncertainty factor; Min: minimum value; X2.5: 2.5th percentile; X5.0: 5th percentile; X25: 25th percentile; X50: 50th percentile; X75: 75th percentile; X95: 95th percentile; X97.5: 97.5th percentile; Max: maximum value; Undisturbed: Reference dose value for the exposure scenario.

Table B4: Sensitivity of organ and tissue committed equivalent dose coefficients (mSv/ (mJh/m^3)) to aerosol parameters of the HRTM deposition model for inhalation of radon progeny by miners performing Job 4.

Organ	Undisturbed	Mean	SD	GM	GSD	UF	Min	X2.5	X5.0	X25	X50	X75	X95	X97.5	Max
Lung	2.33E+01	4.56E+01	4.07E-01	4.56E+01	1.01E+00	1.01E+00	2.33E+01	4.50E+01	4.50E+01	4.53E+01	4.56E+01	4.60E+01	4.62E+01	4.63E+01	4.63E+01
Bronch.bas	4.22E+01	3.82E+01	5.18E-01	3.82E+01	1.01E+00	1.02E+00	3.73E+01	3.74E+01	3.74E+01	3.78E+01	3.82E+01	3.87E+01	3.90E+01	3.91E+01	4.22E+01
Bronch.sec	8.67E+01	9.23E+01	1.39E+00	9.23E+01	1.02E+00	1.03E+00	8.67E+01	9.00E+01	9.01E+01	9.11E+01	9.23E+01	9.35E+01	9.44E+01	9.45E+01	9.47E+01
Bchiol.sec	4.71E+01	6.82E+01	2.61E-01	6.82E+01	1.00E+00	1.01E+00	4.71E+01	6.78E+01	6.79E+01	6.80E+01	6.82E+01	6.85E+01	6.86E+01	6.86E+01	6.87E+01
AI	2.44E+00	3.34E+00	1.22E-02	3.34E+00	1.00E+00	1.01E+00	2.44E+00	3.33E+00	3.33E+00	3.33E+00	3.34E+00	3.35E+00	3.36E+00	3.36E+00	3.36E+00
St.stem	2.60E-02	2.43E-02	1.32E-04	2.43E-02	1.01E+00	1.01E+00	2.41E-02	2.41E-02	2.41E-02	2.42E-02	2.43E-02	2.44E-02	2.45E-02	2.45E-02	2.60E-02
R.marrow	7.28E-03	8.66E-03	1.57E-05	8.66E-03	1.00E+00	1.00E+00	7.28E-03	8.63E-03	8.63E-03	8.64E-03	8.66E-03	8.67E-03	8.68E-03	8.68E-03	8.68E-03
Colon	2.87E-03	8.72E-03	3.21E-05	8.72E-03	1.01E+00	1.00E+00	2.87E-03	8.69E-03	8.69E-03	8.70E-03	8.72E-03	8.73E-03	8.75E-03	8.75E-03	8.75E-03
RC.stem	7.25E-03	8.84E-03	2.13E-05	8.84E-03	1.00E+00	1.00E+00	7.25E-03	8.81E-03	8.81E-03	8.82E-03	8.84E-03	8.86E-03	8.87E-03	8.87E-03	8.87E-03
LC.stem	7.37E-03	8.93E-03	2.07E-05	8.93E-03	1.00E+00	1.00E+00	7.37E-03	8.89E-03	8.89E-03	8.91E-03	8.93E-03	8.94E-03	8.96E-03	8.96E-03	8.96E-03
RS.stem	6.38E-03	8.06E-03	1.57E-05	8.06E-03	1.00E+00	1.00E+00	6.38E-03	8.04E-03	8.04E-03	8.05E-03	8.06E-03	8.07E-03	8.08E-03	8.08E-03	8.08E-03
Liver	8.24E-03	2.51E-02	8.49E-05	2.51E-02	1.01E+00	1.00E+00	8.24E-03	2.51E-02	2.51E-02	2.51E-02	2.52E-02	2.52E-02	2.52E-02	2.52E-02	2.52E-02
Kidneys	8.27E-02	1.01E-01	1.48E-04	1.01E-01	1.00E+00	1.00E+00	8.27E-02	1.01E-01	1.01E-01	1.01E-01	1.01E-01	1.01E-01	1.01E-01	1.01E-01	1.01E-01
Endost.BS	1.88E-02	2.11E-02	3.32E-05	2.11E-02	1.00E+00	1.00E+00	1.88E-02	2.10E-02	2.10E-02	2.10E-02	2.11E-02	2.11E-02	2.11E-02	2.11E-02	2.11E-02
Brain	1.70E-03	4.48E-03	1.55E-05	4.48E-03	1.00E+00	1.00E+00	1.70E-03	4.46E-03	4.46E-03	4.47E-03	4.48E-03	4.49E-03	4.49E-03	4.49E-03	4.49E-03
Ht.wall	6.70E-03	7.92E-03	1.29E-05	7.92E-03	1.00E+00	1.00E+00	6.70E-03	7.90E-03	7.90E-03	7.91E-03	7.92E-03	7.93E-03	7.93E-03	7.93E-03	7.94E-03

SD: Standard deviation; GM: Geometric mean; GSD: Geometric standard deviation; UF: Uncertainty factor; Min: minimum value; X2.5: 2.5th percentile; X5.0: 5th percentile; X25: 25th percentile; X50: 50th percentile; X75: 75th percentile; X95: 95th percentile; X97.5: 97.5th percentile; Max: maximum value; Undisturbed: Reference dose value for the exposure scenario.

Table B5: Sensitivity of organ and tissue committed equivalent dose coefficients (mSv/ (mJh/m^3)) to subject parameters of the HRTM deposition model for inhalation of radon progeny by miners performing Job 1.

Organ	Undisturbed	Mean	SD	GM	GSD	UF	Min	X2.5	X5.0	X25	X50	X75	X95	X97.5	Max
Lung	1.87E+01	3.48E+01	1.10E+00	3.47E+01	1.03E+00	1.06E+00	1.87E+01	3.28E+01	3.30E+01	3.39E+01	3.48E+01	3.57E+01	3.65E+01	3.67E+01	3.74E+01
Bronch.bas	2.72E+01	2.32E+01	8.49E-01	2.32E+01	1.04E+00	1.06E+00	2.14E+00	2.17E+01	2.18E+01	2.25E+01	2.32E+01	2.39E+01	2.45E+01	2.46E+01	2.72E+01
Bronch.sec	5.86E+01	5.66E+01	2.09E+00	5.66E+01	1.04E+00	1.06E+00	5.22E+01	5.31E+01	5.34E+01	5.49E+01	5.67E+01	5.84E+01	5.98E+01	6.01E+01	6.11E+01
Bchiol.sec	3.77E+01	6.15E+01	3.19E+00	6.14E+01	1.05E+00	1.09E+00	3.77E+01	5.61E+01	5.65E+01	5.88E+01	6.16E+01	6.42E+01	6.64E+01	6.69E+01	6.86E+01
AI	1.99E+00	2.82E+00	5.20E-02	2.82E+00	1.02E+00	1.04E+00	1.99E+00	2.72E+00	2.74E+00	2.78E+00	2.82E+00	2.86E+00	2.91E+00	2.92E+00	2.98E+00
St.stem	1.51E-02	1.33E-02	5.35E-05	1.33E-02	1.00E+00	1.01E+00	1.31E-02	1.32E-02	1.32E-02	1.33E-02	1.33E-02	1.33E-02	1.34E-02	1.34E-02	1.51E-02
R.marrow	5.22E-03	6.47E-02	6.43E-05	6.47E-03	1.01E+00	1.02E+00	5.22E-03	6.35E-03	6.36E-03	6.42E-03	6.47E-03	6.51E-03	6.57E-03	6.59E-03	6.64E-03
Colon	2.27E-03	6.42E-02	6.39E-05	6.42E-03	1.01E+00	1.02E+00	2.27E-03	6.30E-03	6.32E-03	6.37E-03	6.42E-03	6.46E-03	6.52E-03	6.53E-03	6.58E-03
RC.stem	5.12E-03	6.48E-02	6.14E-05	6.48E-03	1.01E+00	1.02E+00	5.12E-03	6.36E-03	6.37E-03	6.43E-03	6.48E-03	6.52E-03	6.58E-03	6.59E-03	6.64E-03
LC.stem	5.19E-03	6.52E-03	6.17E-05	6.52E-03	1.01E+00	1.02E+00	5.19E-03	6.41E-03	6.42E-03	6.48E-03	6.52E-03	6.57E-03	6.62E-03	6.64E-03	6.68E-03
RS.stem	4.63E-03	6.09E-03	6.10E-05	6.09E-03	1.01E+00	1.02E+00	4.63E-03	5.98E-03	5.99E-03	6.05E-03	6.09E-03	6.13E-03	6.19E-03	6.21E-03	6.25E-03
Liver	6.62E-03	1.90E-02	1.99E-04	1.90E-02	1.01E+00	1.02E+00	6.62E-03	1.87E-02	1.87E-02	1.89E-02	1.90E-02	1.92E-02	1.94E-02	1.94E-02	1.95E-02
Kidneys	6.02E-02	7.72E-02	7.91E-04	7.72E-02	1.01E+00	1.02E+00	6.02E-02	7.57E-02	7.59E-02	7.66E-02	7.72E-02	7.78E-02	7.85E-02	7.87E-02	7.93E-02
Endost.BS	1.35E-02	1.58E-02	1.58E-04	1.57E-02	1.01E+00	1.02E+00	1.35E-02	1.54E-02	1.55E-02	1.56E-02	1.58E-02	1.59E-02	1.60E-02	1.60E-02	1.62E-02
Brain	1.26E-03	3.17E-03	3.01E-05	3.17E-03	1.01E+00	1.02E+00	1.26E-03	3.12E-03	3.13E-03	3.15E-03	3.17E-03	3.19E-03	3.22E-03	3.23E-03	3.25E-03
Ht.wall	4.81E-03	5.92E-03	5.81E-05	5.92E-03	1.01E+00	1.02E+00	4.81E-03	5.81E-03	5.83E-03	5.88E-03	5.93E-03	5.97E-03	6.02E-03	6.03E-03	6.08E-03

SD: Standard deviation; GM: Geometric mean; GSD: Geometric standard deviation; UF: Uncertainty factor; Min: minimum value; X2.5: 2.5th percentile; X5.0: 5th percentile; X25: 25th percentile; X50: 50th percentile; X75: 75th percentile; X95: 95th percentile; X97.5: 97.5th percentile; Max: maximum value; Undisturbed: Reference dose value for the exposure scenario.

Table B6: Sensitivity of organ and tissue committed equivalent dose coefficients (mSv/ (mJh/m^3)) to subject parameters of the HRTM deposition model for inhalation of radon progeny by miners performing Job 4.

Organ	Undisturbed	Mean	SD	GM	GSD	UF	Min	X2.5	X5.0	X25	X50	X75	X95	X97.5	Max
Lung	2.33E+01	4.65E+01	1.11E+00	4.65E+01	1.02E+00	1.04E+00	2.33E+01	4.46E+01	4.47E+01	4.56E+01	4.65E+01	4.74E+01	4.82E+01	4.84E+01	4.93E+01
Bronch.bas	4.22E+01	3.86E+01	7.67E-01	3.86E+01	1.02E+00	1.03E+00	3.68E+01	3.72E+01	3.73E+01	3.79E+01	3.86E+01	3.92E+01	3.97E+01	3.99E+01	4.22E+01
Bronch.sec	8.67E+01	9.30E+01	1.86E+00	9.30E+01	1.02E+00	1.03E+00	8.67E+01	8.98E+01	9.00E+01	9.14E+01	9.30E+01	9.46E+01	9.59E+01	9.61E+01	9.72E+01
Bchiol.sec	4.71E+01	7.05E+01	3.21E+00	7.04E+01	1.05E+00	1.08E+00	4.71E+01	6.50E+01	6.54E+01	6.78E+01	7.05E+01	7.32E+01	7.54E+01	7.59E+01	7.76E+01
AI	2.44E+00	3.25E+00	6.04E-02	3.25E+00	1.02E+00	1.04E+00	2.44E+00	3.13E+00	3.15E+00	3.21E+00	3.25E+00	3.29E+00	3.35E+00	3.37E+00	3.43E+00
St.stem	2.60E-02	2.42E-02	6.03E-05	2.42E-02	1.01E+00	1.00E+00	2.40E-02	2.40E-02	2.41E-02	2.41E-02	2.42E-02	2.42E-02	2.43E-02	2.43E-02	2.60E-02
R.marrow	7.28E-03	8.53E-03	7.32E-05	8.53E-03	1.01E+00	1.02E+00	7.28E-03	8.39E-03	8.41E-03	8.48E-03	8.53E-03	8.59E-03	8.65E-03	8.67E-03	8.74E-03
Colon	2.87E-03	8.60E-03	7.42E-05	8.60E-03	1.01E+00	1.02E+00	2.87E-03	8.47E-03	8.48E-03	8.55E-03	8.60E-03	8.65E-03	8.71E-03	8.73E-03	8.79E-03
RC.stem	7.25E-03	8.72E-03	6.99E-05	8.72E-03	1.01E+00	1.02E+00	7.25E-03	8.59E-03	8.61E-03	8.67E-03	8.72E-03	8.77E-03	8.84E-03	8.85E-03	8.91E-03
LC.stem	7.37E-03	8.81E-03	7.03E-05	8.80E-03	1.01E+00	1.02E+00	7.37E-03	8.67E-03	8.69E-03	8.76E-03	8.80E-03	8.86E-03	8.92E-03	8.94E-03	9.00E-03
RS.stem	6.38E-03	7.95E-03	6.94E-05	7.95E-03	1.01E+00	1.02E+00	6.38E-03	7.81E-03	7.83E-03	7.90E-03	7.95E-03	8.00E-03	8.06E-03	8.08E-03	8.14E-03
Liver	8.24E-03	2.48E-02	2.30E-04	2.48E-02	1.01E+00	1.02E+00	8.24E-03	2.44E-02	2.44E-02	2.46E-02	2.48E-02	2.49E-02	2.51E-02	2.52E-02	2.54E-02
Kidneys	8.27E-02	9.96E-02	9.00E-04	9.96E-02	1.01E+00	1.02E+00	8.27E-02	9.78E-02	9.81E-02	9.89E-02	9.96E-02	1.00E-01	1.01E-01	1.01E-01	1.02E-01
Endost.BS	1.88E-02	2.08E-02	1.80E-04	2.08E-02	1.01E+00	1.02E+00	1.88E-02	2.04E-02	2.05E-02	2.06E-02	2.08E-02	2.09E-02	2.11E-02	2.11E-02	2.13E-02
Brain	1.70E-03	4.42E-03	3.50E-05	4.42E-03	1.01E+00	1.01E+00	1.70E-03	4.36E-03	4.37E-03	4.40E-03	4.42E-03	4.45E-03	4.48E-03	4.48E-03	4.51E-03
Ht.wall	6.70E-03	7.81E-03	6.63E-05	7.81E-03	1.01E+00	1.02E+00	6.70E-03	7.68E-03	7.70E-03	7.76E-03	7.81E-03	7.85E-03	7.92E-03	7.93E-03	7.99E-03

SD: Standard deviation; GM: Geometric mean; GSD: Geometric standard deviation; UF: Uncertainty factor; Min: minimum value; X2.5: 2.5th percentile; X5.0: 5th percentile; X25: 25th percentile; X50: 50th percentile; X75: 75th percentile; X95: 95th percentile; X97.5: 97.5th percentile; Max: maximum value; Undisturbed: Reference dose value for the exposure scenario.

Table B7: Sensitivity of organ and tissue committed equivalent dose coefficients (mSv/ (mJh/m^3)) to absorption parameters of the HRTM model for inhalation of radon progeny by miners performing Job 1.

Organ	Undisturbed	Mean	SD	GM	GSD	UF	Min	X2.5	X5.0	X25	X50	X75	X95	X97.5	Max
Lung	1.50E+01	3.38E+01	1.52E-01	3.38E+01	1.01E+00	1.01E+00	1.50E+01	3.36E+01	3.36E+01	3.37E+01	3.38E+01	3.39E+01	3.40E+01	3.40E+01	3.41E+01
Bronch.bas	2.10E+01	2.26E+01	8.84E-02	2.26E+01	1.00E+00	1.01E+00	2.10E+01	2.24E+01	2.24E+01	2.25E+01	2.26E+01	2.26E+01	2.27E+01	2.27E+01	2.28E+01
Bronch.sec	4.61E+01	5.51E+01	1.89E-01	5.51E+01	1.00E+00	1.01E+00	4.61E+01	5.48E+01	5.48E+01	5.50E+01	5.51E+01	5.53E+01	5.54E+01	5.55E+01	5.56E+01
Bchiol.sec	2.90E+01	5.97E+01	2.78E-01	5.97E+01	1.01E+00	1.01E+00	2.90E+01	5.92E+01	5.93E+01	5.95E+01	5.97E+01	5.98E+01	6.01E+01	6.01E+01	6.03E+01
AI	1.72E+00	2.93E+00	1.38E-02	2.93E+00	1.00E+00	1.01E+00	1.72E+00	2.91E+00	2.91E+00	2.92E+00	2.93E+00	2.94E+00	2.96E+00	2.96E+00	2.97E+00
St.stem	1.30E-02	1.27E-02	3.31E-04	1.27E-02	1.03E+00	1.05E+00	1.19E-02	1.21E-02	1.22E-02	1.25E-02	1.27E-02	1.30E-02	1.33E-02	1.33E-02	1.35E-02
R.marrow	4.45E-03	5.89E-03	3.46E-04	5.88E-03	1.06E+00	1.12E+00	4.45E-03	5.24E-03	5.32E-03	5.62E-03	5.89E-03	6.14E-03	6.45E-03	6.53E-03	6.74E-03
Colon	1.97E-03	5.79E-03	3.72E-04	5.78E-03	1.07E+00	1.13E+00	1.97E-03	5.10E-03	5.18E-03	5.51E-03	5.79E-03	6.07E-03	6.40E-03	6.48E-03	6.70E-03
RC.stem	4.37E-03	5.85E-03	3.72E-04	5.84E-03	1.07E+00	1.13E+00	4.37E-03	5.15E-03	5.23E-03	5.57E-03	5.85E-03	6.13E-03	6.46E-03	6.54E-03	6.76E-03
LC.stem	4.42E-03	5.90E-03	3.71E-04	5.89E-03	1.07E+00	1.12E+00	4.42E-03	5.21E-03	5.29E-03	5.62E-03	5.90E-03	6.18E-03	6.51E-03	6.59E-03	6.81E-03
RS.stem	3.94E-03	5.46E-03	3.72E-04	5.45E-03	1.07E+00	1.14E+00	3.94E-03	4.77E-03	4.85E-03	5.18E-03	5.46E-03	5.74E-03	6.07E-03	6.15E-03	6.38E-03
Liver	5.73E-03	1.72E-02	1.10E-03	1.71E-02	1.07E+00	1.13E+00	5.73E-03	1.51E-02	1.54E-02	1.63E-02	1.72E-02	1.80E-02	1.90E-02	1.92E-02	1.99E-02
Kidneys	5.12E-02	6.93E-02	4.46E-03	6.92E-02	1.07E+00	1.13E+00	5.12E-02	6.10E-02	6.20E-02	6.60E-02	6.94E-02	7.27E-02	7.66E-02	7.76E-02	8.06E-02
Endost.BS	1.15E-02	1.44E-02	8.01E-04	1.44E-02	1.06E+00	1.11E+00	1.15E-02	1.29E-02	1.30E-02	1.38E-02	1.44E-02	1.50E-02	1.57E-02	1.59E-02	1.64E-02
Brain	1.09E-03	2.88E-03	1.67E-04	2.88E-03	1.06E+00	1.11E+00	1.09E-03	2.57E-03	2.61E-03	2.76E-03	2.89E-03	3.01E-03	3.16E-03	3.19E-03	3.30E-03
Ht.wall	4.09E-03	5.49E-03	2.65E-04	5.49E-03	1.05E+00	1.09E+00	4.09E-03	5.00E-03	5.06E-03	5.29E-03	5.50E-03	5.69E-03	5.93E-03	5.99E-03	6.15E-03

SD: Standard deviation; GM: Geometric mean; GSD: Geometric standard deviation; UF: Uncertainty factor; Min: minimum value; X2.5: 2.5th percentile; X5.0: 5th percentile; X25: 25th percentile; X50: 50th percentile; X75: 75th percentile; X95: 95th percentile; X97.5: 97.5th percentile; Max: maximum value; Undisturbed: Reference dose value for the exposure scenario.

Table B8: Sensitivity of organ and tissue committed equivalent dose coefficients (mSv/ (mJh/m^3)) to absorption parameters of the HRTM model for inhalation of radon progeny by miners performing Job 4.

Organ	Undisturbed	Mean	SD	GM	GSD	UF	Min	X2.5	X5.0	X25	X50	X75	X95	X97.5	Max
Lung	2.33E+01	4.57E+01	1.90E-01	4.57E+01	1.00E+00	1.01E+00	2.33E+01	4.54E+01	4.55E+01	4.56E+01	4.57E+01	4.58E+01	4.60E+01	4.60E+01	4.61E+01
Bronch.bas	4.22E+01	3.82E+01	1.38E-01	3.82E+01	1.00E+00	1.00E+00	3.78E+01	3.79E+01	3.79E+01	3.80E+01	3.82E+01	3.83E+01	3.84E+01	3.84E+01	4.22E+01
Bronch.sec	8.67E+01	9.21E+01	2.87E-01	9.21E+01	1.00E+00	1.00E+00	8.67E+01	9.15E+01	9.16E+01	9.18E+01	9.21E+01	9.23E+01	9.25E+01	9.26E+01	9.27E+01
Bchiol.sec	4.71E+01	6.86E+01	2.91E-01	6.86E+01	1.00E+00	1.00E+00	4.71E+01	6.81E+01	6.82E+01	6.84E+01	6.87E+01	6.89E+01	6.91E+01	6.92E+01	6.93E+01
AI	2.44E+00	3.38E+00	1.51E-02	3.38E+00	1.00E+00	1.00E+00	2.44E+00	3.35E+00	3.36E+00	3.37E+00	3.38E+00	3.39E+00	3.40E+00	3.41E+00	3.42E+00
St.stem	2.60E-02	2.35E-02	4.08E-04	2.35E-02	1.02E+00	1.03E+00	2.25E-02	2.27E-02	2.28E-02	2.32E-02	2.35E-02	2.38E-02	2.41E-02	2.42E-02	2.60E-02
R.marrow	7.28E-03	7.80E-03	4.42E-04	7.78E-03	1.06E+00	1.11E+00	6.70E-03	6.97E-03	7.07E-03	7.47E-03	7.79E-03	8.12E-03	8.53E-03	8.62E-03	8.89E-03
Colon	2.87E-03	7.80E-03	4.74E-04	7.79E-03	1.06E+00	1.12E+00	2.87E-03	6.92E-03	7.02E-03	7.45E-03	7.80E-03	8.16E-03	8.58E-03	8.69E-03	8.96E-03
RC.stem	7.25E-03	7.92E-03	4.74E-04	7.91E-03	1.06E+00	1.12E+00	6.76E-03	7.04E-03	7.14E-03	7.57E-03	7.92E-03	8.28E-03	8.70E-03	8.81E-03	9.09E-03
LC.stem	7.37E-03	8.01E-03	4.73E-04	8.00E-03	1.06E+00	1.12E+00	6.85E-03	7.13E-03	7.23E-03	7.66E-03	8.01E-03	8.36E-03	8.79E-03	8.89E-03	9.17E-03
RS.stem	6.38E-03	7.15E-03	4.75E-04	7.13E-03	1.07E+00	1.13E+00	5.98E-03	6.26E-03	6.36E-03	6.80E-03	7.15E-03	7.50E-03	7.93E-03	8.03E-03	8.31E-03
Liver	8.24E-03	2.24E-02	1.40E-03	2.24E-02	1.06E+00	1.12E+00	8.24E-03	1.98E-02	2.01E-02	2.14E-02	2.24E-02	2.35E-02	2.47E-02	2.50E-02	2.59E-02
Kidneys	8.27E-02	8.97E-02	5.63E-03	8.95E-02	1.07E+00	1.13E+00	7.54E-02	7.91E-02	8.04E-02	8.55E-02	8.97E-02	9.39E-02	9.90E-02	1.00E-01	1.04E-01
Endost.BS	1.88E-02	1.90E-02	1.02E-03	1.90E-02	1.06E+00	1.11E+00	1.64E-02	1.71E-02	1.74E-02	1.83E-02	1.90E-02	1.98E-02	2.07E-02	2.10E-02	2.17E-02
Brain	1.70E-03	4.06E-03	2.12E-04	4.05E-03	1.05E+00	1.10E+00	1.70E-03	3.66E-03	3.71E-03	3.90E-03	4.06E-03	4.21E-03	4.41E-03	4.45E-03	4.59E-03
Ht.wall	6.70E-03	7.26E-03	3.37E-04	7.25E-03	1.05E+00	1.09E+00	6.42E-03	6.63E-03	6.70E-03	7.01E-03	7.26E-03	7.51E-03	7.82E-03	7.89E-03	8.09E-03

SD: Standard deviation; GM: Geometric mean; GSD: Geometric standard deviation; UF: Uncertainty factor; Min: minimum value; X2.5: 2.5th percentile; X5.0: 5th percentile; X25: 25th percentile; X50: 50th percentile; X75: 75th percentile; X95: 95th percentile; X97.5: 97.5th percentile; Max: maximum value; Undisturbed: Reference dose value for the exposure scenario.

Table B9: Sensitivity of organ and tissue committed equivalent dose coefficients (mSv/ (mJh/m^3)) to particle transport parameters of the HRTM model for inhalation of radon progeny by miners performing Job 1.

Organ	Undisturbed	Mean	SD	GM	GSD	UF	Min	X2.5	X5.0	X25	X50	X75	X95	X97.5	Max
Lung	1.50E+01	3.35E+01	2.14E-01	3.35E+01	1.01E+00	1.01E+00	1.50E+01	3.31E+01	3.32E+01	3.34E+01	3.35E+01	3.37E+01	3.39E+01	3.39E+01	3.43E+01
Bronch.bas	2.10E+01	2.24E+01	3.96E-01	2.24E+01	1.02E+00	1.04E+00	2.03E+01	2.16E+01	2.17E+01	2.21E+01	2.24E+01	2.26E+01	2.30E+01	2.31E+01	2.39E+01
Bronch.sec	4.61E+01	5.47E+01	7.98E-01	5.47E+01	1.01E+00	1.03E+00	4.61E+01	5.31E+01	5.34E+01	5.41E+01	5.47E+01	5.52E+01	5.60E+01	5.62E+01	5.78E+01
Bchiol.sec	2.90E+01	5.92E+01	1.43E-01	5.92E+01	1.00E+00	1.00E+00	2.90E+01	5.91E+01	5.91E+01	5.91E+01	5.92E+01	5.92E+01	5.92E+01	5.93E+01	6.12E+01
AI	1.72E+00	2.91E+00	5.43E-03	2.91E+00	1.00E+00	1.00E+00	1.72E+00	2.91E+00	2.91E+00	2.91E+00	2.91E+00	2.91E+00	2.91E+00	2.91E+00	3.04E+00
St.stem	1.30E-02	1.34E-02	3.95E-04	1.34E-02	1.03E+00	1.06E+00	1.18E-02	1.26E-02	1.27E-02	1.31E-02	1.34E-02	1.36E-02	1.40E-02	1.42E-02	1.50E-02
R.marrow	4.45E-03	6.57E-03	5.94E-05	6.57E-03	1.01E+00	1.02E+00	4.45E-03	6.46E-03	6.48E-03	6.53E-03	6.57E-03	6.61E-03	6.67E-03	6.69E-03	7.21E-03
Colon	1.97E-03	6.52E-03	6.05E-05	6.52E-03	1.01E+00	1.02E+00	1.97E-03	6.41E-03	6.43E-03	6.48E-03	6.51E-03	6.55E-03	6.61E-03	6.63E-03	7.54E-03
RC.stem	4.37E-03	6.58E-03	5.98E-05	6.58E-03	1.01E+00	1.02E+00	4.37E-03	6.47E-03	6.48E-03	6.54E-03	6.58E-03	6.62E-03	6.67E-03	6.69E-03	7.59E-03
LC.stem	4.42E-03	6.62E-03	5.69E-05	6.62E-03	1.01E+00	1.02E+00	4.42E-03	6.52E-03	6.53E-03	6.58E-03	6.62E-03	6.66E-03	6.72E-03	6.73E-03	7.65E-03
RS.stem	3.94E-03	6.19E-03	6.15E-05	6.19E-03	1.01E+00	1.02E+00	3.94E-03	6.08E-03	6.09E-03	6.15E-03	6.18E-03	6.23E-03	6.29E-03	6.31E-03	7.21E-03
Liver	5.73E-03	1.93E-02	1.85E-04	1.93E-02	1.01E+00	1.02E+00	5.73E-03	1.90E-02	1.91E-02	1.92E-02	1.93E-02	1.95E-02	1.96E-02	1.97E-02	2.00E-02
Kidneys	5.12E-02	7.85E-02	7.32E-04	7.84E-02	1.01E+00	1.02E+00	5.12E-02	7.72E-02	7.73E-02	7.79E-02	7.84E-02	7.89E-02	7.97E-02	8.00E-02	8.15E-02
Endost.BS	1.15E-02	1.60E-02	1.57E-04	1.60E-02	1.01E+00	1.02E+00	1.15E-02	1.57E-02	1.58E-02	1.59E-02	1.60E-02	1.61E-02	1.63E-02	1.63E-02	1.66E-02
Brain	1.09E-03	3.22E-03	3.58E-05	3.22E-03	1.01E+00	1.02E+00	1.09E-03	3.16E-03	3.17E-03	3.20E-03	3.22E-03	3.24E-03	3.28E-03	3.29E-03	3.56E-03
Ht.wall	4.09E-03	6.02E-03	4.32E-05	6.02E-03	1.01E+00	1.01E+00	4.09E-03	5.94E-03	5.95E-03	5.99E-03	6.01E-03	6.04E-03	6.09E-03	6.10E-03	6.62E-03

SD: Standard deviation; GM: Geometric mean; GSD: Geometric standard deviation; UF: Uncertainty factor; Min: minimum value; X2.5: 2.5th percentile; X5.0: 5th percentile; X25: 25th percentile; X50: 50th percentile; X75: 75th percentile; X95: 95th percentile; X97.5: 97.5th percentile; Max: maximum value; Undisturbed: Reference dose value for the exposure scenario.

Table B10: Sensitivity of organ and tissue committed equivalent dose coefficients (mSv/ (mJh/m^3)) to particle transport parameters of the HRTM model for inhalation of radon progeny by miners performing Job 4.

Organ	Undisturbed	Mean	SD	GM	GSD	UF	Min	X2.5	X5.0	X25	X50	X75	X95	X97.5	Max
Lung	2.33E+01	4.53E+01	3.95E-01	4.53E+01	1.01E+00	1.02E+00	2.33E+01	4.46E+01	4.47E+01	4.51E+01	4.53E+01	4.56E+01	4.60E+01	4.61E+01	5.04E+01
Bronch.bas	4.22E+01	3.79E+01	7.64E-01	3.78E+01	1.02E+00	1.04E+00	3.47E+01	3.63E+01	3.66E+01	3.73E+01	3.79E+01	3.84E+01	3.91E+01	3.93E+01	4.29E+01
Bronch.sec	8.67E+01	9.13E+01	1.54E+00	9.13E+01	1.02E+00	1.03E+00	8.50E+01	8.83E+01	8.87E+01	9.03E+01	9.13E+01	9.24E+01	9.38E+01	9.43E+01	1.02E+02
Bchiol.sec	4.71E+01	6.81E+01	1.25E-01	6.81E+01	1.00E+00	1.00E+00	4.71E+01	6.80E+01	6.80E+01	6.81E+01	6.81E+01	6.81E+01	6.82E+01	6.82E+01	7.93E+01
AI	2.44E+00	3.35E+00	4.37E-03	3.35E+00	1.00E+00	1.00E+00	2.44E+00	3.35E+00	3.35E+00	3.35E+00	3.35E+00	3.35E+00	3.35E+00	3.35E+00	3.54E+00
St.stem	2.60E-02	2.43E-02	1.03E-03	2.42E-02	1.04E+00	1.09E+00	2.01E-02	2.23E-02	2.26E-02	2.36E-02	2.43E-02	2.50E-02	2.60E-02	2.63E-02	2.85E-02
R.marrow	7.28E-03	8.66E-03	1.51E-04	8.66E-03	1.02E+00	1.03E+00	7.28E-03	8.39E-03	8.43E-03	8.56E-03	8.66E-03	8.76E-03	8.92E-03	8.97E-03	9.80E-03
Colon	2.87E-03	8.73E-03	1.49E-04	8.73E-03	1.02E+00	1.03E+00	2.87E-03	8.46E-03	8.50E-03	8.63E-03	8.73E-03	8.83E-03	8.98E-03	9.03E-03	1.04E-02
RC.stem	7.25E-03	8.86E-03	1.52E-04	8.86E-03	1.02E+00	1.03E+00	7.25E-03	8.57E-03	8.62E-03	8.75E-03	8.85E-03	8.96E-03	9.11E-03	9.16E-03	1.04E-02
LC.stem	7.37E-03	8.94E-03	1.44E-04	8.93E-03	1.02E+00	1.03E+00	7.37E-03	8.67E-03	8.71E-03	8.83E-03	8.93E-03	9.03E-03	9.18E-03	9.23E-03	1.06E-02
RS.stem	6.38E-03	8.07E-03	1.56E-04	8.07E-03	1.02E+00	1.04E+00	6.38E-03	7.79E-03	7.83E-03	7.96E-03	8.07E-03	8.18E-03	8.34E-03	8.39E-03	9.77E-03
Liver	8.24E-03	2.52E-02	4.60E-04	2.52E-02	1.02E+00	1.04E+00	8.24E-03	2.44E-02	2.45E-02	2.49E-02	2.52E-03	2.55E-02	2.60E-02	2.61E-02	2.74E-02
Kidneys	8.27E-02	1.01E-01	1.87E-03	1.01E-01	1.02E+00	1.04E+00	8.27E-02	9.79E-02	9.84E-02	9.99E-02	1.01E-01	1.02E-01	1.04E-01	1.05E-01	1.11E-01
Endost.BS	1.88E-02	2.11E-02	3.90E-04	2.11E-02	1.02E+00	1.04E+00	1.88E-02	2.04E-02	2.05E-02	2.08E-02	2.11E-02	2.14E-02	2.18E-02	2.19E-02	2.28E-02
Brain	1.70E-03	4.48E-03	8.98E-05	4.48E-03	1.02E+00	1.04E+00	1.70E-03	4.32E-03	4.35E-03	4.42E-03	4.48E-03	4.54E-03	4.64E-03	4.67E-03	4.94E-03
Ht.wall	6.70E-03	7.92E-03	1.09E-04	7.92E-03	1.01E+00	1.03E+00	6.70E-03	7.73E-03	7.76E-03	7.85E-03	7.92E-03	8.00E-03	8.11E-03	8.15E-03	9.00E-03

SD: Standard deviation; GM: Geometric mean; GSD: Geometric standard deviation; UF: Uncertainty factor; Min: minimum value; X2.5: 2.5th percentile; X5.0: 5th percentile; X25: 25th percentile; X50: 50th percentile; X75: 75th percentile; X95: 95th percentile; X97.5: 97.5th percentile; Max: maximum value; Undisturbed: Reference dose value for the exposure scenario.

Appendix C: This subsection presents a statistical summary of the results from the sensitivity of organ and tissue doses to activity parameters following inhalation of radon progeny by underground miners performing both Job 1 and Job 4.

Table C1: Sensitivity of organ and tissue committed equivalent dose coefficients (mSv/ (mJh/m^3)) to breathing frequency of the HRTM model for inhalation of radon progeny by miners performing Job 1.

Organ	Undisturbed	Mean	SD	GM	GSD	UF	Min	X2.5	X5.0	X25	X50	X75	X95	X97.5	Max
Lung	1.87E+01	3.20E+01	6.66E+00	3.13E+01	1.24E+00	1.43E+00	1.87E+01	2.11E+01	2.17E+01	2.63E+01	3.20E+01	3.78E+01	4.24E+01	4.30E+01	4.39E+01
Bronch.bas	2.72E+01	2.15E+01	4.39E+00	2.10E+01	1.23E+00	1.42E+00	1.35E+01	1.43E+01	1.46E+01	1.77E+01	2.15E+01	2.52E+01	2.83E+01	2.87E+01	2.94E+01
Bronch.sec	5.86E+01	5.25E+01	1.07E+01	5.14E+01	1.23E+00	1.42E+00	3.31E+01	3.49E+01	3.58E+01	4.32E+01	5.24E+01	6.17E+01	6.91E+01	7.00E+01	7.19E+01
Bchiol.sec	3.77E+01	5.64E+01	1.18E+01	5.51E+01	1.24E+00	1.43E+00	3.56E+01	3.69E+01	3.79E+01	4.61E+01	5.63E+01	6.66E+01	7.48E+01	7.59E+01	7.72E+01
AI	2.00E+00	2.78E+00	5.87E-01	2.71E+00	1.24E+00	1.44E+00	1.75E+00	1.81E+00	1.86E+00	2.27E+00	2.77E+00	3.28E+00	3.69E+00	3.74E+00	3.80E+00
St.stem	1.94E-02	1.56E-02	3.24E-03	1.52E-02	1.24E+00	1.43E+00	9.81E-03	1.02E-02	1.05E-02	1.27E-02	1.55E-02	1.84E-02	2.06E-02	2.09E-02	2.13E-02
R.marrow	7.56E-03	7.81E-03	1.64E-03	7.63E-03	1.24E+00	1.43E+00	4.93E-03	5.11E-03	5.25E-03	6.38E-03	7.80E-03	9.23E-03	1.04E-02	1.05E-02	1.07E-02
Colon	3.04E-03	9.34E-03	1.96E-03	9.12E-03	1.24E+00	1.43E+00	3.04E-03	6.11E-03	6.28E-03	7.63E-03	9.33E-03	1.10E-02	1.24E-02	1.26E-02	1.28E-02
RC.stem	9.96E-03	9.39E-03	1.97E-03	9.17E-03	1.24E+00	1.43E+00	5.92E-03	6.15E-03	6.32E-03	7.68E-03	9.38E-03	1.11E-02	1.25E-02	1.26E-02	1.29E-02
LC.stem	1.00E-02	9.44E-03	1.98E-03	9.22E-03	1.24E+00	1.43E+00	5.96E-03	6.18E-03	6.35E-03	7.72E-03	9.43E-03	1.12E-02	1.25E-02	1.27E-02	1.29E-02
RS.stem	9.47E-03	9.02E-03	1.90E-03	8.82E-03	1.24E+00	1.43E+00	5.69E-03	5.90E-03	6.07E-03	7.38E-03	9.02E-03	1.07E-02	1.20E-02	1.21E-02	1.24E-02
Liver	6.32E-03	1.69E-02	3.56E-03	1.66E-02	1.24E+00	1.43E+00	6.32E-03	1.11E-02	1.14E-02	1.39E-02	1.69E-02	2.00E-02	2.25E-02	2.28E-02	2.32E-02
Kidneys	2.45E-02	5.11E-02	1.07E-02	5.00E-02	1.24E+00	1.43E+00	2.45E-02	3.35E-02	3.44E-02	4.18E-02	5.11E-02	6.04E-02	6.79E-02	6.88E-02	7.00E-02
Endost.BS	8.74E-03	1.24E-02	2.61E-03	1.21E-02	1.24E+00	1.43E+00	7.84E-03	8.13E-03	8.35E-03	1.02E-02	1.24E-02	1.47E-02	1.65E-02	1.67E-02	1.70E-02
Brain	1.21E-03	2.95E-03	6.19E-04	2.88E-03	1.24E+00	1.43E+00	1.21E-03	1.93E-03	1.99E-03	2.41E-03	2.95E-03	3.49E-03	3.92E-03	3.97E-03	4.04E-03
Ht.wall	7.20E-03	7.26E-03	1.53E-03	7.10E-03	1.24E+00	1.43E+00	4.58E-03	4.75E-03	4.88E-03	5.94E-03	7.26E-03	8.58E-03	9.64E-03	9.77E-03	9.94E-03

SD: Standard deviation; GM: Geometric mean; GSD: Geometric standard deviation; UF: Uncertainty factor; Min: minimum value; X2.5: 2.5th percentile; X5.0: 5th percentile; X25: 25th percentile; X50: 50th percentile; X75: 75th percentile; X95: 95th percentile; X97.5: 97.5th percentile; Max: maximum value; Undisturbed: Reference dose value for the exposure scenario.

Table C2: Sensitivity of organ and tissue committed equivalent dose coefficients (mSv/ (mJh/m³)) to breathing frequency of the HRTM for inhalation of radon progeny by miners performing Job 4.

Organ	Undisturbed	Mean	SD	GM	GSD	UF	Min	X2.5	X5.0	X25	X50	X75	X95	X97.5	Max
Lung	2.33E+01	4.33E+01	9.09E+00	4.23E+01	1.24E+00	1.44E+00	2.33E+01	2.82E+01	2.90E+01	3.55E+01	4.33E+01	5.12E+01	5.74E+01	5.82E+01	5.91E+01
Bronch.bas	4.22E+01	3.62E+01	7.58E+00	3.54E+01	1.24E+00	1.43E+00	2.28E+01	2.36E+01	2.43E+01	2.97E+01	3.62E+01	4.28E+01	4.80E+01	4.86E+01	4.94E+01
Bronch.sec	8.67E+01	8.73E+01	1.83E+01	8.53E+01	1.24E+00	1.43E+00	5.50E+01	5.70E+01	5.86E+01	7.16E+01	8.74E+01	1.03E+02	1.16E+02	1.17E+02	1.19E+02
Bchiol.sec	4.71E+01	6.49E+01	1.37E+01	6.35E+01	1.24E+00	1.44E+00	4.09E+01	4.23E+01	4.35E+01	5.32E+01	6.50E+01	7.68E+01	8.61E+01	8.74E+01	8.86E+01
AI	2.46E+00	3.20E+00	6.75E-01	3.13E+00	1.24E+00	1.44E+00	2.02E+00	2.08E+00	2.14E+00	2.62E+00	3.21E+00	3.79E+00	4.25E+00	4.31E+00	4.37E+00
St.stem	3.21E-02	2.68E-02	5.63E-03	2.62E-02	1.24E+00	1.44E+00	1.69E-02	1.74E-02	1.79E-02	2.19E-02	2.68E-02	3.16E-02	3.55E-02	3.60E-02	3.65E-02
R.marrow	1.05E-02	1.03E-02	2.16E-03	1.00E-02	1.24E+00	1.44E+00	6.46E-03	6.68E-03	6.87E-03	8.40E-03	1.03E-02	1.21E-02	1.36E-02	1.38E-02	1.40E-02
Colon	3.79E-03	1.24E-02	2.60E-03	1.21E-02	1.24E+00	1.44E+00	3.79E-03	8.06E-03	8.28E-03	1.01E-02	1.24E-02	1.46E-02	1.64E-02	1.67E-02	1.69E-02
RC.stem	1.40E-02	1.25E-02	2.63E-03	1.22E-02	1.24E+00	1.44E+00	7.86E-03	8.13E-03	8.36E-03	1.02E-02	1.25E-02	1.48E-02	1.66E-02	1.68E-02	1.70E-02
LC.stem	1.41E-02	1.26E-02	2.65E-03	1.23E-02	1.24E+00	1.44E+00	7.92E-03	8.19E-03	8.42E-03	1.03E-02	1.26E-02	1.49E-02	1.67E-02	1.69E-02	1.72E-02
RS.stem	1.31E-02	1.18E-02	2.47E-03	1.15E-02	1.24E+00	1.44E+00	7.40E-03	7.65E-03	7.87E-03	9.62E-03	1.18E-02	1.39E-02	1.56E-02	1.58E-02	1.60E-02
Liver	7.90E-03	2.21E-02	4.64E-03	2.16E-02	1.24E+00	1.44E+00	7.90E-03	1.44E-02	1.48E-02	1.81E-02	2.21E-02	2.61E-02	2.93E-02	2.97E-02	3.01E-02
Kidneys	3.31E-02	6.59E-02	1.39E-02	6.43E-02	1.24E+00	1.44E+00	3.31E-02	4.29E-02	4.41E-02	5.39E-02	6.59E-02	7.79E-02	8.74E-02	8.86E-02	8.99E-02
Endost.BS	1.22E-02	1.64E-02	3.45E-03	1.60E-02	1.24E+00	1.44E+00	1.03E-02	1.07E-02	1.10E-02	1.34E-02	1.64E-02	1.94E-02	2.18E-02	2.21E-02	2.24E-02
Brain	1.64E-03	4.12E-03	8.67E-04	4.03E-03	1.24E+00	1.44E+00	1.64E-03	2.68E-03	2.76E-03	3.37E-03	4.12E-03	4.87E-03	5.47E-03	5.54E-03	5.62E-03
Ht.wall	1.00E-02	9.54E-03	2.01E-03	9.32E-03	1.24E+00	1.44E+00	6.01E-03	6.21E-03	6.39E-03	7.81E-03	9.55E-03	1.13E-02	1.27E-02	1.28E-02	1.30E-02

SD: Standard deviation; GM: Geometric mean; GSD: Geometric standard deviation; UF: Uncertainty factor; Min: minimum value; X2.5: 2.5th percentile; X5.0: 5th percentile; X25: 25th percentile; X50: 50th percentile; X75: 75th percentile; X95: 95th percentile; X97.5: 97.5th percentile; Max: maximum value; Undisturbed: Reference dose value for the exposure scenario.

Table C3: Sensitivity of organ and tissue committed equivalent dose coefficients (mSv/ (mJh/m³)) to fraction of air breathed through nose of the HRTM for inhalation of radon progeny by miners performing Job 1.

Organ	Undisturbed	Mean	SD	GM	GSD	UF	Min	X2.5	X5.0	X25	X50	X75	X95	X97.5	Max
Lung	1.87E+01	3.49E+01	8.38E-01	3.49E+01	1.02E+00	1.04E+00	1.87E+01	3.37E+01	3.38E+01	3.42E+01	3.48E+01	3.55E+01	3.64E+01	3.66E+01	3.73E+01
Bronch.bas	2.72E+01	2.40E+01	9.73E-01	2.40E+01	1.04E+00	1.07E+00	2.24E+01	2.26E+01	2.27E+01	2.32E+01	2.38E+01	2.47E+01	2.58E+01	2.60E+01	2.72E+01
Bronch.sec	5.86E+01	5.87E+01	2.45E+00	5.87E+01	1.04E+00	1.08E+00	5.48E+01	5.52E+01	5.54E+01	5.66E+01	5.84E+01	6.05E+01	6.32E+01	6.39E+01	6.59E+01
Bchiol.sec	3.77E+01	6.03E+01	7.71E-01	6.03E+01	1.01E+00	1.02E+00	3.77E+01	5.93E+01	5.93E+01	5.97E+01	6.02E+01	6.09E+01	6.17E+01	6.19E+01	6.24E+01
AI	2.00E+00	2.96E+00	2.96E-02	2.96E+00	1.01E+00	1.02E+00	2.00E+00	2.92E+00	2.92E+00	2.94E+00	2.96E+00	2.98E+00	3.01E+00	3.02E+00	3.04E+00
St.stem	1.94E-02	1.56E-02	4.90E-04	1.56E-02	1.03E+00	1.06E+00	1.44E-02	1.46E-02	1.47E-02	1.52E-02	1.56E-02	1.60E-02	1.63E-02	1.63E-02	1.94E-02
R.marrow	7.56E-03	8.20E-03	6.78E-06	8.20E-03	1.00E+00	1.00E+00	7.56E-03	8.19E-03	8.20E-03	8.20E-03	8.20E-03	8.21E-03	8.21E-03	8.22E-03	8.23E-03
Colon	3.04E-03	9.81E-03	3.14E-05	9.81E-03	1.01E+00	1.00E+00	3.04E-03	9.80E-03	9.80E-03	9.80E-03	9.81E-03	9.81E-03	9.82E-03	9.83E-03	9.85E-03
RC.stem	9.96E-03	9.86E-03	8.05E-06	9.86E-03	1.00E+00	1.00E+00	9.84E-03	9.85E-03	9.85E-03	9.85E-03	9.86E-03	9.86E-03	9.87E-03	9.88E-03	9.96E-03
LC.stem	1.00E-02	9.91E-03	8.31E-06	9.91E-03	1.00E+00	1.00E+00	9.89E-03	9.90E-03	9.90E-03	9.90E-03	9.91E-03	9.92E-03	9.92E-03	9.93E-03	1.00E-02
RS.stem	9.47E-03	9.51E-03	2.10E-05	9.51E-03	1.00E+00	1.00E+00	9.47E-03	9.48E-03	9.48E-03	9.49E-03	9.50E-03	9.52E-03	9.55E-03	9.55E-03	9.59E-03
Liver	6.32E-03	1.78E-02	6.27E-05	1.78E-02	1.01E+00	1.00E+00	6.32E-03	1.78E-02	1.78E-02	1.78E-02	1.78E-02	1.79E-02	1.79E-02	1.79E-02	1.80E-02
Kidneys	2.45E-02	5.40E-02	2.14E-04	5.40E-02	1.00E+00	1.01E+00	2.45E-02	5.37E-02	5.37E-02	5.38E-02	5.39E-02	5.41E-02	5.43E-02	5.43E-02	5.46E-02
Endost.BS	8.74E-03	1.30E-02	2.76E-05	1.30E-02	1.00E+00	1.00E+00	8.74E-03	1.30E-02	1.30E-02	1.30E-02	1.30E-02	1.30E-02	1.30E-02	1.31E-02	1.31E-02
Brain	1.21E-03	3.06E-03	3.01E-05	3.06E-03	1.01E+00	1.02E+00	1.21E-03	3.00E-03	3.00E-03	3.03E-03	3.06E-03	3.08E-03	3.10E-03	3.10E-03	3.10E-03
Ht.wall	7.20E-03	7.64E-03	1.09E-05	7.64E-03	1.00E+00	1.00E+00	7.20E-03	7.63E-03	7.63E-03	7.63E-03	7.64E-03	7.65E-03	7.66E-03	7.67E-03	7.69E-03

SD: Standard deviation; GM: Geometric mean; GSD: Geometric standard deviation; UF: Uncertainty factor; Min: minimum value; X2.5: 2.5th percentile; X5.0: 5th percentile; X25: 25th percentile; X50: 50th percentile; X75: 75th percentile; X95: 95th percentile; X97.5: 97.5th percentile; Max: maximum value; Undisturbed: Reference dose value for the exposure scenario.

Table C4: Sensitivity of organ and tissue committed equivalent dose coefficients (mSv/ (mJh/m³)) to fraction of air breathed through nose of the HRTM for inhalation of radon progeny by miners performing Job 4.

Organ	Undisturbed	Mean	SD	GM	GSD	UF	Min	X2.5	X5.0	X25	X50	X75	X95	X97.5	Max
Lung	2.33E+01	5.38E+01	5.87E+00	5.35E+01	1.11E+00	1.20E+00	2.33E+01	4.58E+01	4.61E+01	4.88E+01	5.28E+01	5.80E+01	6.48E+01	6.64E+01	7.00E+01
Bronch.bas	4.22E+01	4.98E+01	8.32E+00	4.92E+01	1.18E+00	1.33E+00	3.79E+01	3.85E+01	3.89E+01	4.28E+01	4.85E+01	5.58E+01	6.54E+01	6.77E+01	7.28E+01
Bronch.sec	8.67E+01	1.20E+02	2.01E+01	1.19E+02	1.18E+00	1.33E+00	8.67E+01	9.27E+01	9.38E+01	1.03E+02	1.17E+02	1.34E+02	1.58E+02	1.63E+02	1.76E+02
Bchiol.sec	4.71E+01	7.28E+01	3.27E+00	7.27E+01	1.05E+00	1.08E+00	4.71E+01	6.83E+01	6.85E+01	7.00E+01	7.23E+01	7.51E+01	7.89E+01	7.98E+01	8.18E+01
AI	2.46E+00	3.57E+00	1.42E-01	3.56E+00	1.04E+00	1.07E+00	2.46E+00	3.37E+00	3.38E+00	3.45E+00	3.54E+00	3.67E+00	3.83E+00	3.87E+00	3.95E+00
St.stem	3.21E-02	2.71E-02	6.47E-04	2.71E-02	1.02E+00	1.04E+00	2.55E-02	2.58E-02	2.59E-02	2.66E-02	2.72E-02	2.77E-02	2.80E-02	2.80E-02	3.21E-02
R.marrow	1.05E-02	1.11E-02	2.60E-04	1.11E-02	1.02E+00	1.04E+00	1.05E-02	1.08E-02	1.08E-02	1.09E-02	1.11E-02	1.13E-02	1.16E-02	1.17E-02	1.19E-02
Colon	3.79E-03	1.34E-02	3.16E-04	1.34E-02	1.02E+00	1.04E+00	3.79E-03	1.30E-02	1.30E-02	1.32E-02	1.34E-02	1.36E-02	1.40E-02	1.41E-02	1.44E-02
RC.stem	1.40E-02	1.35E-02	3.06E-04	1.35E-02	1.02E+00	1.04E+00	1.31E-02	1.31E-02	1.31E-02	1.33E-02	1.35E-02	1.37E-02	1.41E-02	1.42E-02	1.45E-02
LC.stem	1.41E-02	1.36E-02	3.05E-04	1.36E-02	1.02E+00	1.04E+00	1.32E-02	1.32E-02	1.32E-02	1.34E-02	1.36E-02	1.38E-02	1.42E-02	1.43E-02	1.46E-02
RS.stem	1.31E-02	1.28E-02	3.44E-04	1.28E-02	1.03E+00	1.05E+00	1.23E-02	1.23E-02	1.24E-02	1.25E-02	1.28E-02	1.31E-02	1.35E-02	1.36E-02	1.38E-02
Liver	7.90E-03	2.40E-02	6.29E-04	2.40E-02	1.03E+00	1.05E+00	7.90E-03	2.32E-02	2.32E-02	2.35E-02	2.39E-02	2.45E-02	2.52E-02	2.54E-02	2.58E-02
Kidneys	3.31E-02	7.20E-02	2.03E-03	7.19E-02	1.03E+00	1.05E+00	3.31E-02	6.92E-02	6.93E-02	7.02E-02	7.16E-02	7.34E-02	7.58E-02	7.63E-02	7.76E-02
Endost.BS	1.22E-02	1.77E-02	3.45E-04	1.77E-02	1.02E+00	1.03E+00	1.22E-02	1.72E-02	1.72E-02	1.74E-02	1.76E-02	1.79E-02	1.83E-02	1.84E-02	1.87E-02
Brain	1.64E-03	4.36E-03	3.02E-05	4.36E-03	1.01E+00	1.01E+00	1.64E-03	4.32E-03	4.32E-03	4.34E-03	4.35E-03	4.38E-03	4.41E-03	4.42E-03	4.47E-03
Ht.wall	1.00E-02	1.04E-02	2.68E-04	1.04E-02	1.03E+00	1.05E+00	1.00E-02	1.00E-02	1.00E-02	1.02E-02	1.03E-02	1.06E-02	1.09E-02	1.10E-02	1.11E-02

SD: Standard deviation; GM: Geometric mean; GSD: Geometric standard deviation; UF: Uncertainty factor; Min: minimum value; X2.5: 2.5th percentile; X5.0: 5th percentile; X25: 25th percentile; X50: 50th percentile; X75: 75th percentile; X95: 95th percentile; X97.5: 97.5th percentile; Max: maximum value; Undisturbed: Reference dose value for the exposure scenario.

Table C5: Sensitivity of organ and tissue committed equivalent dose coefficients (mSv/ (mJh/m³)) to tidal volume of the HRTM for inhalation of radon progeny by miners performing Job 1.

Organ	Undisturbed	Mean	SD	GM	GSD	UF	Min	X2.5	X5.0	X25	X50	X75	X95	X97.5	Max
Lung	1.87E+01	4.35E+01	1.50E+01	4.07E+01	1.46E+00	1.89E+00	1.77E+01	1.92E+01	2.05E+01	3.04E+01	4.33E+01	5.64E+01	6.71E+01	6.86E+01	7.03E+01
Bronch.bas	2.72E+01	2.86E+01	9.35E+00	2.69E+01	1.43E+00	1.82E+00	1.22E+01	1.33E+01	1.41E+01	2.04E+01	2.85E+01	3.66E+01	4.32E+01	4.41E+01	4.53E+01
Bronch.sec	5.86E+01	6.97E+01	2.28E+01	6.57E+01	1.43E+00	1.82E+00	2.99E+01	3.26E+01	3.45E+01	4.99E+01	6.96E+01	8.93E+01	1.05E+02	1.08E+02	1.11E+02
Bchiol.sec	3.77E+01	7.68E+01	2.66E+01	7.18E+01	1.46E+00	1.90E+00	3.12E+01	3.36E+01	3.59E+01	5.37E+01	7.66E+01	9.98E+01	1.19E+02	1.21E+02	1.24E+02
AI	2.00E+00	4.60E+00	2.35E+00	3.92E+00	1.82E+00	2.77E+00	1.01E+00	1.15E+00	1.28E+00	2.50E+00	4.38E+00	6.58E+00	8.52E+00	8.79E+00	9.08E+00
St.stem	1.94E-02	2.24E-02	8.92E-03	2.05E-02	1.55E+00	2.10E+00	7.88E-03	8.60E-03	9.24E-03	1.46E-02	2.20E-02	3.01E-02	3.69E-02	3.78E-02	3.89E-02
R.marrow	7.56E-03	1.21E-02	5.59E-03	1.07E-02	1.69E+00	2.43E+00	3.37E-03	3.74E-03	4.09E-03	7.16E-03	1.17E-02	1.69E-02	2.14E-02	2.20E-02	2.27E-02
Colon	3.04E-03	1.45E-02	6.63E-03	1.28E-02	1.69E+00	2.41E+00	3.04E-03	4.50E-03	4.91E-03	8.56E-03	1.40E-02	2.01E-02	2.54E-02	2.62E-02	2.70E-02
RC.stem	9.96E-03	1.45E-02	6.65E-03	1.29E-02	1.68E+00	2.41E+00	4.08E-03	4.53E-03	4.95E-03	8.61E-03	1.41E-02	2.02E-02	2.55E-02	2.63E-02	2.71E-02
LC.stem	1.00E-02	1.46E-02	6.69E-03	1.29E-02	1.68E+00	2.41E+00	4.11E-03	4.56E-03	4.98E-03	8.66E-03	1.41E-02	2.03E-02	2.57E-02	2.64E-02	2.72E-02
RS.stem	9.47E-03	1.40E-02	6.49E-03	1.24E-02	1.69E+00	2.43E+00	3.88E-03	4.31E-03	4.71E-03	8.27E-03	1.36E-02	1.95E-02	2.48E-02	2.55E-02	2.63E-02
Liver	6.32E-03	2.64E-02	1.22E-02	2.33E-02	1.69E+00	2.43E+00	6.32E-03	8.09E-03	8.85E-03	1.55E-02	2.55E-02	3.67E-02	4.65E-02	4.78E-02	4.93E-02
Kidneys	2.45E-02	7.98E-02	3.70E-02	7.03E-02	1.70E+00	2.44E+00	2.19E-02	2.43E-02	2.66E-02	4.68E-02	7.70E-02	1.11E-01	1.41E-01	1.45E-01	1.49E-01
Endost.BS	8.74E-03	1.93E-02	8.89E-03	1.70E-02	1.69E+00	2.43E+00	5.36E-03	5.95E-03	6.51E-03	1.14E-02	1.86E-02	2.68E-02	3.40E-02	3.50E-02	3.60E-02
Brain	1.21E-03	4.52E-03	2.03E-03	4.02E-03	1.66E+00	2.36E+00	1.21E-03	1.46E-03	1.59E-03	2.72E-03	4.38E-03	6.25E-03	7.87E-03	8.09E-03	8.33E-03
Ht.wall	7.20E-03	1.13E-02	5.20E-03	9.96E-03	1.69E+00	2.43E+00	3.13E-03	3.48E-03	3.80E-03	6.66E-03	1.09E-02	1.57E-02	1.99E-02	2.05E-02	2.11E-02

SD: Standard deviation; GM: Geometric mean; GSD: Geometric standard deviation; UF: Uncertainty factor; Min: minimum value; X2.5: 2.5th percentile; X5.0: 5th percentile; X25: 25th percentile; X50: 50th percentile; X75: 75th percentile; X95: 95th percentile; X97.5: 97.5th percentile; Max: maximum value; Undisturbed: Reference dose value for the exposure scenario.

Table C6: Sensitivity of organ and tissue committed equivalent dose coefficients (mSv/ (mJh/m³)) to tidal volume of the HRTM for inhalation of radon progeny by miners performing Job 4.

Organ	Undisturbed	Mean	SD	GM	GSD	UF	Min	X2.5	X5.0	X25	X50	X75	X95	X97.5	Max
Lung	2.33E+01	5.81E+01	1.94E+01	5.46E+01	1.44E+00	1.84E+00	2.33E+01	2.66E+01	2.82E+01	4.12E+01	5.79E+01	7.49E+01	8.87E+01	9.04E+01	9.22E+01
Bronch.bas	4.22E+01	4.79E+01	1.53E+01	4.53E+01	1.41E+00	1.79E+00	2.13E+01	2.28E+01	2.41E+01	3.46E+01	4.79E+01	6.12E+01	7.18E+01	7.31E+01	7.46E+01
Bronch.sec	8.67E+01	1.16E+02	3.69E+01	1.09E+02	1.41E+00	1.79E+00	5.13E+01	5.49E+01	5.82E+01	8.34E+01	1.15E+02	1.48E+02	1.73E+02	1.76E+02	1.80E+02
Bchiol.sec	4.71E+01	8.75E+01	2.96E+01	8.21E+01	1.45E+00	1.86E+00	3.68E+01	3.94E+01	4.20E+01	6.18E+01	8.72E+01	1.13E+02	1.34E+02	1.37E+02	1.40E+02
AI	2.46E+00	5.14E+00	2.53E+00	4.44E+00	1.77E+00	2.64E+00	1.23E+00	1.38E+00	1.53E+00	2.88E+00	4.93E+00	7.30E+00	9.35E+00	9.62E+00	9.89E+00
St.stem	3.21E-02	3.71E-02	1.35E-02	3.45E-02	1.49E+00	1.95E+00	1.46E-02	1.57E-02	1.68E-02	2.53E-02	3.67E-02	4.88E-02	5.87E-02	6.00E-02	6.13E-02
R.marrow	1.05E-02	1.53E-02	6.60E-03	1.38E-02	1.62E+00	2.26E+00	4.78E-03	5.23E-03	5.68E-03	9.46E-03	1.49E-02	2.10E-02	2.61E-02	2.68E-02	2.75E-02
Colon	3.79E-03	1.84E-02	7.88E-03	1.66E-02	1.62E+00	2.25E+00	3.79E-03	6.35E-03	6.89E-03	1.14E-02	1.79E-02	2.52E-02	3.13E-02	3.21E-02	3.29E-02
RC.stem	1.40E-02	1.86E-02	7.93E-03	1.67E-02	1.61E+00	2.24E+00	5.88E-03	6.42E-03	6.97E-03	1.15E-02	1.81E-02	2.54E-02	3.15E-02	3.23E-02	3.31E-02
LC.stem	1.41E-02	1.87E-02	7.98E-03	1.68E-02	1.61E+00	2.24E+00	5.92E-03	6.47E-03	7.02E-03	1.16E-02	1.82E-02	2.55E-02	3.17E-02	3.25E-02	3.34E-02
RS.stem	1.31E-02	1.76E-02	7.61E-03	1.58E-02	1.63E+00	2.27E+00	5.44E-03	5.96E-03	6.48E-03	1.08E-02	1.71E-02	2.41E-02	3.01E-02	3.08E-02	3.16E-02
Liver	7.90E-03	3.30E-02	1.43E-02	2.96E-02	1.63E+00	2.27E+00	7.90E-03	1.12E-02	1.22E-02	2.03E-02	3.21E-02	4.52E-02	5.64E-02	5.78E-02	5.93E-02
Kidneys	3.31E-02	9.88E-02	4.30E-02	8.85E-02	1.63E+00	2.29E+00	3.03E-02	3.32E-02	3.61E-02	6.06E-02	9.61E-02	1.36E-01	1.69E-01	1.74E-01	1.78E-01
Endost.BS	1.22E-02	2.45E-02	1.05E-02	2.20E-02	1.62E+00	2.26E+00	7.65E-03	8.37E-03	9.09E-03	1.51E-02	2.38E-02	3.35E-02	4.17E-02	4.28E-02	4.38E-02
Brain	1.64E-03	6.04E-03	2.51E-03	5.47E-03	1.59E+00	2.18E+00	1.64E-03	2.18E-03	2.36E-03	3.82E-03	5.90E-03	8.20E-03	1.01E-02	1.04E-02	1.06E-02
Ht.wall	1.00E-02	1.42E-02	6.13E-03	1.28E-02	1.62E+00	2.26E+00	4.44E-03	4.86E-03	5.28E-03	8.79E-03	1.39E-02	1.95E-02	2.43E-02	2.49E-02	2.55E-02

SD: Standard deviation; GM: Geometric mean; GSD: Geometric standard deviation; UF: Uncertainty factor; Min: minimum value; X2.5: 2.5th percentile; X5.0: 5th percentile; X25: 25th percentile; X50: 50th percentile; X75: 75th percentile; X95: 95th percentile; X97.5: 97.5th percentile; Max: maximum value; Undisturbed: Reference dose value for the exposure scenario.

Table C7: Sensitivity of organ and tissue committed equivalent dose coefficients (mSv/ (mJh/m³)) to fraction of time spent in each activity of the HRTM for inhalation of radon progeny by miners performing Job 1.

Organ	Undisturbed	Mean	SD	GM	GSD	UF	Min	X2.5	X5.0	X25	X50	X75	X95	X97.5	Max
Lung	1.87E+01	3.37E+01	2.63E+00	3.36E+01	1.08E+00	1.14E+00	1.87E+01	2.94E+01	2.96E+01	3.14E+01	3.37E+01	3.60E+01	3.78E+01	3.80E+01	3.82E+01
Bronch.bas	2.72E+01	2.25E+01	1.67E+00	2.24E+01	1.08E+00	1.13E+00	1.96E+01	1.97E+01	1.99E+01	2.10E+01	2.25E+01	2.39E+01	2.51E+01	2.52E+01	2.72E+01
Bronch.sec	5.86E+01	5.50E+01	4.05E+00	5.48E+01	1.08E+00	1.13E+00	4.79E+01	4.83E+01	4.86E+01	5.14E+01	5.50E+01	5.85E+01	6.13E+01	6.16E+01	6.20E+01
Bchiol.sec	3.77E+01	5.94E+01	4.79E+00	5.92E+01	1.08E+00	1.14E+00	3.77E+01	5.15E+01	5.19E+01	5.52E+01	5.94E+01	6.35E+01	6.69E+01	6.73E+01	6.77E+01
AI	2.00E+00	2.93E+00	2.40E-01	2.92E+00	1.09E+00	1.15E+00	2.00E+00	2.53E+00	2.55E+00	2.72E+00	2.93E+00	3.14E+00	3.30E+00	3.32E+00	3.34E+00
St.stem	1.94E-02	1.64E-02	1.29E-03	1.63E-02	1.08E+00	1.14E+00	1.41E-02	1.42E-02	1.44E-02	1.52E-02	1.64E-02	1.75E-02	1.84E-02	1.85E-02	1.94E-02
R.marrow	7.56E-03	8.23E-03	6.63E-04	8.20E-03	1.08E+00	1.14E+00	7.08E-03	7.13E-03	7.19E-03	7.65E-03	8.23E-03	8.80E-03	9.26E-03	9.32E-03	9.37E-03
Colon	3.04E-03	9.83E-03	7.92E-04	9.80E-03	1.08E+00	1.14E+00	3.04E-03	8.53E-03	8.60E-03	9.15E-03	9.84E-03	1.05E-02	1.11E-02	1.11E-02	1.12E-02
RC.stem	9.96E-03	9.89E-03	7.95E-04	9.86E-03	1.08E+00	1.14E+00	8.51E-03	8.58E-03	8.65E-03	9.20E-03	9.89E-03	1.06E-02	1.11E-02	1.12E-02	1.13E-02
LC.stem	1.00E-02	9.94E-03	8.00E-04	9.91E-03	1.08E+00	1.14E+00	8.56E-03	8.63E-03	8.70E-03	9.25E-03	9.95E-03	1.06E-02	1.12E-02	1.13E-02	1.13E-02
RS.stem	9.47E-03	9.51E-03	7.66E-04	9.48E-03	1.08E+00	1.14E+00	8.18E-03	8.25E-03	8.31E-03	8.84E-03	9.51E-03	1.02E-02	1.07E-02	1.08E-02	1.08E-02
Liver	6.32E-03	1.78E-02	1.44E-03	1.78E-02	1.08E+00	1.14E+00	6.32E-03	1.55E-02	1.56E-02	1.66E-02	1.79E-02	1.91E-02	2.01E-02	2.02E-02	2.03E-02
Kidneys	2.45E-02	5.39E-02	4.35E-03	5.37E-02	1.08E+00	1.14E+00	2.45E-02	4.67E-02	4.71E-02	5.01E-02	5.39E-02	5.76E-02	6.07E-02	6.10E-02	6.14E-02
Endost.BS	8.74E-03	1.31E-02	1.05E-03	1.30E-02	1.08E+00	1.14E+00	8.74E-03	1.14E-02	1.14E-02	1.22E-02	1.31E-02	1.40E-02	1.47E-02	1.48E-02	1.49E-02
Brain	1.21E-03	3.11E-03	2.50E-04	3.10E-03	1.08E+00	1.14E+00	1.21E-03	2.70E-03	2.72E-03	2.89E-03	3.11E-03	3.32E-03	3.50E-03	3.52E-03	3.54E-03
Ht.wall	7.20E-03	7.65E-03	6.17E-04	7.63E-03	1.08E+00	1.14E+00	6.58E-03	6.64E-03	6.69E-03	7.12E-03	7.65E-03	8.18E-03	8.61E-03	8.67E-03	8.72E-03

SD: Standard deviation; GM: Geometric mean; GSD: Geometric standard deviation; UF: Uncertainty factor; Min: minimum value; X2.5: 2.5th percentile; X5.0: 5th percentile; X25: 25th percentile; X50: 50th percentile; X75: 75th percentile; X95: 95th percentile; X97.5: 97.5th percentile; Max: maximum value; Undisturbed: Reference dose value for the exposure scenario.

Table C8: Sensitivity of organ and tissue committed equivalent dose coefficients (mSv/ (mJh/m^3) to fraction of time spent in each activity of the HRTM for inhalation of radon progeny by miners performing Job 4.

Organ	Undisturbed	Mean	SD	GM	GSD	UF	Min	X2.5	X5.0	X25	X50	X75	X95	X97.5	Max
Lung	2.33E+01	4.55E+01	3.74E+00	4.54E+01	1.09E+00	1.15E+00	2.33E+01	3.94E+01	3.97E+01	4.23E+01	4.56E+01	4.88E+01	5.14E+01	5.17E+01	5.20E+01
Bronch.bas	4.22E+01	3.81E+01	3.11E+00	3.79E+01	1.09E+00	1.14E+00	3.27E+01	3.30E+01	3.32E+01	3.54E+01	3.81E+01	4.07E+01	4.29E+01	4.32E+01	4.35E+01
Bronch.sec	8.67E+01	9.18E+01	7.49E+00	9.15E+01	1.09E+00	1.14E+00	7.88E+01	7.95E+01	8.01E+01	8.53E+01	9.18E+01	9.82E+01	1.03E+02	1.04E+02	1.05E+02
Bchiol.sec	4.71E+01	6.83E+01	5.65E+00	6.81E+01	1.09E+00	1.15E+00	4.71E+01	5.91E+01	5.95E+01	6.34E+01	6.84E+01	7.32E+01	7.71E+01	7.76E+01	7.81E+01
AI	2.46E+00	3.37E+00	2.80E-01	3.36E+00	1.09E+00	1.15E+00	2.46E+00	2.91E+00	2.94E+00	3.13E+00	3.37E+00	3.62E+00	3.81E+00	3.84E+00	3.86E+00
St.stem	3.21E-02	2.82E-02	2.32E-03	2.81E-02	1.09E+00	1.15E+00	2.41E-02	2.43E-02	2.45E-02	2.61E-02	2.82E-02	3.02E-02	3.18E-02	3.20E-02	3.22E-02
R.marrow	1.05E-02	1.08E-02	8.94E-04	1.08E-02	1.09E+00	1.15E+00	9.25E-03	9.33E-03	9.41E-03	1.00E-02	1.08E-02	1.16E-02	1.22E-02	1.23E-02	1.23E-02
Colon	3.79E-03	1.30E-02	1.08E-03	1.30E-02	1.09E+00	1.15E+00	3.79E-03	1.13E-02	1.13E-02	1.21E-02	1.30E-02	1.40E-02	1.47E-02	1.48E-02	1.49E-02
RC.stem	1.40E-02	1.31E-02	1.09E-03	1.31E-02	1.09E+00	1.15E+00	1.13E-02	1.14E-02	1.14E-02	1.22E-02	1.31E-02	1.41E-02	1.48E-02	1.49E-02	1.50E-02
LC.stem	1.41E-02	1.32E-02	1.10E-03	1.32E-02	1.09E+00	1.15E+00	1.13E-02	1.14E-02	1.15E-02	1.23E-02	1.32E-02	1.42E-02	1.49E-02	1.50E-02	1.51E-02
RS.stem	1.31E-02	1.24E-02	1.02E-03	1.23E-02	1.09E+00	1.15E+00	1.06E-02	1.07E-02	1.08E-02	1.15E-02	1.24E-02	1.33E-02	1.40E-02	1.41E-02	1.41E-02
Liver	7.90E-03	2.32E-02	1.92E-03	2.31E-02	1.09E+00	1.15E+00	7.90E-03	2.01E-02	2.02E-02	2.16E-02	2.32E-02	2.49E-02	2.62E-02	2.64E-02	2.66E-02
Kidneys	3.31E-02	6.93E-02	5.74E-03	6.91E-02	1.09E+00	1.15E+00	3.31E-02	5.99E-02	6.04E-02	6.43E-02	6.93E-02	7.43E-02	7.83E-02	7.88E-02	7.93E-02
Endost.BS	1.22E-02	1.73E-02	1.43E-03	1.72E-02	1.09E+00	1.15E+00	1.22E-02	1.49E-02	1.50E-02	1.60E-02	1.73E-02	1.85E-02	1.95E-02	1.96E-02	1.97E-02
Brain	1.64E-03	4.34E-03	3.59E-04	4.32E-03	1.09E+00	1.15E+00	1.64E-03	3.75E-03	3.78E-03	4.03E-03	4.34E-03	4.65E-03	4.90E-03	4.93E-03	4.96E-03
Ht.wall	1.00E-02	1.00E-02	8.31E-04	1.00E-02	1.09E+00	1.15E+00	8.60E-03	8.67E-03	8.75E-03	9.32E-03	1.00E-02	1.08E-02	1.13E-02	1.14E-02	1.15E-02

SD: Standard deviation; GM: Geometric mean; GSD: Geometric standard deviation; UF: Uncertainty factor; Min: minimum value; X2.5: 2.5th percentile; X5.0: 5th percentile; X25: 25th percentile; X50: 50th percentile; X75: 75th percentile; X95: 95th percentile; X97.5: 97.5th percentile; Max: maximum value; Undisturbed: Reference dose value for the exposure scenario.

Appendix D: This subsection presents a statistical summary of the results from the uncertainty analysis of organ and tissue doses following inhalation of uranium ore dust by underground miners performing both Job 1 and Job 4.

Table D1: Summary statistics of organ and tissue committed equivalent dose coefficients (mSv/ (kBqh/m^3)) from inhalation of uranium ore dust by underground miners performing Job 1.

Organ	Undisturbed	Mean	SD	GM	GSD	UF	Min	X2.5	X5.0	X25	X50	X75	X95	X97.5	Max
Lung	5.64E-01	4.17E-02	4.03E-02	2.97E-02	2.28E+00	4.97E+00	1.88E-03	6.07E-03	7.85E-03	1.67E-02	2.96E-02	5.19E-02	1.18E-01	1.50E-01	5.64E-01
Bronch.bas	5.13E-01	3.93E-02	3.50E-02	2.91E-02	2.17E+00	4.52E+00	2.28E-03	6.41E-03	8.09E-03	1.72E-02	2.92E-02	4.93E-02	1.05E-01	1.31E-01	5.13E-01
Bronch.sec	4.83E-01	3.77E-02	3.44E-02	2.75E-02	2.23E+00	4.76E+00	1.87E-03	5.67E-03	7.32E-03	1.60E-02	2.77E-02	4.74E-02	1.02E-01	1.28E-01	4.83E-01
Bchiol.sec	6.58E-01	4.88E-02	4.75E-02	3.46E-02	2.29E+00	5.05E+00	2.18E-03	6.97E-03	8.84E-03	1.94E-02	3.46E-02	6.10E-02	1.38E-01	1.78E-01	6.58E-01
AI	5.37E-01	3.77E-02	4.10E-02	2.46E-02	2.54E+00	6.15E+00	1.24E-03	3.97E-03	5.28E-03	1.28E-02	2.47E-02	4.71E-02	1.14E-01	1.50E-01	5.37E-01
St.stem	1.36E-02	9.71E-04	1.01E-03	6.54E-04	2.45E+00	5.85E+00	3.36E-05	1.09E-04	1.52E-04	3.54E-04	6.59E-04	1.21E-03	2.89E-03	3.73E-03	1.36E-02
R.marrow	2.05E-02	1.71E-03	1.37E-03	1.32E-03	2.07E+00	4.17E+00	9.89E-05	3.04E-04	3.88E-04	8.15E-04	1.34E-03	2.17E-03	4.34E-03	5.29E-03	2.05E-02
Colon	3.63E-03	2.56E-04	2.42E-04	1.84E-04	2.25E+00	4.99E+00	1.20E-05	3.69E-05	4.80E-05	1.07E-04	1.85E-04	3.21E-04	7.18E-04	9.17E-04	3.63E-03
RC.stem	3.40E-03	2.40E-04	2.24E-04	1.74E-04	2.23E+00	4.86E+00	1.16E-05	3.58E-05	4.61E-05	1.01E-04	1.75E-04	3.02E-04	6.63E-04	8.47E-04	3.40E-03
LC.stem	5.06E-03	3.58E-04	3.52E-04	2.52E-04	2.32E+00	5.23E+00	1.51E-05	4.83E-05	6.35E-05	1.41E-04	2.52E-04	4.48E-04	1.03E-03	1.32E-03	5.06E-03
RS.stem	1.24E-03	8.47E-05	6.42E-05	6.70E-05	2.00E+00	3.93E+00	6.23E-06	1.67E-05	2.08E-05	4.29E-05	6.81E-05	1.08E-04	2.06E-04	2.58E-04	1.24E-03
Liver	2.70E-02	1.97E-03	1.66E-03	1.50E-03	2.10E+00	4.27E+00	1.26E-04	3.50E-04	4.33E-04	9.21E-04	1.50E-03	2.51E-03	5.15E-03	6.38E-03	2.70E-02
Kidneys	1.63E-02	1.12E-03	8.77E-04	8.73E-04	2.06E+00	4.12E+00	7.39E-05	2.01E-04	2.59E-04	5.42E-04	8.86E-04	1.44E-03	2.77E-03	3.40E-03	1.63E-02
Endost.BS	7.17E-02	6.75E-03	5.31E-03	5.17E-03	2.10E+00	4.24E+00	4.42E-04	1.16E-03	1.44E-03	3.20E-03	5.25E-03	8.77E-03	1.70E-02	2.09E-02	7.17E-02
Brain	4.35E-03	2.26E-04	1.55E-04	1.89E-04	1.80E+00	3.23E+00	2.70E-05	5.89E-05	7.17E-05	1.27E-04	1.88E-04	2.81E-04	5.10E-04	6.15E-04	4.35E-03
Ht.wall	5.53E-02	4.66E-03	4.49E-03	3.24E-03	2.40E+00	5.54E+00	1.54E-04	5.39E-04	7.25E-04	1.82E-03	3.31E-03	5.89E-03	1.30E-02	1.65E-02	5.53E-02

SD: Standard deviation; GM: Geometric mean; GSD: Geometric standard deviation; UF: Uncertainty factor; Min: minimum value; X2.5: 2.5th percentile; X5.0: 5th percentile; X25: 25th percentile; X50: 50th percentile; X75: 75th percentile; X95: 95th percentile; X97.5: 97.5th percentile; Max: maximum value; Undisturbed: Reference dose value for the exposure scenario

Table D2: Summary statistics of organ and tissue committed equivalent dose coefficients (mSv/ (kBqh/m³)) from inhalation of uranium ore dust by underground miners performing Job 4.

Organ	Undisturbed	Mean	SD	GM	GSD	UF	Min	X2.5	X5.0	X25	X50	X75	X95	X97.5	Max
Lung	8.24E-01	6.14E-02	5.73E-02	4.41E-02	2.28E+00	4.88E+00	3.07E-03	8.84E-03	1.12E-02	2.49E-02	4.43E-02	7.82E-02	1.64E-01	2.10E-01	8.24E-01
Bronch.bas	7.37E-01	5.72E-02	4.98E-02	4.25E-02	2.18E+00	4.50E+00	3.76E-03	9.02E-03	1.14E-02	2.49E-02	4.28E-02	7.35E-02	1.50E-01	1.83E-01	7.37E-01
Bronch.sec	6.98E-01	5.52E-02	4.90E-02	4.03E-02	2.23E+00	4.72E+00	3.24E-03	8.06E-03	1.03E-02	2.33E-02	4.09E-02	7.10E-02	1.46E-01	1.79E-01	6.98E-01
Bchiol.sec	9.65E-01	7.25E-02	6.76E-02	5.18E-02	2.29E+00	4.93E+00	3.32E-03	1.02E-02	1.27E-02	2.94E-02	5.22E-02	9.24E-02	1.95E-01	2.48E-01	9.65E-01
AI	7.89E-01	5.57E-02	5.83E-02	3.67E-02	2.54E+00	5.97E+00	1.38E-03	5.84E-03	7.62E-03	1.92E-02	3.75E-02	7.08E-02	1.61E-01	2.08E-01	7.89E-01
St.stem	1.99E-02	1.43E-03	1.44E-03	9.70E-04	2.46E+00	5.59E+00	5.12E-05	1.66E-04	2.13E-04	5.27E-04	9.97E-04	1.82E-03	4.01E-03	5.18E-03	1.99E-02
R.marrow	2.94E-02	2.53E-03	1.99E-03	1.96E-03	2.06E+00	4.14E+00	1.60E-04	4.51E-04	5.76E-04	1.21E-03	1.99E-03	3.27E-03	6.26E-03	7.73E-03	2.94E-02
Colon	5.29E-03	3.77E-04	3.44E-04	2.73E-04	2.25E+00	4.79E+00	2.13E-05	5.56E-05	7.00E-05	1.57E-04	2.76E-04	4.82E-04	9.96E-04	1.28E-03	5.29E-03
RC.stem	4.94E-03	3.53E-04	3.18E-04	2.58E-04	2.23E+00	4.72E+00	2.02E-05	5.32E-05	6.70E-05	1.49E-04	2.60E-04	4.52E-04	9.27E-04	1.18E-03	4.94E-03
LC.stem	7.37E-03	5.27E-04	5.00E-04	3.73E-04	2.32E+00	5.08E+00	2.75E-05	7.16E-05	9.06E-05	2.09E-04	3.78E-04	6.74E-04	1.43E-03	1.85E-03	7.37E-03
RS.stem	1.80E-03	1.25E-04	9.16E-05	9.94E-05	1.98E+00	3.83E+00	9.66E-06	2.45E-05	3.08E-05	6.25E-05	1.01E-04	1.61E-04	2.92E-04	3.59E-04	1.80E-03
Liver	3.92E-02	2.91E-03	2.36E-03	2.23E-03	2.09E+00	4.17E+00	1.91E-04	5.14E-04	6.38E-04	1.35E-03	2.27E-03	3.70E-03	7.23E-03	8.92E-03	3.92E-02
Kidneys	2.35E-02	1.65E-03	1.25E-03	1.29E-03	2.04E+00	4.02E+00	1.25E-04	3.00E-04	3.76E-04	8.03E-04	1.32E-03	2.13E-03	3.97E-03	4.85E-03	2.35E-02
Endost.BS	1.03E-01	1.01E-02	8.02E-03	7.79E-03	2.09E+00	4.13E+00	4.25E-04	1.84E-03	2.25E-03	4.78E-03	7.93E-03	1.30E-02	2.53E-02	3.14E-02	1.03E-01
Brain	5.39E-03	3.00E-04	2.08E-04	2.48E-04	1.85E+00	3.31E+00	2.92E-05	7.43E-05	9.01E-05	1.64E-04	2.47E-04	3.78E-04	6.77E-04	8.12E-04	5.39E-03
Ht.wall	8.09E-02	6.86E-03	6.44E-03	4.78E-03	2.40E+00	5.45E+00	2.74E-04	7.92E-04	1.04E-03	2.68E-03	4.96E-03	8.83E-03	1.91E-02	2.35E-02	8.09E-02

SD: Standard deviation; GM: Geometric mean; GSD: Geometric standard deviation; UF: Uncertainty factor; Min: minimum value; X2.5: 2.5th percentile; X5.0: 5th percentile; X25: 25th percentile; X50: 50th percentile; X75: 75th percentile; X95: 95th percentile; X97.5: 97.5th percentile; Max: maximum value; Undisturbed: Reference dose value for the exposure scenario

Appendix E: This sub section presents the results for fitting a probability distribution to the posterior dataset following inhalation of uranium ore dust in underground mines under Job 4 conditions.

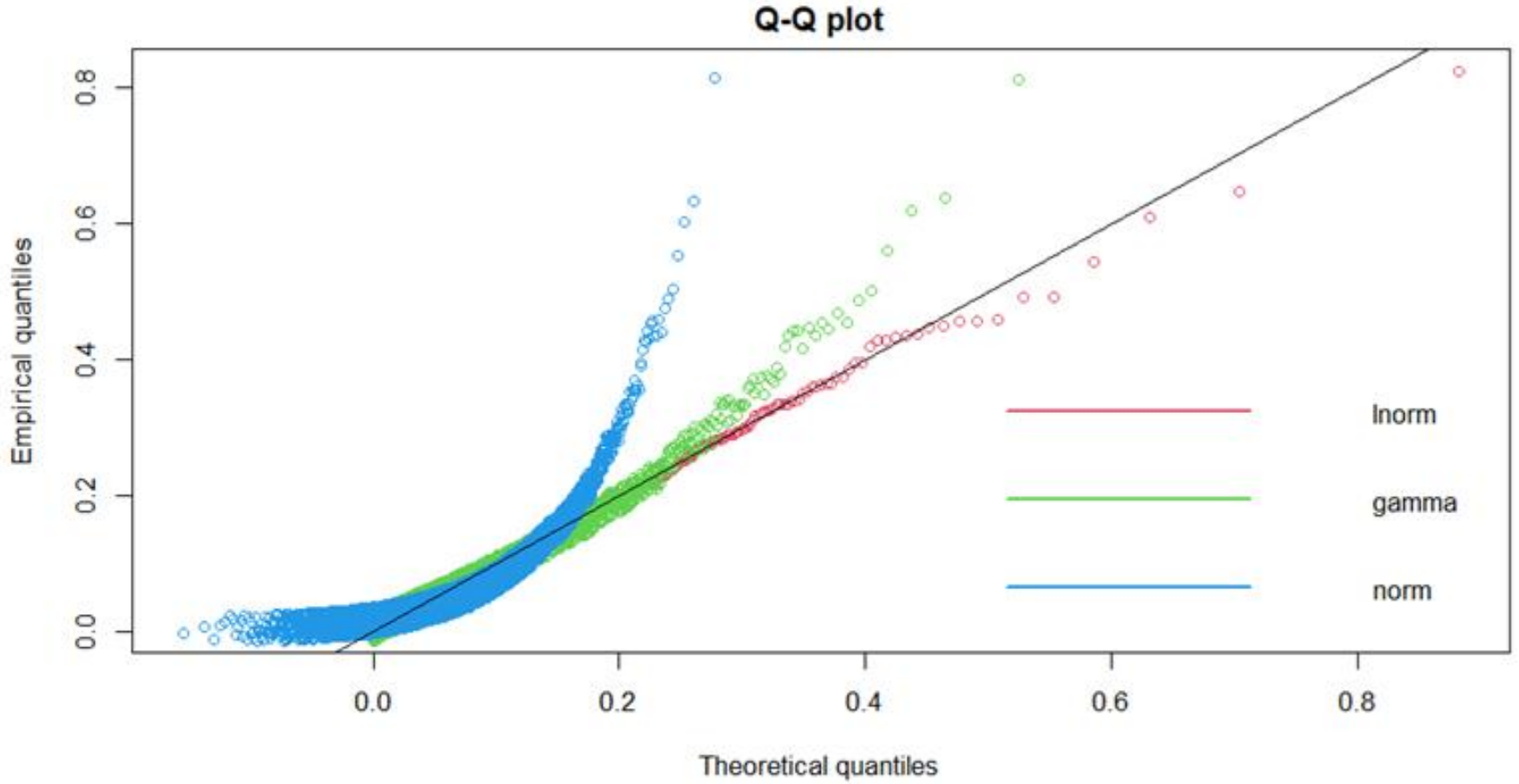

Figure E1: Fitting probability distributions using a Q-Q plot to the posterior dataset of the committed equivalent lung dose coefficient following inhalation of uranium ore dust in underground mines under Job 4 conditions.

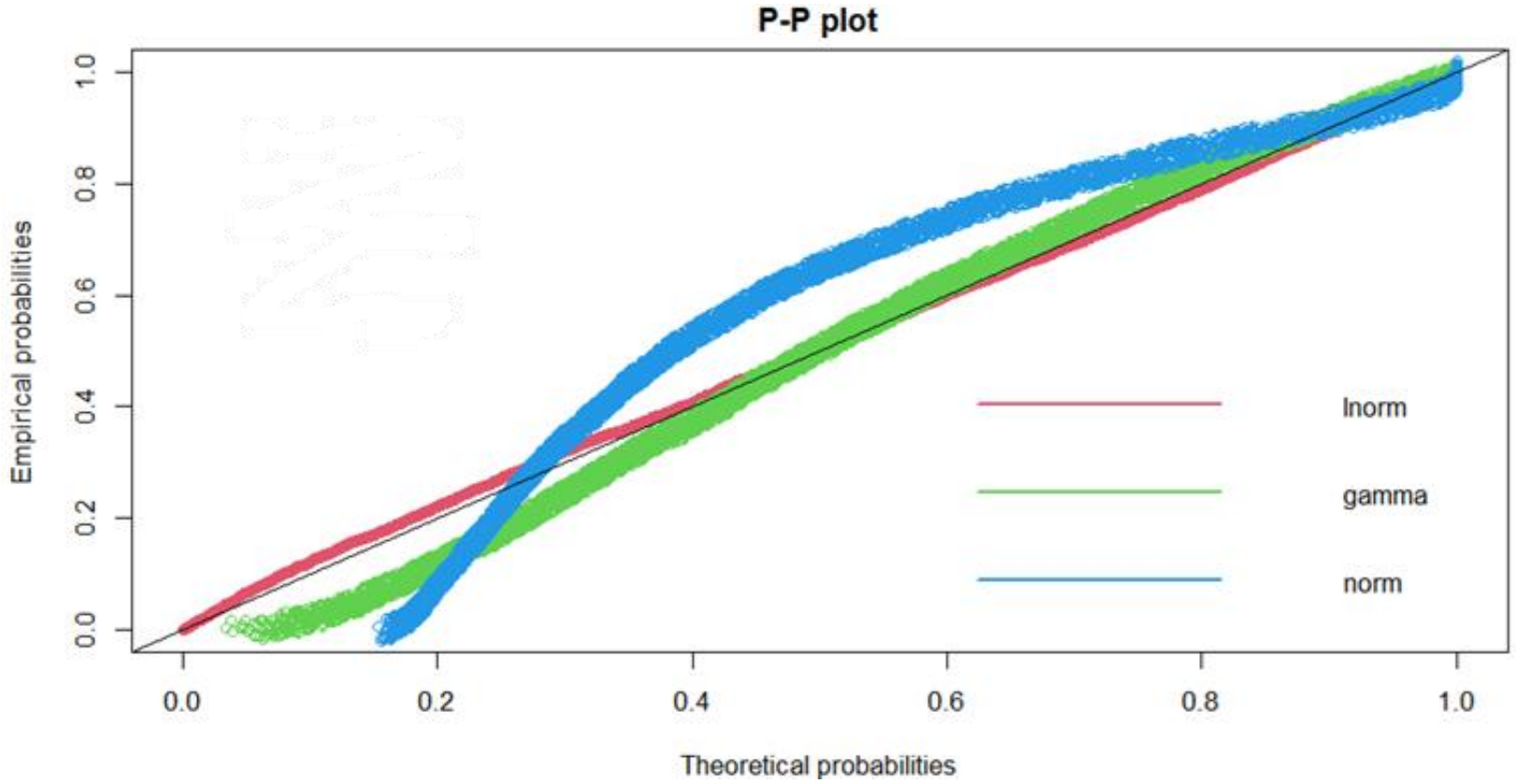

Figure E2: Fitting probability distributions using a P-P plot to the posterior dataset of the committed equivalent lung dose coefficient following inhalation of uranium ore dust in underground mines under Job 4 conditions.

Appendix F: This subsection presents a statistical summary of the results from the sensitivity of organ and tissue doses to parameter groups following inhalation of uranium ore dust by underground miners performing both Job 1 and Job 4.

Table F1: Sensitivity of organ and tissue committed equivalent dose coefficients (mSv/ (kBqh/m^3)) to particle transport parameters of the HRTM model for inhalation of uranium ore dust by underground miners performing Job 1.

Organ	Undisturbed	Mean	SD	GM	GSD	UF	Min	X2.5	X5.0	X25	X50	X75	X95	X97.5	Max
Lung	5.64E-01	2.77E-02	1.87E-02	2.34E-02	1.78E+00	3.04E+00	3.91E-03	8.07E-03	9.44E-03	1.57E-02	2.28E-02	3.46E-02	6.29E-02	7.48E-02	5.64E-01
Bronch.bas	5.13E-01	2.57E-02	1.54E-02	2.22E-02	1.72E+00	2.83E+00	3.56E-03	7.75E-03	8.87E-03	1.54E-02	2.24E-02	3.26E-02	5.31E-02	6.20E-02	5.13E-01
Bronch.sec	4.83E-01	2.47E-02	1.52E-02	2.12E-02	1.76E+00	2.96E+00	2.98E-03	6.92E-03	8.05E-03	1.45E-02	2.16E-02	3.16E-02	5.20E-02	6.08E-02	4.83E-01
Bchiol.sec	6.58E-01	3.27E-02	2.21E-02	2.75E-02	1.79E+00	3.07E+00	4.74E-03	9.41E-03	1.09E-02	1.82E-02	2.68E-02	4.09E-02	7.36E-02	8.89E-02	6.58E-01
AI	5.37E-01	2.53E-02	2.02E-02	1.98E-02	2.02E+00	3.83E+00	2.71E-03	5.26E-03	6.32E-03	1.20E-02	1.95E-02	3.27E-02	6.36E-02	7.74E-02	5.37E-01
St.stem	1.36E-02	6.50E-04	4.90E-04	5.21E-04	1.94E+00	3.64E+00	6.31E-05	1.43E-04	1.75E-04	3.32E-04	5.14E-04	8.30E-04	1.59E-03	1.90E-03	1.36E-02
R.marrow	2.05E-02	1.16E-03	5.34E-04	1.07E-03	1.49E+00	2.18E+00	2.52E-04	4.89E-04	5.51E-04	8.23E-04	1.08E-03	1.40E-03	2.06E-03	2.31E-03	2.05E-02
Colon	3.63E-03	1.72E-04	1.11E-04	1.48E-04	1.72E+00	2.87E+00	2.85E-05	5.42E-05	6.22E-05	1.02E-04	1.43E-04	2.11E-04	3.75E-04	4.48E-04	3.63E-03
RC.stem	3.40E-03	1.61E-04	1.02E-04	1.40E-04	1.70E+00	2.81E+00	2.78E-05	5.21E-05	6.00E-05	9.70E-05	1.36E-04	1.98E-04	3.46E-04	4.11E-04	3.40E-03
LC.stem	5.06E-03	2.40E-04	1.65E-04	2.01E-04	1.79E+00	3.13E+00	3.39E-05	6.71E-05	7.90E-05	1.35E-04	1.96E-04	2.99E-04	5.48E-04	6.58E-04	5.06E-03
RS.stem	1.24E-03	5.73E-05	2.46E-05	5.42E-05	1.39E+00	1.91E+00	1.92E-05	2.86E-05	3.12E-05	4.39E-05	5.45E-05	6.69E-05	9.30E-05	1.04E-04	1.24E-03
Liver	2.70E-02	1.34E-03	7.06E-04	1.22E-03	1.52E+00	2.31E+00	3.32E-04	5.66E-04	6.37E-04	9.16E-04	1.17E-03	1.59E-03	2.57E-03	3.02E-03	2.70E-02
Kidneys	1.63E-02	7.59E-04	3.45E-04	7.06E-04	1.46E+00	2.08E+00	1.99E-04	3.21E-04	3.64E-04	5.49E-04	7.26E-04	9.24E-04	1.26E-03	1.38E-03	1.63E-02
Endost.BS	7.17E-02	4.63E-03	1.97E-03	4.29E-03	1.49E+00	2.14E+00	1.15E-03	1.87E-03	2.14E-03	3.26E-03	4.40E-03	5.74E-03	7.92E-03	8.54E-03	7.17E-02
Brain	4.35E-03	1.66E-04	6.98E-05	1.60E-04	1.29E+00	1.63E+00	7.89E-05	1.02E-04	1.08E-04	1.34E-04	1.57E-04	1.88E-04	2.51E-04	2.72E-04	4.35E-03
Ht.wall	5.53E-02	3.09E-03	1.99E-03	2.56E-03	1.89E+00	3.47E+00	2.20E-04	6.49E-04	8.22E-04	1.70E-03	2.66E-03	4.06E-03	6.79E-03	7.81E-03	5.53E-02

SD: Standard deviation; GM: Geometric mean; GSD: Geometric standard deviation; UF: Uncertainty factor; Min: minimum value; X2.5: 2.5th percentile; X5.0: 5th percentile; X25: 25th percentile; X50: 50th percentile; X75: 75th percentile; X95: 95th percentile; X97.5: 97.5th percentile; Max: maximum value; Undisturbed: Reference dose value for the exposure scenario

Table F2: Sensitivity of organ and tissue committed equivalent dose coefficients (mSv/ (kBqh/m^3)) to particle transport parameters of the HRTM model for inhalation of uranium ore dust by underground miners performing Job 4.

Organ	Undisturbed	Mean	SD	GM	GSD	UF	Min	X2.5	X5.0	X25	X50	X75	X95	X97.5	Max
Lung	8.24E-01	4.08E-02	2.75E-02	3.43E-02	1.79E+00	3.06E+00	6.04E-03	1.16E-02	1.35E-02	2.27E-02	3.34E-02	5.10E-02	9.19E-02	1.09E-01	8.24E-01
Bronch.bas	7.37E-01	3.72E-02	2.26E-02	3.20E-02	1.75E+00	2.89E+00	4.76E-03	1.06E-02	1.22E-02	2.20E-02	3.26E-02	4.80E-02	7.69E-02	8.89E-02	7.37E-01
Bronch.sec	6.98E-01	3.62E-02	2.23E-02	3.08E-02	1.78E+00	3.02E+00	4.11E-03	9.61E-03	1.12E-02	2.10E-02	3.15E-02	4.69E-02	7.55E-02	8.74E-02	6.98E-01
Bchiol.sec	9.65E-01	4.82E-02	3.26E-02	4.04E-02	1.80E+00	3.05E+00	7.43E-03	1.37E-02	1.58E-02	2.62E-02	3.95E-02	6.14E-02	1.09E-01	1.28E-01	9.65E-01
AI	7.89E-01	3.75E-02	2.96E-02	2.92E-02	2.03E+00	3.80E+00	4.31E-03	7.75E-03	9.35E-03	1.73E-02	2.89E-02	4.84E-02	9.35E-02	1.12E-01	7.89E-01
St.stem	1.99E-02	9.60E-04	7.19E-04	7.68E-04	1.95E+00	3.62E+00	1.03E-04	2.10E-04	2.56E-04	4.84E-04	7.56E-04	1.22E-03	2.30E-03	2.76E-03	1.99E-02
R.marrow	2.94E-02	1.70E-03	7.82E-04	1.56E-03	1.49E+00	2.19E+00	3.38E-04	7.07E-04	8.06E-04	1.20E-03	1.57E-03	2.05E-03	3.00E-03	3.38E-03	2.94E-02
Colon	5.29E-03	2.53E-04	1.63E-04	2.17E-04	1.73E+00	2.91E+00	4.31E-05	7.70E-05	9.11E-05	1.47E-04	2.11E-04	3.14E-04	5.51E-04	6.50E-04	5.29E-03
RC.stem	4.94E-03	2.37E-04	1.49E-04	2.05E-04	1.70E+00	2.84E+00	4.19E-05	7.41E-05	8.74E-05	1.41E-04	1.99E-04	2.93E-04	5.08E-04	5.98E-04	4.94E-03
LC.stem	7.37E-03	3.53E-04	2.42E-04	2.96E-04	1.80E+00	3.14E+00	5.25E-05	9.62E-05	1.15E-04	1.95E-04	2.89E-04	4.42E-04	8.01E-04	9.50E-04	7.37E-03
RS.stem	1.80E-03	8.35E-05	3.56E-05	7.89E-05	1.39E+00	1.91E+00	2.45E-05	4.11E-05	4.53E-05	6.36E-05	7.97E-05	9.73E-05	1.35E-04	1.51E-04	1.80E-03
Liver	3.92E-02	1.95E-03	1.03E-03	1.77E-03	1.53E+00	2.30E+00	4.80E-04	8.19E-04	9.25E-04	1.31E-03	1.71E-03	2.32E-03	3.77E-03	4.32E-03	3.92E-02
Kidneys	2.35E-02	1.11E-03	5.03E-04	1.03E-03	1.47E+00	2.11E+00	2.78E-04	4.65E-04	5.25E-04	8.11E-04	1.06E-03	1.35E-03	1.85E-03	2.06E-03	2.35E-02
Endost.BS	1.03E-01	6.71E-03	2.89E-03	6.20E-03	1.50E+00	2.19E+00	1.47E-03	2.66E-03	3.06E-03	4.73E-03	6.34E-03	8.30E-03	1.17E-02	1.28E-02	1.03E-01
Brain	5.39E-03	2.14E-04	9.26E-05	2.05E-04	1.33E+00	1.74E+00	9.39E-05	1.22E-04	1.32E-04	1.66E-04	2.02E-04	2.48E-04	3.34E-04	3.69E-04	5.39E-03
Ht.wall	8.09E-02	4.58E-03	2.92E-03	3.79E-03	1.91E+00	3.43E+00	3.50E-04	9.68E-04	1.20E-03	2.53E-03	3.98E-03	6.07E-03	9.95E-03	1.14E-02	8.09E-02

SD: Standard deviation; GM: Geometric mean; GSD: Geometric standard deviation; UF: Uncertainty factor; Min: minimum value; X2.5: 2.5th percentile; X5.0: 5th percentile; X25: 25th percentile; X50: 50th percentile; X75: 75th percentile; X95: 95th percentile; X97.5: 97.5th percentile; Max: maximum value; Undisturbed: Reference dose value for the exposure scenario

Table F3: Sensitivity of organ and tissue committed equivalent dose coefficients (mSv/ (kBqh/m^3)) to absorption parameters of the HRTM deposition model for inhalation of uranium ore dust by underground miners performing Job 1.

Organ	Undisturbed	Mean	SD	GM	GSD	UF	Min	X2.5	X5.0	X25	X50	X75	X95	X97.5	Max
Lung	5.64E-01	3.15E-02	6.89E-03	3.14E-02	1.04E+00	1.02E+00	3.05E-02	3.07E-02	3.08E-02	3.12E-02	3.14E-02	3.16E-02	3.19E-02	3.20E-02	5.64E-01
Bronch.bas	5.13E-01	2.66E-02	6.29E-03	2.66E-02	1.04E+00	1.02E+00	2.58E-02	2.60E-02	2.60E-02	2.64E-02	2.66E-02	2.68E-02	2.70E-02	2.71E-02	5.13E-01
Bronch.sec	4.83E-01	2.57E-02	5.91E-03	2.56E-02	1.04E+00	1.02E+00	2.49E-02	2.50E-02	2.51E-02	2.54E-02	2.56E-02	2.58E-02	2.61E-02	2.61E-02	4.83E-01
Bchiol.sec	6.58E-01	3.77E-02	8.02E-03	3.77E-02	1.04E+00	1.02E+00	3.65E-02	3.68E-02	3.69E-02	3.74E-02	3.77E-02	3.79E-02	3.83E-02	3.84E-02	6.58E-01
AI	5.37E-01	3.05E-02	6.55E-03	3.04E-02	1.04E+00	1.02E+00	2.95E-02	2.98E-02	2.98E-02	3.02E-02	3.05E-02	3.07E-02	3.10E-02	3.10E-02	5.37E-01
St.stem	1.36E-02	7.55E-04	1.66E-04	7.53E-04	1.04E+00	1.02E+00	7.27E-04	7.35E-04	7.38E-04	7.47E-04	7.53E-04	7.59E-04	7.67E-04	7.69E-04	1.36E-02
R.marrow	2.05E-02	1.18E-03	2.50E-04	1.18E-03	1.04E+00	1.03E+00	1.11E-03	1.14E-03	1.15E-03	1.17E-03	1.18E-03	1.19E-03	1.21E-03	1.21E-03	2.05E-02
Colon	3.63E-03	1.92E-04	4.45E-05	1.92E-04	1.04E+00	1.03E+00	1.81E-04	1.86E-04	1.87E-04	1.90E-04	1.92E-04	1.94E-04	1.97E-04	1.98E-04	3.63E-03
RC.stem	3.40E-03	1.79E-04	4.16E-05	1.79E-04	1.04E+00	1.03E+00	1.68E-04	1.73E-04	1.74E-04	1.77E-04	1.79E-04	1.81E-04	1.83E-04	1.84E-04	3.40E-03
LC.stem	5.06E-03	2.73E-04	6.19E-05	2.72E-04	1.04E+00	1.03E+00	2.60E-04	2.65E-04	2.66E-04	2.69E-04	2.72E-04	2.74E-04	2.78E-04	2.79E-04	5.06E-03
RS.stem	1.24E-03	5.87E-05	1.55E-05	5.85E-05	1.06E+00	1.08E+00	5.09E-05	5.37E-05	5.44E-05	5.69E-05	5.85E-05	6.02E-05	6.23E-05	6.29E-05	1.24E-03
Liver	2.70E-02	1.45E-03	3.39E-04	1.45E-03	1.07E+00	1.11E+00	1.20E-03	1.29E-03	1.31E-03	1.39E-03	1.45E-03	1.50E-03	1.57E-03	1.59E-03	2.70E-02
Kidneys	1.63E-02	7.55E-04	2.01E-04	7.53E-04	1.05E+00	1.04E+00	6.94E-04	7.21E-04	7.26E-04	7.42E-04	7.53E-04	7.64E-04	7.78E-04	7.82E-04	1.63E-02
Endost.BS	7.17E-02	4.39E-03	8.81E-04	4.38E-03	1.05E+00	1.07E+00	3.89E-03	4.09E-03	4.14E-03	4.28E-03	4.39E-03	4.49E-03	4.61E-03	4.65E-03	7.17E-02
Brain	4.35E-03	1.68E-04	5.41E-05	1.67E-04	1.05E+00	1.04E+00	1.56E-04	1.60E-04	1.62E-04	1.65E-04	1.67E-04	1.69E-04	1.72E-04	1.73E-04	4.35E-03
Ht.wall	5.53E-02	3.09E-03	6.75E-04	3.08E-03	1.04E+00	1.02E+00	2.99E-03	3.01E-03	3.02E-03	3.06E-03	3.08E-03	3.11E-03	3.14E-03	3.14E-03	5.53E-02

SD: Standard deviation; GM: Geometric mean; GSD: Geometric standard deviation; UF: Uncertainty factor; Min: minimum value; X2.5: 2.5th percentile; X5.0: 5th percentile; X25: 25th percentile; X50: 50th percentile; X75: 75th percentile; X95: 95th percentile; X97.5: 97.5th percentile; Max: maximum value; Undisturbed: Reference dose value for the exposure scenario

Table F4: Sensitivity of organ and tissue committed equivalent dose coefficients (mSv/ (kBqh/m^3)) to absorption parameters of the HRTM model for inhalation of uranium ore dust by underground miners performing Job 4.

Organ	Undisturbed	Mean	SD	GM	GSD	UF	Min	X2.5	X5.0	X25	X50	X75	X95	X97.5	Max
Lung	8.24E-01	4.58E-02	1.01E-02	4.57E-02	1.04E+00	1.02E+00	4.43E-02	4.47E-02	4.49E-02	4.54E-02	4.57E-02	4.61E-02	4.65E-02	4.66E-02	8.24E-01
Bronch.bas	7.37E-01	3.82E-02	9.04E-03	3.81E-02	1.04E+00	1.02E+00	3.70E-02	3.72E-02	3.74E-02	3.78E-02	3.81E-02	3.84E-02	3.88E-02	3.88E-02	7.37E-01
Bronch.sec	6.98E-01	3.71E-02	8.54E-03	3.70E-02	1.04E+00	1.02E+00	3.59E-02	3.61E-02	3.63E-02	3.67E-02	3.70E-02	3.73E-02	3.76E-02	3.77E-02	6.98E-01
Bchiol.sec	9.65E-01	5.51E-02	1.18E-02	5.50E-02	1.04E+00	1.02E+00	5.32E-02	5.38E-02	5.39E-02	5.46E-02	5.50E-02	5.54E-02	5.60E-02	5.61E-02	9.65E-01
AI	7.89E-01	4.47E-02	9.62E-03	4.46E-02	1.04E+00	1.02E+00	4.32E-02	4.36E-02	4.38E-02	4.43E-02	4.46E-02	4.50E-02	4.54E-02	4.55E-02	7.89E-01
St.stem	1.99E-02	1.10E-03	2.43E-04	1.10E-03	1.04E+00	1.02E+00	1.06E-03	1.07E-03	1.08E-03	1.09E-03	1.10E-02	1.11E-03	1.12E-03	1.12E-03	1.99E-02
R.marrow	2.94E-02	1.71E-03	3.59E-04	1.70E-03	1.04E+00	1.03E+00	1.61E-03	1.65E-03	1.66E-03	1.68E-03	1.70E-03	1.72E-03	1.75E-03	1.76E-03	2.94E-02
Colon	5.29E-03	2.80E-04	6.48E-05	2.80E-04	1.04E+00	1.03E+00	2.64E-04	2.71E-04	2.72E-04	2.76E-04	2.80E-04	2.83E-04	2.87E-04	2.88E-04	5.29E-03
RC.stem	4.94E-03	2.61E-04	6.06E-05	2.60E-04	1.04E+00	1.03E+00	2.45E-04	2.52E-04	2.53E-04	2.57E-04	2.60E-04	2.63E-04	2.67E-04	2.68E-04	4.94E-03
LC.stem	7.37E-03	3.98E-04	9.02E-05	3.97E-04	1.04E+00	1.03E+00	3.78E-04	3.86E-04	3.88E-04	3.93E-04	3.97E-04	4.00E-04	4.05E-04	4.07E-04	7.37E-03
RS.stem	1.80E-03	8.50E-05	2.24E-05	8.47E-05	1.06E+00	1.08E+00	7.40E-05	7.80E-05	7.90E-05	8.23E-05	8.48E-05	8.73E-05	9.02E-05	9.11E-05	1.80E-03
Liver	3.92E-02	2.10E-03	4.93E-04	2.10E-03	1.07E+00	1.11E+00	1.73E-03	1.87E-03	1.90E-03	2.01E-03	2.10E-03	2.18E-03	2.28E-03	2.31E-03	3.92E-02
Kidneys	2.35E-02	1.10E-03	2.90E-04	1.09E-03	1.05E+00	1.04E+00	1.01E-03	1.05E-03	1.06E-03	1.08E-03	1.09E-03	1.11E-03	1.13E-03	1.14E-03	2.35E-02
Endost.BS	1.03E-01	6.37E-03	1.26E-03	6.35E-03	1.05E+00	1.06E+00	5.67E-03	5.94E-03	6.01E-03	6.21E-03	6.36E-03	6.50E-03	6.68E-03	6.73E-03	1.03E-01
Brain	5.39E-03	2.15E-04	6.70E-05	2.14E-04	1.05E+00	1.04E+00	1.99E-04	2.05E-04	2.06E-04	2.11E-04	2.14E-04	2.17E-04	2.21E-04	2.22E-04	5.39E-03
Ht.wall	8.09E-02	4.51E-03	9.87E-04	4.50E-03	1.04E+00	1.02E+00	4.36E-03	4.40E-03	4.41E-03	4.47E-03	4.50E-03	4.54E-03	4.58E-03	4.59E-03	8.09E-02

SD: Standard deviation; GM: Geometric mean; GSD: Geometric standard deviation; UF: Uncertainty factor; Min: minimum value; X2.5: 2.5th percentile; X5.0: 5th percentile; X25: 25th percentile; X50: 50th percentile; X75: 75th percentile; X95: 95th percentile; X97.5: 97.5th percentile; Max: maximum value; Undisturbed: Reference dose value for the exposure scenario

Table F5: Sensitivity of organ and tissue committed equivalent dose coefficients (mSv/ (kBqh/m^3)) to particle deposition parameters of the HRTM model for inhalation of uranium ore dust by underground miners performing Job 1.

Organ	Undisturbed	Mean	SD	GM	GSD	UF	Min	X2.5	X5.0	X25	X50	X75	X95	X97.5	Max
Lung	5.64E-01	4.03E-02	2.24E-02	3.50E-02	1.71E+00	2.80E+00	5.17E-03	1.18E-02	1.41E-02	2.42E-02	3.55E-02	5.15E-02	8.18E-02	9.28E-02	5.64E-01
Bronch.bas	5.13E-01	3.45E-02	1.87E-02	3.03E-02	1.67E+00	2.69E+00	4.91E-03	1.07E-02	1.27E-02	2.12E-02	3.05E-02	4.38E-02	6.87E-02	7.77E-02	5.13E-01
Bronch.sec	4.83E-01	3.30E-02	1.81E-02	2.89E-02	1.69E+00	2.73E+00	4.49E-03	1.01E-02	1.19E-02	2.01E-02	2.92E-02	4.21E-02	6.64E-02	7.51E-02	4.83E-01
Bchiol.sec	6.58E-01	4.82E-02	2.68E-02	4.19E-02	1.71E+00	2.81E+00	6.11E-03	1.41E-02	1.68E-02	2.89E-02	4.25E-02	6.18E-02	9.82E-02	1.12E-01	6.58E-01
AI	5.37E-01	3.88E-02	2.19E-02	3.36E-02	1.73E+00	2.87E+00	4.69E-03	1.10E-02	1.31E-02	2.30E-02	3.42E-02	4.98E-02	7.95E-02	9.04E-02	5.37E-01
St.stem	1.36E-02	9.54E-04	5.37E-04	8.27E-04	1.72E+00	2.84E+00	1.17E-04	2.74E-04	3.26E-04	5.68E-04	8.41E-04	1.22E-03	1.96E-03	2.21E-03	1.36E-02
R.marrow	2.05E-02	1.49E-03	8.26E-04	1.30E-03	1.71E+00	2.79E+00	1.89E-04	4.41E-04	5.26E-04	8.98E-04	1.32E-03	1.91E-03	3.03E-03	3.44E-03	2.05E-02
Colon	3.63E-03	2.43E-04	1.37E-04	2.11E-04	1.72E+00	2.84E+00	3.01E-05	7.00E-05	8.38E-05	1.45E-04	2.14E-04	3.12E-04	4.99E-04	5.63E-04	3.63E-03
RC.stem	3.40E-03	2.26E-04	1.27E-04	1.96E-04	1.72E+00	2.83E+00	2.81E-05	6.54E-05	7.83E-05	1.35E-04	1.99E-04	2.91E-04	4.64E-04	5.24E-04	3.40E-03
LC.stem	5.06E-03	3.45E-04	1.94E-04	2.99E-04	1.72E+00	2.84E+00	4.25E-05	9.89E-05	1.18E-04	2.05E-04	3.03E-04	4.42E-04	7.07E-04	7.98E-04	5.06E-03
RS.stem	1.24E-03	7.43E-05	4.22E-05	6.46E-05	1.71E+00	2.81E+00	9.37E-06	2.18E-05	2.61E-05	4.46E-05	6.54E-05	9.52E-05	1.51E-04	1.72E-04	1.24E-03
Liver	2.70E-02	1.84E-03	1.03E-03	1.60E-03	1.71E+00	2.82E+00	2.39E-04	5.39E-04	6.46E-04	1.10E-03	1.62E-03	2.36E-03	3.75E-03	4.29E-03	2.70E-02
Kidneys	1.63E-02	9.57E-04	5.45E-04	8.31E-04	1.71E+00	2.81E+00	1.19E-04	2.80E-04	3.34E-04	5.72E-04	8.44E-04	1.22E-03	1.95E-03	2.21E-03	1.63E-02
Endost.BS	7.17E-02	5.62E-03	3.10E-03	4.89E-03	1.71E+00	2.80E+00	6.98E-04	1.65E-03	1.98E-03	3.37E-03	4.96E-03	7.19E-03	1.15E-02	1.30E-02	7.17E-02
Brain	4.35E-03	1.93E-04	1.01E-04	1.75E-04	1.55E+00	2.33E+00	3.49E-05	7.37E-05	8.47E-05	1.29E-04	1.75E-04	2.43E-04	3.58E-04	3.99E-04	4.35E-03
Ht.wall	5.53E-02	3.91E-03	2.20E-03	3.39E-03	1.72E+00	2.84E+00	4.82E-04	1.12E-03	1.34E-03	2.33E-03	3.44E-03	5.01E-03	8.01E-03	9.07E-03	5.53E-02

SD: Standard deviation; GM: Geometric mean; GSD: Geometric standard deviation; UF: Uncertainty factor; Min: minimum value; X2.5: 2.5th percentile; X5.0: 5th percentile; X25: 25th percentile; X50: 50th percentile; X75: 75th percentile; X95: 95th percentile; X97.5: 97.5th percentile; Max: maximum value; Undisturbed: Reference dose value for the exposure scenario

Table F6: Sensitivity of organ and tissue committed equivalent dose coefficients (mSv/ (kBqh/m^3) to particle deposition parameters of the HRTM for inhalation of uranium ore dust by underground miners performing Job 4.

Organ	Undisturbed	Mean	SD	GM	GSD	UF	Min	X2.5	X5.0	X25	X50	X75	X95	X97.5	Max
Lung	8.24E-01	5.95E-02	3.24E-02	5.19E-02	1.70E+00	2.73E+00	7.11E-03	1.78E-02	2.07E-02	3.59E-02	5.31E-02	7.67E-02	1.18E-01	1.33E-01	8.24E-01
Bronch.bas	7.37E-01	5.03E-02	2.68E-02	4.43E-02	1.67E+00	2.65E+00	6.59E-03	1.57E-02	1.83E-02	3.11E-02	4.51E-02	6.44E-02	9.84E-02	1.10E-01	7.37E-01
Bronch.sec	6.98E-01	4.84E-02	2.61E-02	4.24E-02	1.69E+00	2.69E+00	6.08E-03	1.48E-02	1.72E-02	2.96E-02	4.34E-02	6.22E-02	9.53E-02	1.07E-01	6.98E-01
Bchiol.sec	9.65E-01	7.15E-02	3.90E-02	6.23E-02	1.71E+00	2.74E+00	8.54E-03	2.14E-02	2.49E-02	4.30E-02	6.38E-02	9.24E-02	1.43E-01	1.61E-01	9.65E-01
AI	7.89E-01	5.76E-02	3.19E-02	5.00E-02	1.72E+00	2.79E+00	6.47E-03	1.67E-02	1.96E-02	3.43E-02	5.13E-02	7.45E-02	1.16E-01	1.30E-01	7.89E-01
St.stem	1.99E-02	1.41E-03	7.81E-04	1.23E-03	1.72E+00	2.78E+00	1.61E-04	4.13E-04	4.83E-04	8.45E-04	1.26E-03	1.83E-03	2.84E-03	3.18E-03	1.99E-02
R.marrow	2.94E-02	2.19E-03	1.19E-03	1.91E-03	1.71E+00	2.72E+00	2.58E-04	6.57E-04	7.63E-04	1.32E-03	1.96E-03	2.83E-03	4.38E-03	4.88E-03	2.94E-02
Colon	5.29E-03	3.59E-04	1.99E-04	3.12E-04	1.72E+00	2.76E+00	4.11E-05	1.05E-04	1.23E-04	2.15E-04	3.21E-04	4.63E-04	7.21E-04	8.06E-04	5.29E-03
RC.stem	4.94E-03	3.34E-04	1.85E-04	2.91E-04	1.71E+00	2.76E+00	3.83E-05	9.81E-05	1.15E-04	2.00E-04	2.99E-04	4.31E-04	6.71E-04	7.49E-04	4.94E-03
LC.stem	7.37E-03	5.09E-04	2.82E-04	4.43E-04	1.72E+00	2.77E+00	5.82E-05	1.49E-04	1.75E-04	3.05E-04	4.55E-04	6.58E-04	1.02E-03	1.15E-03	7.37E-03
RS.stem	1.80E-03	1.09E-04	6.10E-05	9.51E-05	1.71E+00	2.74E+00	1.25E-05	3.26E-05	3.79E-05	6.57E-05	9.77E-05	1.41E-04	2.18E-04	2.44E-04	1.80E-03
Liver	3.92E-02	2.71E-03	1.50E-03	2.36E-03	1.71E+00	2.75E+00	3.09E-04	8.04E-04	9.41E-04	1.63E-03	2.43E-03	3.49E-03	5.43E-03	6.09E-03	3.92E-02
Kidneys	2.35E-02	1.41E-03	7.90E-04	1.23E-03	1.71E+00	2.74E+00	1.62E-04	4.19E-04	4.88E-04	8.47E-04	1.26E-03	1.82E-03	2.82E-03	3.15E-03	2.35E-02
Endost.BS	1.03E-01	8.26E-03	4.48E-03	7.20E-03	1.71E+00	2.74E+00	9.44E-04	2.47E-03	2.87E-03	4.98E-03	7.38E-03	1.07E-02	1.65E-02	1.86E-02	1.03E-01
Brain	5.39E-03	2.56E-04	1.34E-04	2.30E-04	1.59E+00	2.39E+00	4.74E-05	9.19E-05	1.05E-04	1.66E-04	2.33E-04	3.21E-04	4.77E-04	5.25E-04	5.39E-03
Ht.wall	8.09E-02	5.79E-03	3.19E-03	5.03E-03	1.72E+00	2.77E+00	6.64E-04	1.69E-03	1.99E-03	3.47E-03	5.16E-03	7.49E-03	1.16E-02	1.30E-02	8.09E-02

SD: Standard deviation; GM: Geometric mean; GSD: Geometric standard deviation; UF: Uncertainty factor; Min: minimum value; X2.5: 2.5th percentile; X5.0: 5th percentile; X25: 25th percentile; X50: 50th percentile; X75: 75th percentile; X95: 95th percentile; X97.5: 97.5th percentile; Max: maximum value; Undisturbed: Reference dose value for the exposure scenario

Appendix G: In this subsection, the curriculum vitae provides an overview of the author's academic background, research experience, and professional development. It summarizes the educational trajectory, key qualifications, and relevant activities that have contributed to this dissertation.

Thomas Makumbi

WORK EXPERIENCE

SCIENTIST – KARLSRUHE INSTITUTE OF TECHNOLOGY (KIT) – 15/01/2021 – Current – KARLSRUHE, GERMANY

Business or Sector: Education **Department:** Institute for Thermal Energy Technology and Safety

Address: Campus North, Hermann-von-Helmholtz Platz 1, 76344, Karlsruhe, Germany

Website: www.kit.edu

-Application of AI in scientific research.

-Data collection and analysis.

-Software development.

-Modelling and simulation of biokinetic and dosimetric models.

-Literature search.

-Uncertainty and sensitivity analysis in internal dosimetry.

-Statistical data analysis.

-Programming.

-Technical report writing.

-Publication of academic research.

europass

ASSISTANT LECTURER – MAKERERE UNIVERSITY (MUK) – 01/09/2014 – 31/12/2020 – KAMPALA, UGANDA

Business or Sector: Education **Department:** Department of Electrical and Computer Engineering

Address: College of Engineering, Design, Art and Technology (CEDAT), Makerere Hill Road, P.O Box 7062, Kampala, Uganda

Website: www.mak.ac.ug

-Teaching, marking and grading undergraduate students.

-Supervision of undergraduate internship.
-Co-supervision of bachelor thesis on energy systems (energy efficiency and conservation, power systems, renewable energy, refrigeration and air conditioning, power generation, etc).
-Conducting tutorials and research.

-Assisting senior colleagues with data collection, analysis of results and documentation of their research findings and research proposals.

-Offering consultancy services in the department on behalf of energy technology, power system design and protection, electrical machines and machine design, etc.

-Performance of feasibility studies for small hydropower schemes.

-Design, construction and testing of solar irrigation pumps and solar PV systems.

-Design of thermal power plants.

GUEST RESEARCHER/ SCIENTIST – KARLSRUHE UNIVERSITY OF APPLIED SCIENCES (HKA) – 01/01/2019 – 30/06/2019 – KARLSRUHE, GERMANY

Business or Sector: Education **Department:** Institute of Refrigeration, Air Conditioning and Environmental Engineering (IKKU)

Address: Faculty of Mechanical Engineering and Mechatronics (MMT), Moltkestrasse 30, 76133, Karlsruhe, Germany

Website: www.hs-karlsruhe.de

-Writing research proposals on refrigeration and air conditioning.

-Performing laboratory experiments on ice slurry generation and utilisation.

-Evaluating the performance of heat exchangers.

-Modelling and simulation of HVAC systems with ice slurry thermal energy storage.

-Modelling of solar air conditioning systems with ice slurry thermal energy storage.

-Evaluating the performance of refrigeration and air conditioning systems.

-Literature search.

-Teaching and conducting tutorials.

TEACHING ASSISTANT – MAKERERE UNIVERSITY (MUK) – 01/09/2008 – 30/06/2013 – KAMPALA, UGANDA

Business or Sector: Education **Department:** Department of Agricultural and Biosystems Engineering

Address: College of Agricultural and Environmental Sciences (CAES), Makerere Hill Road, P.O Box 7062, Kampala, Uganda

Website: www.mak.ac.ug

-Assisting with teaching, marking and grading of undergraduate students.

-Conducting tutorials and laboratories for undergraduate students.

-Supervision of undergraduate internship.

-Offering consultancy services.

-Assisting senior colleagues with their research data collection, analysis and documentation.

MAINTENANCE AND REPAIR ENGINEER – VOLUNTEERS EFFORT FOR DEVELOPMENT CONCERNS (VEDCO) – 01/06/2008 – 01/09/2010 – KAMPALA, UGANDA

Business or Sector: Agriculture, forestry and fishing **Department:** Department of Agricultural Mechanisation and Irrigation

Address: Plot 504, Kibuga Block 8, Rubaga, P.O Box 1244, Kampala, Uganda **Email:** info@vedcouganda.org

Website: www.vedcouganda.org

-Supervision of motor vehicle repair and maintenance.

-Design and construction of rainwater harvesting tanks for rural households.

-Design, construction and maintenance of biogas systems for rural households.

-Design and construction of biomass cooking stoves for rural households.

-Design and construction of briquette machines for rural households.

-Design, installation and maintenance of drip irrigation systems for farmers.

MANAGEMENT ASSISTANT – IBERO(UGANDA) LIMITED – 01/06/2007 – 25/09/2007 – KAMPALA, UGANDA

Business or Sector: Manufacturing **Department:** Department of Engineering

Address: Plot 44/50, 7th Street Namuwongo Road, P.O Box 23139, Kampala, Uganda

Email: management@ibero.co.ug

Website: www.ibero.co.ug

-Supervision of repair and maintenance of coffee processing equipment and machinery.

-Supervision of civil, electrical and mechanical works (i.e., repair and maintenance of engines, generators, motors, pumps, fans and compressors, electrical wiring and installation, water supply and plumbing works, wastewater treatment, etc).

-Technical report writing.

-Production planning and control.

-Computer repair and maintenance.

STUDENT ENGINEER – SUGAR CORPORATION OF UGANDA LIMITED (SCOUL) – 01/06/2006 – 23/09/2006 – LUGAZI, UGANDA

Business or Sector: Manufacturing **Department:** Department of Engineering

Address: Plot 133/135, 6th Street Industrial Area, P.O Box 1, Lugazi, Uganda **Email:** scoul@mehtagroup.com

Website: www.mehtagroup.com

-Engine repair and maintenance

-Repair and maintenance of turbo machinery (pumps, fans, steam turbines and compressors).

-Repair and maintenance of electrical machines and equipment (control panels, switch gears, motors and generators).

-House wiring and instrumentation.

-Manufacturing processes and machining.

-Preparation of production and machine drawings.

EDUCATION AND TRAINING

01/07/2021 – 13/11/2025 Karlsruhe, Germany

DOCTOR OF PHILOSOPHY (PhD) Karlsruhe Institute of Technology (KIT)

-Technical and scientific expertise (physics of ionizing radiation, radiation biology and health effects, dosimetry and instrumentation, modelling and simulation).

-Regulatory and compliance competence (radiation protection standards, licensing and safety cases, environmental and waste management).

-Risk assessment and safety management (radiological risk analysis, emergency preparedness and response, safety culture and human factors).

-Research and analytical skills (experimental design, statistics and data analysis, scientific computing).

-Project and program management (research project leadership, interdisciplinary collaboration, quality assurance).

-Communication and stakeholder engagement (technical writing, oral communication, training and instruction, risk communication).

-Professional and ethical practice (ethics and responsible conduct, professional standards, continuous learning).

-Transferable skills (critical thinking and problem structuring, independent work under ambiguity, high-level quantitative reasoning, negotiation and influence in technical settings, policy analysis and advisory capability).

Address Kaiserstrasse 12, 76131, Karlsruhe, Germany **Website** www.kit.edu

Field of study Environmental protection technology **Level in EQF** EQF level 8

Thesis Assessment of uncertainties affecting dosimetric calculations for the intake of radon and NORM.

01/09/2010 – 30/09/2014 Kampala, Uganda

europass

MASTER OF SCIENCE IN RENEWABLE ENERGY Makerere University (MUK)

Principal Subjects: Electrical Energy Systems, Solar Energy, Bioenergy, Hydropower, Statistics and Research Methods, Energy Systems Optimisation, Entrepreneurship, Project Planning and Management, Energy Policies, Geothermal Energy, Wind Energy, Tidal and Wave Energy, Development of Small Hydropower Systems, Design and Maintenance of Hydraulic Structures for Hydropower, Design and Maintenance of Electromechanical Equipment for Hydropower, Power System Design and Protection, Laboratories and Thesis Project.

Occupational Skills: How to draft a renewable energy policy, how to design a standalone (off grid) and grid (on grid) solar photovoltaic systems, how to plan and design a solar thermal power plant, how to design and install solar water heating systems based on flat plate collectors, design and construction of a solar water desalination system, design, construction and testing of solar crop dryers, design, construction and testing of solar cookers, how to design, install and maintain a solar powered irrigation system, how to read and prepare electrical and electronics circuit drawings (block , highway, layout, sankey and schematics), how to read and prepare power systems drawings(generation, transmission, substation and distribution), how to test for the performance parameters of electrical machines (open circuit test, short circuit test, voltage regulation, efficiency, etc), how to select a turbine for a given hydropower site, how to start and manage an energy business, how to manage an energy project, how to design, maintain and repair electromechanical equipment for hydropower (turbines, pumps, transformers, generators, switch gears, etc), operation and maintenance of power plants, how to mitigate technical losses in a power system, how to perform a feasibility study for a hydropower project, how to design and maintain various hydraulic structures for hydropower (weirs, gates, valves, canals, reservoirs, spillways, dams, penstock, draft tube, surge tanks, power house, trash racks, etc), how to design and optimise a hybrid energy system, how to plan and design a solar energy system for a homestead and how to write a business proposal.

Address Makerere Hill Road, P.O Box 7062, Kampala, Uganda **Website** www.mak.ac.ug **Field of study** Renewable Energy

Final grade A **Level in EQF** EQF level 7

Thesis Design of a sustainable energy system for an eco-village: a case study of Bulindo village

01/09/2010 – 07/11/2013 Gavle, Sweden

MASTER OF SCIENCE IN ENERGY SYSTEMS University of Gavle (HIG)

Principal subjects: Introduction to Energy Technology, Renewable Energy Technology, Sustainable Power Generation, Sustainable Energy Utilisation, Energy and Environment, Computational Fluid Dynamics, Thermal Comfort and Indoor Climate, Applied Refrigeration and Heat Pump Technology, Energy Management, Modelling of Energy systems, Green Buildings, Advanced Refrigeration and Heat Pump Technology, Energy Policies, Applied Energy Technology (project course), Measurement Techniques and Thesis Project.

Occupational skills: Operation and maintenance of power plants (hydro, solar, wind, geothermal, thermal, nuclear, etc), how to plan eco-cities, how to draft an energy policy, how to design, optimise and install a heat driven cooling system using a geothermal, biomass or solar absorption chiller, techniques on how to instrument, measure and evaluate the performance of refrigeration systems, how to reduce the emission of greenhouse gases in large scale power plants, how to design, model and optimise a hybrid energy system, how to use LEED and BREEAM, flow measurement, flue gas analysis, engine testing, how to use building codes in structural and HVAC systems design, how to design an air conditioning system for residential and commercial buildings, how to model and simulate the performance of a heat pump under different operating conditions, how to perform a CFD analysis on energy systems, energy and exergy analysis of thermodynamic systems, how to perform an energy audit of a company, how to characterise a fuel (proximate and ultimate analysis) and how to perform a risk assessment.

Address Kungschbacksvagen 47, 80176, Gavle, Sweden **Website** www.hig.se **Field of study** Sustainable Energy Engineering

Final grade B **Level in EQF** EQF level 7

Thesis Investigating the application of environmentally friendly solutions in the refrigeration industry

24/09/2004 – 31/08/2008 Kampala, Uganda

BACHELOR OF SCIENCE IN AGRICULTURAL ENGINEERING Makerere University (MUK)

Principal subjects: Engineering Mathematics, Engineering Drawing, Engineering Mechanics (Statics and Dynamics), Mechanics of Materials, Fluid Mechanics, Thermodynamics, Computer Aided Design, Theory of Machines and Mechanisms, Circuit Theory, Electrical Machines, Instrumentation, Power Systems, Computer Programming, Design of Machine Elements, Operations Research, Soil Mechanics, Renewable Energy Technologies, Structural Engineering, Soil and Water Engineering, Design of Processing Equipment, Design of Agricultural Machinery, Irrigation System Design and Management, Engineering Experimental Design, Hydraulics and Hydrology, Business Management, Entrepreneurship, Industrial Case Study (project course), Farm Power, Farm Machinery, Engineering Surveying, Environmental Engineering, Earth Moving Equipment, Land Use Policy and Law, Sociology and Thesis Project.

Occupational skills: Computing skills, basic mechanics, how to design the various agricultural machinery, design of machine elements (brakes, clutches, shafts, gears, bearings, linkages, cams, belts and pulleys, chain and sprocket, etc), how to design and construct farm structures, how to survey land and generate a topographical map, how to prepare and read engineering drawings, how to design and install an irrigation system, how to write a business proposal, how to evaluate the economic feasibility of a project/venture, how to design water and earth retention structures, how to hitch various equipment and machinery onto a tractor, how to service and maintain motor vehicles, motor vehicle driving and painting skills.

Address Makerere Hill Road, P.O Box 7062, Kampala, Uganda **Website** www.mak.ac.ug

Field of study Engineering, manufacturing and construction **Final grade** B **Level in EQF** EQF level 6

Thesis Assessment of thermodynamic properties of agricultural waste briquettes

01/03/2002 – 12/12/2003 Kampala, Uganda

UGANDA ADVANCED CERTIFICATE OF EDUCATION (UACE) Old Kampala Senior Secondary School

Main subjects: Physics, Chemistry, Mathematics and Art

Occupational skills: Drawing skills, arithmetic skills, how to prepare and read algorithms.

Address P.O Box 330, Kampala, Uganda **Field of study** Physical Science **Final grade** B **Level in EQF** EQF level 5

01/03/1998 – 30/11/2001 Kampala, Uganda

UGANDA CERTIFICATE OF EDUCATION (UCE) Kampala Secondary School

Principal Subjects: English language, Mathematics, Physics, Chemistry, Biology, Geography, Commerce, Art and History.

Occupational skills: Drawing skills, arithmetic skills, basic science, leadership skills and map reading.

Address P.O Box 4916, Kampala, Uganda **Field of study** Basic Science **Final grade** B **Level in EQF** EQF level 4

europass

LANGUAGE SKILLS

Mother tongue(s): **ENGLISH** | **LUGANDA**

Other language(s):

	UNDERSTANDING		SPEAKING		WRITING
	Listening	Reading	Spoken production	Spoken interaction	
SWAHILI	B2	B2	B1	B1	B1
FRENCH	A2	A2	A2	A2	A2
GERMAN	B1	B1	A2	A2	A2

Levels: A1 and A2: Basic user; B1 and B2: Independent user; C1 and C2: Proficient user

SKILLS

Content Creation | good commands of C++ programming | Software Development | Microsoft Office: Word, Excel, Access, Power Point, Outlook. | Social media communicator | Computational Fluid Dynamics (CFD) | Internet use information processing | Computer-Aided Design | Video Conferencing (Zoom Skype Google Hangout) | Data management and data analysis | Programming with R | good command of Java programming

PUBLICATIONS

2015

Investigating the opportunities for environmentally benign options in the refrigeration industry of Uganda

Using synthetic refrigerants has led to ozone depletion, global warming and the associated climate change. This study therefore aimed at investigating the application of environmentally friendly options in the refrigeration industry of Uganda with the main emphasis on refrigerants. A field study was done to assess the status of refrigeration in Uganda as well as to obtain relevant information for the study using questionnaires, interviews, field measurements and observations. The required data included evaporation and condensing temperatures and pressure, refrigerant mass flow rate, system type, refrigerant type, etc. Using the above data as input, models of the available systems were developed using EES and their efficiencies determined; also, models were proposed for each sector in the industry using an appropriate natural refrigerant(s) and comparison of the efficiencies obtained with those of installed systems was made. EES also assisted in the performance of a parametric study on the system operating parameters. Results from the field survey showed that synthetic refrigerants dominate the industry and the systems installed are single stage vapour compression while those from modelling and simulation reveal that natural refrigerants offer a promising solution in the refrigeration industry of Uganda and should be adopted for energy, safety and environmental reasons. Nevertheless, it is recommended that rigorous testing of the systems with alternate refrigerants proposed be conducted to verify the results of the simulations before full adoption. Furthermore, performing an economic analysis would give better justification for adoption from an industrial point of view. However, the major challenges to be encountered in case of adoption are safety, system modifications especially in systems that are to use R744, lack of technical expertise to design, install, operate and service the systems as well as lack of government policy to spearhead the transition. Therefore, for the transition to be realised there is need to come up with policy concerning the use of environmentally harmful refrigerants and create awareness in the industry.

Thomas Makumbi, John Baptist Kirabira, Adam Sebbit, Bjoern Palm; BJAST .18033

2014

Design of a sustainable energy system for an eco-village: a case study of Bulindo village

The aim was to plan Bulindo village to accommodate 10,000 residents with the main emphasis on the sustainable energy system that meets the energy demand under available constraints. The planning and design were accomplished by ascertaining the current state of Bulindo village as well as determining the energy requirements of this village and the available resource potential in the area. Using the above data as input to computer simulation model using HOMER software an energy system configuration that meets the energy demand for this village was obtained. After gathering the relevant information for the study i.e. energy demand of the village using a field survey and the primary energy resource potential at Bulindo got from a climate file for Wakiso district provided by Meteonorm software, HOMER was used to model, simulate and optimize the energy system that meets the energy requirements of the village under available constraints. HOMER also assisted in determining both the technical and economic feasibility of the designed system. From computer modelling and simulation, it was found that Bulindo has an overall electrical energy demand of 49 MWh/day. The demand is maximum from 18:00-22:00hrs with a peak of 4.6 MW. The fresh water supply system for the village which was modelled as a

deferrable load had an energy demand of 680 kWh/day. The demand is highest during the dry season i.e., from January to March and from June to September with a peak demand of 170 kW. The designed energy system consisted of a PV array, a wind generator, the grid, battery bank, a converter and a biomass generator which acts as backup. This system can meet up to 95% of the annual energy demand while the remaining 5% will be supplied by the national grid. The unit cost of the electricity is $0.028, and the project life is 50 years. In conclusion, the sustainable energy system for Bulindo village to be moved in by 2025 was designed. The designed system is believed to offer a better performance due to its sustainability as well as its ability to meet all the energy requirements of the village i.e., both energy and freshwater demand. Simulation results demonstrated that using green energy sources such as solar PV and wind generators will reduce the operating costs, greenhouse gas emissions and particulate matter. In addition, the system also supplies fresh water for residential, commercial and industrial usage. The amount of energy produced by the system is 63,658,616 kWh/year at a unit cost of $0.028 /kWh. 76% of the generated energy is consumed by the system i.e., AC primary load and the deferrable load while the surplus (24%) is sold to the national grid which earns crucial revenue to the village for better management of the system, hence guaranteeing sustainability. However, the challenge will be getting the human resource to maintain and manage this system.

Thomas Makumbi, Samuel Baker Kucel, John Baptist Kirabira, Adam Sebbit; JSRR.2015.100

2015

Phase developments during natural evaporation simulation of lake Katwe brine based on Pitzer's model

Lake Katwe is the largest of the eight saline crater lakes in the pleistocene Katwe-Kikorongo volcanic field situated in the western arm of the great East African Rift system in southwestern Uganda. The salt lake is hydro-chemically of a carbonate type with its brines representing an important source of mineral salts of high economic value. In the present work, the geochemical simulation of the crystallisation route of the natural evaporation of the lake brine in PHREEQC based on Pitzer's thermodynamic model was done. The precipitation sequence of the different mineral salts that crystallised step by step from the brine during natural evaporation at 30ºC was obtained. The results show that the mineral salt precipitation sequence following the saturation data is Sulfates, chlorides and carbonates. During the evaporative concentration process, the brines become enriched in Na^+, K^+, HCO_3^- + CO_3^{2-}, and depleted in Cl^- and SO_4^{2-} with massive halite precipitation. The study provides the basis for the future comprehensive utilisation of the natural brine resource in Lake Katwe.

John Baptist Kirabira, Hillary Kasedde, Matthaeus U. Baebler, Thomas Makumbi; BJAST.20598

2014

Energy management practices in Ugandan SME foundries

Foundry is one of the most energy intensive metallurgical industries. In Uganda, foundries are associated with large energy consumption necessitating the need to seek for ways to minimise their energy consumption. This study sought to establish the energy efficiency of the SMEs in Uganda with the view of devising means to reduce on their energy consumption. This was accomplished by studying the energy consumption trends in the industry using primary and secondary data obtained from several SME foundry operators in Uganda and basing on this data, energy efficiency and conservation measures have been devised. The major energy sources used in these foundries include used oil at a consumption rate of 72%, biomass (charcoal and firewood) at 21%, diesel at 6%, and electricity at 1%. The specific energy consumptions (SEC) of the firms studied range from 7.35 MJ/kg to 14.61 MJ/kg which is considerably on the higher side. The melting process consumes the biggest part of the total energy consumed, at 70% in the foundries. This necessitates the employment of more energy efficient melting technologies. Implementation of energy management programs in order to reduce energy requirements per unit of output is thus recommended. Different energy saving measures that can be employed in this sector were identified. Some of these can be implemented by adopting simple courses of action while others require high capital investment. It is thus recommended that these firms start by implementing the low-cost solutions and progressively move to the capital-intensive solutions.

John Baptist Kirabira, Angella Nalweyiso, Thomas Makumbi; IJSTR ISSN 2277-8616

2015

Estimating energy conservation potential of local metal casting units in Uganda using data envelopment analysis

This study sought to determine the relative energy efficiency of metal casting units in Uganda with a view of estimating the energy conservation potential. Data Envelopment Analysis (DEA) tool was used to accomplish this task. Energy consumption data was collected through interviews and field observations from the different foundries and was used as the input data for the model. Six foundries in the Central region of Uganda were surveyed following a snowball sampling technique. This consisted mainly of the annual energy consumption by the different foundries while the model outputs were annual total sales and annual total profits. Results showed that all the foundries were energy efficient except for one, foundry E, as indicated by its energy efficiency score of less than unity. There exists potential in foundry E for energy savings and this may be accomplished by emulating energy management practices in the other units most especially foundry A and foundry D. The findings in this study can also be extended to other energy intensive industries in the country like the cement industry.

John Baptist Kirabira, Angella Nalweyiso Semakula, Thomas Makumbi; IJSTR, ISSN 2277-8616

2024

Parameter uncertainty analysis of the equivalent lung dose coefficient for the intake of radon in mines: a review

Radon presents significant health risks due to its short-lived progeny. The evaluation of the equivalent lung dose coefficient is crucial for assessing the potential health effects of radon exposure. This review focuses on the uncertainty analysis of the parameters associated with the calculation of the equivalent lung dose coefficient attributed to radon inhalation in mines. This analysis is complex due to various factors, such as geological conditions, ventilation rates, and occupational practices. The literature review systematically examines the sources of radon and its health effects among underground miners. It also discusses the human respiratory tract model used to calculate the equivalent lung dose coefficient and the associated parameters leading to uncertainties in the calculated lung dose. Additionally, the review covers the different methodologies employed for uncertainty quantification and their implications on dose assessment. The text discusses challenges and limitations in current research practices and provides recommendations for future studies. Accurate risk assessment and effective safety measures in mining environments require understanding and mitigating parameter uncertainties.

Thomas Makumbi, Bastian Breustedt, Wolfgang Raskob; Journal of Environmental Radioactivity

Authors: Thomas Makumbi, Bastian Breustedt, Wolfgang Raskob | **Journal Name**: Journal of Environmental Radioactivity |

Volume, Issue and Pages: 276(1–4):107446 | **Publisher**: Elsevier

Link https://doi.org/10.1016/j.jenvrad.2024.107446

2024

INTDOSKIT: An R Code for calculation of dose coefficients and studying their uncertainties.

An R-code, which allows based on ICRP reference models the calculation of the time dependent activity distribution, the number of decays in a commitment period and the dose coefficients for tissues and organs of the human body, has been developed. R Language was chosen due to its powerful mathematical and statistical modelling features, as well as its graphical capabilities. The developed set of functions and constants (called “INTDOSKIT”) can be sourced in R-scripts that define or import the models and calculations to be performed. The code has been tested on models of several radionuclides and was successfully validated against reference data taken from ICRP OIR Data Viewer software (ICRP 2022). Furthermore, the code has been tested and verified on the modelling of the radioactivity of decay chains using data of the Ra-223 model presented by Höllriegl and colleagues (Höllriegl 2021). The results of calculations with INTDOSKIT demonstrated that the code can reproduce the ICRP bioassay data and dose coefficients.

Deviations are few percents only and are mainly due to rounding in the original data. Lastly, the code is able to handle uncertainty and sensitivity studies as demonstrated by the results in a pilot study of injection of Am-241, which estimated geometric standard deviations (GSD) for dose coefficients ranging between 1.25 (bone-surface) and 1.66 (testes); these results are consistent with those obtained from similar studies done by other researchers who reported GSD values ranging from 1.13 to 1.73.

Bastian Breustedt, Niranjan Chavan, Thomas Makumbi; Health Physics

Authors: Bastian Breustedt, Niranjan Chavan, Thomas Makumbi | **Journal Name**: Health Physics | **Publisher**: Health physics Society

Link https://journals.lww.com/health-physics/fulltext/9900/intdoskit__an_r_code_for_calculation_of_dose.185.aspx

2024

Application of INTDOSKIT tool for assessment of uncertainties on dose coefficients for ingestion of uranium by workers

The International Commission on Radiological Protection (ICRP) has developed the Human Alimentary Tract Model (HATM) to calculate radiation doses from the ingestion of radionuclides for the protection of workers and the public. In parallel, the ICRP's Occupational Intake of Radionuclides (OIR) series provides biokinetic models and dose coefficients based on a reference human, primarily for regulatory purposes. Although these coefficients are not usually checked for uncertainties, the investigation of such uncertainties is crucial to ensure their reliability in radiation protection. This study uses INTDOSKIT, a software tool developed using the R programming language and RStudio as the Integrated Development Environment (IDE), to calculate doses and explore uncertainties following ingestion of U-238 by workers. Two scenarios were investigated: Case I, using the latest HATM model and the systemic uranium model from ICRP publications, and Case II, based on data from Puncher and Burt (2013), using older ICRP models. In both cases, uptake of U-238 in its soluble form (Type F) was modelled and the results were validated using the ICRP OIR dataviewer software. Following validation, uncertainty and sensitivity analyses were performed. In Case I, uncertainties were assigned to particle transport parameters in the HATM and uranium uptake fraction (f_A) into the blood, while in Case II they were limited to the uptake fraction (f_1) and the systemic uranium model. A Monte Carlo simulation of 60,000 runs was performed for both cases, sampling model parameters from their respective probability distributions to generate dose distributions. The influence of each parameter on these distributions was also analysed. Probability distributions were inferred to the calculated dose values using the maximum likelihood estimation method and the Kolmogorov-Smirnov goodness-of-fit. The results showed that for both cases the committed effective dose coefficient, e (50), followed a lognormal distribution. Case I had a geometric mean of 3.2E-08 Sv/Bq and GSD of 2.0, while case II had a slightly lower geometric mean of 3.1E-08 Sv/Bq and GSD of 1.9. Sensitivity analysis showed that the main contributor to dose uncertainty was the fraction of uranium absorbed from the small intestine into the blood. Both cases showed similar trends, with slightly higher results in case I. Overall, this study demonstrates the effectiveness of INTDOSKIT in calculating dose coefficients and analysing uncertainties. It suggests that while the ICRP reference values

remain useful for protection, the incorporation of additional statistical measures and distribution characteristics could further enhance radiation protection strategies.

Thomas Makumbi, Bastian Breustedt, Wolfgang Raskob, Sadeeb Simon Ottenburger

Authors: Thomas Makumbi, Bastian Breustedt, Wolfgang Raskob, Sadeeb Simon Ottenburger | **Journal Name**: Radiation Physics and Chemistry | **Volume, Issue and Pages**: 226(1):112247 | **Publisher**: Elsevier

Link https://doi.org/10.1016/j.radphyschem.2024.112247

2025

Parameter uncertainty analysis of the committed equivalent dose coefficients from inhalation of radon progeny in underground uranium mines

This study evaluates the uncertainties in committed equivalent dose coefficients from inhalation of radon progeny in underground uranium mines. The work focuses on two exposure scenarios: wet drilling with good ventilation (Job 1) and dry drilling with poor ventilation (Job 4). The use of Monte Carlo simulations informed by the International Commission on Radiological Protection (ICRP) latest biokinetic models and parameter probability distributions obtained from published literature, revealed that Job 4 conditions yield higher lung dose coefficients than Job 1, despite both scenarios exhibiting similar uncertainty levels. The committed equivalent lung dose coefficients followed lognormal distributions, with geometric means of 61.87 mSv/(mJh/m^3) and geometric standard deviation of 1.56 for Job 4 and 47.05 mSv/(mJh/m^3) and geometric standard deviation of 1.58 for Job 1. The alveolar-interstitial region showed the greatest uncertainty, while the bronchial secretory cells received the highest doses. Among systemic organs, the kidneys received the largest dose. Statistical tests confirmed significant differences between the two job types. Sensitivity analysis identified tidal volume as main contributor to committed equivalent lung dose coefficient uncertainty. These findings support revising model parameters and improving breathing parameter measurements to enhance dose accuracy. The study emphasizes the necessity for enhanced ventilation, stricter air quality standards, and advanced personal protective equipment to mitigate health risks in radon-prone mining environments.

Authors: Thomas Makumbi, Bastian Breustedt, Wolfgang Raskob, Sadeeb Simon Ottenburger | **Journal Name**: Journal of Environmental Radioactivity | **Publisher**: Elsevier

NETWORKS AND MEMBERSHIPS

10/05/2022 – CURRENT Oberschleissheim, Germany

European Radiation Dosimetry Group e.V (EURADOS)

I have been an active member of EURADOS for the last 2 years attached to work group 7 that deals with internal dosimetry.

15/01/2021 – 31/08/2025 Oberschleissheim, Germany

RADONORM Early Researchers Council

I am currently an active member of the RadoNorm Early Career Researchers Council attached to work package 3 that deals with radiation protection dosimetry.

01/03/2024 – CURRENT

European NORM Association (ENA)

I am an active member of ENA since March 2024.

DRIVING LICENCE

Driving Licence: AM Driving Licence: A1

Driving Licence: A2 Driving Licence: A

Driving Licence: B1 Driving Licence: B

Driving Licence: BE Driving Licence: C1

Driving Licence: D1

CONFERENCES AND SEMINARS

22/11/2021 – 24/11/2021 Vienna, Austria

europass

5th European Radiation Protection Week (ERPW)

I was invited to give an oral talk concerning my PhD work at this conference.

14/07/2014 – 15/07/2014 Entebbe, Uganda

SIDA/ SAREC Regional Collaboration Conference

I was invited to give an oral talk about the possible to introduce natural refrigerants in the refrigeration industry of Uganda.

30/05/2022 – 03/06/2022 Budapest, Hungary

6th European Congress on Radiation Protection

I was invited to give an oral talk concerning my PhD work at this conference.

09/10/2022 – 14/10/2022 Estoril, Portugal

6th European Radiation Protection Week (ERPW)

I was invited to present a poster about my PhD work at this conference.

23/05/2023 – 25/05/2023 Munich, Germany

International Workshop on Uranium Miners and Millers

I was invited to present a poster at this workshop.

09/10/2023 – 13/10/2023 Dublin, Ireland

7th European Radiation Protection Week (ERPW)

I was invited to present a poster at this conference.

15/05/2024 – 17/05/2024 Rome, Italy

3rd European NORM Association (ENA) Workshop

I was invited to present a poster at this workshop.

20/06/2022 – 24/06/2022 Belgrade, Serbia

European Radiation Dosimetry (EURADOS) Group Annual Meeting

I was invited to give an oral took to the work group 7 internal meeting during this event.

12/06/2023 – 15/06/2024 Porto, Portugal

European Radiation Dosimetry (EURADOS) Group Annual Meeting

I was invited to give an oral took to the work group 7 internal meeting during this event.

10/05/2023 – 12/05/2023 Domodossola, Italy

ITES Artificial Intelligence Seminar

I participated and gave an oral talk on neural networks at the ITES artificial intelligence seminar held in Domodossola, Italy in spring 2023.

11/11/2024 – 15/11/2024 Rome, Italy

8th European Radiation Protection Week (ERPW)

I was invited to give an oral talk at this conference.

24/02/2025 – 27/02/2025 Bucharest, Romania

European Radiation Dosimetry (EURADOS) Group Annual Meeting

I was invited to give an oral took to the work group 7 internal meeting during this event.

29/09/2025 – 03/10/2025 London, United Kingdom

9th European Radiation Protection Week (ERPW)

I was invited to give an oral talk at this conference.